

**Study of Complexation and
Redox Reactions Using
Capillary Electrophoresis Inductively Coupled
Plasma Mass Spectrometry (CE-ICP-MS)**

Dissertation
zur Erlangung des Grades
"Doktor der Naturwissenschaften"
im Promotionsfach Chemie

am Fachbereich 09 - Chemie, Pharmazie, Geographie und
Geowissenschaften
der Johannes Gutenberg-Universität Mainz

Christian Willberger

geb. in Koblenz

Mainz, 2019

Dekan:

1. Berichterstatter:

2. Berichterstatter:

Datum der mündlichen Prüfung: 10.07.2019

ABSTRACT

In the context of the long-term safety assessment of a future disposal for high-level nuclear waste the actinides uranium, neptunium, plutonium and americium are of particular importance since they all exhibit very long-lived isotopes. As part of spent nuclear fuels, for example the isotopes ^{238}U ($t_{1/2} = 4.47 \cdot 10^9$ a), ^{237}Np ($t_{1/2} = 2.14 \cdot 10^6$ a) and ^{239}Pu ($t_{1/2} = 2.41 \cdot 10^4$ a) must be named. Because it is planned to safely embed the radioactive waste up to 1 million years in deep geological formations with argillaceous rocks, crystalline rocks or salt as host rock it is of great importance to have a deep knowledge of the actinide behavior in these conditions.

In order to investigate these systems, in the present work the coupling of a capillary electrophoresis (CE) to an inductively coupled plasma mass spectrometer (ICP-MS) was employed. Here, the combination of the high separation capability of the CE with the possibility of multi element detection with very low detection limits of the ICP-MS was utilized. This analytical method provides very good results, especially in the case of very low concentration ranges of the actinides in environmentally relevant systems.

First, in the frame of this work, investigations on the redox speciation of actinides in 1 M acetic acid as the background electrolyte (BGE) were conducted. The electrophoretic mobilities μ_i of the redox stable actinides Am(III), Th(IV), Np(V) and U(VI) could be determined and based on that the μ_i of all Pu species with the oxidation states +III – +VI. The trend in the μ_i turned out to be $\text{An(III)} > \text{An(VI)} > \text{An(V)} > \text{An(IV)}$ for all actinides. Additionally, an approach for the estimation of the μ_i of non-stable oxidation states of actinides, e.g. Np(III) or U(V), was developed. By comparing the so determined μ_i with experimentally determined values, the applicability of this proceeding could be validated.

Furthermore, the stability constants of the actinides Am(III), Th(IV), Np(V) and U(VI) with the ligands acetate, propionate, gluconate and citrate at an ionic strength of $I = 0.3$ M were examined. For each system a complete set of stability constants could be obtained, the results were extrapolated to zero ionic strength by means of the Davies equation.

The basics for the determination of kinetic parameters of redox reactions by CE-ICP-MS were investigated for the reduction of Np(V) by hydroxylamine hydrochloride. In doing so, the rate constants of the reaction at different temperatures and based on that the Arrhenius parameters could be determined. In addition, the rate constants at different temperatures and the Arrhenius parameters were obtained for the reduction of Pu(VI) by Fe(II).

It could be shown clearly by the results presented in this work, that the coupling of CE to ICP-MS is a powerful analytical method for the investigation of actinides in low concentration ranges. The resulting electrophoretic mobilities can deal as the basis for the interpretation of CE experiments. The determined stability constants are of great importance in the long-term safety assessment of a future nuclear waste disposal for high-level nuclear waste. With a prove-of-principle study the applicability of CE-ICP-MS for the determination of kinetic parameters of redox reactions could be shown.

ZUSAMMENFASSUNG

Im Zusammenhang mit der Langzeitsicherheitsanalyse eines zukünftigen Endlagers für hochradioaktive Abfälle sind die Aktinide Uran, Neptunium, Plutonium und Americium von Bedeutung, da diese alle sehr langlebige Isotope besitzen. Als Bestandteile von abgebrannten Brennelementen sind hierbei zum Beispiel die Isotope ^{238}U ($t_{1/2} = 4,47 \cdot 10^9 \text{ a}$), ^{237}Np ($t_{1/2} = 2,14 \cdot 10^6 \text{ a}$) und ^{239}Pu ($t_{1/2} = 2,41 \cdot 10^4 \text{ a}$) zu nennen. Da es geplant ist, die radioaktiven Abfälle in tiefegeologischen Formationen mit Ton, Salz oder Granit als Wirtsgestein für bis zu 1 Million Jahre sicher zu lagern, ist es von großer Wichtigkeit, das Verhalten der Aktinide unter den dort vorherrschenden Bedingungen genau zu kennen um damit Aussagen über die Langzeitsicherheit treffen zu können. Als besondere Eigenschaften weisen die Aktinide ein sehr breites Spektrum an möglichen Oxidationszuständen und Speziationen auf und gehen eine Vielzahl an Komplex- und Redoxreaktionen mit unterschiedlichsten Reaktionspartnern ein.

Um diese Systeme zu untersuchen, wurde in der vorliegenden Arbeit die Kopplung einer Kapillarelektrophorese (CE) mit einem induktiv-gekoppeltem Plasma Massenspektrometer (ICP-MS) verwendet. Hierbei wurde sich die Kombination der hohen Trennfähigkeit einer CE mit der Möglichkeit der Multi-Element Detektion mit sehr niedrigen Nachweisgrenzen der ICP-MS zunutze gemacht. Vor allem für die Herausforderung der sehr niedrigen Konzentrationsbereiche der Aktinide in natürlichen Systemen lieferte diese analytische Methode sehr gute Ergebnisse.

Zunächst wurden im Rahmen dieser Arbeit Untersuchungen zur Redoxspeziation von Aktiniden in 1 M Essigsäure als Background Elektrolyt (BGE) durchgeführt. Es konnten die elektrophoretischen Mobilitäten μ_i der redoxstabilen Aktinide Am(III), Th(IV), Np(V) und U(VI) bestimmt werden und davon ausgehend auch die aller Pu-Spezies in den Oxidationsstufen +III – +VI. Als Reihenfolge der μ_i ergab sich für alle Aktinide $\text{An(III)} > \text{An(VI)} > \text{An(V)} > \text{An(IV)}$. Zusätzlich wird ein Ansatz zur Abschätzung der μ_i von nicht stabilen Oxidationsstufen der Aktiniden, z.B. Np(III) oder U(V), erarbeitet. Über einen Vergleich der so berechneten μ_i mit experimentell bestimmten Werten konnte die Anwendbarkeit dieses Vorgehens bestätigt werden.

Weiterhin wurden in dieser Arbeit die Komplexbildungskonstanten der Aktinide Am(III), Th(IV), Np(V) und U(VI) mit den Liganden Acetat, Propionat, Gluconat und Citrat bei einer Ionenstärke von $I = 0,3 \text{ M}$ untersucht. Es wurde für jedes System ein vollständiger Satz an Stabilitätskonstanten ermittelt, die Ergebnisse wurden mittels Davies-Gleichung auf die Ionenstärke $I = 0 \text{ M}$ extrapoliert.

Die Grundlagen der Bestimmung von kinetischen Parametern von Redox Reaktionen mit Hilfe der CE-ICP-MS wurden an der Reduktion von Np(V) mit Hydroxylamin-Hydrochlorid untersucht. Es konnten hierbei die Geschwindigkeitskonstanten der Reaktion bei unterschiedlichen Temperaturen und darauf aufbauend die Arrhenius-Parameter bestimmt werden. Zusätzlich wurden die Geschwindigkeitskonstanten bei unterschiedlichen Temperaturen und die Arrhenius-Parameter für die Reduktion von Pu(VI) mittels Fe(II) bestimmt.

Durch die erzielten Ergebnisse kann deutlich gezeigt werden, dass die Kopplung von CE mit ICP-MS eine sehr gut geeignete analytische Methode zur Untersuchung von Aktiniden in niedrigen Konzentrationsbereichen ist. Die erhaltenen elektrophoretischen Mobilitäten können als Basis zur Interpretation von CE Experimenten verwendet werden. Die Stabilitätskonstanten sind von großer Bedeutung bei der Langzeitsicherheitsanalyse eines zukünftigen Endlagers für hochradioaktive Abfälle. Außerdem konnte in einer Machbarkeitsstudie die Anwendbarkeit von CE-ICP-MS für die Bestimmung von kinetischen Parametern von Redox Reaktionen gezeigt werden.

TABLE OF CONTENT

ABSTRACT.....	i
ZUSAMMENFASSUNG.....	ii
1. INTRODUCTION AND MOTIVATION	1
2. CE-ICP-MS	3
2.1 CAPILLARY ELECTROPHORESIS	3
2.1.1 BASIC PRINCIPLES	3
THEORY	3
APPARATUS AND EXPERIMENTAL PARAMETERS	5
2.1.2 ELECTROSMOTIC FLOW	8
2.1.3 FACTORS THAT INFLUENCE THE ELECTROPHORETIC MOBILITY	11
JOULE HEATING	11
VISCOSITY	13
PERMITTIVITY.....	13
CO-IONS AND COUNTER -IONS.....	14
IONIC STRENGTH.....	14
2.2 ICP-MS.....	14
2.2.1 MAIN COMPONENTS.....	15
2.2.2 INTERFERENCES AND OCTOPOLE REACTION SYSTEM	17
2.3 COUPLING DEVICE.....	18
2.4 SUMMARY OF ALL PARAMETERS OF THE CE-ICP-MS SYSTEM	21
2.5 LITERATURE REVIEW OF APPLICATIONS OF CE-ICP-MS WITH FOCUS ON THE INVESTIGATION OF ACTINIDES	22
EXPERIMENTAL SECTION.....	28
3. DETERMINATION OF ELECTROPHORETIC MOBILITIES WITH CE-ICP-MS.....	28
3.1 THEORETICAL CONSIDERATIONS.....	28
3.2 COMPARISON OF TWO EOF-MARKERS	30
3.3 PUBLICATION: INVESTIGATION OF THE ELECTROPHORETIC MOBILITY OF THE ACTINIDES TH AND U-AM IN DIFFERENT OXIDATION STATES.....	34
4. DETERMINATION OF STABILITY CONSTANTS WITH CE-ICP-MS	57
4.1 THEORETICAL CONSIDERATIONS.....	57
4.2 DETERMINATION OF THE FREE MOBILITIES OF THE ACTINIDES WITHOUT LIGANDS	60
4.2.1 EXPERIMENTAL PROCEDURE.....	60
4.2.2 RESULTS AND DISCUSSION.....	61
4.3 PUBLICATION: DETERMINATION OF THE STABILITY CONSTANTS OF THE ACETATE COMPLEXES OF THE ACTINIDES AM(III), TH(IV), Np(V), AND U(VI) USING CE-ICP-MS.....	64
4.4 PROPIONATE LIGAND	73

TABLE OF CONTENT

4.4.1 INTRODUCTION	73
4.4.2 EXPERIMENTAL PROCEDURE.....	74
4.4.3 RESULTS AND DISCUSSION	75
4.5 COMPARISON OF ACETATE AND PROPIONATE.....	80
4.6 GLUCONATE LIGAND	81
4.6.1 INTRODUCTION	81
4.6.2 EXPERIMENTAL PROCEDURE.....	82
4.6.3 RESULTS AND DISCUSSION	83
4.7 CITRATE LIGAND.....	88
4.7.1 INTRODUCTION	88
4.7.2 CITRATE SPECIATION.....	90
4.7.3 EXPERIMENTAL PROCEDURE.....	91
4.7.4 DATA EVALUATION.....	92
4.7.5 RESULTS AND DISCUSSION	93
AMERICIUM(III)	93
THORIUM(IV).....	96
NEPTUNIUM(V).....	98
URANIUM(VI).....	101
4.7.6 CONCLUSION.....	104
5. DETERMINATION OF REDOX KINETICS WITH CE-ICP-MS.....	105
5.1 INTRODUCTION.....	105
5.2 DETERMINATION OF KINETIC PARAMETERS OF THE REDOX REACTION OF NP(V) WITH HAHCL BY CE-ICP-MS	106
5.2.1 PUBLICATION: DETERMINATION OF KINETIC PARAMETERS OF REDOX REACTIONS USING CE-ICP-MS: A CASE STUDY FOR THE REDUCTION OF NP(V) BY HYDROXYLAMINE HYDROCHLORIDE.....	106
5.2.2 SUPPLEMENTARY INVESTIGATIONS: INFLUENCE OF IRON ON THE REDOX KINETICS OF THE REDUCTION OF NP(V) TO NP(IV) BY HYDROXYLAMINE HYDROCHLORIDE.....	117
5.3 DETERMINATION OF KINETIC PARAMETERS OF THE REDOX REACTION OF PU(VI) WITH Fe(II) BY CE-ICP-MS	121
5.3.1 INTRODUCTION	121
5.3.2 PRECEDING STUDY 1: MEASUREMENT OF IRON WITH THE ORS	124
5.3.3 PRECEDING STUDY 2: CE-ICP-MS MEASUREMENT OF Fe(II)-PHEN AND Fe(III)-EDTA COMPLEXES.....	126
5.3.4 KINETICS OF THE REDOX REACTION OF PU(VI) WITH Fe(II).....	129
SAMPLE PREPARATION AND EXPERIMENTAL PROCEDURE.....	130
LLE/LSC MEASUREMENTS	130
CE-ICP-MS MEASUREMENTS	135

TABLE OF CONTENT

5.3.5 DISCUSSION.....	137
6. SUMMARY AND CONCLUSION.....	139
REFERENCES.....	142
APPENDIX A1 – CALCULATION OF TEMPERATURE RISE DUE TO JOULE HEATING	159
APPENDIX A2 – CALCULATION OF UNCERTAINTIES.....	161
APPENDIX A3 – DETAILS ABOUT EXPERIMENTAL PROCEDURES.....	163
APPENDIX A4 – SUPPORTING INFORMATION FOR THE MOBILITY PAPER (SECTION 3.3)	165
APPENDIX A5 – DETAILED SAMPLE PREPARATIONS, RESULTS AND ELECTROPHEROGRAMS FROM STABILITY CONSTANT DETERMINATION	168
A5.1 ACETATE.....	168
A5.2 PROPIONATE	189
A5.3 GLUCONATE	194
A5.4 CITRATE.....	199
APPENDIX A6 – SUPPORTING INFORMATION FOR THE KINETIC PAPER (SECTION 5.2.1).....	203
DANKSAGUNG	206
LIST OF ABBREVIATIONS	208
LIST OF CHEMICALS	210
LIST OF UNITS.....	212
LIST OF VARIABLES AND CONSTANTS.....	213
LIST OF FIGURES.....	215
LIST OF TABLES.....	218

1. INTRODUCTION AND MOTIVATION

Nuclear energy has been used in Germany for many decades for the production of electrical energy. With the Federal Government's decision to opt out of this energy by the year 2022 [18AtG], this age will come to an end in Germany. Nevertheless, other countries adhere to the use of nuclear energy for power generation or even expand their nuclear energy production. Regardless of exit, continuation or expansion, the safe disposal of accruing radioactive waste is an important issue. Every country that uses nuclear energy has its own strategy and research program to find the best and most secure place. Most concepts have in common to store the radioactive material underground. In Germany it is planned to use deep geological formations with argillaceous rocks, crystalline rocks or salt as host rock for the storage of radioactive waste. Before the final decision about the definite conditions and the location of such a disposal in Germany can be made, a lot of research is needed to gain the desired background knowledge about risks and challenges.

In this context, the safe deposit has to be ensured for up to 1 Mio years [17SAG], only then the activity of long-lived isotopes has receded to the activity of the natural radiation [00GOM]. The neighboring population and the environment have to be protected from the radioactivity under any circumstances. In the case of a possible leakage of radionuclides from their casks, the geological surrounding has to act as a barrier to prevent the radionuclides from being transported away from the deposit, e.g. dissolved in ground waters. For the long-term safety assessment of a future geological disposal for high-level radioactive waste, it is thus of utmost importance to have a deep understanding and knowledge about the behavior and the properties of long-lived radioactive isotopes in the respective host rock systems and the corresponding pore waters.

One group of such long-lived radionuclides are the early actinides. Uranium, neptunium, plutonium and americium all exhibit long-lived isotopes which are part of the high-level radioactive waste resulting from spent nuclear fuels. The purpose of this work is thus the investigation of some aspects of the chemistry of the actinides named and their interaction with components being present in the geological system of a possible disposal.

As an analytical technique, the coupling of a capillary electrophoresis system (CE) with an inductively-coupled plasma mass spectrometer (ICP-MS) has been applied. This analysis method is very powerful for the investigation of actinides for two main reasons. First, it allows the investigation at low concentrations (down to $1 \cdot 10^{-9}$ M, [12STO]), which is important for environmentally relevant systems since the concentration of actinides in the surrounding biosphere after the leakage from the disposal is expected to be also very small.

1. Introduction and Motivation

Second, the actinides are known to exhibit a complex redox chemistry with a range of possible oxidation states and species. To clearly identify all of the occurring species, the separation capability of CE is of great benefit.

In the course of this work, three different possible applications of CE-ICP-MS were examined: the determination of electrophoretic mobilities, the determination of stability constants and the determination of kinetic parameters of redox reactions. The results of these investigations are presented in the following Sections 3 – 5. Important aspects about CE, ICP-MS and the coupling device are summarized in the Chapters 2.1 - 2.4. Chapter 2.5 provides a literature overview of the works conducted in the field of actinide CE-ICP-MS, Section 6 gives a summary and a conclusion.

2. CE-ICP-MS

In this work, capillary electrophoresis (CE), an analytical separation technique, was hyphenated to inductively coupled plasma mass spectrometry (ICP-MS) allowing to combine the advantages of both methods. CE is characterized by great separation capabilities, e.g. high efficiency and resolution, good reproducibility, relatively short analysis times and a very low sample consumption. ICP-MS, used as a multi-element detection method, provides a very high sensitivity and selectivity. Thus, this system enables to investigate the speciation of actinides in environmentally-relevant systems in very low concentration ranges.

The present chapter gives an overview of the theoretical aspects of the individual parts, namely CE, ICP-MS and the coupling device, and creates a link to the application in the speciation of actinides.

2.1 CAPILLARY ELECTROPHORESIS

The following descriptions of the theory of electrophoretic separation and instrumentation are mainly based, if not stated otherwise, on [10LAU] and [93ENG]. Some of these parts can also be found in the 'Mobility Manuscript' [19WIL1] but are also given here for the sake of completeness and for more comprehensive considerations.

2.1.1 BASIC PRINCIPLES

THEORY

The separation of different ions during electrophoretic experiments is based on the different migration velocity v of the respective ion in the applied electric field E . As can be seen from Equation (2.1), these two quantities are directly proportional to each other, the proportional constant is the so called electrophoretic mobility μ .

$$v = \mu E. \quad (2.1)$$

This electrophoretic mobility μ is a characteristic constant for a given ion in a given medium. The electric field E is defined as the quotient of the applied voltage U and the capillary length l . In the case of the experiments in this work, capillaries with a length of $l = 76$ cm were used. The voltage applied to the capillary was either $U = 10$ kV during stability constant determinations (see Section 4) or $U = 25$ kV during mobility measurements and kinetic experiments (Sections 3 and 5). This leads to electric field strengths of $E = 132$ V cm⁻¹ and $E = 329$ V cm⁻¹, respectively.

During their electrophoretic migration, the ions are driven forward by the electric force F_e given in Equation (2.2).

2. CE-ICP-MS

$$F_e = qE. \quad (2.2)$$

Here, q is the electric charge of the respective ion, defined as the charge number z multiplied by the elementary charge e .

This forward movement opposed is the frictional force F_f which is dependent on the viscosity η of the surrounding medium and the radius of the ion r . For spherical ions it can be expressed by Stoke's Law (see Equation (2.3)). The negative sign indicates the opposite direction of F_f compared to F_e .

$$F_f = -6\pi\eta r v. \quad (2.3)$$

After a very short time, the system is in equilibrium and the two forces counterbalance each other ($F_e = -F_f$), resulting in Equation (2.4).

$$qE = 6\pi\eta r v. \quad (2.4)$$

By combining Equation (2.1) and Equation (2.4) and rearranging for the electrophoretic mobility μ one finally obtains Equation (2.5).

$$\mu = \frac{q}{6\pi\eta r}. \quad (2.5)$$

The electrophoretic mobility μ of a given ion thus depends both on its charge q and its radius r . Hence, the smaller an ion and the higher its charge, the faster it migrates in electrophoretic experiments.

It must be noted that the radius r is not just the ionic radius but rather the radius of the first or even second coordination sphere of the ion since this significantly expands the overall radius and thus influences the migration velocity. This sphere can either be build up by water molecules leading to the so called hydration sphere [84FOU], [01DAV1], [01DAV2], by other complexing agents or by a mixture of both. Furthermore, in the case of a charged complexing partner, it has to be taken into account that the effective charge q_{eff} seen by the electric field is, due to shielding effects, not identical with the nominal charge q of the pure ion. A more detailed discussion on these topics can be found in the Sections 3 and 4.

Equation (2.5) is only valid in the case of infinite dilution (zero ionic strength $I = 0$ M). For considering other ions in the vicinity of the central ion i , the extended Onsager-Fuoss model [31ONS] given in Equation (2.6) can be used. The formula is valid for $I < 0.1$ M. Further ionic strength models for the electrophoretic mobility are summarized and compared in [10BAH].

2.1 Capillary Electrophoresis

$$\mu_i = \mu_i^0 - (A\mu_i^0 + B) \frac{\sqrt{\Gamma}}{1 + \frac{aD}{\sqrt{2}}\sqrt{\Gamma}},$$

with $A = z_i \frac{e^3}{12\pi} \sqrt{\frac{N}{(\varepsilon kT)^3}} \sum_{n=0}^{\infty} C_n R_i^n,$

$$B = |z_i| \frac{e^2}{6\pi\eta} \sqrt{\frac{N}{\varepsilon kT}}, \quad (2.6)$$
$$D = \sqrt{\frac{2e^2 N}{\varepsilon kT}}$$

and $\Gamma = \sum_{i=1}^s c_i z_i^2.$

In Equation (2.6), μ^0 is the electrophoretic mobility extrapolated to zero ionic strength, N is the Avogadro constant, ε is the permittivity of the solution, k is the Boltzmann constant, T the temperature, c the concentration, s the number of species and Γ is the twice ionic strength. The coefficients C_n and the vectors R^n are defined in more detail in [16AUP]. The A term describes the relaxation effect caused by the cloud of counter ions around the central ion i , the B term considers the electrophoretic effect. The factor $\frac{aD}{\sqrt{2}}$ is usually set as 1.5 [10BAH], whereby a is the distance from the middle of the central ion to the beginning of the ionic vicinity.

It can be seen from Equation (2.6) that the electrophoretic mobility of an ion i is not just dependent on the ionic strength of a solution but also on further physical parameters such as the temperature, the viscosity and the permittivity. For reliable experimental results these parameters must be kept constant during measurements ensuring that changes in the mobility are solely due to chemical differences in the samples. A closer look on this topic can be found in Section 2.1.3.

APPARATUS AND EXPERIMENTAL PARAMETERS

For performing capillary electrophoresis experiments, an Agilent 7100 apparatus (Agilent Technologies, Santa Clara, California, USA) was used. A schematic overview of the main parts of such a setup is given in Figure 1.

The separation of the ions is carried out in thin capillaries filled with a buffer solution, also called background electrolyte (BGE). At both ends, the capillary is immersed into two vials filled with the same BGE. An electrical contact is thus established and a high voltage can be applied by the platinum electrodes. In this work, fused silica capillaries (TSP0503753, Polymicro Technologies, Phoenix, Arizona, USA) with an inner diameter of 50 μm were used.

2. CE-ICP-MS

Since the capillary was supplied in 25 m rolls it had to be broken to the required length of 76 cm. This was done by the use of a ceramic plate. Both ends of each capillary were controlled with a magnifying glass to ensure that the cut is preferably plain. Crooked ends would lead to band broadening due to irregular elution. Prior to the first utilization the capillaries were preconditioned using the flushing program given in Table 1 to remove impurities remaining from the manufacturing process. At the beginning of every measuring day, the rinsing program presented in Table 2 was used. At the end of each series this program was passed through again, but in the last step air instead of BGE was employed in order to dry the capillary for the storage until the next measurements.

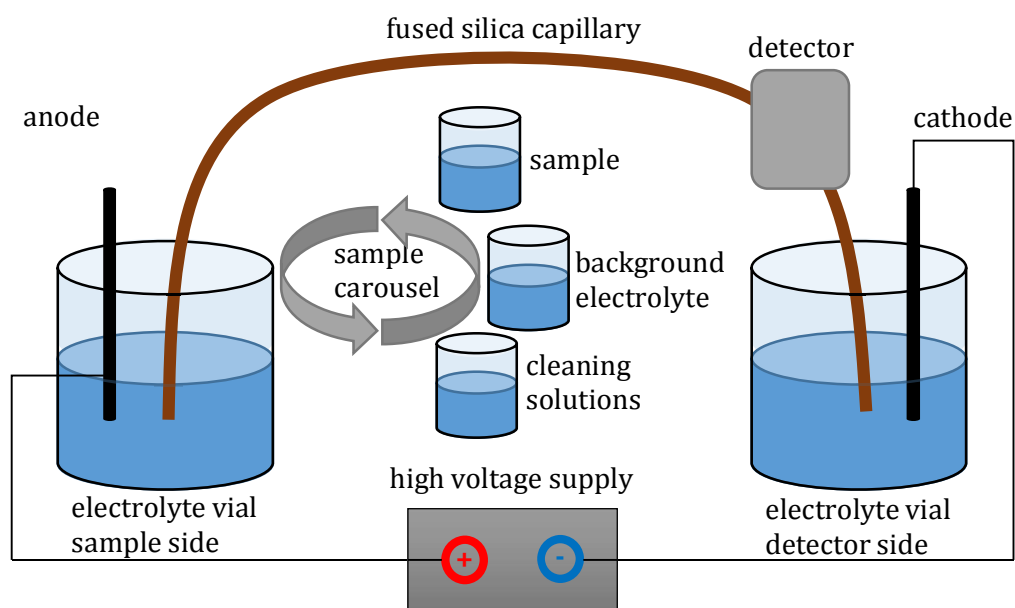


Figure 1: Schematic layout of a capillary electrophoresis system.

The rinsing solutions were in all cases inserted into the capillary by applying an external pressure of 1 bar. Between every measurement, the capillary was additionally flushed for 15 min with the BGE needed for the following sample. This step is very important, because the degree of deprotonation of the silanol groups on the inside of the capillary has to be adapted to the pH value of the BGE in use. The choice of the BGE depends on the particular experiments and can be found in the respective experimental sections. It has to be noted that the applied high voltage alters the BGE due to electrolysis effects. This is why a fresh portion was used for every flushing step.

The samples for CE measurements were prepared by dissolving the analyte solution in the BGE medium in conical micro-inserts of borosilicate glass (Carl Roth AG, Arlesheim, Switzerland). These micro-inserts were placed in polyethylene vials sealed with polyethylene olefin snap caps (both Agilent Technologies, Santa Clara, California, USA) and

2.1 Capillary Electrophoresis

thus transferred to the CE system. To prevent a clogging of the capillary, all solutions were filtered through 0.2 μm syringe filters (Nalgene, Rochester, New York, USA) prior to their application. For the same reason, a small pressure of 60 mbar was applied during measurements.

Table 1: Preconditioning program for new capillaries.

step	solution	duration
1.	acetone	5 min
2.	H ₂ O	3 min
3.	0.1 M NaOH	5 min
4.	H ₂ O	3 min
5.	0.1 M HCl	5 min
6.	H ₂ O	3 min
7.	0.1 M NaOH	5 min
8.	H ₂ O	3 min
9.	0.1 M HCl	5 min
10.	H ₂ O	3 min
11.	BGE	15 min

Table 2: Flushing program at the beginning of every measurement day.

step	solution	duration
1.	0.1 M NaOH	5 min
2.	H ₂ O	3 min
3.	0.1 M HCl	5 min
4.	H ₂ O	3 min
5.	BGE	15 min

In principle, sample injection into the capillary can be carried out by two different methods, namely hydrodynamic and electrokinetic injection. For the first method, a difference in pressure between the inlet and the outlet of the capillary is used. This can be achieved by either applying an external pressure at the injection side, a vacuum at the exit side or by a syphoning effect created by a difference in height between the sample vial and the exit vial. The electrokinetic injection on the other hand is characterized by the application of a voltage at the sample side. This method has the disadvantage that the migration speed of the sample ions is different for each ion depending on the charge and the size. Consequently, for samples with different analytes in the same solution, the injected quantity differs for each ion. In the present work, a hydrodynamic injection with an external pressure was used. In this case, the injected sample volume V_{inj} is defined by the pressure difference Δp across the capillary with the length l and the inner radius r_c , the injection time t_{inj} and the viscosity η of the solution and can be calculated by the Hagen-Poiseuille equation shown in Equation (2.7).

2. CE-ICP-MS

$$V_{\text{inj}} = \frac{\pi \Delta p r_c^4 t_{\text{inj}}}{8 \eta l}. \quad (2.7)$$

For the parameters used in this work ($\Delta p = 100$ mbar, $t_{\text{inj}} = 8$ s, $r_c = 25$ μm), an injected sample volume V_{inj} of about 15 nL results. This, on the one hand, mirrors one of the advantages of CE, the low sample consumption. On the other hand, reproducibility becomes a challenge due to these very small sample volumes. It has to be ensured that the amount of analyte injected is always consistent for each sample of the same solution.

After the introduction the sample vial is removed from the capillary and replaced by the BGE vial via a sample carousel. Thereafter, the high voltage is applied and the electrophoretic migration of the sample ion starts.

At the end of the separation, the analytes have to be detected. For this purpose various methods are possible, among other things, UV-Vis absorption spectroscopy, fluorescence detection, electrochemical detectors such as contactless conductivity detection (CCD), atomic emission detection and mass spectrometry. Since, as already mentioned, in this work an online coupling to an ICP-MS was used, this detection method is described in more detail in Section 2.2.

2.1.2 ELECTROSMOTIC FLOW

A very important effect in CE is the so called electroosmotic flow (EOF). It describes the migration of the entire solution inside the capillary due to an electric field. An elaborate examination of different aspects concerning the EOF is given in [92GRO]. The most important parts for the present work are summarized in the following section.

The reason for the appearance of the EOF is the surface charge of the inner capillary wall. The silanol groups on the inside of the fused silica capillaries are dissociated to varying extend in dependence of the pH value, they are thus negatively charged. Because of this excess of negative charges a layer of positive ions accumulates nearby to compensate the charge difference. As shown in Figure 2 a), a diffuse electric double layer forms, consisting of a rigid layer next to the capillary wall and a mobile layer somewhat further to the middle. By applying an electric field, the positive layer is attracted in direction of the cathode. This leads to a migration of the whole BGE, because the complete solution is dragged along by this movement.

The building of an electrical double layer leads to a decrease of the potential φ from the wall potential φ_0 in the direction of the middle of the capillary. A general plot of this curve in dependence of the distance x to the wall is shown in Figure 2 b). The mathematical description is given in Equation (2.8), following the derivation in [97HIE].

$$\varphi(x) = \varphi_0 \exp\left(-\frac{x}{\kappa^{-1}}\right),$$

(2.8)

$$\text{with } \kappa = \sqrt{\frac{1000 \text{ Ne}^2}{\epsilon kT} \sum_i z_i^2 c_i}.$$

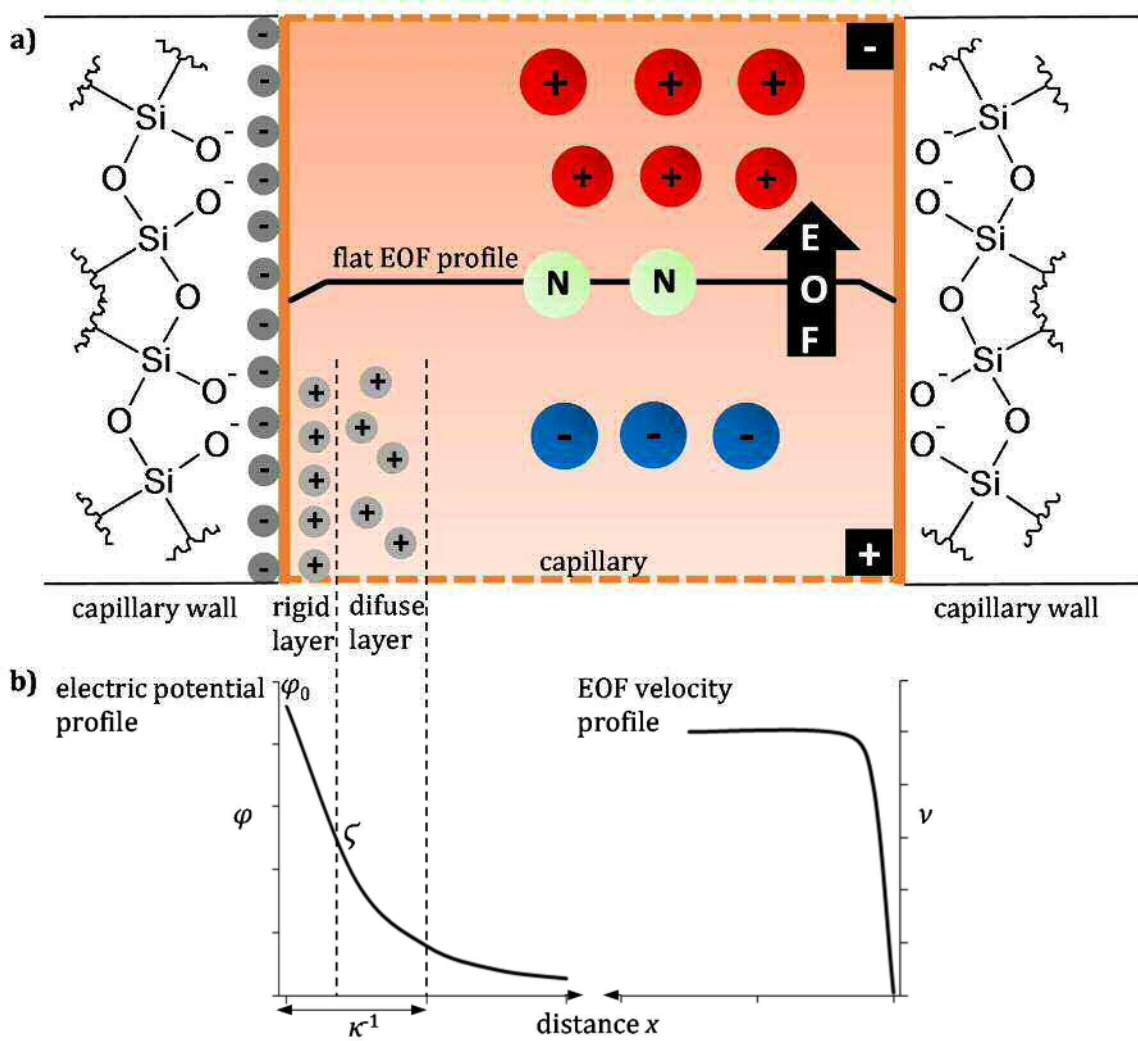


Figure 2: a) Cross section of a fused silica capillary with a schematic depiction of the electric double layer creating a flat EOF profile. b) Potential curve and EOF velocity profile. Figure based on a combination of [10LAU] and [92GRO].

The constant κ^{-1} is called the double layer thickness. The described potential difference close to the capillary wall is often called zeta potential ζ . The electrophoretic mobility of the EOF μ_{EOF} is given in terms of this potential according to Equation (2.9) [65RIC].

$$\mu_{\text{EOF}} = \frac{\epsilon \zeta}{\eta}. \quad (2.9)$$

2. CE-ICP-MS

By combining the information in Equation (2.8) and (2.9), it reveals that the electrophoretic mobility of the EOF is independent of the diameter of the capillary but dependent on the ionic strength of the BGE. Furthermore, it also depends on the pH of the BGE since this value defines the degree of deprotonation of the silanol groups and thus the surface charge on the capillary wall and the zeta potential, respectively. The point of zero charge for fused silica capillaries was determined to be approximately at pH 2.0 [81CHU]. Generally, one can say that a BGE with a high pH and a low ionic strength exhibits a faster EOF compared to a BGE with lower pH and higher ionic strength.

The mobility of the EOF superimposes the electrophoretic mobility of the analytes but it is constant for every ion and thus does not affect the separation. Nevertheless, it has to be kept in mind that the experimentally determined electrophoretic mobility of a given ion, called apparent mobility μ_{app} , is the sum of the EOF mobility and the electrophoretic mobility of the respective ion (see Equation (2.10)).

$$\mu_{app} = \mu_{EOF} + \mu. \quad (2.10)$$

Under conventional experimental conditions the electrophoretic mobility of the EOF is in the same order of magnitude as the mobility of the analyte ions ($10^{-4} \text{ cm}^2\text{V}^{-1}\text{s}^{-1}$) and can in some cases even be the main contributor to the apparent mobility μ_{app} .

Due to the fact that the whole electrolyte solution in the capillary is moved forward by the EOF and not by an applied external pressure, a flat flow profile forms. After only very few nanometers from the capillary wall, the flow velocity of the EOF becomes constant (see Figure 2 b)). For a capillary with an inner diameter of 50 μm , as used in the present work, this means that more than 99.9% of the cross section of the capillary show this flat profile. That, compared to a parabolic flow profile arising from a pressure-driven, laminar migration, is beneficial for electrophoretic separation experiments since the separation capability is preserved and very sharp peaks can be obtained. Another benefit of the EOF is, that anions can be investigated together with cations in one run, as long as the electrophoretic mobility of the anion is smaller than that of the EOF. Regardless of their negative charge, in such a case the anions migrate with an effective velocity, defined by the difference of their electrophoretic mobility and that of the EOF, in direction of the cathode.

Alongside the positive characteristics mentioned above, the EOF can have negative effects in electrophoretic experiments that have to be considered. If, for example, the EOF is too fast during a measurement, the ions cannot be separated satisfactorily because of a too short residence time inside the capillary. In some cases it can therefore be necessary to manipulate the magnitude of the EOF. Different methods for that purpose have been investigated,

2.1 Capillary Electrophoresis

amongst others the coating of the capillary inner wall enabling to even reverse the EOF [10HUH].

For the determination of the EOF, neutral molecules (called EOF marker) that are transported just by the electroosmotic flow and not by an applied voltage can be used. The electrophoretic mobility of an ion can then be experimentally determined by the comparison of the migration times of the ion under investigation t_i and of the EOF t_{EOF} according to Equation (2.11).

$$\mu = \frac{l_d l}{U} \left(\frac{1}{t_i} - \frac{1}{t_{\text{EOF}}} \right). \quad (2.11)$$

Here, l_d is the capillary length to the detector, l is the complete capillary length and U is the applied voltage. In the case of a coupling of CE to ICP-MS, as employed in this work, the length to the detector is identical with the entire capillary length and Equation (2.11) simplifies to Equation (2.12).

$$\mu = \frac{l^2}{U} \left(\frac{1}{t_i} - \frac{1}{t_{\text{EOF}}} \right). \quad (2.12)$$

As EOF marker, 2-bromopropane was used. It was detected via ICP-MS on the mass of ^{79}Br .

Further insight into the determination of electrophoretic mobilities and a comparative examination of two different EOF markers can be found in Section 3.1.

2.1.3 FACTORS THAT INFLUENCE THE ELECTROPHORETIC MOBILITY

As already depicted in Equation (2.6) the electrophoretic mobility is dependent on several physical parameters which all have to be considered for obtaining reliable experimental results [06JOU]. The most important aspects of these parameters will be examined below in a little more detail. For factors that influence the peak width and thus the resolution instead of the electrophoretic mobility, see Section 4.1.

JOULE HEATING

Due to the high voltages that are applied during electrophoretic measurements, the temperature inside the capillary may rise significantly under certain circumstances. This effect is called Joule heating and leads to an inhomogeneous, radial temperature profile along the capillary. Since the electrophoretic mobility is temperature dependent, the accuracy of the results may be influenced negatively. As a rule of thumb one can say that the electrophoretic mobility rises by about 2% with every 1 °C [90HJE]. Additionally to that, further parameters, such as the density of the BGE, show a temperature dependence and not controlling the temperature rise could lead to band broadening. At this point, it is not so much the overall temperature rise that causes problems but rather the development of a

2. CE-ICP-MS

temperature profile [04PET]. For very high temperature increases even the analyte could be affected due to shifts in the chemical equilibrium or decomposition.

In order to make qualitative assessments about the magnitude of the temperature rise Equation (2.13) can be used. It is given in terms of the difference between the temperature of the middle of the capillary T_0 and the ambient temperature of the surrounding medium T_a . A cross section of the capillary with the respective radii and the calculated temperature profile is shown in Figure 3. For a detailed derivation one can consult [92GRO] (another approach for the calculation can be found in [06EVE]).

$$T_0 - T_a = \frac{Sr_c^2}{2} \left(\frac{1}{2k_{\text{BGE}}} + \frac{1}{k_f} \ln \left(\frac{r_2}{r_c} \right) + \frac{1}{k_p} \ln \left(\frac{r_3}{r_2} \right) + \frac{1}{r_3 h} \right). \quad (2.13)$$

Here, S is the rate of power generation within the capillary per unit volume, k_{BGE} , k_f and k_p are the thermal conductivities of the BGE, the fused silica layer and the polymer coating, respectively. The radii r_c , r_2 and r_3 refer to the inner capillary radius, the radius of the fused silica layer and the radius of the complete capillary including the polymer coating (see Figure 3) and h is the heat transfer coefficient between the capillary and the surrounding medium. Equation (2.13) considers all factors that are relevant for the temperature rise during electrophoresis experiments, which are the applied electrical field and properties of the capillary, the BGE and the surrounding medium.

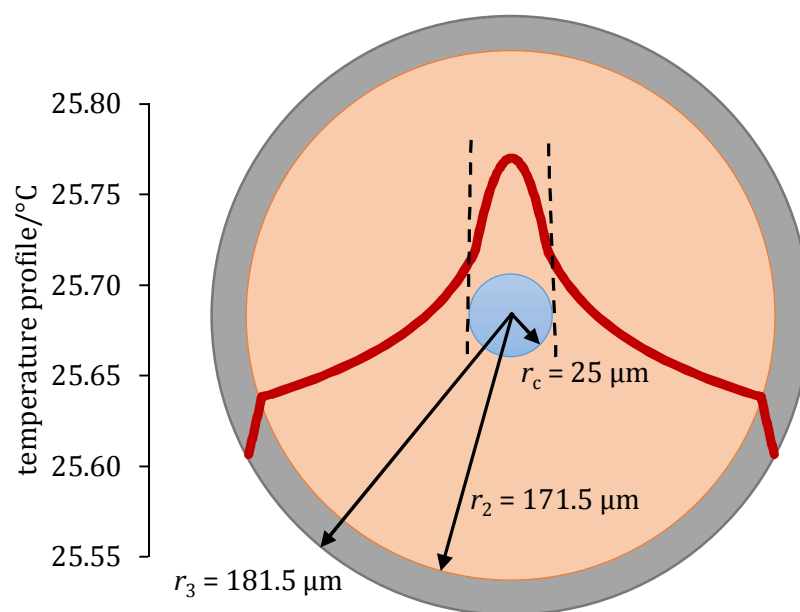


Figure 3: Cross section of the fused silica capillary with polymer coating (not true to scale). The temperature profile shown in red was evaluated with the conditions used in this work ($U = 25$ kV, 10 m s⁻¹ forced air cooling at 25 °C). More details on the calculations are given in APPENDIX A1.

2.1 Capillary Electrophoresis

A great advantage of performing electrophoretic separations in very thin capillaries is the beneficial surface to volume ratio that allows to effectively dissipate the generated heat. Furthermore, in our experiments the forced air cooling device of the Agilent electrophoresis apparatus was used to temper the system at 25 °C [09AGI]. An active cooling of the capillary increases the heat transfer coefficient h and thus further improves the dissipation of heat. For an even more effective cooling, special capillaries with a sheath that enables the application of liquid cooling agents can be used. Nevertheless, one has to keep in mind that a very short part at the inlet side and a short part at the end of the capillary that is inside the nebulizer cannot be temperature controlled [11EVE], [10MUS1], [10MUS2], [12SLA]. Recently, some improvements to this problem could be achieved by using a customized, 3D printed cartridge that enables to guide the tempered air stream from the apparatus to the interface and thus extend the cooled area of the capillary [18FRA].

An application of Equation (2.13) to typical conditions in this work yields a rise of the temperature of about 0.4 °C at 10 kV and 0.8 °C at 25 kV. The detailed calculation is presented in the APPENDIX A1. The temperature profile presented in Figure 3 is also based on parameters used in this work.

VISCOSITY

The viscosity η of the BGE has the second largest influence on the electrophoretic mobility μ of a given ion. As can be seen from Equation (2.6), a rise in the viscosity leads to a decrease in μ . If the same BGE is used throughout different experiments, the viscosity is also constant and the measured mobilities are comparable. Changes in the viscosity within one series can occur, if a parameter of the BGE, e.g. the concentration of a ligand, is varied systematically. In such cases, the influence on the electrophoretic mobility has to be considered. The discrepancies can reach up to 20% under disadvantageous conditions [17NOW]. Additionally, the temperature dependence of the viscosity has to be taken into account.

On the other hand, intended modification of the viscosity can be used to adjust the mobility of the EOF if necessary. For example, by increasing the viscosity near the capillary wall with adsorbing polymers, the electrophoretic mobility of the EOF can be reduced [87HER].

PERMITTIVITY

The permittivity ε can be interpreted as a measure of the permeability of a material for an electrical field. In this connection, the permittivity in vacuum ε_0 is a constant and ε is a multiple of this value. The relative permittivity ε_r is the ratio $\varepsilon/\varepsilon_0$ and specifies the degree of attenuation of the Coulomb interaction of ions in the respective medium [06ATK]. Hence, a smaller ε implies a stronger impact of the applied electric field on the migrating ions and

2. CE-ICP-MS

consequently a higher electrophoretic mobility. The same consideration regarding the experimental consequences and the temperature dependency as for the viscosity applies for the permittivity, but the magnitude of the effect is much smaller.

The permittivity can be used to diminish the double layer thickness κ^{-1} and thereby influence the EOF profile and velocity. As can be seen from Equation (2.8), a smaller ε of the BGE results in a smaller κ^{-1} . In practice, the addition of organic solvents, for example acetonitrile or methanol, can be used for this purpose [87FUJ].

CO-IONS AND COUNTER -IONS

As already indicated above, the Coulomb interaction of analyte ions with other ions in their vicinity can also affect the electrophoretic mobility. This fact is considered by the sum $\sum_{n=0}^{\infty} C_n R_i^n$ in Equation (2.6). If co-ions exhibit electrophoretic mobilities different from those of the analyte but not different enough for being completely separated, they migrate in the same zone and thus they can influence each other; both an acceleration and a retardation of the ions under investigation is possible [02MUZ]. Furthermore, the ions of the BGE are omnipresent and therefore may also have an impact. Aupiais et al. [16AUP] investigated this topic for different tetravalent actinides complexed with DTPA (diethylene triamine pentaacetic acid). They found out that the effects start at a concentration of co-ions of $c = 10^{-4}$ M and increase rapidly for $c > 1$ mM. However, the overall impact on the electrophoretic mobility is very small.

IONIC STRENGTH

The last parameter given in Equation (2.6) that is discussed here is the ionic strength I of the BGE (given there as I , the twice ionic strength). In general terms, it can be said that the electrophoretic mobility decreases with increasing ionic strength because of the relaxation effect depending on the relative permittivity and because of the electrophoretic effect depending on both the viscosity and the relative permittivity [02MUZ]. Additional to that, the effect of Joule heating is also raised by a higher ionic strength because more ions lead to a higher electrical current through the capillary.

2.2 ICP-MS

ICP-MS is established as an efficient and widely used detector for ions previously separated by capillary electrophoresis. The considerably higher effort of the coupling of CE to ICP-MS compared to the simpler, commonly used UV-Vis detection is willingly being accepted due to the great benefits of very low detection limits combined with a wide linear range. In fact, there are two different operation modes applicable: scanning all masses for completely unknown samples or the scan of just particular masses if the overall sample content has

already been identified before. The second case is faster and offers a higher sensitivity and is thus utilized in this work for the detection of the actinides investigated. Another advantage of the CE-ICP-MS coupling is the capability of clearly distinguishing two different ions from each other, even though they exhibit similar or even identical electrophoretic mobilities. After their migration on the capillary, they can be separated by their different masses via ICP-MS.

2.2.1 MAIN COMPONENTS

Main components of the ICP-MS used in this work (Agilent 7500ce) are shown in Figure 4 described in the following on basis of [01AGI] and [08AGI1].

After elution from the capillary, the sample ions are guided through the nebulizer and the spray chamber (the coupling device is discussed in more detail in Section 2.3). Thereby, an aerosol is created inside the nebulizer by means of an argon gas flow, the so called carrier gas. Droplets that are too big are stopped at the walls of the spray chamber and thus cannot negatively influence the stability of the plasma. The remaining aerosol is transported towards the plasma torch (Fassel type, constructed of three concentric quartz tubes) by a second argon gas flow (make-up gas). The sample is then finally atomized and ionized inside the plasma because of the very high temperatures of 8000 – 10000 K. Plasma generation takes place at the end of the torch by a radio frequency (RF) coil with a current oscillating at 27.12 MHz. This provides electrons and after ignition, the collision of Ar atoms in the RF field maintains the plasma. Ar is used as the plasma gas for several reasons. First, it is inert and can quite easily be obtained at high purities. Second and more important, Ar has a very high first ionization potential, higher than that of most other elements and a second ionization potential that is lower. Consequently, most analytes can efficiently be ionized as single charged ions.

The analyte ions are thereafter extracted to the first vacuum chamber. This so called interface is made up from two cones, the sample cone followed by the skimmer cone. As the opening of the second cone is smaller than that of the first one, a pre-focusing of the ion beam results. The first vacuum level is produced by a rotary pump which also deals as a backing pump for the molecular pump. Leaving the interface, the ions are collimated and accelerated by two conical extraction lenses.

In order to achieve a preferably low background signal, the ion beam is guided to the lens system following the interface. This region is working under a higher vacuum, generated by a molecular pump. Its function is both further focusing the beam by Einzel lenses and eliminating neutral species and photons that would cause a noise signal at the detector by

2. CE-ICP-MS

the Omega lenses. The Omega lenses deflect the ion beam from its original axis by alternately attracting and repelling the ions. Photons and neutral particles are not affected by this and thus can be separated from the beam. Before leaving the lens system the ion beam is re-focused again by the quadrupole focusing lens.

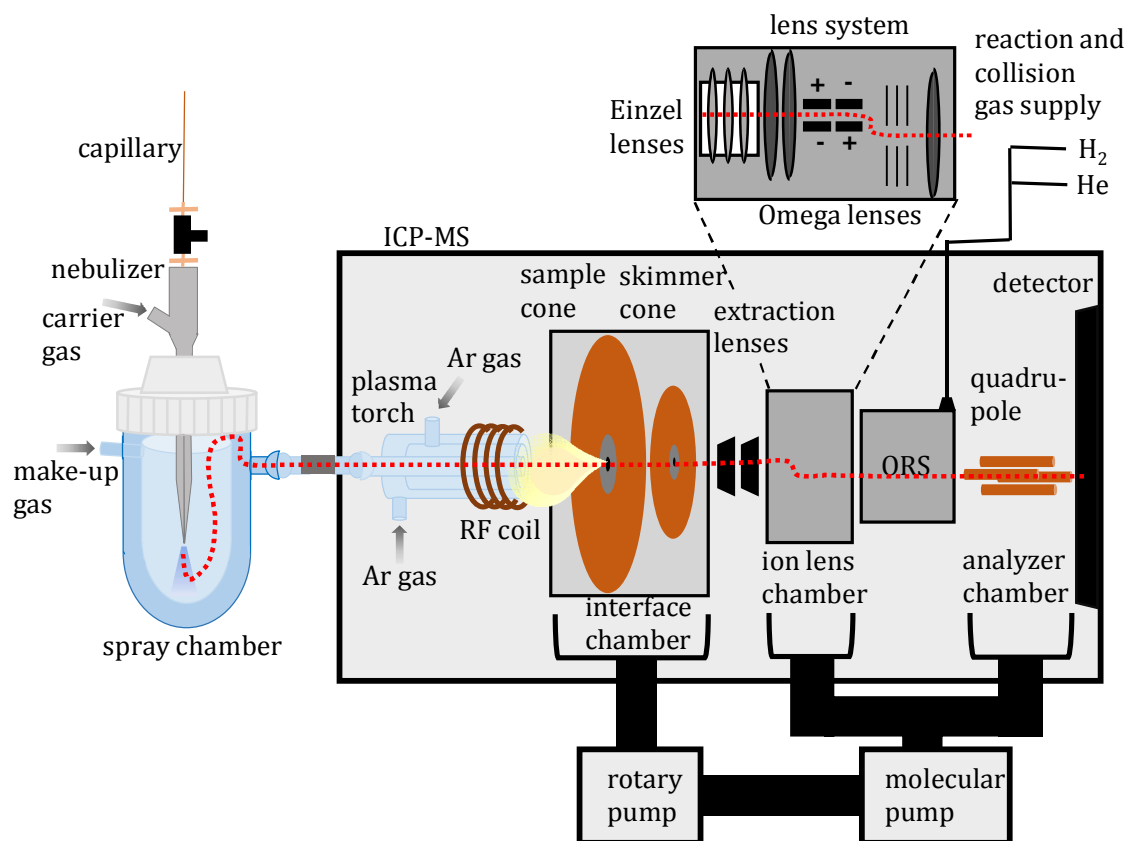


Figure 4: Schematic overview of the general structure of the ICP-MS system with nebulizer and spray chamber used in this work. The figure is based on a combination of different illustrations in [08AGI1]. The red dotted line describes the path of the sample through the system.

The octapole reaction system (ORS) can be found between the ion lens system and the quadrupole mass filter. It can be filled with a reaction or collision gas and by that, interferences can be reduced. More details about such interferences arising in ICP-MS measurements and the use of the ORS are given in the following chapter. If the no-gas-mode is used, the ion beam just passes through the reaction cell into the quadrupole mass filter.

The last component of an ICP-MS system is the analyzer chamber consisting of the quadrupole mass filter and the detector. It is the lowest pressure region also evacuated by a molecular pump. Varying voltages can be applied to the quadrupole magnet and by that, only one specific ion is able to pass through the mass filter due to its defined mass-to-charge ratio. All other ions with different mass-to-charge ratios exhibit unstable flight paths and thus collide with the rods of the quadrupole. The applied voltages can be changed very rapidly

with a dwell time of 100 ms so that the determination of different masses is possible within the same run. The ions separated in this way are finally detected by an electron multiplier detector. This detector can either operate in a pulse mode for low sample concentrations or in an analog mode for high sample concentrations.

Data processing of the detected signals were undertaken with the MassHunter Workstation software (G7200B, Agilent Technologies, Santa Clara, California, USA).

2.2.2 INTERFERENCES AND OCTOPOLE REACTION SYSTEM

A problem in ICP-MS measurements is the occurrence of interferences that can have a negative impact on the experimental results. Isobaric nuclides for example cannot be discriminated due to their identical masses. In that case, the coupling with CE is beneficial because isobars can already be separated by their differences in the electrophoretic mobilities and thus reach the ICP-MS detector successively.

A second source of interferences originates from the ionization of the sample in the plasma. Even though, like mentioned above, Ar as plasma gas has favorable properties in producing consistently single charged ions, the generation of doubly charged species cannot be prevented completely. Such ions exhibit different stable flight paths inside the quadrupole mass filter because of their altered mass-to-charge ratio and consequently they are detected at the wrong masses. Since in the plasma also other elements from the air or from aqueous solvents are present, for example hydrogen or oxygen, the formation of Ar oxides and hydrides are to be considered. The detection of these dimers occurs then at masses that are 16 amu or 1 amu higher than the original ion, respectively. On top of that, the formation of dimers with other elements and even of trimers is conceivable. To suppress these interferences as good as possible, a tuning was performed at the beginning of every measurement series to identify the optimal plasma parameters. For that purpose, ^{140}Ce was used because it has a high oxide bond strength and hence will reveal a high oxide ion generation rate. Furthermore, it readily generates doubly charged ions [08AGI2]. The ratio in the masses of 70/140 for the +2 ions and 156/140 for the oxides is determined and the tuning should result in values of < 5% and < 1%, respectively. An overview of different isotopes and potential interferences can be found in the literature [94REE].

A major challenge is the measurement of iron via ICP-MS. This is because distinct interferences with different Ar dimers (and trimers) exist for all naturally occurring Fe isotopes, for example $^{40}\text{Ar}^{16}\text{O}^+$ for ^{56}Fe , $^{40}\text{Ar}^{14}\text{N}^+$ for ^{54}Fe and $^{40}\text{Ar}^{16}\text{O}^1\text{H}^+$ for ^{57}Fe . These interferences lead to a background signal on these masses that is too high for iron measurements without further optimizations. Remedy can be provided by the application of

2. CE-ICP-MS

the already mentioned ORS. The utilization of a collision or reaction cell for the reduction of interferences is described in great detail e.g. in [02TAN] and [04KOP]. However, at this point just the background for the iron case will be discussed in a little more detail because it is a naturally often occurring element that can also influence the speciation of actinides in the environment due to the redox activity of the Fe(II)/Fe(III) couple. In this work, examinations with CE coupled to ICP-MS with the additional use of the ORS were conducted for iron measurements and the results can be found in Section 5.3.

The basic principle of the ORS is the interaction of the interference dimers with a reaction or collision gas inside the ORS chamber. In the case of this work, helium as a collision gas and hydrogen as a reaction gas were applied, but the use of other gases is also possible. In He mode, the dimers collide with the He atoms and by that, they are destroyed. They are now detected at the individual masses of the single atoms. Fe⁺ is not affected by that process because it is a monomer and thus can be detected on its respective mass with a much lower background. In H₂ mode in contrast, a reaction of the hydrogen with the interference particles takes place. H₂O for example is generated by an atom transfer reaction of ArO⁺ and H₂. A drawback of this method is, that side reactions, especially with the analyte ions, cannot be controlled satisfactorily. This significantly decreases the sensitivity of the ICP-MS measurement. Furthermore it has to be noted, that in both modes unwanted collisions between gas molecules and analyte ions reduce the amount of sample reaching the detector and thus the detection limit is further decreased. Therefore, the use of the ORS is just reasonable for measurements that otherwise would not be possible because of interferences that produce a very high background signal. The choice of the respective mode depends on the analyte under investigation. In the case of iron, the H₂ mode turned out to be more efficient.

2.3 COUPLING DEVICE

The application of an ICP-MS apparatus as a detector for CE experiments is only worthwhile if an effective coupling of both devices can be assured. Only in this case, the high separation capability of the CE can be preserved and the advantages of the very low detection limits of the ICP-MS can be used in its entirety. To achieve this, the individual components have to meet certain requirements which are explicated in the following.

In general, the coupling device is composed of four main parts, which are the nebulizer containing the end of the capillary, the spray chamber, the make-up electrolyte supply and the connecting tube between the spray chamber and the plasma torch of the ICP-MS (see Figure 4).

2.3 Coupling Device

The nebulizer is the heart piece of the coupling device. Review articles about the importance of nebulizers for coupling purposes can be found in the literature, e.g. [98MCL], [04YAN], [05YAN]. In this work, a MiraMist CE nebulizer (Burgener Research, Mississauga, Canada) is employed. In a former work by Stöbener [13STO], the combination of this nebulizer with a Scott-type spray chamber (AHS Analysentechnik, Tübingen, Germany) has proven to be a suitable setup for the investigation of actinides. The choice of the spray chamber is of great importance for the aerosol creation and thus for the sensitivity of the whole measurement. A comparison of different types of spray chambers was conducted by Todoli et al. [00TOD]. Sonke et al. [03SON] investigated the dispersion effects of spray chamber volumes. The schematic layout of the setup used in this work is shown in Figure 5 a). As one can see, the nebulizer is a parallel path model, which means that the capillary and the carrier gas are guided through two separated, individual tubes. The make-up electrolyte is supplied rectangular to this by a syringe pump (PicoPlus, Harvard Apparatus, Holliston, USA). A mixture of these three components takes place in just a very small volume at the tip of the nebulizer. This is the reason why the correct position of the capillary outlet in the nebulizer tip is such a crucial point for obtaining reliable and reproducible experimental results. The details of the gas and liquid flows at the tip of the nebulizer are depicted in Figure 5 b).

When assembling the system it has to be ensured that the ends of the capillary, both the inlet and the outlet side, are positioned at the same height. Otherwise an additional siphoning effect occurs. Moreover, the connecting tube between the spray chamber outlet and the plasma torch of the ICP-MS has to be as short as possible because the transport of the different analyte species should be kept preferably short in order to conserve the separation of the analyte species.

One of the biggest challenges of coupling CE to ICP-MS are the different flow rates. While in CE just very small sample volumes less than one microliter per minute elute from the capillary, in ICP-MS a significantly higher flow, large enough to generate a stable aerosol, is required. This problem is avoided by the introduction of the make-up electrolyte. The additional flow rate enables for a satisfactory aerosol production. Furthermore, due to the high carrier gas flow which forms the aerosol, a suction effect is generated inside the capillary. Because of this, a laminar flow profile arises and the beneficial flat EOF flow profile (already subject of discussion in Section 2.1.2) is destructed. By adding the make-up electrolyte one is able to oppress this suction effect. Last but not least, the make-up electrolyte is used to close the electric circuit at the outlet side of the capillary. This is not trivial, because the capillary at this end does not extend into a second BGE vial as it usually does in standard CE mode but rather is guided inside the nebulizer. The make-up electrolyte

2. CE-ICP-MS

is connected with the CE via an electrode and thus the electric circuit can be closed. Besides these benefits, one has to keep in mind that the introduction of the make-up electrolyte leads to a great dilution of the sample and this, in turn, results in a loss of sensitivity for the ICP-MS measurement.

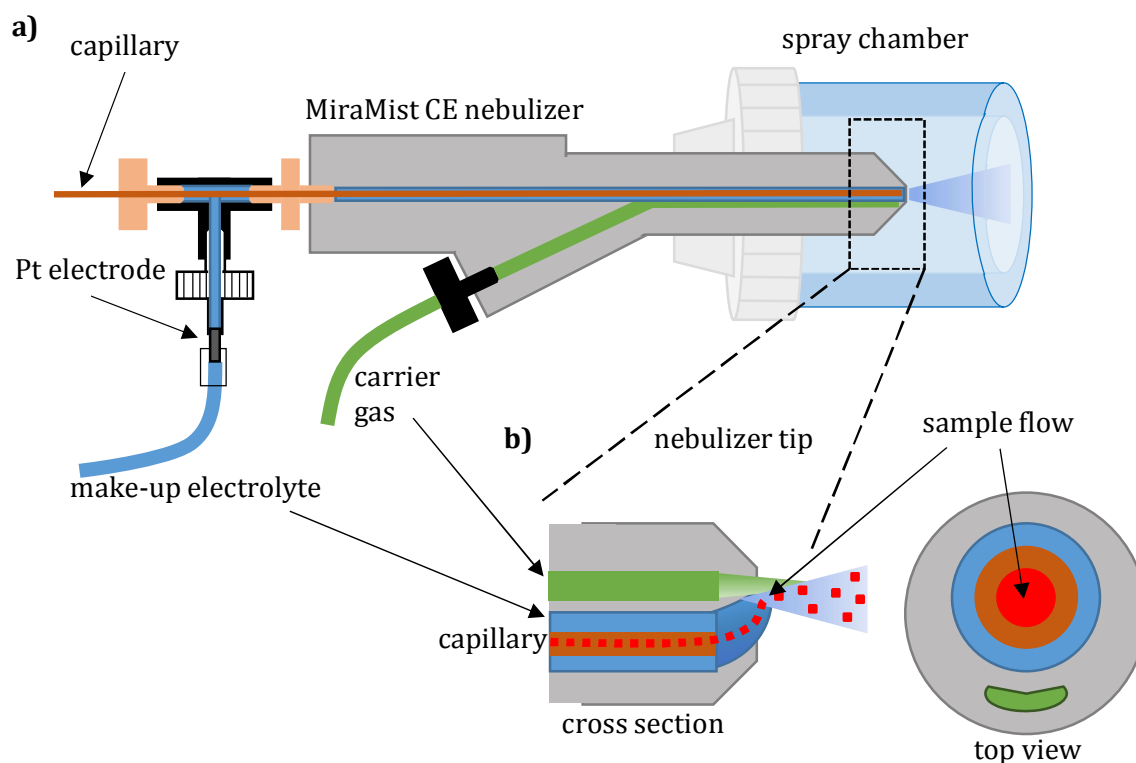


Figure 5: a) Schematic cross-section of the MiraMist CE nebulizer used in this work. b) Details of the tip of the nebulizer in cross section and top view with the respective gas and liquid flows. The figures are based on the Burgener Research Operating Instructions Manual [19BUR].

As make-up electrolyte a solution of 1.25% HNO_3 with 10% ethanol was used in this work. The use of ethanol promotes the formation of smaller droplets for the aerosol by a reduction of the surface tension. Further, 5 ppb each of ^{89}Y , ^{103}Rh , ^{140}Ce and ^{209}Bi were added as internal standards. The tuning of the ICP-MS parameters was performed on these masses with special focus on the optimization of the higher masses for the measurements of actinides. The ^{89}Y signal was additionally monitored during all measurements in order to detect systematic fluctuations. The optimal make-up electrolyte flow rate was determined experimentally to be $5 \mu\text{L min}^{-1}$. A lower flow rate would not completely eliminate the laminar flow profile, a higher one in contrast would lead to a sample tailback in the capillary.

2.4 Summary of all Parameters of the CE-ICP-MS System

2.4 SUMMARY OF ALL PARAMETERS OF THE CE-ICP-MS SYSTEM

In Table 3 all parameters and devices used in this work for the CE-ICP-MS measurements are summarized. More detailed information about the individual parts can be found in the previous sections.

Table 3: Summary of the parameters and devices used in this work.

device	parameter	value	
capillary (TSP0503753, Polymicro Technologies)	material	fused silica	
	length	76 cm	
	inner diameter	50 μm	
CE (Agilent 7100)	sample vials	micro-inserts of borosilicate glass placed in polyethylene vials sealed with polyethylene olefin snap caps	
	sample introduction	hydrodynamic 8 s with 100 mbar	
	EOF-marker	2-bromopropane detected at the mass of ^{79}Br	
		<i>experiments</i>	
		<i>mobility measurements, kinetic studies (Sections 3 and 5)</i>	<i>stability constant determination (Sections 4)</i>
	BGE	1 M acetic acid pH 2.4	several ligands with the respective acids at varying pH values
	voltage	25 kV	10 kV
	current	10 – 15 μA	10 – 120 μA
	temperature control	forced air cooling at 25 $^{\circ}\text{C}$	
	coupling device	nebulizer	MiraMist CE (Burgener Research)
spray chamber		Scott-type (AHF Analysentechnik)	

2. CE-ICP-MS

Table 3: continued.

device	parameter	value
coupling device	make-up electrolyte	1.25% HNO ₃ and 10% ethanol, 5 ppb ⁸⁹ Y, ¹⁰³ Rh, ¹⁴⁰ Ce and ²⁰⁷ Bi as internal standards, flow rate: 5 µL min ⁻¹
	carrier gas (Ar) flow rate	0.9 – 1.1 L min ⁻¹
	make-up (Ar) gas flow rate	0.2 – 0.4 L min ⁻¹
ICP-MS (Agilent 7500ce)	plasma gas	argon
	plasma torch	Fassel typ
	plasma power	1550 W
	radio frequency	27.12 MHz
	dwel time	100 ms
	detection mode	time resolved analysis
	data processing	MassHunter Workstation software (G7200B, Agilent Technologies)

2.5 LITERATURE REVIEW OF APPLICATIONS OF CE-ICP-MS WITH FOCUS ON THE INVESTIGATION OF ACTINIDES

As mentioned before, the coupling of CE to ICP-MS was employed in this work to examine different aspects of actinide speciation analysis. For that purpose this section will give a short literature overview of CE and CE-ICP-MS applications with the focus on actinide investigations. At the beginning, some general aspects are reviewed.

The capability of capillary electrophoresis for elemental speciation is well described in the literature and several overview articles on this topic can be found, for example by Timerbaev et al. [00TIM], [01TIM], [10TIM] (and also the five previous articles cited therein), [13TIM1], [14KUB] or others [93ENG], [97MAC], [03LIU], [03PAU], [05ALI], [09JOH]. The coupling of CE to ICP-MS was first described by Olesik et al. [95OLE] in 1995. Since then, a wide variety of different works concerning the development of the method and its application to metal speciation has been conducted. Again, several review articles are available for an extended

2.5 Literature Review of Applications of CE-ICP-MS with Focus on the Investigation of Actinides

overview, e.g. [97SUT], [98BAR], [02KAN], [05ALV], [05MIC] (and previous reviews by Michalke et al. cited therein), [17TYC] (as the last of a frequently every two years appearing series, for earlier versions see the citations within this article). A comparison with the hitherto commonly used UV detection shows the considerably improved detection limits while retaining constant separation quality [98SUT]. The coupling of CE to a high resolution sector field ICP-MS (HR-SF-ICP-MS) enables to extend the limits of detection to even lower concentrations [07SON]. More specialized applications are also described, for example the investigation of metalloproteomics [05PRA], the interactions between metals and biomolecules [08YIN], biospeciation analysis [09TIM] and element ligand interactions [16CHE]. For the sake of completeness it should be mentioned that there exist, besides CE, also other separation techniques that can be hyphenated to ICP-MS [12PRO]. More recently, the separation and detection of nanoparticles by CE-ICP-MS [16MEB], [17ALE] and the coupling of CE to single particle ICP-MS (CE-SP-ICP-MS) [18MEE], in particular for Ag [17MOZ1], [17MOZ2], [18MIC] and Au [17FRA] nanoparticles, have gained a growing interest.

Instead of an ICP-MS detection, sometimes an ICP-AES (inductively coupled plasma atomic emission spectroscopy), or also referred to as ICP-OES (inductively coupled plasma optical emission spectroscopy) detector coupled to a CE is used. A comparison of the two shows, that the limits of detections are lower in ICP-MS, but for lighter metals (e.g. Ca or Mg), higher salt contents and more complex matrices the use of an ICP-AES detector may have benefits if the analyte concentrations are not too low [13TIM1]. Recently, a new transient method has been developed to enable the use of ICP-MS detection also with high salinities [17HEI]. A more gentle ionization method for MS detection often used instead of the inductively coupled plasma is the so called electrospray ionization (ESI-MS). While in ICP-MS all analytes are completely destroyed due to the high plasma energies, in ESI-MS it is possible to study chemical compounds [13KLE]. The electrochemical detection with C⁴D (capacitively coupled contactless conductivity detector) detectors is sometimes used as an alternative to the MS detection [98ZEM], [18KUB].

Lanthanides (Ln) are often studied as chemical analogues for trivalent actinides and many works concerning their investigation by CE(-ICP-MS) can be found in the literature. One of the major challenges is the separation of the individual Ln(III) ions due their very similar electrophoretic mobilities resulting from their chemical likeness. One approach to increase the differences in the electrophoretic mobilities is the complexation with suitable complex forming agents [03JAN], for example cupferron (*N*-nitroso-*N*-phenylhydroxylamine) with hydroxyisobutyric acid (HIBA) as buffer [00OZT], aromatic polyaminocarboxylate together

2. CE-ICP-MS

with nitrilotriacetic acid [06SAI] or arsenazo III for the separation of both Ln(III) and U(VI) [98MAC], [01COL]. The separation of Ln(III), Th(IV) and U(VI) via CE by complexation with different ligands is described by Liu et al. [98LIU1], [98LIU2] and Shiri-Yekta et al. [14SHI], the separation of U(VI) and different transition metals by 4-(2-thiazolylazo)resorcinol in [01EVA]. CE was further used for the investigation of oxalate and tartrate complexes of Ln(III) [87ROS] and for carbonate complexes [08PHI] (CE-ICP-MS in the last case). Furthermore, Ln are one of the main proportions in fission products and CE was employed for the determination of the isotopic composition of such samples [08PIT]. Day et al. [00DAY] determined the nuclide abundance of Ln produced in a spallation reaction in an irradiated tantalum target by CE-double focusing SF-ICP-MS.

Kautenburger et al. investigated the influence of humic acid (HA) on the migration behavior of lanthanides in the environment due to complexation or colloid formation by CE-ICP-MS [06KAU], [07KAU], [09KAU], [14KAU]. HA is part of naturally occurring large organic macromolecules, summarized under the term natural organic matter (NOM) and is thus interesting in the context of the migration behavior of radionuclides in the environment. The interaction of lanthanides with humic substances was further examined by Sonke and Salters et al. by an EDTA-ligand competition method via CE-ICP-MS [06SON], [07STE]. The actinides Th(IV) and U(VI) have also been investigated with respect to their interaction with NOM. Benes [09BEN] applied a free ligand electrophoresis for the study of Th(IV) complexation with HA. In [14STE] the same question was addressed by ligand competition experiments. U(VI) was examined by [01PAC] and again by the group of Kautenburger et al. [12MOS], [17HAH], [17KAU].

In the field of actinide speciation, CE has been used as an analytical tool in a number of investigations. A comprehensive overview up until the year 2013, especially in combination with ICP-MS, is given by Timerbaev et al. [13TIM2]. The application in the speciation of geological and environmental samples is summarized by Hein et al. [14HEI].

Ion mobilities of Am(III) and Ln(III) have been determined by Rösch et al. [89ROS1], [90ROS1] (in this paper also Cf(III) is investigated), [03MAU] by a custom-made free electrolyte continuous electromigration technique. In 2003, Kuczewski et al. were the first to coupled CE and ICP-MS for the investigation of actinides [03KUC]. They were able to separate the four different Pu oxidation states +III to +VI and Np(V)/Np(IV) with 1 M acetic acid as the BGE. Further examinations on the redox speciation of Pu followed this work [05AMB], [07BUR]. Graser et al. investigated the kinetics of the reduction of Pu(VI) by Fe(II) and also determined the electrophoretic mobilities of different Np species [15GRA]. The absolute mobility and the equivalent ionic conductivity of Np(V) was measured by Aupiais et al.

2.5 Literature Review of Applications of CE-ICP-MS with Focus on the Investigation of Actinides

[03AUP]. Stöbener et al. studied the redox speciation of Np in samples contacted with natural Opalinus clay [12STO]. The redox speciation of Pa(V) and different hydrolyzed species as well as the complexation of U(VI) by anionic forms of some long-lived fission products MO_x^{n-} ($M = I, Se$) were investigated in [05FOU]. A detailed scheme of the electrophoretic mobilities of several actinides in different oxidation states is one of the results of this work (for more detailed information see Section 3 and [19WIL1]). Furthermore in this work, the redox kinetics of the reduction of Np(V) by hydroxylamine hydrochloride (HAHCl) are investigated and the results can be found in Section 5 and in [18WIL].

A very important and extensively used field of the application of CE-(ICP-MS) is the investigation of metal ligand interactions and the determination of stability constants of actinides [16SLA]. An overview of the works conducted concerning An(V) ions is reviewed in [16TOP]. The capability of this method as an appropriate analytical tool for the study of complex binding interactions at low concentrations is also emphasized in [01RUN], [08CHE], [13DVO]. In Table 4, the different actinide-ligand systems examined by CE are summarized and the respective literature source is given. In this work, CE-ICP-MS was also used to determine the stability constants of the actinides Am(III), Th(IV), Np(V) and U(VI) with acetate [19WIL2], propionate, gluconate and citrate. The results and more details about the experimental conditions and the data treatment is given in Section 4.

Table 4: Summary of the publications on the determination of stability constants of actinides with different ligands. For more details concerning the experimental conditions such as BGE, ionic strength, temperature etc. and the results see the respective reference.

ligand	actinide					
	Th	Pa	U	Np	Pu	Am
chloride				Np(V) [09TOP2]	Pu(V) [09TOP2]	
sulfate				Np(V) [89ROS2] [90ROS4] [09TOP2]	Pu(V) [09TOP2]	Am(III) [90ROS2]
nitrate				Np(V) [10TOP]	Pu(V) [10TOP]	
periodate			U(VI) [04KAR]			
carbonate				Np(V) [09TOP1]	Pu(V) [09TOP1]	

2. CE-ICP-MS

Table 4: continued.

ligand	actinide					
	Th	Pa	U	Np	Pu	Am
acetate	Th(IV) [19WIL2]		U(VI) [13SLA] [14SLA] [19WIL2]	Np(V) [90ROS3] [90ROS4] [19WIL2]		Am(III) [19WIL2]
propionate	Th(IV) [this work]		U(VI) [this work]	Np(V) [this work]		Am(III) [this work]
oxalate		Pa(V) [10MEN]	U(VI) [09PET] [10PET] [15BRU]	Np(V) [89ROS2] [90ROS4] [15BRU]	Pu(V) [15BRU]	Am(III) [90ROS2] [15BRU]
gluconate	Th(IV) [this work]		U(VI) [this work]	Np(V) [this work]		Am(III) [this work]
succinate			U(VI) [18SLA]		Pu(VI) [18SLA]	
tartrate				Np(V) [89ROS2] [90ROS4]		
citrate	Th(IV) [this work]		U(VI) [15ZHA] [this work]	Np(V) [90ROS3] [90ROS4] [this work]		Am(III) [this work]
adipate	Th(IV) [81SIN]		U(VI) [81SIN]			
nitrioltri- acetic acid		Pa(V) [18LUC]				
DTPA	Th(IV) [16AUP] [16BON]	Pa(V) [13MEN]	U(VI) [16AUP]	Np(IV) [16AUP]	Pu(IV) [16AUP] [16BON]	Am(III) [12LEG] (also Cm(III) and Cf(III))
3,4,3- LI(1,2- HOPO) and 5-LIO(Me- 3,2-HOPO)	Th(IV) [17AUP]				Pu(IV) [17AUP]	

Besides this application in the complexation chemistry of actinides, the study of the interactions of actinides with biologically relevant molecules by CE is of growing interest [07USE], [10JIA], [15GAL], [15STE]. For example, a uranium-protein interaction in human

2.5 Literature Review of Applications of CE-ICP-MS with Focus on the Investigation of Actinides

blood was investigated by Huynh et al. by CE-ICP-MS [15HUY], [16HUY]. The interaction of U with transferrin is described in [97SCA], [98SCA]. The stability constants of Pu(IV) with this protein can be found in [17SAU], that of Th(IV) in [18BRU]. In the last paper, for the first time the coupling of capillary isoelectric focusing with ICP-MS is described. The binding of beta-cyclodextrine was investigated in [16LI] by affinity capillary electrophoresis (ACE).

For the investigation of dissolved and colloidal uranium species in carbonated soil after a leaching process, CE-ICP-MS was used in order to determine the uranium-colloid interactions [11CLA]. Martelat et al. recently published the use of CE-multi collector (MC)-ICP-MS for the precise U/Pu isotope ratio measurement in nuclear samples [18MAR].

EXPERIMENTAL SECTION

Preliminary remark: A list of all chemicals used in this work together with the respective supplier can be found in the appendix ('LIST OF CHEMICALS' on Page 194 f). The indicated error limits are calculated, if not stated otherwise, on basis of a Gaussian error propagation. The respective equations and the estimated errors for the calculations are presented in APPENDIX A2.

3. DETERMINATION OF ELECTROPHORETIC MOBILITIES WITH CE-ICP-MS

For the interpretation of electropherograms, which are a result of CE-ICP-MS experiments, the electrophoretic mobilities μ of all species under investigation must be known. Only then it is possible to assign the observed peaks unambiguously to a particular species. Since the electrophoretic mobilities are dependent on the experimental conditions such as BGE, pH value and ionic strength, it has to be kept in mind that a given μ is only valid for the exact conditions it has been determined for.

The following chapter provides an overview of the experiments conducted in this work for the investigation of the electrophoretic mobilities of different actinides in varying oxidation states as well as a comparison of two different EOF markers. For the start, some important theoretical considerations concerning this topic are summarized.

3.1 THEORETICAL CONSIDERATIONS

For the calculation of electrophoretic mobilities from experimental results, the migration times of the respective species have to be determined experimentally. Then Equation (2.12) can be employed (see Section 2.1.1 for further information). Because of the importance of this formula and for reasons of simplicity it is repeated in Equation (3.1).

$$\mu = \frac{l^2}{U} \left(\frac{1}{t_i} - \frac{1}{t_{\text{EOF}}} \right). \quad (3.1)$$

The migration times t_i and t_{EOF} are defined by the maximum of the particular peaks in the electropherogram. Since these peaks always exhibit a certain expansion due to the non-ideality of the experimental system, they can overlap if the differences in the migration times of the respective species are too small for full separation. In such a case the two peaks are not completely resolved.

A measure for the capability of the separation of two species under given conditions is the resolution R_s . It is defined as the distance between two peak maxima (so the migration times t) divided by the average of their baseline widths w (Equation (3.2)).

3.1 Theoretical Considerations

$$Rs = \frac{t_2 - t_1}{\frac{1}{2}(w_1 + w_2)} \quad (3.2)$$

In general, a resolution of $Rs \geq 1.5$ is considered as resolved to baseline [92GRO].

Factors that affect the electrophoretic mobility are discussed in Section 2.1.3. The peak width w in contrast is a result of diffusion and other dispersive phenomena, which are briefly elucidated in the following based on [92GRO], [10LAU]. For more details and mathematical derivations is referred to these references.

Diffusion: Axial diffusion of the analyte has an equal extent in both directions along the capillary. Consequently this effect leads to a symmetrical peak broadening. Radial diffusion can be neglected due to the flat EOF profile.

Parabolic temperature profile: In this case the considerations already discussed in Section 2.1.3 apply.

Injection volume: It is not possible to inject the sample as an infinitely thin zone into the capillary. Since in hydrodynamic injection mode, as used in this work, the pressure is applied for a certain period of time, an expanded sample zone occurs resulting in broader peaks. For minimizing this effect, it is commonly said that the length of the injected sample plug should not exceed 1 – 2% of the total capillary length l_c . In the present case, the injected sample volume of ca. 15 nL as calculated with the conditions given in Equation (2.7) results in a sample plug length of 7.6 mm for an inner diameter of 50 μm (calculated with the volume equation of a cylinder). This precisely corresponds to 1% of $l_c = 76 \text{ cm}$ and thus the effect of the finite injection volume is negligibly small.

Analyte and capillary wall interaction: As mentioned before in the theory section, the inner capillary wall is composed of silanol groups which are partly negatively charged in dependence of the pH value due to deprotonation. The analyte cations can now interact with these negative charges and by that their migration velocity is slowed down or they can even be completely adsorbed to the surface. The deceleration of a part of the analyte ions will lead to a back-tailing of the respective peak. Because of the large surface-to-volume ratio in thin capillaries, this effect can become significant in CE experiments. In the case of this work, most experiments were conducted with 1 M acetic acid as BGE with a pH value of 2.4. Even though the acidity constant of the silanol surface groups are difficult to determine, the degree of deprotonation at such a low pH value should be quite small and thus the effect will not excessively influence the migration of the ions.

3. Determination of Electrophoretic Mobilities with CE-ICP-MS

Siphon effect: This effect is already mentioned in Section 2.3. By positioning the ends of the capillary, both the inlet and the outlet side, at the same height, the siphon effect can be avoided.

Electrodispersion: Due to the presence of the analyte ions in the BGE, a different conductivity in the sample zone compared to the rest of the BGE occurs. This in turn leads to local differences in the applied electric field. Since the electrophoretic mobility of a given ion depends on the applied electric field, it varies relative to the analyte concentration. This effect can result in both front-tailing and back-tailing, depending on whether the conductivity in the respective zone decreases or increases leading to a faster or slower electrophoretic mobility. The low concentrations of actinide sample ions used in this work are beneficial for minimizing this effect because it is all the more pronounced the higher the analyte concentration is.

Detection volume: As the injection volume always has a certain spatial expansion the same is true for the analyte volume detected at the end of the separation. It takes a certain time for the sample zone to elute and the ICP-MS is just able to detect the incoming analyte ions as a function of time. This results in a peak broadening defined by the analyte distribution in the sample zone. Again, the low sample concentrations are advantageous because of smaller sample zones.

All the dispersive processes listed above can be considered as independent from each other and the overall effect is the sum of all single contributions. Generally speaking, as already implied above, CE is a method exhibiting a small amount of dispersion effects and thus a good resolution. Nevertheless it is important to adjust the experimental parameters as suitable as possible to minimize the individual effects in order to obtain reliable results for the determination of electrophoretic mobilities.

3.2 COMPARISON OF TWO EOF-MARKERS

Besides the migration time t_i of the analyte species under investigation, also the migration time of the EOF t_{EOF} must be known for the calculation of the electrophoretic mobility μ (compare Equation (3.1)). For this reason, a so called EOF marker is added to every sample before CE-ICP-MS measurements. Neutral molecules are used for this purpose since they are not accelerated by the applied electric field but rather dragged along by the EOF. Consequently, they eluate simultaneously with the EOF and their detection thus allows the determination of its migration time.

In the literature, the application of different EOF markers is described. The group of Aupiais and Topin et al. used DMF (*N,N*-dimethylformamide) which is detected by UV-Vis

3.2 Comparison of Two EOF-Markers

spectroscopy (see e.g. [10TOP] or other citations given in Section 2.5). Graser et al. employed 2-bromoethanol detected on the mass of ^{79}Br via SF-ICP-MS [15GRA]. In order to ensure that the EOF marker used in this work, namely 2-bromopropane, can also be applied, comparison experiments were conducted with 2-bromoethanol since in that case the detection methods are identical.

The measurements were executed with $^{237}\text{Np(V)}$ as analyte ion. This species was chosen due to the fact that it is chemically stable under the given conditions and its electrophoretic mobility is known from former experiments and the literature [15GRA], [12STO].

A 0.2 M 2-bromoethanol solution was produced by diluting 97% 2-bromoethanol with 0.1 M nitric acid, exact as described in the literature. 2-Bromopropane was used without further dilution.

The CE-ICP-MS samples were prepared by dissolving 2 μL of a $^{237}\text{Np(V)}$ stock solution in 198 μL 1 M acetic acid yielding a neptunium concentration of $c(^{237}\text{Np(V)}) = 5 \cdot 10^{-7}$ M. The 1 M acetic acid was also employed as the BGE. To these samples, the appropriate volume of the respective EOF marker was given. Measurements were undertaken with both 25 kV and 10 kV to show that the results are independent of the applied high voltage. For both high voltages, three measurements were performed, each with 1 μL 2-bromopropane, 5 μL 0.2 M 2-bromoethanol and a mixture of both. The mixture was investigated in order to see if still one peak on the mass 79 is obtained. This must be true if both compounds migrate together with the EOF. If one substance exhibits an electrophoretic mobility different from zero, a separation of the peak would arise.

The resulting electropherograms are shown in Figure 6. As one can see, in each electropherogram only one peak is obvious for the mass 79.

In Table 5 the measured migration times and the electrophoretic mobility of Np(V) calculated from these by Equation (3.1) are depicted. It can be clearly observed that the results agree with each other within the limits of error. Both for the different EOF markers and for the varying voltage, the same electrophoretic mobility for Np(V) was obtained. Furthermore, the results are in good agreement with the literature. A more detailed discussion of this topic will be given in the following chapter.

3. Determination of Electrophoretic Mobilities with CE-ICP-MS

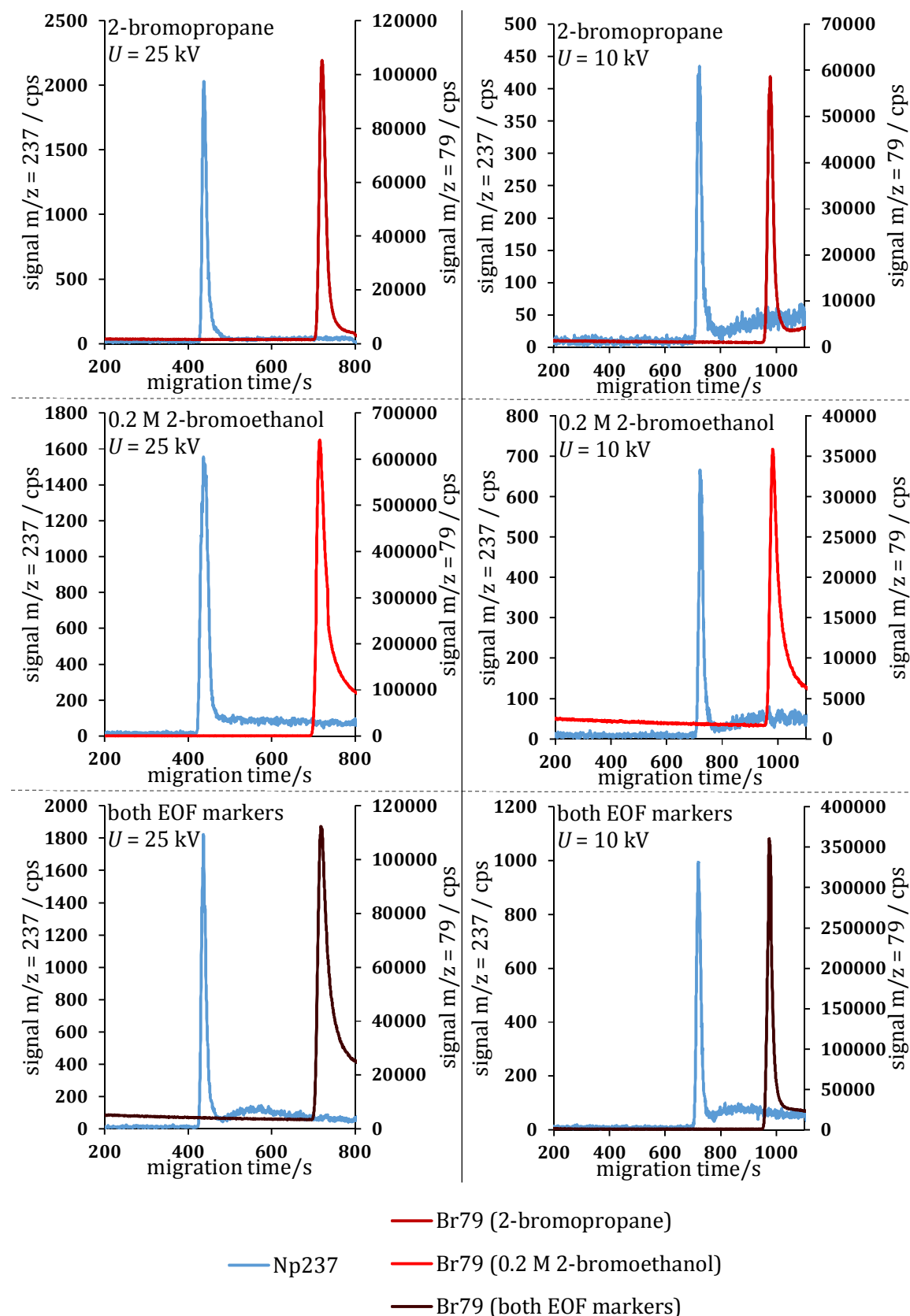


Figure 6: Resulting electropherograms for the comparison of two different EOF markers, 2-bromopropane and 2-bromoethanol, at $U = 25$ kV and $U = 10$ kV.

3.2 Comparison of Two EOF-Markers

Table 5: Results of the comparison of two different EOF markers, 2-bromopropane and 0.2 M 2-bromoethanol, at $U = 25$ kV and $U = 10$ kV.

EOF marker	voltage/ kV	migration time/s		electrophoretic mobility/ $10^{-4} \text{ cm}^2 \text{ V}^{-1} \text{ s}^{-1}$
		$^{237}\text{Np(V)}$	^{79}Br	Np(V)
2-bromopropane	25	438.3	720.8	2.07 ± 0.07
0.2 M 2-bromoethanol		436.5	715.3	2.06 ± 0.07
both		436.5	718.1	2.08 ± 0.07
2-bromopropane	10	723.5	978.7	2.08 ± 0.07
0.2 M 2-bromoethanol		719.9	982.3	2.14 ± 0.07
both		719.9	975.0	2.10 ± 0.07

As a result it can be concluded that 2-bromopropane provides findings comparable to EOF markers described in the literature. The utilization of this compound thus is reasonable.

REMARKS:

The investigation presented above was undertaken within the framework of the diploma thesis of Saskia Leidich [17LEI1] under the guidance of Christian Willberger and Tobias Reich. Samples preparation and CE-ICP-MS measurements were conducted by Saskia Leidich and Christian Willberger. The evaluation was conducted individually by both Saskia Leidich and Christian Willberger.

3. Determination of Electrophoretic Mobilities with CE-ICP-MS

3.3 PUBLICATION: INVESTIGATION OF THE ELECTROPHORETIC MOBILITY OF THE ACTINIDES TH AND U-AM IN DIFFERENT OXIDATION STATES

TABLE OF CONTENT GRAPHIC FOR PUBLICATION:

The graphic shows the combined electropherograms of different neptunium and plutonium species separated by CE. Furthermore the migration and separation process of the different species and of the EOF inside the capillary is indicated.

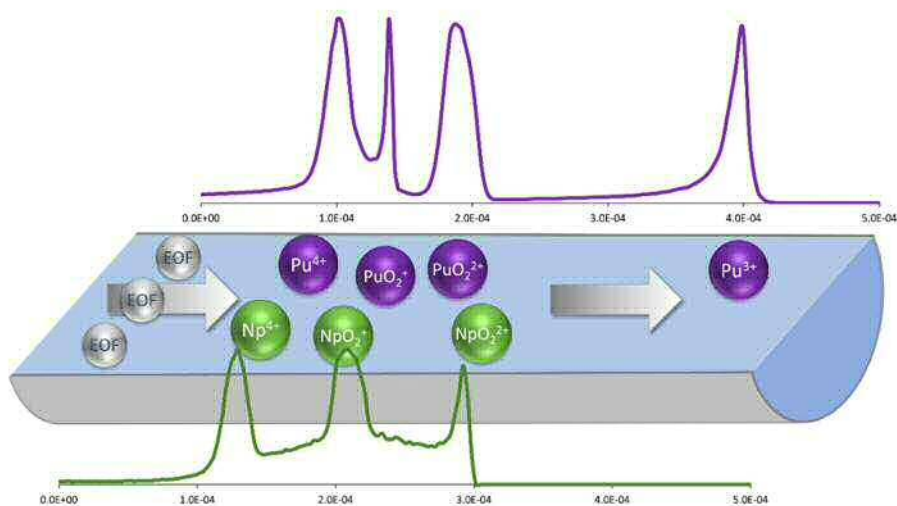


Figure 7: Table of Content Graphic for publication of the electrophoretic mobility manuscript.

AUTHOR CONTRIBUTIONS:

The samples and stock solutions of the actinides were prepared by Samer Amayri, Raphael Scholze, Verena Schneiders and Christian Willberger. The ICP-MS measurements were performed by Christian Willberger and Samer Amayri. The conceptual planning of this investigation and the layout of the manuscript were done by Christian Willberger and Tobias Reich. The manuscript was written by Christian Willberger with contributions from Tobias Reich.

REMARKS:

Detailed calculations for the acetate speciation of the metal ions and the resulting mean effective charge q_{eff} and the corresponding species distribution in 1 M acetic acid at pH 2.38 calculated with Visual MINTEQ are presented in the Supporting Information that can be found in the APPENDIX A4. The numbering of the tables, figures and equations within the manuscript has remained unchanged and thus is not in accordance with the numbering of the rest of this work. The same is true for the citations. The version presented here is not the final one and may be changed before publication since the manuscript was in the status of revision in the publication process at the time of the printing of this work.

Investigation of the Electrophoretic Mobility of the Actinides Th and U–Am in Different Oxidation States

Christian Willberger*, Samer Amayri, Verena Häußler, Raphael Scholze, Tobias Reich*

Institute of Nuclear Chemistry, Johannes Gutenberg University Mainz, 55099 Mainz, Germany

ABSTRACT: The electrophoretic mobilities (μ_e) of the actinides Th and U–Am in different oxidation states (prepared in 1 M HCl and 1 M HClO₄) have been determined by CE-ICP-MS using 1 M acetic acid as the background electrolyte, which has proven to provide an excellent setup for trace analysis at environmentally relevant concentrations ($1 \cdot 10^{-9}$ M). The values are independent of the respective acid solution. The μ_e of the Pu oxidation states +III to +VI have been measured. They agree with both the available literature data and with the redox-stable analogues (Eu(III), Th(IV), Np(V), U(VI)) that have also been investigated. The trend in the μ_e for the actinides U–Pu was found to be An(III) > An(VI) > An(V) > An(IV). The μ_e of Am(III) ($\mu_e(\text{Am(III)}) = 3.86 \cdot 10^{-4} \frac{\text{cm}^2}{\text{Vs}}$), U(IV) ($\mu_e(\text{U(IV)}) = 0.34 \cdot 10^{-4} \frac{\text{cm}^2}{\text{Vs}}$) and U(VI) ($\mu_e(\text{U(VI)}) = 1.51 \cdot 10^{-4} \frac{\text{cm}^2}{\text{Vs}}$) have been measured for the first time under these experimental conditions. Furthermore, a systematic approach for calculating values for the μ_e of actinides in instable oxidation states that are not feasible for CE-ICP-MS experiments is introduced. This schema is confirmed by measurements of already estimated values, measured after their estimation. The estimated value for U(IV), for example, is $\mu_e(\text{U(IV)}) = 0.28 \cdot 10^{-4} \frac{\text{cm}^2}{\text{Vs}}$. This is in agreement with the experimental data given above.

1. INTRODUCTION

Nuclear power has been used as a source of energy for many years and is still in use in many countries. During the operation of a nuclear power plant, a large amount of high-level radioactive waste is generated, for which safe entombment has to be ensured for periods up to one million years. Most notably, the spreading of radionuclides into the environment has to be prevented at all times. Nuclear waste will in future be stored in a deep geological repository with argillaceous and crystalline rocks or salt as potential host rocks.¹⁻² It is very important to gain a deep understanding of the chemical behavior of the relevant radionuclides in the respective geological formation.

Long-lived actinides such as ²³⁸U ($t_{1/2} = 4.47 \cdot 10^9$ a), ²³⁷Np ($t_{1/2} = 2.14 \cdot 10^6$ a), ²³⁹Pu ($t_{1/2} = 2.41 \cdot 10^4$ a) and ²⁴¹Am ($t_{1/2} = 432.2$ a) are part of the high-level radioactive waste in

3. Determination of Electrophoretic Mobilities with CE-ICP-MS

spent nuclear fuels. After a long period of enclosure these nuclides account for a significant percentage of the total radiotoxicity of the nuclear waste.³

Under environmental conditions actinides exhibit a wide distribution of possible oxidation states, with different speciations in aquifers. Plutonium, for example, displays a wide range of oxidation states from Pu(III) up to Pu(VI) in aqueous solution, whereby the lower ones exist as the free cations Pu^{3+} and Pu^{4+} and the higher ones as the plutonyl cations PuO_2^+ and PuO_2^{2+} , not to mention the versatile possibilities of different complexation partners and coordination numbers.⁴ For this reason it is essential for the safety assessment of a possible repository to have an extensive knowledge of the exact speciation of the considered actinides under the expected conditions.

The determination of the exact speciation of the actinides at environmentally relevant concentrations in the worst case of a possible leakage from the repository requires a reliable and effective analytical method. For analyzing the different oxidation states, the separation capability of capillary electrophoresis (CE) was coupled with the high sensitivity of inductively coupled plasma mass spectrometry (ICP-MS). With this setup we achieved the separation and quantification of different actinide oxidation states within less than 20 minutes and limits of detection of approximately $1 \cdot 10^{-9}$ M, which is expected for actinides in the far field of a repository.⁵⁻⁶

In the present work we measured the electrophoretic mobilities of different oxidation states of the actinides Th and U–Am diluted in 1 M acetic acid medium. The migration of actinides in a capillary is strongly affected by their speciation in solution, which is dependent on several parameters such as pH, redox potential and ligand complexation. Hence the results of such measurements under model conditions are very helpful for the realization and interpretation of investigations of authentic environmental samples in complex media concerning the long-term safety analysis of possible nuclear repositories.

CE-ICP-MS measurements of actinides have been carried out before, our studies focus on the actinides Pu and Np. The results for these elements will be discussed in comparison with the values of redox-stable homologues and will be compared with the available data in the literature.⁶⁻⁸ Furthermore, for the first time we measured values for the U oxidation states +VI and +IV and for Th(IV) under the experimental conditions used here. Concluding, a systematic approach for estimating unknown electrophoretic mobilities from experimental data is introduced.

3.3 Publication: Investigation of the Electrophoretic Mobility of the Actinides Th and U-Am in Different Oxidation States

2. EXPERIMENTAL

As already mentioned, the coupling between the CE and the ICP-MS system provides a powerful method to determine the exact speciation of actinides at near environmentally relevant concentrations. The method was first described by Olesik et al. in 1995.⁹ Since then, much work in the field of elemental speciation analysis has been done and many review articles can be found in the literature.¹⁰⁻¹²

2.1 CAPILLARY ELECTROPHORESIS

The importance of CE with regard to element speciation was described by Timberbaev et al.,¹³ especially to the speciation of actinides.¹⁴ Basic considerations for CE can be found elsewhere.¹⁵

The principle of separation in electrophoresis techniques is the varying velocity of migration of different ions in solution in an applied electric field. The electrophoretic mobility μ_e , which is measured during capillary electrophoresis experiments, is a characteristic quantity of each ion in a particular medium. For performing capillary electrophoresis, ca. 50 μm thin fused silica capillaries are used, which are filled with a background electrolyte (in our case 1 M acetic acid). The sample is dissolved in the same medium and transferred to the capillary via hydrodynamic injection. A high voltage is applied between two platinum electrodes and the electric circuit is closed by the background electrolyte solution.

One can calculate the electrophoretic mobility of an ion μ_i by knowing the retention times of the electroosmotic flow (EOF) t_{EOF} and of the examined species t_i at a given capillary length l_k and applied voltage U .

$$\mu_i = \frac{l_k^2}{U} \left(\frac{1}{t_i} - \frac{1}{t_{\text{EOF}}} \right) \quad (1)$$

The EOF describes the movement of the whole electrolyte solution inside the electric field. Neutral species eluate together with the EOF, which can be used for measuring the retention time of the EOF.

In the present case 2-bromopropane was used as the neutral EOF marker. We tested the capability of this chemical to really act as a neutral marker by comparing its behavior during CE experiments with the behavior of 2-bromoethanol, another EOF marker used in the literature⁸. Both ⁷⁹Br signals had exact the same retention time whereof we concluded that the 2-bromopropane is a suitable EOF marker, too.

3. Determination of Electrophoretic Mobilities with CE-ICP-MS

2.2 ICP-MS SYSTEM

Mass spectrometry with inductively coupled plasma is an appropriate detection method for analyzing eluates previously separated by capillary electrophoresis. The system combines the advantages of mass spectrometry, which is a very sensitive and specific method for simultaneous multi-element detection at very low concentrations, with the benefits of inductively coupled plasma, namely a high efficiency of atomization and ionization of the sample. A detailed summary of possible applications of ICP-MS as a detection method for CE can be found in the literature.¹⁶

At the beginning of every measurement, a tuning was performed to find the optimal plasma parameters for the system and thus to prevent the formation of higher-charged ions, hydroxides, and oxides, which can cause interferences.

2.3 COUPLING DEVICE

For an effective coupling of the CE (Agilent 7100, Agilent Technologies, Santa Clara, California, USA) with the ICP-MS (Agilent 7500 ce, Agilent Technologies, Santa Clara, California, USA), a functional connection between both systems is of utmost importance. Figure 1 shows a picture of the coupling system that was used in this work. The centerpiece of the device is a MiraMist CE nebulizer (Burgener Research, Mississauga, Canada) leading to a Scott-type spray chamber (AHS Analysentechnik, Tübingen, Germany). The nebulizer used in our experiments is a parallel path model. In this layout, the carrier gas flow and the capillary are separated in two parallel tubes and the make-up electrolyte is applied rectangularly to those. Accordingly, the mixture of the three components takes place just at the very tip of the nebulizer in a very small volume. Reviews of the importance of nebulizers for performing CE-ICP-MS measurements can be found in the literature.¹⁷⁻¹⁹

The make-up electrolyte is introduced via a syringe pump (PicoPlus, Harvard Apparatus, Holliston, Massachusetts, USA). Its flow rate has to be adjusted experimentally to avoid a laminar flow profile from too small flow rates and a tailback of the sample in the capillary from too high flow rates. In the present experiments a 1.25% HNO₃ solution with 10% ethanol was used. Additionally, the make-up solution contained 5 ppb ⁸⁹Y, ¹⁰⁷Rh, ¹⁴⁰Ce, and ²⁰⁹Bi as internal standards.

3.3 Publication: Investigation of the Electrophoretic Mobility of the Actinides Th and U-Am in Different Oxidation States

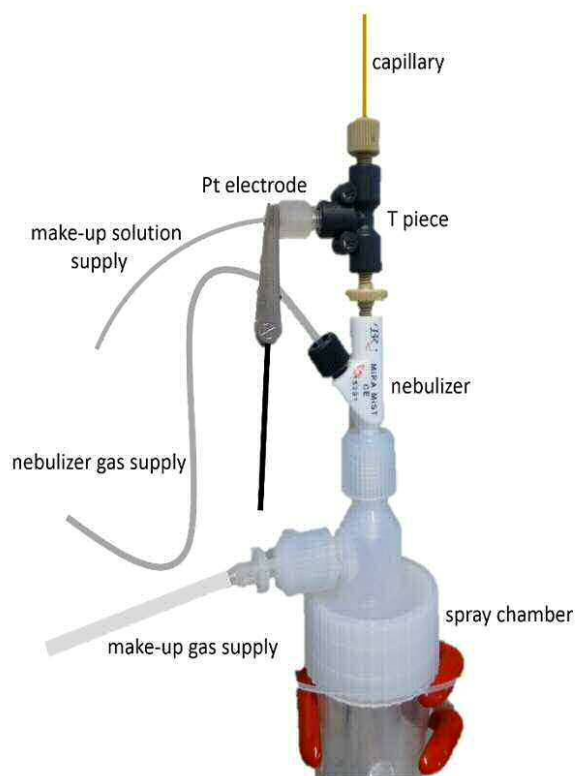


Figure 1. Coupling system between CE and ICP-MS as used for the actinide mobility measurements.

2.4 REAGENTS

Nitric acid, 2-bromopropane, hydroxylamine hydrochloride ($\text{NH}_3\text{OH}^+\text{Cl}^-$), ^{238}U wires, and Rh ICP standard solution were supplied by Merck (Darmstadt, Germany). Acetic acid and perchloric acid were received from Riedel-de Haën (Seelze, Germany), and hydrochloric acid from Fisher Scientific (Loughborough, UK). The ICP-MS elemental standards were supplied by High-Purity Standards (Charleston, South Carolina, USA) (Bi, Ce and Y), Peak Performance (CPI International, Santa Rosa, California, USA) (Eu and U) and Accu Trace™ (Accu Standard, New Haven, Connecticut, USA) (Th). All reagents were of pro-analysis quality or better. Milli-Q water (18.2 M Ω , Synergy™ Millipore water system, Millipore GmbH, Schwalbach, Germany) was used for dilutions. All solutions were filtered through 0.2 μm syringe filters (Nalgene, Rochester, New York, USA) prior to their application in CE to prevent clogging.

All actinide stock solutions were prepared both in 1 M HCl and in 1 M HClO_4 to see if there is an effect on the electrophoretic mobility of the ions after diluting in 1 M acetic acid depending on the medium of the stock solution.

$^{239}\text{Pu}(\text{VI})$ and $^{237}\text{Np}(\text{VI})$ stock solutions were prepared by repeated evaporation with 1 M HClO_4 or 1 M HCl respectively under the addition of very small amounts of NaF to prevent

3. Determination of Electrophoretic Mobilities with CE-ICP-MS

colloid formation. Starting from this hexavalent state, the tri-, tetra- and pentavalent oxidation states were obtained by electrolytic reduction and oxidation reactions.

Besides this, a $^{237}\text{Np(V)}$ stock solution was prepared as described in the literature.²⁰ Proceeding from this, $^{237}\text{Np(IV)}$ was yielded by chemical reduction with hydroxyl ammonium hydrochloride.

$^{238}\text{U(VI)}$ was obtained by dilution of the ICP-MS standard solution to the required concentration. Dissolving ^{238}U wires in 1 M HCl produced $^{238}\text{U(IV)}$ solutions.

As Am(III) is stable in the trivalent oxidation state, there was only the need to adjust the medium of the stock solution by evaporation until near dryness and dissolving the residue in 1 mL of the respective 1 M acid.

The Th(IV) and Eu(III) solutions were diluted from the ICP-MS standard solutions with 1 M HCl or 1 M HClO_4 , respectively.

The purity of the different oxidation states of the investigated actinides was controlled by UV-Vis measurements (Tidas 100, J & M Analytik AG, Essingen, Germany). The concentrations of the respective solutions were measured via liquid-scintillation counting for Pu or γ -ray spectrometry measurements for U, Np, and Am.

Some oxidation states turned out to be much more instable than we expected under the used conditions, which required certain additions. These were chosen to ensure a reducing ($\text{NH}_3\text{OH}^+\text{Cl}^-$) or oxidizing (NaClO) environment to stabilize the very reactive oxidation states without further complexation properties.²¹ Therefore, NaClO was added to the Np(VI) samples and hydroxyl ammonium hydrochloride to the Pu(III) samples.

If the concentration of the stock solutions exceeded $5 \cdot 10^{-5}$ M, the respective solutions were diluted to this specific concentration. Solutions with concentrations less than $5 \cdot 10^{-5}$ M were used without further dilution.

2.5 SAMPLE PREPARATION AND PARAMETERS FOR CE-ICP-MS

Unless stated otherwise, samples for CE-ICP-MS measurements were prepared by diluting 2 μL of the analyte solution with 198 μL 1 M acetic acid in conical micro-inserts of borosilicate glass (Carl Roth AG, Arlesheim, Switzerland). To each sample, 1 μL 2-bromopropane was added as the EOF marker. The final concentration of the analyte was $(5.00 \pm 0.45) \cdot 10^{-7}$ M. The micro-inserts were transferred into the CE system by placing them in polyethylene vials sealed with polyethylene olefin snap caps (both Agilent Technologies, Santa Clara, California, USA).

3.3 Publication: Investigation of the Electrophoretic Mobility of the Actinides Th and U-Am in Different Oxidation States

The fused silica capillaries (Polymicro Technologies, Phoenix, Arizona, USA) were preconditioned before every use by flashing several times with MilliQ-Water, 0.1 M sodium hydroxide solution, 0.1 M hydrochloric acid and 1 M acetic acid. In between the measurements the capillary was flushed with 1 M freshly prepared acetic acid to remove the remaining analytes and to prevent effects caused by altered acetic acid due to the applied high voltage.

Temperature stability is a crucial point in performing CE experiments since a variation of 1 °C can lead to a change in the electrophoretic mobility of about 2%. We controlled the temperature at 25 °C by the air cooling device of the Agilent apparatus. Only a short part of the capillary leading out of the CE apparatus inside the nebulizer could not be temperature controlled. The temperature rise inside the capillary due to Joule heating was calculated following a procedure given in the literature²² to be on average about 0.5 °C and to not exceed 1 °C under the used experimental conditions.

All evaluations were undertaken with the MassHunter Workstation software (G7200B, Agilent Technologies, Santa Clara, California, USA). All parameters during the measurements are summarized in Table 1.

Table 1. Parameters for the CE-ICP-MS system during measurements.

Capillary electrophoresis	
system	Agilent 7100 ce (Agilent Technologies, Santa Clara, California, USA)
voltage	25 kV
current	10–20 µA
capillary	fused-silica capillaries, inner diameter: 50 µm, length: 76 cm
sample introduction	hydrodynamic, 8 s with 100 mbar
background electrolyte	1 M acetic acid, pH 2.4
temperature control	25 °C
Coupling device	
nebulizer	Mira Mist CE (Burgener Research, Mississauga, Canada)
spray chamber	Scott-type

3. Determination of Electrophoretic Mobilities with CE-ICP-MS

Table 1. continued.

make-up electrolyte	1.25% HNO ₃ and 10% ethanol, 5 ppb Y, Rh, Ce and Bi as internal standard, flow rate: 5 $\frac{\mu\text{L}}{\text{min}}$
carrier gas	Ar, flow rate: 0.86–1.15 $\frac{\text{L}}{\text{min}}$
make-up gas	Ar, flow rate: 0.28–0.77 $\frac{\text{L}}{\text{min}}$
ICP-MS	
system	Agilent 7500 ce (Agilent Technologies, Santa Clara, California, USA)
plasma power	1550 W
detection mode	time-resolved analysis
dwelt time	100 ms

3. RESULTS AND DISCUSSION

The electrophoretic mobilities of the Pu oxidation states +III to +VI in the given medium were determined. To assign the observed peaks in the measured electropherograms to the correct oxidation states, a set of redox-stable analogues was investigated and the obtained retention times were compared with those of the Pu measurements.

In Sections 3.1 and 3.2, first the electropherograms of the redox-stable analogues and then the results for the Pu mobility measurements are presented and discussed. In Section 3.3, a more systematic approach for the calculation of electrophoretic mobilities is introduced.

3.1 ELECTROPHORETIC MOBILITIES OF REDOX-STABLE OXIDATION STATES

As already mentioned, a set of redox-stable elements as homologues for the different Pu oxidation states was investigated first. These analogues for the +III to the +VI oxidation states were ¹⁵³Eu(III), ²³²Th(IV), ²³⁷Np(V), and ²³⁸U(VI). All elements were mixed in one and the same solution with a concentration of $c_i = 5 \cdot 10^{-7}$ M each. The measurements were undertaken with both 1 M HCl and 1 M HClO₄ as sample background to test whether there exists an influence of the acidic medium on the electrophoretic mobility measured in the 1 M acetic acid medium. If this was the case, a difference between a non-complexing agent (HClO₄) and a weakly complexing agent (HCl) with respect to the obtained electrophoretic mobilities would occur. A typical electropherogram is shown in Figure 2. The electrophoretic mobilities

3.3 Publication: Investigation of the Electrophoretic Mobility of the Actinides Th and U-Am in Different Oxidation States

calculated using Equation (1) for the different elements in both 1 M HCl and 1 M HClO₄ solutions are given in Table 2. As one can see from these values, the choice of the medium in which the oxidation states were prepared has no significant effect on the electrophoretic migration of the ions. The two values for the electrophoretic mobility of each element are nearly identical within the limits of error. The 100-fold dilution during sample preparation for CE-ICP-MS measurements and the high excess of acetic acid on the capillary create a medium in which the acid of the initial solution, i.e., HCl or HClO₄, becomes negligible.

Table 2. Results for the electrophoretic mobilities of the redox analogues (stock solutions: 1 M HCl and 1 M HClO₄).

medium stock solution	mobilities/10 ⁻⁴ $\frac{\text{cm}^2}{\text{Vs}}$				
	Eu(III)	Am(III)	Th(IV)	Np(V)	U(VI)
1 M HClO ₄	4.19 (± 0.11)	3.86 (± 0.10)	2.18 (± 0.04)	2.09 (± 0.14)	1.51 (± 0.09)
1 M HCl	4.10 (± 0.09)	3.92 (± 0.03)	2.24 (± 0.11)	2.03 (± 0.08)	1.48 (± 0.04)

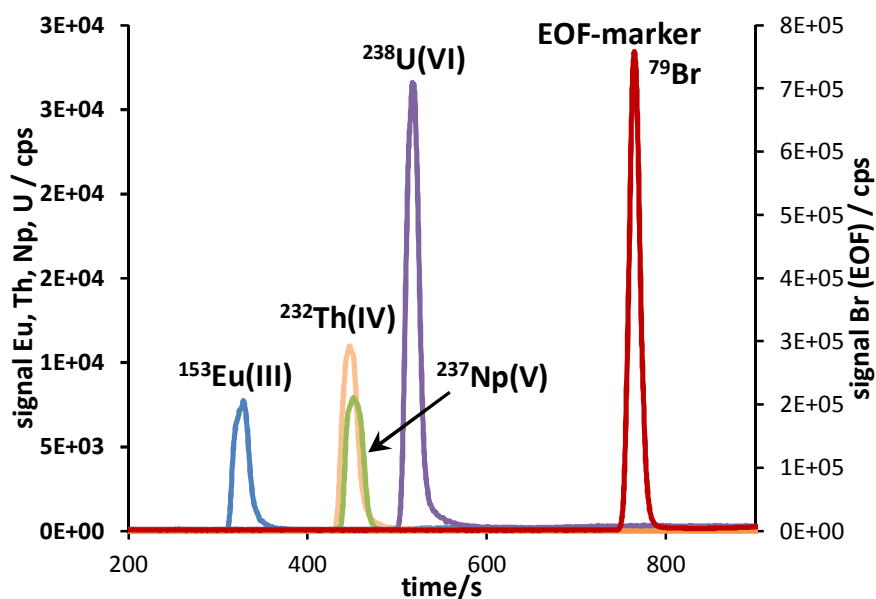


Figure 2. Electropherogram of the redox-stable analogues (stock solution: 1 M HCl).

As can be seen in the figure above, both for the masses of the investigated species and the mass of the EOF marker a sharp signal was obtained. The apparent differences in the peak areas result from discrepancies in the ionization efficiencies of the elements in the plasma of the ICP-MS system and, in case of Eu, from the fact that only mass 153 was detected, which has a natural abundance of just 52.2% (mass 151 with 47.8% was not detected).

3. Determination of Electrophoretic Mobilities with CE-ICP-MS

The detected retention times increase from ^{153}Eu via ^{232}Th and ^{237}Np to ^{238}U , which corresponds to the reverse of the trend for the electrophoretic mobilities. Eu(III) migrates fastest, which results in the highest electrophoretic mobility, followed by Th(IV) and Np(V) . The slowest ion on the capillary is U(VI) , so this species has the lowest electrophoretic mobility. Following this order of elution for the different oxidation states of the analogues, we can summarize the order of the electrophoretic mobilities from high to low as follows:

$$\text{Eu(III)} > \text{Th(IV)} \approx \text{Np(V)} > \text{U(VI)} \quad (2)$$

At first sight this sequence seems to be the wrong way round, since generally speaking an ion is the faster the smaller its radius and the higher its electric charge. To explain the order shown in Equation (2) one has to examine the exact speciation of the ion instead of just looking at the formal oxidation number.

The investigated ions of uranium(VI) and neptunium(V) exist as uranyl and neptunyl cations. U(VI) occurs as UO_2^{2+} and Np(V) as NpO_2^+ . The effective charge of the ion on which the electric field acts is thus just +2 and +1, respectively. Eu(III) and Th(IV) appear as the free ions Eu^{3+} and Th^{4+} . This explains why Np(V) and U(VI) have smaller electrophoretic mobilities than Eu(III) and Th(IV) .

To understand the inverted elution of both Np(V) and U(VI) and also Eu(III) and Th(IV) one has to take into account the different complexation behavior of the individual ions with the surrounding ligands. In the present case, the main ligand is the acetate ion. The complexation with acetic acid leads to a shielding effect, so the applied electric field acts upon only a smaller effective charge. Furthermore in performing CE experiments one has to take into account not only the crystallographic or ionic radius, respectively, of the investigated ion but rather the radius of the first or even the second hydration sphere. This coordination radius significantly affects the overall size of the migrating ions. Investigations and theoretical considerations on this topic, especially on the trivalent lanthanide and actinide series, can be found in the literature by several groups (Lundqvist et al.²³, David, Fourest et al.²⁴⁻³⁰ and Rösch et al.³¹⁻³³). The order of elution for ions with similar speciation is consequently a measure of the degree of complexation as well as a measure of the values for the radii of the particular hydration spheres.

As a comparable measure of the hydration radius the mean metal-oxygen distance in the hydrated ion can be considered. In EXAFS studies the following bond distances were determined: 2.42 Å³⁴ for U(VI) , 2.49 Å³⁵ for Np(V) , 2.45 Å³⁶ for Th(IV) and 2.424 Å³⁷ for Eu(III) . Since the electrophoretic mobility is proportional to the quotient of charge q and radius r one has to compare these values to understand the order of elution in electrophoretic

3.3 Publication: Investigation of the Electrophoretic Mobility of the Actinides Th and U-Am in Different Oxidation States

measurements. By calculating this ratio with the ionic charge of the respective ions the following order results (q/r values in brackets): Np(V) (0.40) < U(VI) (0.83) < Eu(III) (1.24) < Th(IV) (1.63). Since the difference in the metal oxygen bond distances given above is $\leq 0.07 \text{ \AA}$, the order of the q/r values is governed by the ionic charge of the aquo ions. As one can see from Table 2, this calculated order of μ_i is not consistent with the experimental order. Because of the shielding effect of the acetate complexation the effective charge is lower than the ionic charge of the ion. For taking this influence into account we conducted a speciation calculation with the experimental conditions used in this work. From the speciation of each ion a mean effective charge q_{eff} was calculated (for details see the supplementary section). They resulted as 0.68 for U(VI), 0.85 for Np(V), 0.97 for Th(IV), and 2.15 for Eu(III). Neglecting size differences between different species, the predicted order of electrophoretic mobilities based on q_{eff} is: Eu(III) > Th(IV) \approx Np(V) > U(VI). This agrees with the experimental results (Figure 2, Table 2). Additionally, it is known for tetravalent actinides to have a strong tendency toward sorption on surfaces, so that it cannot completely be ruled out that the migration of the +IV actinides is slowed down by interactions with the inner capillary wall.³⁸

One can conclude that all the factors mentioned above have to be taken into account for the interpretation of a given order of electrophoretic mobilities. On the other hand it is possible to rationalize the measured mobilities of the ions based on their speciation during CE.

Besides the already discussed elements, a sample of Am(III) was investigated to compare the electrophoretic mobility of a trivalent actinide with the value of the lanthanide Eu(III). The results show that Am(III) has a similar mobility as Eu(III) whereby the migration of Am(III) is slightly slower. Nevertheless, it is also the fastest of all oxidation states. The metal-oxygen distance for Am(III) is 2.48 \AA ³⁹. This is also slightly higher than the value for Eu(III) aquo ion. The complex binding constants β for acetate given by the NIST database⁴⁰ are in a comparable range (for Am(III): $\log(\beta_1) = 2.8$, $\log(\beta_2) = 4.62$, $\log(\beta_3) = 5.51$; for Eu(III): $\log(\beta_1) = 2.77$, $\log(\beta_2) = 4.71$, $\log(\beta_3) = 5.52$). However, data provided by the Andra database⁴¹ indicate that Am(III) forms slightly more stable complexes ((for Am(III): $\log(\beta_1) = 2.94$, $\log(\beta_2) = 5.07$, $\log(\beta_3) = 6.54$; for Eu(III): $\log(\beta_1) = 2.9$, $\log(\beta_2) = 4.8$, $\log(\beta_3) = 5.6$). Besides this, actinides are known to have a greater degree of hydration than lanthanides^{23, 26}, which leads to a better shielding and thus to a lower effective charge.^{29, 30} Regarding these aspects it is conceivable that Am(III) migrates slower than Eu(III) under our experimental conditions. It should be noted, that some literature data show the opposite trend. Lundqvist et al.²³ obtained a faster relative migration velocity for Am(III) compared to Eu(III) in a (H,Na)ClO₄ medium (varying pH and ionic strength I) at 25 °C, but the values seem to be very similar to each other. The same was found by Fourest et al.²⁴ in a (H,Li)Cl medium (pH = 4 and varying

3. Determination of Electrophoretic Mobilities with CE-ICP-MS

I) at 25 °C, while in a later work²⁶ they state, that the actinides are less mobile than the respective lanthanides. Marin et al.⁴² published $\mu_e(\text{Am(III)}) = 4.25 \cdot 10^{-4} \frac{\text{cm}^2}{\text{Vs}}$ and $\mu_e(\text{Eu(III)}) = 3.75 \cdot 10^{-4} \frac{\text{cm}^2}{\text{Vs}}$ in (H,K)Cl medium determined by paper electrophoresis (15 °C, pH < 2.5 and $I = 5 \cdot 10^{-3}$ M). Furthermore in their work it is shown that the order of the electrophoretic mobilities is turned around for pH > 3.5 for the hydroxides ($\mu_e(\text{Am(OH)}^{2+}) = 0.90 \cdot 10^{-4} \frac{\text{cm}^2}{\text{Vs}}$ and $\mu_e(\text{Eu(OH)}^{2+}) = 2.38 \cdot 10^{-4} \frac{\text{cm}^2}{\text{Vs}}$). Rösch et al.³² determined ion mobilities by means of a glass capillary apparatus. Their values for the electrophoretic mobilities are $\mu_e(\text{Am(III)}) = 5.48(15) \cdot 10^{-4} \frac{\text{cm}^2}{\text{Vs}}$ and $\mu_e(\text{Eu(III)}) = 5.12(29) \cdot 10^{-4} \frac{\text{cm}^2}{\text{Vs}}$ for pH > 2.5 (25 °C, $I = 0.1$ M) in a (Na,H)ClO₄ medium. In a work using CE-ICP-MS by Topin⁴³ the electrophoretic mobilities are given as $\mu_e(\text{Am(III)}) = 4.62(15) \cdot 10^{-4} \frac{\text{cm}^2}{\text{Vs}}$ and about $\mu_e(\text{Eu(III)}) = 4.4(2) \cdot 10^{-4} \frac{\text{cm}^2}{\text{Vs}}$ in a (H,Na)Cl medium (25 °C, pH = 2.0 and $I = 0.1$ M). This given overview shows that the absolute values for the electrophoretic mobilities of Eu(III) and Am(III) are difficult to compare among each other since they have been measured under different experimental conditions (temperature, pH, ionic strength, and medium) that affect the migration velocity of a given ion. As to our knowledge the mobilities of Am(III) and Eu(III) have never been investigated before under the experimental conditions used in this work. The same is true for the electrophoretic mobilities of Th(IV) and U(VI), where no data are given in the literature for measurements in 1 M acetic acid.

The redox speciation of neptunium under comparable experimental conditions was investigated by Stöbener et al.⁵ However, in that work, no EOF marker was used, so no values for the electrophoretic mobility were available. In his later work,⁴⁴ the electrophoretic mobility is given as $\mu_e(\text{Np(V)}) = 2.0 \cdot 10^{-4} \frac{\text{cm}^2}{\text{Vs}}$, which is in good agreement with the present study. Graser et al.⁸ published a value of $\mu_e(\text{Np(V)}) = 2.4 (\pm 0.03) \cdot 10^{-4} \frac{\text{cm}^2}{\text{Vs}}$. This value is significantly higher than ours and Stöbener's, and cannot be reconciled with them without further analysis. A thorough discussion of this deviation, by interpreting additional Np oxidation states, can be found in Section 3.3. Other studies on the electrophoretic mobility of Np(V) were done by Aupiais et al.⁴⁵ They determined a value of $\mu_e(\text{Np(V)}) = 2.94(7) \cdot 10^{-4} \frac{\text{cm}^2}{\text{Vs}}$ for zero ionic strength (25 °C, HClO₄ medium with creatinine buffer, pH = 5.00). Rösch et al.⁴⁶ published a value of $\mu_e(\text{Np(V)}) = 2.25(20) \cdot 10^{-4} \frac{\text{cm}^2}{\text{Vs}}$ in 1 M (Na,H)ClO₄ solution (25 °C, $1 < \text{pH} < 2$). Furthermore it is shown in their work that the electrophoretic mobility of Np(V) in

3.3 Publication: Investigation of the Electrophoretic Mobility of the Actinides Th and U-Am in Different Oxidation States

acetic acid medium decreases of about 50% with the acetate concentration increasing from $c(\text{acetate}) = 10^{-3}$ M to $c(\text{acetate}) = 10^{-1}$ M. Once again, direct comparison of these data with our results is not possible because of the differences in the experimental conditions, but our values seem to fit well in the overall picture.

3.2 SEPARATION AND IDENTIFICATION OF PU OXIDATION STATES

For the investigation of the Pu oxidation states, the samples were prepared electrochemically starting from Pu(VI) as described above. With this method we were able to produce all four Pu oxidation states in the range from +III to +VI in 1 M HClO₄. During the CE-ICP-MS measurements it emerged that only Pu(IV) and Pu(VI) were stable under the given experimental conditions. Pu(III) was oxidized and Pu(V) disproportionated during dilution in 1 M acetic acid, so that only electropherograms of Pu(IV) and Pu(VI) were obtained. We were able to stabilize the +III oxidation state by adding an excess amount of hydroxyl ammonium hydrochloride. It was not possible to stabilize the +V oxidation state for the duration of one experiment. Due to this, a Pu(VI) aliquot was added to synthetic Opalinus Clay pore water (OPA PW) at pH 7.6 (the composition is described elsewhere)⁴⁷, yielding Pu(V) after several days.

The results are presented in Figure 3. Here the ICP-MS signal for mass 239 is plotted as a function of the electrophoretic mobility as calculated via Equation (1).

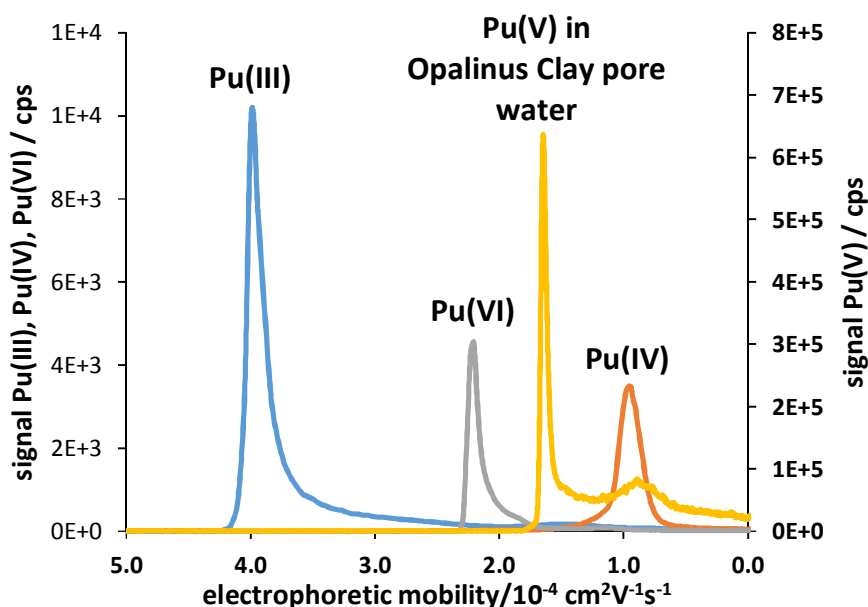


Figure 3. Electrophoretic mobilities of the different Pu species.

For the oxidation states +III, +IV, and +VI one peak was obtained. These samples contained no other oxidation states at concentrations higher than the detection limit of the used

3. Determination of Electrophoretic Mobilities with CE-ICP-MS

method. In the OPA PW sample, beside the dominant peak with the mobility assigned to Pu(V), a second, smaller peak with the mobility of Pu(IV) can be seen. Evidently, the medium here was also unable to completely preserve the +V oxidation state. In the UV-Vis spectrum only Pu(V) could be seen, so in this case a partial reduction from Pu(V) to Pu(IV) took place during the dilution step with 1 M acetic acid.

Table 3. Results for the electrophoretic mobilities of the Pu oxidation states (stock solution: 1 M HClO₄) and comparison with literature.

this work	mobility/ $10^{-4} \frac{\text{cm}^2}{\text{Vs}}$			
	Pu(III)	Pu(IV)	Pu(V)	Pu(VI)
1 M HClO ₄	3.92 (± 0.06)	0.96 (± 0.04)		2.20 (± 0.03)
OPA PW			1.65 (± 0.05)	
literature	Pu(III)	Pu(IV)	Pu(V)	Pu(VI)
Kuczewski ⁶ *	3.85	0.82	1.69	2.10
Graser ⁸	4.0 (± 0.07)	1.2 (± 0.08)	1.6 (± 0.06)	2.4 (± 0.08)
Topin ⁴³ **	4.61 (± 0.15)			
Topin ⁴⁹ **			1.93 (± 0.12)	
Topin ⁵⁰⁻⁵¹ **			2.360–2.405	

* calculated from the electropherograms shown in the publication

** different pH values and ionic strengths

The detected retention times increase from Pu(III) via Pu(VI) and Pu(V) to Pu(IV). Accordingly the order of the electrophoretic mobilities of the different Pu oxidation states can be summarized as follows:

$$\text{Pu(III)} > \text{Pu(VI)} > \text{Pu(V)} > \text{Pu(IV)} \quad (3)$$

The comparison of this order with the order of the redox-stable analogues in (2) shows that the +III and the +V oxidation states exhibit the same trend for Pu and the redox analogues. In both cases the +III ion is the one with the highest mobility. Eu(III) is here faster than Pu(III) (and also Am(III)), which can be explained by the considerations summarized in section 3.1. The hydrated radius of Pu(III) is with 4.65 Å²⁶ identical with the one of Am(III). This leads to electrophoretic mobilities that are also identical within the limits of error. Topin also determined identical values for $\mu_e(\text{Am(III)})$ and $\mu_e(\text{Eu(III)})$.⁴³ The absolute values must not be compared due to different experimental conditions.

3.3 Publication: Investigation of the Electrophoretic Mobility of the Actinides Th and U-Am in Different Oxidation States

In contrast, the order of elution for the tetravalent and the hexavalent oxidation state is interchanged. Th(IV) is the tetravalent ion with the highest electrophoretic mobility. In the order of the redox analogues it is the second fastest ion, whereas Pu(IV) is the slowest ion among the Pu oxidation states. Th(IV) has a lower effective charge Z_{eff} than Pu(IV)²⁹ ($Z_{\text{eff}}(\text{Th(IV)}) = 3.82$ and $Z_{\text{eff}}(\text{Pu(IV)}) = 3.97$)³⁰ which leads to a higher coordination number of water molecules in the first hydration sphere N ($N(\text{Th(IV)}) = 10.8$ and $N(\text{Pu(IV)}) = 9.8$)²⁹ and thus to a lower number of water molecules in the second hydration sphere H ($H(\text{Th(IV)}) = 13.41$ and $H(\text{Pu(IV)}) = 16.28$)²⁹. The overall number of hydrating water molecules and with that the size of the hydrated ion is accordingly lower for Th(IV) which leads to a higher overall electrophoretic mobility. The explanation for the order measured under our experimental conditions may be found in the values for the complexation constant with acetate. They are smaller for Th(IV) ($\log(\beta_1) = 5.24$, $\log(\beta_2) = 9.44$)⁴¹ than for Pu(IV) ($\log(\beta_1) = 5.39$, $\log(\beta_2) = 10.09$)⁴⁸ This means that thorium has a lower degree of complexation, so that its charge is less shielded and due to this the mobility is higher.

The order given in (3) is identical for all the other probed actinides. The values of their electrophoretic mobilities and a detailed discussion are given in Section 3.3.

In Table 3 a summary of the Pu electrophoretic mobilities is given. Literature values are shown for comparison.

The comparison of our results with the literature shows that the values for the Pu oxidation states are in very good agreement. They are nearly identical within the limits of error in the studies that were performed under the same conditions as in our experiment.^{6,8}

The first investigation on the different Pu oxidation states was carried out by Kuczewski et al.⁶ In that work no electrophoretic mobilities were given due to the fact that no EOF marker was measured. We tried to recalculate the values from the electropherograms shown in that publication by calculating a theoretical retention time of the EOF marker from the electrophoretic mobility of the Np(V) species (which was also measured as a +V analogue) and our value for its electrophoretic mobility. All plutonium mobilities could then be determined using Equation (1) as explained above. As one can see, this leads to results that are in good agreement with our values; deviations can be explained by the difficulty of the exact reading of the particular retention times. The elution order of the Pu oxidation states are the same, which is also confirmed in other works.^{7,52}

3. Determination of Electrophoretic Mobilities with CE-ICP-MS

Recently Graser et al.⁸ published values for the electrophoretic mobilities of different plutonium species. They were measured under the same conditions as used in the present work and, as shown in Table 3, they also agree with our results. In the case of Pu the order of elution is identical.

The comparison of our results with the results for Pu(III) and Pu(V) given in the works of Topin et al.⁴⁹⁻⁵¹ shows the necessity of comparing electrophoretic mobilities under the same experimental conditions, such as pH, ionic strength and temperature. The present work was carried out with a pH value of 2.4 and ionic strengths of $I = 1.0 \frac{\text{mol}}{\text{L}}$, whereas Topin et al. measured at lower ionic strengths and variable pH values. The deviations of the electrophoretic mobilities can thus be seen as a consequence of the varying experimental conditions.

3.3 TRENDS IN MOBILITY VALUES AND ESTIMATION OF MOBILITIES OF NON-MEASURABLE SPECIES

As already mentioned, it is difficult to measure very instable oxidation states with CE-ICP-MS because they are rapidly oxidized or reduced to more stable species. In the case of some instable ions such as Pu(III) we were able to stabilize them by adding a reducing agent without influencing their migration time. Unfortunately, some species, for example Np(III), are so instable that it was not possible to stabilize them for the duration of one experiment. Np(III) is oxidized to Np(IV) very rapidly and only a peak with an electrophoretic mobility attributable to the tetravalent species was obtained. The same problem occurred for U(III) and U(V).

Nevertheless, it is very interesting to know the electrophoretic mobilities for these species, so we tried a systematic approach to estimate them. In Table 4 a proposed schema of all investigated actinides with their possible oxidation states is shown. Besides the already discussed Np(V) electrophoretic mobility, we also measured the value for Np(IV), which was found to be $\mu_e(\text{Np(IV)}) = 1.42 \cdot 10^{-4} \frac{\text{cm}^2}{\text{Vs}}$. This is in good agreement with the literature data.^{5,8}

The values written in black are the ones we were able to measure with CE-ICP-MS. By arranging them in a systematic order as shown above, it is noticeable that the intervals between two corresponding pairs of values for the electrophoretic mobilities are always the same. This is true for both following a row of oxidation states for the same element or a column of elements with the same oxidation states.

3.3 Publication: Investigation of the Electrophoretic Mobility of the Actinides Th and U-Am in Different Oxidation States

Table 4. Schema of all investigated actinides and their possible oxidation states.

	electrophoretic mobilities of the oxidation states/ $10^{-4} \frac{\text{cm}^2}{\text{Vs}}$			
	III	IV	V	VI
Th		2.18		
U	3.25 ↓ 1.13	-2.91 → 0.34* ↓ 1.08	0.62 → 0.96 ↓ 1.13	0.55 → 1.51 ↓ 1.09
Np	4.38 ↓ -0.46	-2.96 → 1.42 ↓ -0.46	0.67 → 2.09 ↓ -0.44	0.51 → 2.60** ↓ -0.40
Pu	3.92 ↓ -0.06	-2.96 → 0.96	0.69 → 1.65	0.55 → 2.20
Am	3.86			

* sample was diluted in 1 M HCl instead of 1 M acetic acid

** sample was diluted in 1 M HClO₄ instead of 1 M acetic acid

For example, the difference between Np(IV) and Np(V) is $\Delta\mu_e(\text{Np(IV)} \rightarrow \text{Np(V)}) = 0.67 \cdot 10^{-4} \frac{\text{cm}^2}{\text{Vs}}$, while the difference for the Pu analogues is $\Delta\mu_e(\text{Pu(IV)} \rightarrow \text{Pu(V)}) = 0.69 \cdot 10^{-4} \frac{\text{cm}^2}{\text{Vs}}$.

Going down the particular oxidation state columns one can notice that the difference for the Np(IV)/Pu(IV) couple is, at $\Delta\mu_e(\text{Pu(IV)} \rightarrow \text{Np(IV)}) = 0.46 \cdot 10^{-4} \frac{\text{cm}^2}{\text{Vs}}$, identical within the errors with the value for the Np(V)/Pu(V) couple $\Delta\mu_e(\text{Pu(V)} \rightarrow \text{Np(V)}) = 0.44 \cdot 10^{-4} \frac{\text{cm}^2}{\text{Vs}}$. Knowing this one can now assume that the differences in the electrophoretic mobilities are also the same for other pairs of elements or oxidation states. Although Np(III) cannot be measured, we can predict its mobility by comparing the Np(III)/Np(IV) couple with the Pu(III)/Pu(IV) couple. By assuming the difference to be $\Delta\mu_e(\text{Np(III)} \rightarrow \text{Np(IV)}) = -2.96 \cdot 10^{-4} \frac{\text{cm}^2}{\text{Vs}}$ which is the same as for $\Delta\mu_e(\text{Pu(III)} \rightarrow \text{Pu(IV)})$, we obtained an electrophoretic mobility of Np(III) of $\mu_e(\text{Np(III)}) = 4.38 \cdot 10^{-4} \frac{\text{cm}^2}{\text{Vs}}$. Since there are no known literature data, this is currently the only possible way to estimate this mobility using experimental results from CE-ICP-MS measurements. With the same procedure we calculated the electrophoretic mobilities of the other elements written in red, U(III) and U(V). For them we estimated $\mu_e(\text{U(III)}) = 3.25 \cdot 10^{-4} \frac{\text{cm}^2}{\text{Vs}}$ and $\mu_e(\text{U(V)}) = 0.96 \cdot 10^{-4} \frac{\text{cm}^2}{\text{Vs}}$. These values have also not been previously published in the literature.

3. Determination of Electrophoretic Mobilities with CE-ICP-MS

To prove that this systematic approach is reasonable, we paid attention to the values written in green. In these cases we first calculated the electrophoretic mobilities by using the method explained above. It appeared therefore that the mobilities should be $\mu_e(\text{U(IV)}) = 0.29 \cdot 10^{-4} \frac{\text{cm}^2}{\text{Vs}}$ and $\mu_e(\text{Np(VI)}) = 2.64 \cdot 10^{-4} \frac{\text{cm}^2}{\text{Vs}}$. In later experiments we were then able to measure the experimental values as $\mu_e(\text{U(IV)}) = 0.34 \cdot 10^{-4} \frac{\text{cm}^2}{\text{Vs}}$ and $\mu_e(\text{Np(VI)}) = 2.60 \cdot 10^{-4} \frac{\text{cm}^2}{\text{Vs}}$. The comparison indicates clearly that the predicted mobilities are in very good agreement with the measured ones. Consequently, the presented approach seems to provide reliable results and the electrophoretic mobilities in red can be seen as reasonable values.

With the set of electrophoretic mobilities shown in Table 4 for the actinides uranium, neptunium and plutonium, a distinct trend is clearly visible. The sequence of the oxidation states for all elements is in the same order as given in Formula (4).

$$\mu_e(\text{Ac(III)}) > \mu_e(\text{Ac(VI)}) > \mu_e(\text{Ac(V)}) > \mu_e(\text{Ac(IV)}) \quad (4)$$

This order is also confirmed for plutonium by previous works.^{6,8}

For neptunium there are discrepancies: the electrophoretic mobilities of Np(V) and Np(VI) are given by Graser et al.⁸ as $\mu_e(\text{Np(V)}) = 2.4 (\pm 0.06) \cdot 10^{-4} \frac{\text{cm}^2}{\text{Vs}}$ and $\mu_e(\text{Np(VI)}) = 2.2 (\pm 0.05) \cdot 10^{-4} \frac{\text{cm}^2}{\text{Vs}}$, so here the order of the An(V) and An(VI) is contrary to the trend in the plutonium row and to our results. Since neptunium and plutonium are chemically very similar, no explanation for the reversed order in the electrophoretic mobilities of Np(V) and Np(VI) can be given there. Therefore, due to the overall trend for the actinides (Formula 4) and the systematic treatment shown in Table 4, we consider our sequence for the Np(V) and Np(VI) species to be valid.

4. SUMMARY AND CONCLUSION

CE-ICP-MS has proven to provide an appropriate experimental setup for trace analysis of actinides in different oxidation states and speciations in aqueous solutions. With the described setup it was also possible to carry out multi-element measurements in one solution.

We were able to measure all Pu oxidation states that are relevant under environmental conditions (III–VI) and to compare them with redox-stable analogues (Eu(III), Am(III), Th(IV), Np(V), U(VI)). The trend in the electrophoretic mobilities for the actinides U to Pu

3.3 Publication: Investigation of the Electrophoretic Mobility of the Actinides Th and U-Am in Different Oxidation States

using 1 M acetic acid as the background electrolyte was found to be $An(III) > An(VI) > An(V) > An(IV)$.

With a systematic approach we were able to predict values for the electrophoretic mobilities of actinides in instable oxidation states, which due to their instability cannot be measured by CE-ICP-MS.

In future works the results from this broad overview of the separation of different actinide speciations in model samples can be used for the investigation of unknown samples, for example from experiments being carried out in connection with the long-term safety analysis for a possible nuclear repository. By comparison of the electrophoretic mobilities measured for the species in an unknown sample with the ones known from the present work, one can infer the qualitative and (by calibration) quantitative composition of the sample.

Furthermore, with CE-ICP-MS measurements it is possible to gain insight into the complexation processes of actinides with several ligands in different oxidation states. This offers the possibility of a better understanding of the exact speciation of an actinide ion in a given solution.

ASSOCIATED CONTENT

Supporting Information

S-1: Detailed calculations for the acetate speciation of the metal ions and the resulting mean effective charge q_{eff} .

Table S-1: Species distribution of $5 \cdot 10^{-7}$ M metal ion in 1 M acetic acid at pH 2.38 calculated with Visual MINTEQ.

AUTHOR INFORMATION

Corresponding Author

* E-Mail: willberg@uni-mainz.de, treich@uni-mainz.de

ACKNOWLEDGMENT

We thank Dr. J. Aupiais for the inspiring discussions and the very helpful advices on the topic of determining electrophoretic mobilities of actinides by CE-ICP-MS.

We thank the two reviewers of the first version of this manuscript for their qualified and elaborate remarks.

This work was financially supported by the Federal Ministry for Economic Affairs and Energy under contract No. 02E10981.

3. Determination of Electrophoretic Mobilities with CE-ICP-MS

REFERENCES

- (1) Hoth, P.; Wirth, H.; Reinhold, K.; Bräuer, V.; Krull, P.; Feldrappe, H. *Endlagerung radioaktiver Abfälle in Deutschland*; BGR Bundesanstalt für Geowissenschaften und Rohstoffe: Hannover/Berlin, Germany, **2007**.
- (2) NAGRA: Projekt Opalinuston: *Bericht NTB 02-03*, **2002**.
- (3) Gompper, K. *Radioaktivität und Kernenergie*; Forschungszentrum Karlsruhe: Karlsruhe, Germany, **2000**; pp. 153–168.
- (4) Yoshida, Z.; Johnson, S. G.; Kimura, T.; Krsul, J. R.; Morss, L. R.; Edelstein, N. M.; Fuger, J.; Katz, J. J. *The Chemistry of the Actinide and Transactinide Elements – Chapter 7: Plutonium*, 3rd ed.; Springer: Heidelberg, Germany, **2006**.
- (5) Stöbener, N.; Amayri, S.; Gehl, A.; Kaplan, U.; Malecha, K.; Reich, T. *Anal. Bioanal. Chem.* **2012**, *404*, 2143–2150.
- (6) Kuczewski, B.; Marquardt, C. M.; Seibert, A.; Geckeis, H.; Kratz, J. V.; Trautmann, N. *Anal. Chem.* **2003**, *75*, 6769–6774.
- (7) Bürger, S.; Banik, N. L.; Buda, R. A.; Kratz, J. V.; Kuczewski, B.; Trautmann, N. *Radiochim. Acta* **2007**, *95*, 433–438.
- (8) Graser, C.-H.; Banik, N.; Bender, K. A.; Lagos, M.; Marquard, C. M.; Marsac, R.; Montoya, V.; Geckeis, H. *Anal. Chem.* **2015**, *87*, 9786–9794.
- (9) Olesik, J. W.; Kinzer, J. A.; Olesik, S. V. *Anal. Chem.* **1995**, *67*, 1–12.
- (10) Michalke, B. *Electrophoresis* **2005**, *26*, 1584–1597.
- (11) Kannamkumarath, S. S.; Wrobel, K.; Wrobel, K.; B'Hymer, C.; Caruso, J. A. *J. Chromatogr., A* **2002**, *975*, 245–266.
- (12) Hein, C.; Sander, J. M.; Kautenburger, R. *J. Anal. Bioanal. Tech.* **2014**, *5*, 225–233.
- (13) Timberbaev, A. R. *Chem. Rev.* **2013**, *113*, 778–812.
- (14) Timberbaev, A. R.; Timberbaev, R. M. *Trends Anal. Chem.* **2013**, *51*, 44–50.
- (15) Engelhardt, H.; Beck, W.; Kohr, J.; Schmitt, T. *Angew. Chem.* **1993**, *105*, 659–680.
- (16) Sutton, K.; Sutton, R. M. C.; Caruso, J. A. *J. Chromatogr., A* **1997**, *789*, 85–126.
- (17) Yanes, G. E.; Miller-Ihli, N. I. *Spectrochim. Acta, Part B* **2004**, *59*, 883–890.
- (18) Yanes, G. E.; Miller-Ihli, N. I. *Spectrochim. Acta, Part B* **2005**, *60*, 555–561.

3.3 Publication: Investigation of the Electrophoretic Mobility of the Actinides Th and U-Am in Different Oxidation States

- (19) McLean, J. A.; Minnich, M. G.; Iacone, L. A.; Liu, H.; Montaser, A. *J. Anal. At. Spectrom.* **1998**, *13*, 829–842.
- (20) Amayri, S.; Jermolajev, A.; Reich, T. *Radiochim. Acta* **2011**, *99*, 349–357.
- (21) Gaona, X.; Wieland, E.; Tits, J.; Scheinost, A.; Dähn, R. *Appl. Geochem.* **2013**, *28*, 109–118.
- (22) Grossman, P.D.; Colburn, J.C.; Eds. *Capillary Electrophoresis Theory and Practice*; Academic Press: San Diego, 1992.
- (23) Lundqvist, R.; Hulet, E. K.; Baisden, P. A. *Acta Chem. Scand. A* **1981**, *35*, 653–661.
- (24) Fourest, B.; Duplessis, J.; David, F. *Radiochim. Acta* **1984**, *36*, 191–195.
- (25) Fourest, B.; Duplessis, J.; David, F. *Radiochim. Acta* **1989**, *46*, 131–135.
- (26) David, F. H.; Fourest, B. *New J. Chem.* **1997**, *21*, 167–176.
- (27) David, F. H.; Vokhmin, V. *J. Phys. Chem. A* **2001**, *105*, 9704–9709.
- (28) David, F.; Vokhmin, V.; Ionova, G. *J. Mol. Liq.* **2001**, *90*, 45–62.
- (29) David, F. H.; Vokhmin, V. *J. Nucl. Sci. Technol.* **2002**, *39*, 286–289.
- (30) David, F. H.; Vokhmin, V. *New J. Chem.* **2003**, *27*, 1627–1632.
- (31) Rösch, F.; Reimann, T.; Buklanov, G. V.; Milanov, M.; Khalkin, V. A.; Dreyer, R. *J. Radioanal. Nucl. Chem. Art.* **1989**, *134*, 109–128.
- (32) Rösch, F.; Khalkin, V. A. *Radiochim. Acta* **1990**, *51*, 101–106.
- (33) Mauerhofer, E.; Rösch, F. *Phys. Chem. Chem. Phys.* **2003**, *5*, 117–126.
- (34) Moll, H.; Geipel, G.; Reich, T.; Bernhard, G.; Fanghänel, T.; Grenthe, I. *Radiochim. Acta* **2003**, *91*, 11–20.
- (35) Reich, T.; Bernhard, G.; Geipel, G.; Funke, H.; Hennig, C.; Rossberg, A.; Matz, W.; Schell, N.; Nitsche, H. *Radiochim. Acta* **2000**, *88*, 633–637.
- (36) Moll, H.; Denecke, M. A.; Jalilehvand, F.; Sandström, M.; Grenthe, I. *Inorg. Chem.* **1999**, *38*, 1795–1799.
- (37) Persson, I.; D'Angelo, P.; De Panfilis, S.; Sandström, M.; Eriksson, L. *Chem. Eur. J.*, **2008**, *14*, 3056–3066.
- (38) Runde, W. *Los Alamos Sci.* **2000**, *26*, 392–411.

3. Determination of Electrophoretic Mobilities with CE-ICP-MS

- (39) Allen, P. G.; Bucher, J. J.; Shuh, D. K.; Edelstein, N. M.; Craig, I. *Inorg. Chem.* **2000**, *39*, 595–601.
- (40) Smith, R. M.; Martell, A. E.; Motekaitis, R. J. *NIST standard reference database 46, version 6.0*, NIST, Gaithersburg, MD, USA, **2003**.
- (41) Grivé, M.; Duro, L.; Colàs, E.; Giffaut, E. *Appl. Geochem.* **2015**, *55*, 85–94.
- (42) Marin, R.; Kikindai, T. *Compt. Ren. Ser. C* **1969**, *268*, 1–4.
- (43) Topin, S. Etude des Interactions Entre les Éléments Transuraniens et quelques Ligands Environnementaux par le Couplage Électrophorèse Capillaire Spectrométrie de Masse à Source Plasma Générée par Couplage Inductif. Ph.D. Thesis, Université de Paris-Sud, Faculté des Sciences d'Orsay (Essonne), France, **2009**.
- (44) Stöbener, N. Elementspeziation von Neptunium im Ultraspurenbereich. Ph.D. Thesis, Johannes Gutenberg University, Germany, **2013**.
- (45) Aupiais, J.; Delorme, A.; Baglan, N. *J. Chromatogr. A*, **2003**, *994*, 199–206.
- (46) Rösch, F.; Hung, T. K.; Dittrich, S.; Ludwig, R.; Buklanov, G. V.; Dreyer, R.; Khalkin, V. A. *Isotopenpraxis*, **1990**, *26*, 355–363.
- (47) Van Loon, L. R.; Soler, J. M.; Bradbury, M. H. *J. Contam. Hydrol.* **2003**, *61*, 73–83.
- (48) Schwabe, K.; Nebel, D. *Z. Phys. Chem.* **1962**, *220*, 339–354.
- (49) Topin, S.; Aupiais, J.; Moisy, P. *Electrophoresis* **2009**, *30*, 1747–1755.
- (50) Topin, S.; Aupiais, J.; Baglan, N. *Radiochim. Acta* **2010**, *98*, 71–75.
- (51) Topin, S.; Aupiais, J.; Baglan, N.; Vercouter, T.; Vitorge, P.; Moisy, P. *Anal. Chem.* **2009**, *81*, 5354–5363.
- (52) Ambard, C.; Delorme, A.; Baglan, N.; Aupiais, J.; Pointurier, F.; Madic, C. *Radiochim. Acta* **2005**, *93*, 665–673.

4. DETERMINATION OF STABILITY CONSTANTS WITH CE-ICP-MS

Besides the measurement of electrophoretic mobilities of metal ions as described in the previous chapter, CE-ICP-MS can also be used for the determination of stability constants.

In this work, this method was employed for the investigation of complexes of actinides, namely Am(III), Th(IV), Np(V) and U(VI), with several ligands (acetate, propionate, gluconate, citrate). In this context, it can again be taken advantage of the low detection limits of the CE-ICP-MS coupling compared to otherwise applied methods such as UV-Vis spectroscopy. This enables for the investigation of environmentally-relevant systems as pictured in the introduction section.

In the following chapter, the experiments are described for each respective ligand and the results are compared among each other. Furthermore, the theoretical and mathematical background of the evaluation of the measured results is explained.

4.1 THEORETICAL CONSIDERATIONS

CE, also in combination with ICP-MS, has often been employed for the determination of stability constants of metal complexes with various ligands. In Section 2.5 (and in the Introduction Section in the acetate publication following hereafter), a literature overview of this topic is provided with special attention being paid to the complexation of actinides (see Table 4). At this point it is therefore just referred to the references cited therein. In the acetate publication, also a short theoretical consideration of the mathematical background in determining stability constants by CE is given. Since this is only done for the special case of acetate as a ligand, in the following a more general description is given being valid for all the ligands investigated in this work. Furthermore, some additional aspects are depicted here for more detailed insight. The basis of these information again is the literature mentioned above if not stated otherwise.

In the complexation reaction of an actinide An^{n+} with the charge $n+$ with a Ligand L^{m-} with the charge $m-$, in principle several complexes can be formed differing in their number of ligands i and thus in the overall charge $(n + i \cdot m)$. The general formula of such a complex is $An-L_i^{(n+i \cdot m)}$. For $i = 0$ only the non-complexed actinide is described. Even so the formation of complexes with more than one central metal ion is also possible this is skipped in this introductory explanation.

Each of these complexes exhibit an individual, well-defined electrophoretic mobility μ_i , but two different cases have to be considered. In the first case, the complexes are stable on the time scale of a CE experiment. This means, that two or more species can be separated on basis of their differences in the electrophoretic mobilities and thus can be detected as several

4. Determination of Stability Constants with CE-ICP-MS

separated peaks. This also applies if a mixture of different oxidation states of one and the same actinide is present in the sample solution. Such a case is discussed and experimentally examined in Section 5.

The complexes investigated in the present chapter in contrast are all so called labile complexes. They are not stable on the time scale of an electrophoretic separation because a fast exchange of the ligands between the metal ions takes place. More details about disequilibrium effects in CE and the concept of stabile and labile complexes is given in [04SON].

The ligands have a shielding effect on the positive charge of the central ion. As a consequence, the applied electric field acts on an average charge of the respective actinide defined by the average number of ligands present in its vicinity. Consequently, the measured electrophoretic mobility is an effective electrophoretic mobility μ_{eff} composed of the sum of the μ_i of the individual free species weighted by their mole fractions x_i (Equation (4.1)). N represents the maximum number of ligands in the respective complex system.

$$\mu_{\text{eff}} = \sum_{i=0}^N \mu_i x_i. \quad (4.1)$$

In the electropherograms therefore only one peak with the corresponding effective electrophoretic mobility is obtained.

If two or more metal ions are hard to separate by CE because of very small differences in their electrophoretic mobilities μ_i , this effect can also be exploited to improve the separability. Differences in the stability constants of the respective metal ions with a given ligand lead to greater differences in the effective electrophoretic mobilities μ_{eff} [99JAN].

As already mentioned, the aim of the experiments described in this chapter was to determine the successive stability constants β_i of actinides with several ligands. The β_i are defined as given in Equation (4.2). The square brackets indicate molar concentrations.

$$\beta_i = \frac{[\text{An-L}_i^{(n+i\cdot m)}]}{[\text{An}^{n+}][\text{L}^{m-}]^i}. \quad (4.2)$$

For the free actinide ($i = 0$) of course no stability constant can be calculated and $\beta_0 = 1$.

The mole fraction x_i are defined as depicted in Equation (4.3).

$$x_i = \frac{[\text{An-L}_i^{(n+i\cdot m)}]}{\sum_{j=0}^N [\text{An-L}_j^{(n+j\cdot m)}]}. \quad (4.3)$$

By combining Equations (4.2) and (4.3) and inserting the result in Equations (4.1) one obtains Equations (4.4).

4.1 Theoretical Considerations

$$\mu_{\text{eff}} = \frac{\mu_0 + \sum_{i=1}^N \mu_i \beta_i [L^{m-}]^i}{1 + \sum_{i=1}^N \beta_i [L^{m-}]^i} \quad (4.4)$$

Hereby, μ_0 describes the electrophoretic mobility of the non-complexed actinide. As one can see, the stability constants β_i can be obtained from the relationship of the free ligand concentration $[L^{m-}]$ and the corresponding effective electrophoretic mobility μ_{eff} .

$[L^{m-}]$ was adjusted by varying the pH value of the sample solution. The concentration of free ligands $[L^{m-}]$ is then defined by the acidity constant pK_a of the corresponding protonated acid with the initial concentration c_0 by Equation (4.5) for monoprotic acids.

$$[L^{m-}] = \frac{c_0 \cdot 10^{-pK_a}}{10^{-pK_a} + 10^{-pH}} \quad (4.5)$$

By plotting the free ligand concentration $[L^{m-}]$ against the effective electrophoretic mobility μ_{eff} and fitting these experimental data with the function given in Equation (4.4), values for the electrophoretic mobility of the individual free species μ_i and the complex binding constants β_i can be obtained. The maximum number of ligands N for a given actinide ligand system is usually not known from the start. Because of this, different fits for varying numbers of N were conducted. The results presented in the following sections are always relating to the best achievable fits. The fits were performed with Origin 7 software (OriginLab Corporation, Northampton, Massachusetts, USA) by a least-squares curve fitting method using the Levenberg–Marquardt algorithm. In order to obtain reliable values, constraints can be formulated. The choice of these constraints is based on physical and chemical requirements. In general, four requirements were presumed, as follows:

1. The electrophoretic mobility of a neutral complex is zero.
2. Complexes with a positive charge have an electrophoretic mobility greater than zero; for negative complexes the electrophoretic mobility is less than zero.
3. The values for the electrophoretic mobilities decrease with increasing number of associated ligands.
4. The values for the complex binding constants β_i are greater than zero and increase with increasing ligand number. (This constraint is based on the available literature data.)

Additionally to that, in some cases individual constraints based on the experimental results were formulated. These are described in the following in the respective Sections.

It is important to note that stability constants thus determined are just apparent constants. They are only valid for the applied experimental conditions, e.g. the ionic strength.

4. Determination of Stability Constants with CE-ICP-MS

Thermodynamic stability constants β_i^0 for $I = 0$ M can be derived from these values by Equation (4.6).

$$\beta_i^0 = \beta_i \frac{\gamma_{\text{An-L}_i^{(n+i\cdot m)}}}{\gamma_{\text{An}^{n+}} \gamma_{\text{L}_i^{m-}}}. \quad (4.6)$$

For the calculation of the activity coefficients γ_i different models can be used in dependence of the ionic strength I . For $I = 0.3$ M, as employed in this work, the Davies equation, based on the Debye-Hückel theory, is a suitable approximation (Equation (4.7)) [12POI]. z_i is the charge of the compound i .

$$\log(\gamma_i) = -0.509 z_i^2 \left(\frac{\sqrt{I}}{1+\sqrt{I}} - 0.3 I \right). \quad (4.7)$$

4.2 DETERMINATION OF THE FREE MOBILITIES OF THE ACTINIDES WITHOUT LIGANDS

Before starting with the determination of the stability constants it seemed reasonable to first examine the electrophoretic mobilities of the actinides under investigation without any complexing ligand. This is because according to Equation (4.4), the electrophoretic mobility μ_i of the free, uncomplexed actinide An^{n+} is one of the required fitting parameters. Knowing that value allows to define narrow limits for this parameter during the fitting procedure since it should be identical (or at least very similar) in all the investigated systems. The percentage of uncomplexed actinides increases with decreasing pH value of the sample solution because the free ligand concentration also decreases (see Equation (4.5)). Consequently, the measurements of μ_i for the free actinides An^{n+} were also carried out in a low pH region in order to achieve a preferably good comparability.

4.2.1 EXPERIMENTAL PROCEDURE

Four samples with pH values of 0.56, 1.07, 1.48 and 1.82 were prepared in a perchloric acid medium because ClO_4^- is known to be a non-complexing ligand [06CHO]. The ionic strength was set to $I = 0.3$ M in accordance with the stability constant experiments by the addition of appropriate amounts of sodium perchlorate monohydrate. These solutions were used as the BGE for the initial flushing of the capillary. To the rest of the solutions, few μL of the respective actinides were added to yield concentrations of $c(\text{Am}^{3+}) = c(\text{NpO}_2^+) = 5 \cdot 10^{-8}$ M and $c(\text{Th}^{4+}) = c(\text{UO}_2^{2+}) = 2 \cdot 10^{-7}$ M. The total sample volume was 20 mL each to make the addition of the actinide stock solutions negligible. Nevertheless, the pH values were controlled after sample preparation. 200 μL of the sample solution together with 1 μL 2-bromopropane as the EOF marker were then measured by CE-ICP-MS at $U = 10$ kV. For the pH = 0.56 sample, just 9 kV could be applied due to a high electric current.

4.2 Determination of the Free Mobilities of the Actinides Without Ligands

4.2.2 RESULTS AND DISCUSSION

The resulting electropherograms of the four CE-ICP-MS measurements are shown in Figure 8.

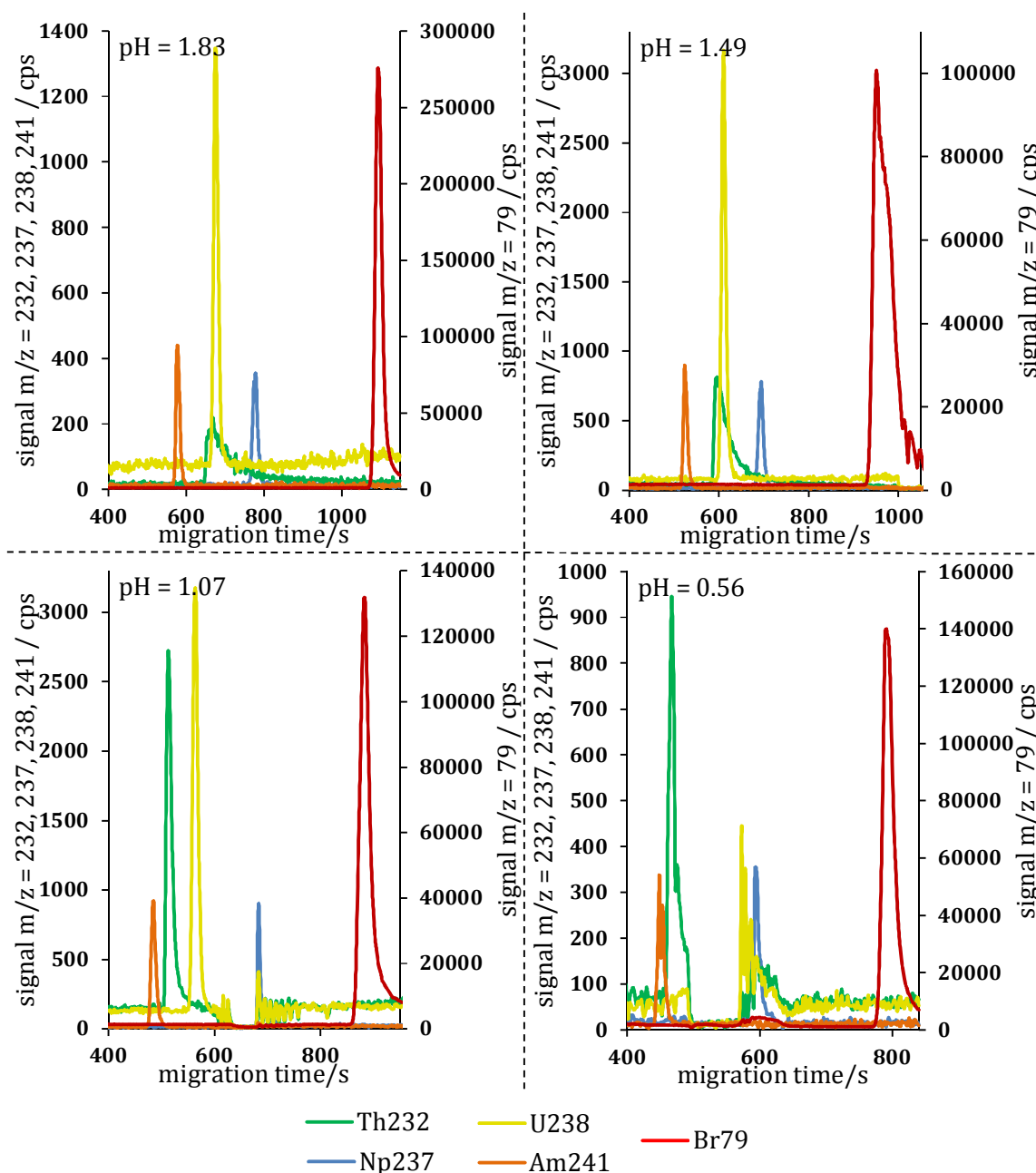


Figure 8: Electropherograms of the CE-ICP-MS measurements of the actinides Am(III), Th(IV), Np(V) and U(VI) in a non-complexing medium in dependence of the pH value at $I = 0.3$ M and $U = 10$ kV ($U = 9$ kV for the sample at pH = 0.56).

As one can see, for every actinide just one peak was obtained in all experiments. The corresponding values for the electrophoretic mobilities are depicted in Table 6. It has to be noted that the electropherogram obtained from the sample with the lowest pH value (and in parts of the second lowest, too) is difficult to evaluate because of a rather unsteady background signal. This results from a high electrical current at low pH values, which is a

4. Determination of Stability Constants with CE-ICP-MS

known problem in this pH region. To take this into account, the errors for the migration times of the respective species were set at $\Delta t_i = \Delta t_{\text{EOF}} = 8$ s in these samples which is considerably higher compared to the commonly applied values (see APPENDIX A2).

In Figure 9 a diagram with the obtained electrophoretic mobilities for the actinides as a function of the respective pH value of the sample solution is shown.

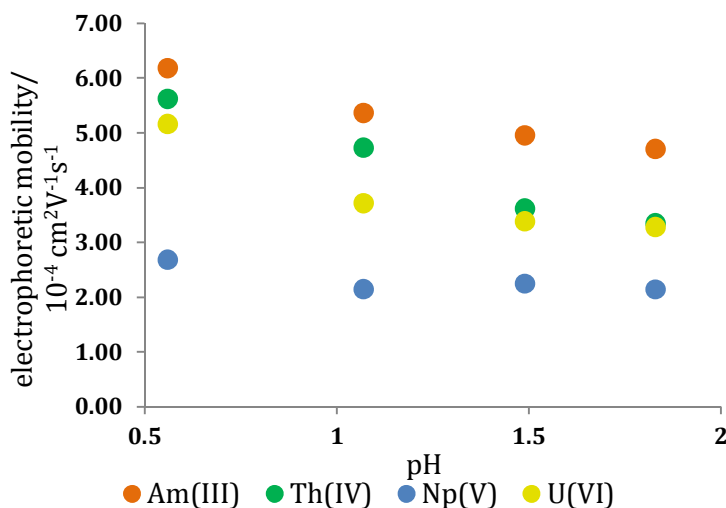


Figure 9: Trend of the electrophoretic mobilities of the actinides Am(III), Th(IV), Np(V) and U(VI) in a non-complexing medium in dependence of the pH value measured by CE-ICP-MS at $U = 10$ kV ($U = 9$ kV for the sample at $\text{pH} = 0.56$).

Table 6: Values of the electrophoretic mobilities of the actinides Am(III), Th(IV), Np(V) and U(VI) in a non-complexing medium at different pH values.

pH	electrophoretic mobility/ $10^{-4} \text{ cm}^2 \text{ V}^{-1} \text{ s}^{-1}$			
	Am(III)	Th(IV)	Np(V)	U(VI)
0.56	6.18 ± 0.28	5.62 ± 0.26	2.68 ± 0.17	5.16 ± 0.24
1.07	5.36 ± 0.22	4.73 ± 0.20	2.14 ± 0.12	3.71 ± 0.16
1.49	4.96 ± 0.13	3.61 ± 0.10	2.24 ± 0.07	3.38 ± 0.09
1.83	4.71 ± 0.11	3.35 ± 0.08	2.14 ± 0.06	3.28 ± 0.08

All four actinides exhibit decreasing electrophoretic mobilities with increasing pH. The differences in the electrophoretic mobilities from low to higher pH for a given ion shows a strong dependency on the oxidation state. It follows the order $\text{Th(IV)} > \text{U(VI)} > \text{Am(III)} > \text{Np(V)}$, whereby for Np(V) nearly no effect is noticeable. This order exactly corresponds with the strength of hydrolysis of actinides in different oxidation states [06CHO]. Since it is known that hydrolysis of actinides occurs even at low pH values and no other complexing partners are present in the sample solution, it can therefore be

4.2 Determination of the Free Mobilities of the Actinides Without Ligands

concluded that the differences in the electrophoretic mobilities result from different degrees of hydrolysis.

To verify this suspicion, a species calculation with the program Visual MINTEQ [14GUS] was conducted with the exact conditions applied in this experiments. The results show, that at the low pH values investigated only the 1:1 actinide:OH⁻ species has to be considered. Th(IV) has a share of 0.16% of Th(OH)³⁺ at pH 0.56 which rises up to 4.63% of Th(OH)³⁺ at pH 1.83. For U(VI) and Am(III) the values are 0.001% to 0.03% and 0.00003% to 0.001%, respectively. No Np(V)-OH⁻ species was found at all pH values. The percentage of the hydrolyzed species thus follows, as expected, the same order mentioned above. The decrease in the electrophoretic mobilities can consequently be attributed to a higher degree of complexation with OH⁻ ions at higher pH which shields parts of the positive charge of the actinide ions.

As a result of these investigations it can be noted that it is difficult to establish one fixed value for the electrophoretic mobilities of the free actinides at the given experimental conditions, because even without complexing agents present in the samples and at low pH values hydrolysis has to be considered. For determining the electrophoretic mobilities without any influence of hydrolyzed species it would be necessary to measure samples at even lower pH than conducted in this work. This is hardly possible because of the electrical current being too high while electrophoresis. This would lead to electropherograms that cannot be evaluated properly anymore. Nevertheless, it is beneficial to have a first estimation of an upper limit of the μ_i that can be used to refine the constraints and the starting values for this parameter during the fitting procedure for the determination of the stability constants. Consequently, in the following evaluations it was taken advantage of the findings presented here.

4. Determination of Stability Constants with CE-ICP-MS

4.3 PUBLICATION: DETERMINATION OF THE STABILITY CONSTANTS OF THE ACETATE COMPLEXES OF THE ACTINIDES AM(III), Th(IV), Np(V), AND U(VI) USING CE-ICP-MS

TABLE OF CONTENT GRAPHIC FOR PUBLICATION:

The graphic shows the mobility shift of the actinide peaks in selected electropherograms in dependence of the pH value. The red curve indicates a fitting result obtained by data evaluation as described in the manuscript.

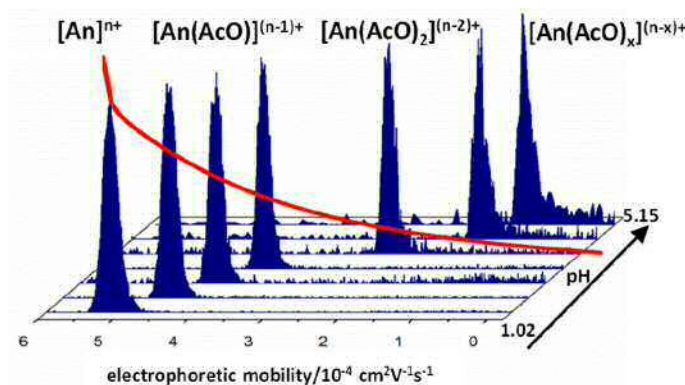


Figure 10: Table of Content Graphic for publication of the acetate manuscript.

AUTHOR CONTRIBUTIONS:

The samples were prepared by Daniel Leichtfuß under the guidance of Christian Willberger, Samer Amayri and Tobias Reich. The CE-ICP-MS measurements were performed by Christian Willberger, one UO_2^{2+} series and the NpO_2^+ series were measured by Samer Amayri. Data evaluation was performed by Christian Willberger. The conceptual planning of this investigation and the layout of the manuscript were done by Christian Willberger and Tobias Reich. The manuscript was written by Christian Willberger.


FURTHER REMARKS:

All sample compositions, measured electropherograms and detailed results are presented in the Supporting Information that can be found in the Appendix A5.1.


The numbering of the tables, figures and equations within the manuscript has remained unchanged and thus is not in accordance with the numbering of the rest of this work. The same is true for the citations.

One additional constrain in all fitting procedures was the restriction of the fitting parameter of the electrophoretic mobility of the free actinides to a certain range defined by the lowest measured electrophoretic mobility as the lower limit and the highest electrophoretic mobility as evaluated in Section 4.2 for the system without any ligands as the upper limit.

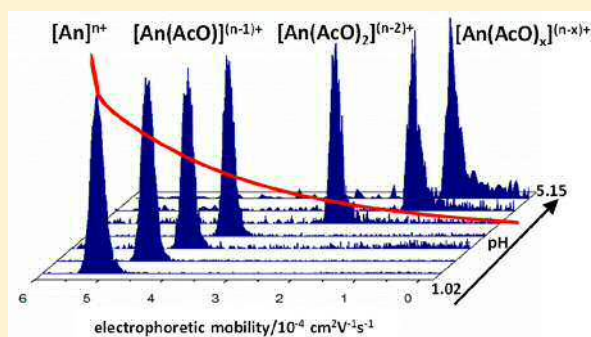
Determination of the Stability Constants of the Acetate Complexes of the Actinides Am(III), Th(IV), Np(V), and U(VI) Using Capillary Electrophoresis-Inductively Coupled Plasma Mass Spectrometry

Christian Willberger,* Daniel Leichtfuß, Samer Amayri, and Tobias Reich*

Institut für Kernchemie, Johannes Gutenberg-Universität Mainz, 55099 Mainz, Germany

 Supporting Information

ABSTRACT: Capillary electrophoresis-inductively coupled plasma mass spectrometry (CE-ICP-MS) was used to determine the stability constants of the actinides Am(III), Th(IV), Np(V), and U(VI) at an ionic strength of $I = 0.3$ M. The obtained stability constants were extrapolated to zero ionic strength by means of the Davies equation. For both U(VI) and Am(III), three consecutive acetate complexes with $\log(\beta_1^0) = 3.01 \pm 0.12$, $\log(\beta_2^0) = 5.27 \pm 0.07$, $\log(\beta_3^0) = 6.82 \pm 0.09$, and $\log(\beta_1^0) = 3.70 \pm 0.09$, $\log(\beta_2^0) = 5.35 \pm 0.08$, $\log(\beta_3^0) = 6.45 \pm 0.09$, respectively, could be identified. For Np(V), there was just one acetate complex, with $\log(\beta_1^0) = 1.56 \pm 0.03$. In the case of Th(IV), five different complex species could be determined: $\log(\beta_1^0) = 4.73 \pm 0.16$, $\log(\beta_2^0) = 8.92 \pm 0.09$, $\log(\beta_3^0) = 12.16 \pm 0.11$, $\log(\beta_4^0) = 12.96 \pm 0.87$, and $\log(\beta_5^0) = 14.39 \pm 0.16$. The actinides were selected with regard to their most stable oxidation state in aqueous solution so that four different oxidation states from +III to +VI could be investigated. A great benefit of CE-ICP-MS is the opportunity to measure at significantly lower concentrations compared to the available literature, allowing the study of actinide complexation in environmentally relevant concentration ranges. Furthermore, it is possible to analyze all four actinides simultaneously in one and the same sample.



1. INTRODUCTION

Geological clay formations are considered as host rocks for future high-level nuclear waste repositories. In deep geological repositories, the most toxic and long-lived radionuclides contained in spent nuclear fuels must be isolated as effectively as possible from human beings and the environment for up to one million years.¹ In case of a possible leakage of radionuclides from the repository, their chemical and geochemical behavior and their interaction with the surrounding biosphere must be evaluated.² Some actinides, namely, uranium (^{238}U , $t_{1/2} = 4.47 \times 10^9$ a), neptunium (^{237}Np , $t_{1/2} = 2.14 \times 10^6$ a), plutonium (^{239}Pu , $t_{1/2} = 2.41 \times 10^4$ a), and americium (^{241}Am , $t_{1/2} = 432.2$ a) are the main contributors to the long-term radiotoxicity of spent nuclear fuels in a radioactive waste repository.³ Therefore, a detailed knowledge of the aqueous speciation and thermodynamic data of these actinides is of great importance for the safety assessment of a possible nuclear waste repository since they provide the basis for modeling sorption and transportation of radionuclides. Besides a deep understanding of the redox-chemistry and hydrolysis of actinides in environmental systems, their complexation behavior with natural organic and inorganic ligands plays a key role in predicting their long-term migration in the near- and far-field of the repository.^{4,5}

Many studies have shown that in pore waters of different clay formations, such as Opalinus clay (OPA) and Callovo-

Oxfordian clay (COX), the content of low molecular weight organic compounds plays an important role making up large fractions of the total dissolved organic matter (DOM) (i.e., 36% in OPA, 88% in COX). The greatest proportion of the DOM is acetate, with the highest concentrations of 203 μM (OPA)⁶ and 1865 μM (COX).⁷ The acetate can act as a ligand for the actinides and thus affects their speciation, solubility, mobility, and toxicity in the aquatic environment. Besides this, acetate, being a small carboxylic acid, can be used as a model for more complex DOMs such as humic or fulvic acids. These substances are bigger organic molecules holding several carboxylic groups, which can also influence the geochemical behavior of radionuclides in the environment.⁸ Consequently, obtaining reliable thermodynamic data about the stability of these complexes at environmentally relevant concentrations ($<10^{-9}$ M) supports the safety assessment of a possible nuclear waste repository.

In the available literature the interactions of actinides with acetate ligands have been investigated using different methods such as extraction techniques, potentiometric and calorimetric approaches, X-ray absorption spectroscopy (XAS), and infrared absorption (IR), Raman scattering, and ultraviolet–visible (UV–vis) absorption spectroscopy.

Received: December 6, 2018

Published: March 28, 2019

The U(VI)–acetate system is the one most intensively studied. The first works were carried out by Ahrlund et al.^{9,10} who determined stability constants of three U(VI)–acetate complexes in sodium perchlorate solution using a potentiometric method. Subsequent studies by different groups on both stability constants and structural aspects are summarized in the literature.^{11–14} Most recently the stability constant for the 1:1 acetate/U(VI) complex was determined by Meinrath et al.¹⁵ by means of UV–vis spectroscopy. The majority of the works mentioned identified three successive complexes (1:1, 1:2, and 1:3) with a bidentate binding of the acetate ligand.

Less data are given in the literature for the NpO₂⁺–acetate system. Many works mention stability constants for just one or two different neptunyl complexes with acetate (see references given by Takao et al.¹⁶ and the publication of Rao et al.¹⁷). Takao et al.¹⁶ however showed the three-step complexation of Np(V) by acetate in aqueous solution by means of UV–vis–near-IR (NIR) and X-ray absorption fine structure (XAFS) spectroscopy and determined three successive values for log(β).

Since Th⁴⁺ is the ion with the highest charge investigated, it should be expected to be able to bind the highest number of acetate ligands. However, most of the available literature only gives data for thorium/acetate ratios up to 1:1,^{18,19} 1:2,^{20,21} or 1:3.²² Only Portanova et al.²³ and Rao et al.²⁴ identified five successive complexes.

The Am³⁺–acetate system was investigated in the 1960s and early 1970s by Choppin et al.²⁵ (1:1 complex only) and by Grenthe et al.²⁶ and Moskvina et al.^{27–29} (three successive complexes). The results are rather inconclusive since the values differ in part by about one logarithmic unit. Later works^{30–32} just mention the 1:1 complex. More recently, the Am complexation with acetate was investigated by means of extended X-ray absorption fine structure (EXAFS) spectroscopy, identifying bidentate acetate binding for all the three possible complexes.³³

Because of the difficulty of comparing different values for the stability constants determined under different experimental conditions (e.g., ionic strength, temperature, ligand concentration, or pH), we will just refer to the values given in the ANDRA Thermodynamic Database³⁴ and the NIST Standard Reference Database.³⁵ In both databases, the thermodynamic stability constants log(β^0) for zero ionic strength are given. The particular values are listed and compared to the values determined in our work in Section 3.6.

What all these mentioned publications (and analytical techniques, respectively) have in common is a detection limit considerably higher than the concentration range required for environmental investigations.

In this work, a coupling between capillary electrophoresis (CE) and inductively coupled plasma mass spectrometry (ICP-MS) was used for the determination of the complex binding constants of Am³⁺, Th⁴⁺, NpO₂⁺, and UO₂²⁺ with acetate ligands, representing a set of possible oxidation states for the actinides. Since these are the most stable oxidation states for each respective element, any impact of redox processes on our results can be ruled out. The benefit of the coupling between CE and ICP-MS is the possibility to investigate the complexation reactions at environmentally relevant concentrations due to the combination of the high separation capability of CE with the high sensitivity and the opportunity for multielement analysis of ICP-MS.^{36–39} Furthermore, the affinity CE method has proved to be an appropriate analytical

tool for the determination of complex binding interactions at low concentrations.^{40–42} Besides a wide utilization in the field of biochemistry,^{43–46} its application to metal complexation^{47,48} and more especially to actinide systems^{49,50} is also described extensively in the literature. Moreover, the coupling of CE to ICP-MS for this purpose has been reviewed.^{51,52}

Complex binding constants have been determined for actinides with CE-ICP-MS for various ligands by Aupiais et al.⁵³ such as sulfate and chloride,⁵⁴ carbonate,⁵⁵ nitrate,⁵⁶ oxalate,^{57–60} and diethylenetriaminepentaacetic acid.^{61,62} Furthermore, affinity CE has been used for the investigation of the interaction of Np(V)⁶³ and U(VI)¹³ with acetate, but no coupling with ICP-MS was performed. Therefore, for the actinide–acetate system there are no studies described using a coupling between CE and ICP-MS, and, as mentioned above, all the available literature for this system provides data for actinide concentrations orders of magnitude higher than those used in this work.

2. EXPERIMENTAL SECTION

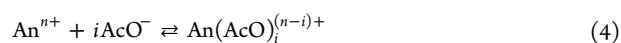
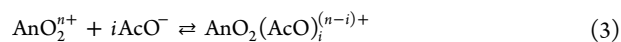
2.1. Determination of Complex Binding Constants by Capillary Electrophoresis. The capability to separate different species in CE is based on the fact that the different ions vary in their radius r and their charge q and by that in their electrophoretic mobilities μ_i . The electrophoretic mobility is determined experimentally by relating the retention time of the analyte t_i to the retention time of the electroosmotic flow (EOF) t_{EOF} at a given capillary length l and applied high voltage U (eq 1):

$$\mu_i = \frac{l^2}{U} \left(\frac{1}{t_i} - \frac{1}{t_{\text{EOF}}} \right) \quad (1)$$

In determining the complex binding constant of a given central ion with a certain type of ligand, the electrophoretic mobility of the central ion decreases with an increase in the number of ligands. This is because the ligand has a shielding effect on the positive charge of the metal ion, which is thus less influenced by the applied voltage. In the case of acetate there are labile complexes formed, meaning that the exchange of ligands and the adjustment of the chemical equilibrium is fast on the time scale of an electrophoretic experiment (more details can be found in the literature^{44,50,64}). Hence, only one peak is present in every electropherogram. The so-called effective electrophoretic mobility μ_{eff} of this peak is dependent on the relative ratios of the different complex species in the sample solution. It can be expressed as the sum of the electrophoretic mobility of each individual species μ_i , weighted by its mole fraction x_i (eq 2):

$$\mu_{\text{eff}} = \sum_{i=0}^N x_i \mu_i \quad (2)$$

The investigated complex equilibria are given in general in eq 3 for the neptunyl ($n = 1$) and uranyl ($n = 2$) acetate complexes and in eq 4 for the americium ($n = 3$) and thorium ($n = 4$) complexes.



An stands for the respective actinide and AcO[−] represents the acetate ligand. On the basis of this, the successive complex binding constants β_i are defined in eqs 5 and 6. The square brackets indicate molar concentrations.

$$\beta_i = \frac{[\text{AnO}_2(\text{AcO})_i^{(n-i)+}]}{[\text{AnO}_2^{n+}][\text{AcO}^-]^i} \quad (5)$$

$$\beta_i = \frac{[\text{An}(\text{AcO})_i^{(n-i)+}]}{[\text{An}^{n+}][\text{AcO}^-]^i} \quad (6)$$

The change of the effective electrophoretic mobility μ_{eff} of the actinide ions with respect to their degree of complexation was investigated as a function of the concentration of free acetate in the sample solution. The free acetate concentration $[\text{AcO}^-]$ can be calculated and adjusted through the pH value of the solution by means of the initial concentration c_0 and the acidity constant of the acetic acid as given in eqs 7 and 8. The ionic strength was kept constant at $I = 0.3$ M unless stated otherwise.

$$K_a = \frac{[\text{H}^+][\text{AcO}^-]}{[\text{AcOH}]} = \frac{[\text{H}^+][\text{AcO}^-]}{c_0 - [\text{AcO}^-]} \quad (7)$$

$$[\text{AcO}^-] = \frac{c_0 \cdot K_a}{K_a + [\text{H}^+]} = \frac{c_0 \cdot 10^{-\text{p}K_a}}{10^{-\text{p}K_a} + 10^{-\text{pH}}} \quad (8)$$

For the determination of the free acetate concentration $[\text{AcO}^-]$, the $\text{p}K_a$ value of acetic acid ($\text{p}K_a = 4.756 \pm 0.003^{65}$ at zero ionic strength) was corrected to an ionic strength of $I = 0.3$ M with activity coefficients calculated with the Davies equation (see eq 13). In the following evaluations the corrected value of $\text{p}K_a = 4.50$ was thus used. This value satisfyingly fits with experimental results for $I = 0.3$ M presented in the literature, e.g., $\text{p}K_a = 4.59 \pm 0.01$ by Tedesco et al.⁶⁶ and $\text{p}K_a = 4.42$ by Hynes et al.⁶⁷ with an average of $\text{p}K_a = 4.505$.

Now, the mole fractions x_i in eq 2 can be expressed as a function of the complex binding constant β_i and the free acetate concentration $[\text{AcO}^-]$ as shown in eq 9:

$$x_0 = \frac{1}{1 + \sum_{i=1}^N \beta_i [\text{AcO}^-]^i} \quad \text{and} \quad x_i = \frac{\beta_i [\text{AcO}^-]^i}{1 + \sum_{i=1}^N \beta_i [\text{AcO}^-]^i} \quad (9)$$

In this equation $i = 1, 2, \dots, N$ represents the complexed species with the respective number of ligands. Finally, combining eq 2 with eq 9 results in eq 10, which allows the determination of the complex binding constants β_i from the measured electrophoretic mobility μ_{eff} as a function of the free acetate concentration $[\text{AcO}^-]$. μ_0 is the electrophoretic mobility of the noncomplexed actinide.

$$\mu_{\text{eff}} = \frac{\mu_0 + \sum_{i=1}^N \mu_i \beta_i [\text{AcO}^-]^i}{1 + \sum_{i=1}^N \beta_i [\text{AcO}^-]^i} \quad (10)$$

At this point, a further benefit of the CE-ICP-MS method for the determination of stability constants becomes obvious. Because of the capability of analyzing very low actinide concentrations, a large ligand to metal ratio arises which drastically simplifies the data evaluation since the consumption of acetate ligand for the formation of the complex species can be neglected.

In order to extrapolate the stability constants to zero ionic strength, the results were corrected by the correspondent activity coefficients γ_i (see eq 11 for uranyl and neptunyl and eq 12 for thorium and americium).

$$\beta_i^0 = \beta_i \frac{\gamma_{\text{AnO}_2(\text{AcO})_i^{(n-i)+}}}{\gamma_{\text{AnO}_2^{n+}} \gamma_{\text{AcO}^-}} \quad (11)$$

$$\beta_i^0 = \beta_i \frac{\gamma_{\text{An}(\text{AcO})_i^{(n-i)+}}}{\gamma_{\text{An}^{n+}} \gamma_{\text{AcO}^-}} \quad (12)$$

For calculating the activity coefficients at 25 °C and at a given ionic strength I , the Davies equation was used, as given in eq 13.

$$\log(\gamma_i) = -0.509z_i^2 \left(\frac{\sqrt{I}}{1 + \sqrt{I}} - 0.3I \right) \quad (13)$$

In the ionic strength range employed in this work, this theory is described to be a suitable approximation. A comparison of some $\log(\beta_i^0)$ values of higher charged actinide-acetate species derived from the Davies equation with results obtained from the specific ion interaction (SIT) theory further proved the suitability of this extrapolation since the values were identical within the limits of error (see Table S10 in SI).

2.2. CE-ICP-MS System. For performing the electrophoresis experiments, an Agilent 7100 CE system was hyphenated to an Agilent 7500 ce ICP-MS (both Agilent Technologies, Santa Clara, California, USA). An effective coupling was realized using a MiraMist CE nebulizer (Burgener Research, Mississauga, Canada) in connection with a Scott-type spray chamber (AHS Analysentechnik, Tübingen, Germany). As a makeup electrolyte, a 1.25% HNO_3 solution with 10% ethanol and 5 ppb ^{89}Y , ^{103}Rh , ^{140}Ce , and ^{209}Bi (internal standards) was inserted via a syringe pump (PicoPlus, Harvard Apparatus, Holliston, Massachusetts, USA). The flow rate was adjusted experimentally to $5 \mu\text{L min}^{-1}$ as the optimal value.

The electrophoretic runs were performed in fused silica capillaries (Polymicro Technologies, Phoenix, Arizona, USA) with an inner diameter of 50 μm and a length of 76 cm. The high voltage was set to 10 kV. The capillary was filled with the background electrolyte of the respective experiment. The samples were prepared in conical microinserts of borosilicate glass (Carl Roth AG, Arlesheim, Switzerland), which were placed in polyethylene vials sealed with polyethylene olefin snap caps (both Agilent Technologies, Santa Clara, California, USA). The introduction into the capillary was by hydrodynamic injection (100 mbar for 8 s). Before every use the capillary was preconditioned by flushing with Milli-Q water, 0.1 M NaOH solution, 0.1 M HCl, and the background electrolyte. In order to change the complete background electrolyte between all measurements, the capillary was flushed for 15 min with the respective solution needed for the next experiment. Temperature was controlled at 25 °C by the air cooling device of the Agilent apparatus. Temperature rise in this system due to Joule heating was calculated to be on average 0.5 °C and to not exceed 1 °C.⁶⁸

Detection was carried out with the ICP-MS using a time-resolved analysis detection mode with a dwell time of 100 ms and a plasma power of 1550 W. To find the optimal parameters for the lens system and the argon flow rates before each day of measurement, tuning to the masses of the internal standards was executed. Carrier gas and makeup gas flow rates were adjusted to 0.86–1.15 L min^{-1} and 0.28–0.77 L min^{-1} , respectively. Data processing was conducted with MassHunter Workstation software (G7200B, Agilent Technologies, Santa Clara, California, USA).

2.3. Reagents. All chemicals employed were of pro-analysis quality or better. The dilutions were performed with Milli-Q water (18.2 M Ω , Synergy Millipore water system, Millipore GmbH, Schwalbach, Germany), and all solutions were filtered through 0.2 μm syringe filters (Nalgene, Rochester, New York, USA) to prevent a clogging of the capillary.

Sodium hydroxide, 2-bromopropane, and rhodium ICP-MS standard solution were from Merck (Darmstadt, Germany). Acetic acid and perchloric acid were supplied by Riedel-de Haën (Seelze, Germany), hydrochloric acid by Fisher Scientific (Loughborough, UK), and sodium perchlorate by Sigma-Aldrich (St. Louis, Missouri, USA). The ICP-MS elemental standard solution for bismuth, cerium, and yttrium were ordered from High-Purity Standards (Charleston, South Carolina, USA). As plasma gas, 4.6 Ar was used (Westfalen AG, Münster, Germany).

In-house stock solutions of known concentrations of $^{237}\text{Np(V)}$ and U(VI) (dep.) in 1 M perchloric acid were used. A stock solution of $^{241}\text{Am(III)}$ was prepared by evaporating an in-house Am(III) solution in nitric acid five times until near dryness and dissolving the residue in 1 M perchloric acid. The concentrations of Np(V) and Am(III) were checked by γ -ray spectrometry using the γ -lines at 86.5 keV for ^{237}Np and 59.5 keV for ^{241}Am with a high-purity Ge-detector (GMX-13280-S, EG & G ORTEC, USA) and the Canberra InSpector 2000 DSP Portable Spectroscopic Workstation (model IN2K, Canberra Industries Inc., USA), and Genie 2000 Gamma software (V. 3.0, Canberra Industries Inc., USA). The γ -ray spectrometer was calibrated with a multiple γ -ray emitting solution (serial number: 1850–27, Eckert & Ziegler Isotope Products, Braunschweig, Germany). The $^{232}\text{Th(IV)}$ stock solution was obtained by diluting the ICP-MS standard solution (Accu Trace, Accu Standard, New Haven, Connecticut, USA) of known concentration in 1 M perchloric acid.

2.4. Sample Preparation. Each sample was prepared starting from a 0.3 M acetic acid solution. By adding certain amounts of 11.6 M perchloric acid or 10 M sodium hydroxide solution, the different desired pH values were set. Experiments were conducted in a pH range starting from pH 1, where the actinides should be completely uncomplexed, to a maximum pH value at which hydroxide formation did not significantly influence the actinide–acetate system (pH 4.8 for Th(IV), pH 5.8 for U(VI), pH 6.0 for Np(V), and pH 5.7 for Am(III)). All samples were brought to an equal ionic strength of $I = 0.3$ M by adding appropriate amounts of sodium perchlorate. The detailed sample compositions are summarized in the Supporting Information, Tables S1–S9. Volumes of 200 μL of each of these solutions were added to a CE glass vial as the background electrolyte of the respective sample and were used for flushing the capillary before every experiment.

For every measuring series, solutions containing only one particular actinide were prepared. To 10 mL of the background electrolyte solutions, a few μL of the respective actinide stock solution was added to obtain the following actinide sample concentrations: $c(\text{Th}) = (1.00 \pm 0.09) \times 10^{-6}$ M, $c(\text{U}) = (1.42 \pm 0.13) \times 10^{-7}$ M, $c(\text{Np}) = (5.00 \pm 0.45) \times 10^{-8}$ M, and $c(\text{Am}) = (5.27 \pm 0.47) \times 10^{-8}$ M. The volume of added actinide solution was kept as small as possible so as to not significantly alter the ionic strength of the solution. Again, 200 μL of the actinide sample solution was transferred to a CE glass vial, together with 1 μL of 2-bromopropane as the EOF marker (detected via ICP-MS on the bromine mass 79). As can be seen from the data given above, the ligand concentration by far exceeds the concentration of the actinide ion, which is known to be a crucial point in accurately determining stability constants by measuring effective electrophoretic mobilities.⁶⁹

The pH value of the solution was controlled before and after the addition of the actinide stock solution, and no significant difference was observed. For the pH measurements, an inoLab/Cond pH 720 pH meter (WTW GmbH, Weilheim, Germany) equipped with a blue line 16 pH electrode (SI Analytics, Mainz, Germany) and temperature sensor (TFK 150, WTW GmbH, Weilheim, Germany) was used. Calibration was realized with certified commercial buffers (pH 4.01 and 6.87, SI Analytics, Mainz, Germany).

2.5. Data Treatment. By plotting the free acetate concentration $[\text{AcO}^-]$ against the effective electrophoretic mobility μ_{eff} and fitting these experimental data with the function given in eq 10, values for the electrophoretic mobility of the individual species μ_i and the complex binding constants β_i were obtained. The individual equations for the different actinide–acetate systems employed are given in the Supporting Information (eqs S1–S4). The fit was performed with Origin 7 software (OriginLab Corporation, Northampton, Massachusetts, USA) by a least-squares curve fitting method using the Levenberg–Marquardt algorithm. In order to obtain reliable values, constraints were formulated. The choice of these constraints was based on physical and chemical requirements. In general, four requirements were presumed, as follows:

- (1) The electrophoretic mobility of a neutral complex is zero.
- (2) Complexes with a positive charge have an electrophoretic mobility greater than zero; for negative complexes the electrophoretic mobility is less than zero.
- (3) The values for the electrophoretic mobilities decrease with increasing number of associated ligands.
- (4) The values for the complex binding constants β_i are greater than zero and increase with increasing ligand number. (This constraint is based on the available literature data.)

3. RESULTS AND DISCUSSION

All electropherograms are shown in the Supporting Information, Figures S1 and S2 (Am(III) series), S3 and S4 (Th(IV) series), S5–S7 (Np(V) series) and S8 and S9 (U(VI) series).

3.1. U(VI)–acetate System. In the case of the U(VI)–acetate system, three successive acetate complexes were determined. The respective function used for the fit is thus

given in eq 10 for $i = 0, 1, 2, 3$. The experimental data and the related results for the fit are shown in Figure 1.

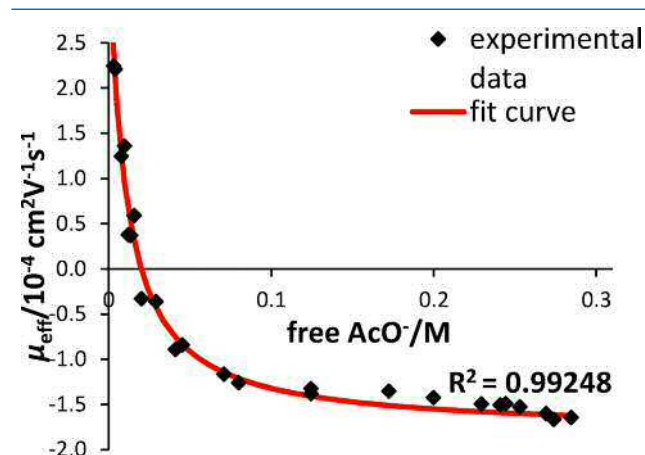


Figure 1. Measured effective electrophoretic mobilities μ_{eff} of the U(VI)–acetate series as a function of the free acetate concentration $[\text{AcO}^-]$ at $I = 0.3$ M with the related fit curve.

Since both positively and negatively charged complexes are formed depending on the free acetate concentration, it is reasonable that the values for the effective electrophoretic mobilities also change from positive at the beginning to negative for higher free acetate concentrations. As one can further see, the experimental data could be fitted satisfactorily with a coefficient of determination R^2 of 99.2%. The determined values for the complex binding constants at $I = 0.3$ M are given in Table 1. All electrophoretic mobilities of the

Table 1. Complex Binding Constants β_i for the Three Successive U(VI)–Acetate Complexes ($I = 0.3$ M)^a

i	β_i/M^{-i}	$\Delta(\beta_i)/\text{M}^{-i}$	$\log(\beta_i)$	$\Delta(\log(\beta_i))$
1	2.99×10^2	8.49×10^1	2.48	0.12
2	2.94×10^4	4.97×10^3	4.47	0.07
3	1.03×10^6	2.05×10^5	6.01	0.09

^aThe standard errors $\Delta(\beta_i)$ result from the fitting procedure.

individual species μ_i are summarized in Table 2 and discussed in Section 3.5. The results for extrapolation the complex binding constants to zero ionic strength and the comparison with literature data can be found in Section 3.6 (the same is true for the following actinide–acetate systems).

3.2. Np(V)–acetate System. For the Np(V)–acetate system, only the 1:1 complex could be identified, and the respective complex binding constant was determined (Table 3). Since in some parts of the literature^{16,34} the formation of three successive Np–acetate complexes has been described, we also tried to fit our experimental data with a function representing three binding constants. But with the constraints mentioned in Section 2.5, no solution could be obtained. The same result occurred, when considering the formation of 1:1 and 1:2 Np(V)–acetate complexes.

The experimental data and the respective fit can be seen in Figure 2. In contrast to the U(VI) data, no negative values for the electrophoretic mobilities were measured, even for high concentrations of free acetate. This is also an indication for just a 1:1 complex being formed because if the negatively charged 1:2 and 1:3 Np–acetate species were present to a significant

Table 2. Electrophoretic Mobility of the Individual Species μ_i^a

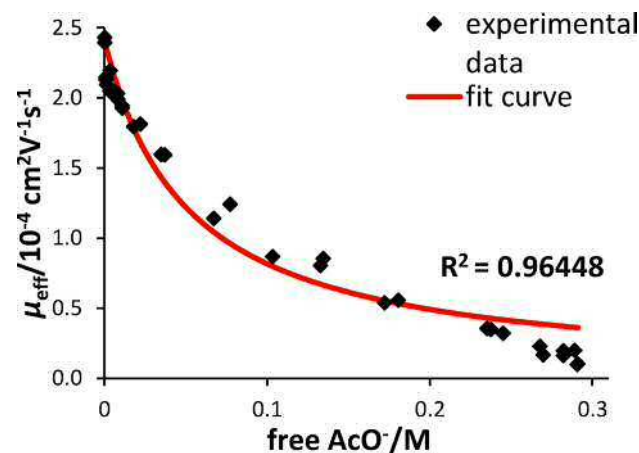
	$\mu_i/10^{-4} \text{ cm}^2 \text{ V}^{-1} \text{ s}^{-1}$	
U(VI)	UO_2^{2+}	3.4
	$[\text{UO}_2(\text{AcO})]^+$	1.9
	$[\text{UO}_2(\text{AcO})_2]_{\text{aq}}$	0.0 ^b
	$[\text{UO}_2(\text{AcO})_3]^-$	-1.8
Np(V)	NpO_2^+	2.4
	$[\text{NpO}_2(\text{AcO})]_{\text{aq}}$	0.0 ^b
Th(IV)	Th^{4+}	5.0
	$[\text{Th}(\text{AcO})]^{3+}$	3.4
	$[\text{Th}(\text{AcO})_2]^{2+}$	1.9
	$[\text{Th}(\text{AcO})_3]^+$	0.3
	$[\text{Th}(\text{AcO})_4]_{\text{aq}}$	0.0 ^b
	$[\text{Th}(\text{AcO})_5]^-$	-0.5
Am(III)	Am^{3+}	5.1
	$[\text{Am}(\text{AcO})]^{2+}$	3.8
	$[\text{Am}(\text{AcO})_2]^+$	1.7
	$[\text{Am}(\text{AcO})_3]_{\text{aq}}$	0.0 ^b

^aThe uncertainties are estimated to be $\Delta\mu_i = 0.1 \times 10^{-4} \text{ cm}^2 \text{ V}^{-1} \text{ s}^{-1}$ in all cases. ^bHeld constant during the fits.

Table 3. Complex Binding Constant β_1 for the Np(V)–Acetate Complex ($I = 0.3 \text{ M}$)^a

β_1/M^{-1}	$\Delta(\beta_1)/\text{M}^{-1}$	$\log(\beta_1)$	$\Delta(\log(\beta_1))$
19.4	1.4	1.29	0.03

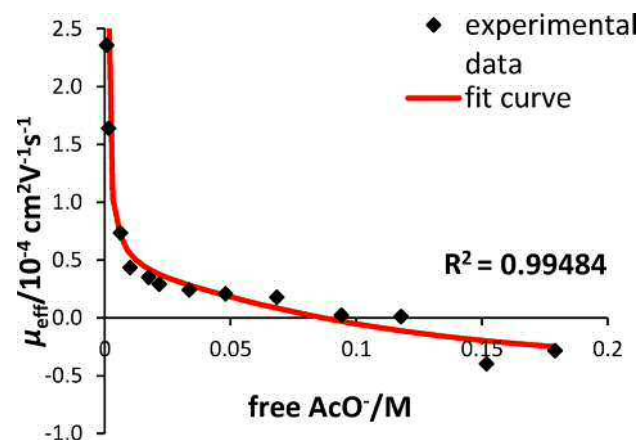
^aThe standard error $\Delta(\beta_1)$ results from the fitting procedure.

**Figure 2.** Measured effective electrophoretic mobilities μ_{eff} of the Np(V)–acetate series as a function of the free acetate concentration $[\text{AcO}^-]$ at $I = 0.3 \text{ M}$ with the related fit curve.

extent the overall electrophoretic mobility would become negative. The results for μ_i and β_i are given in Tables 2, 3, and 6.

3.3. Th(IV)–Acetate System. The complexation of Th(IV) with acetate leads to the most elaborate system. Because of the high charge of +4 of the thorium ion, it is able to bind the highest number of ligands of all the actinides investigated in this work. The experimental data and the related results for the fit for five successive complexes are shown in Figure 3.

In contrast to the other systems, in this case the results of the two data series are quite inconsistent. Consequently, the first data series was not used for the data evaluation, and the

**Figure 3.** Measured effective electrophoretic mobilities μ_{eff} of the Th(IV)–acetate series as a function of the free acetate concentration $[\text{AcO}^-]$ at $I = 0.3 \text{ M}$ with the related fit curve.

second measurement series was considered to be more reliable. As in the U(VI) example, both positive and negative effective electrophoretic mobilities were measured, substantiating the formation of a 1:5 thorium–acetate complex that is negatively charged. Since in this case the fit function (eq 10) contained 11 parameters, it was the most difficult system to process with the Origin software, and the errors are somewhat higher than in the other systems (for $\log(\beta_4)$ even higher than the absolute value itself). The results presented in Table 4 are the best

Table 4. Complex binding constants β_i for the five successive Th(IV)–acetate complexes ($I = 0.3 \text{ M}$)^a

i	β_i/M^{-i}	$\Delta(\beta_i)/\text{M}^{-i}$	$\log(\beta_i)$	$\Delta(\log(\beta_i))$
1	4.53×10^3	1.63×10^3	3.66	0.16
2	1.09×10^7	6.30×10^7	7.04	0.09
3	5.58×10^9	7.62×10^{10}	9.75	0.11
4	1.89×10^{10}	7.92×10^{11}	10.28	0.87
5	5.09×10^{11}	1.51×10^{13}	11.71	0.16

^aThe standard errors $\Delta(\beta_i)$ result from the fitting procedure.

values that could be calculated using all constraints mentioned above. In spite of these difficulties, the values for the complex binding constants are in good agreement with the literature, as discussed in Section 3.6.

3.4. Am(III)–Acetate System. As can be seen in Figure 4, for the Am(III)–acetate system no negative effective electrophoretic mobilities could be measured over the whole pH range. This indicates, as in the case of Np(V), that no negatively charged americium–acetate complexes are formed under these conditions. Consequently, three was set as the highest ligand number for the fit shown in Figure 4, which led to satisfactory results. The complex binding constants β_i at $I = 0.3 \text{ M}$ are given in Table 5.

3.5. Electrophoretic Mobilities of the Individual Species μ_i . In addition to the complex binding constants, the electrophoretic mobilities of the individual species μ_i have also been determined by means of the fit function given in eq 10. For the fitting procedure, the constraints given in Section 2.5 were used. As one can see from the results given in Table 2, a set of individual electrophoretic mobilities complying with these conditions could be obtained.

The order in the individual electrophoretic mobilities of the noncomplexed species corresponds to the charge of the

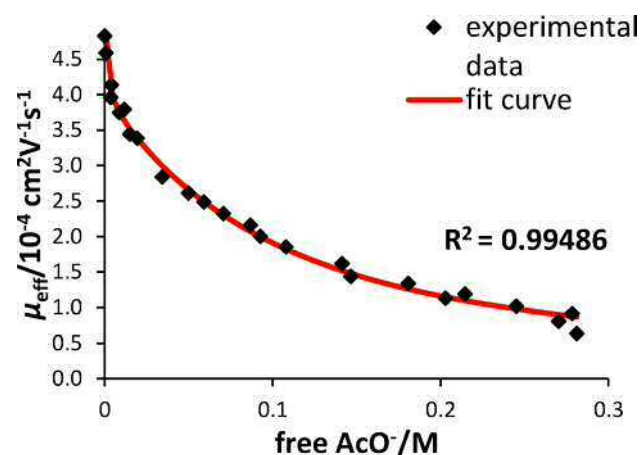


Figure 4. Measured effective electrophoretic mobilities μ_{eff} of the Am(III)–acetate series as a function of the free acetate concentration $[\text{AcO}^-]$ at $I = 0.3 \text{ M}$ with the related fit curve.

Table 5. Complex Binding Constants β_i for the Three Successive Am(III)–Acetate Complexes ($I = 0.3 \text{ M}$)^a

i	β_i/M^{-i}	$\Delta(\beta_i)/\text{M}^{-i}$	$\log(\beta_i)$	$\Delta(\log(\beta_i))$
1	7.80×10^2	1.57×10^2	2.89	0.09
2	1.01×10^4	1.90×10^3	4.00	0.08
3	6.82×10^4	1.36×10^4	4.83	0.09

^aThe standard errors $\Delta(\beta_i)$ result from the fitting procedure.

respective actinide ion. Thorium and americium, with the highest charges of +4 and +3, respectively, have the highest mobility; the least charged neptunyl ion is the slowest. Species with the same charge have comparable electrophoretic mobilities.

3.6. Extrapolation to Zero Ionic Strength. The complex binding constants β_i determined by CE-ICP-MS were extrapolated to thermodynamic stability constants β_i^0 at zero ionic strength by eqs 11 and 12, respectively, by means of the Davies equation given in eq 13.

The results are summarized in Table 6. For comparison with the literature, data available from the ANDRA database³⁴ as well as from the NIST database³⁵ are also given.

The binding constants of the different actinide–acetate systems obtained in this work are, in general, in good agreement with the literature data mentioned above; they all follow the same trends. Small deviations of our values from the literature data may be explained by the orders of magnitude differences in the concentrations of the actinides. As mentioned earlier, we investigated systems at environmentally relevant concentrations ($\sim 10^{-7} \text{ M}$), while the literature data are given for mostly millimolar concentrations. According to our experimental results, Np(V) forms just one complex under the given experimental conditions; this is in accordance with the findings of Pokrovsky and Choppin⁷⁰ and Rao et al.¹⁷ but disagrees with the results of Takao et al.,¹⁶ who quote values for three successive complexes. Since the CE-ICP-MS method enables reliable statements about the charge of a complex species, and no negative effective electrophoretic mobilities referring to a negatively charged Np(V)–acetate species were detected, it is reasonable that only the 1:1 complex is formed.

For the oxidation states III, IV, and VI of the investigated actinides, the successive acetate complexes exhibit increasing $\log(\beta_i^0)$ values, indicating an increase in the stability of the

Table 6. Thermodynamic Stability Constants β_i^0 for the Different Actinide–Acetate Systems and Comparison with the Literature

	$\log(\beta_i^0)$		
	this work	ANDRA database ³⁴	NIST database ³⁵
U(VI)	3.01 ± 0.12	3.02 ± 0.2	3.11
	5.27 ± 0.07	5.20 ± 0.3	5.04
	6.82 ± 0.09	7.03 ± 0.4	7.06
Np(V)	1.56 ± 0.03	1.32 ± 1.0	1.35
		3.42 ± 0.01	
		3.57 ± 0.01	
Th(IV)	4.73 ± 0.16	5.24 ± 0.15	4.69
	8.92 ± 0.09	9.44 ± 0.15	8.18
	12.16 ± 0.11	12.56 ± 0.50	10.85
	12.96 ± 0.87	14.38 ± 0.50	12.44
Am(III)	14.39 ± 0.16	15.37 ± 1.00	13.04
	3.70 ± 0.09	2.94 ± 0.5	2.8
	5.35 ± 0.08	5.07 ± 0.5	4.62
	6.45 ± 0.09	6.54 ± 0.5	5.51

complexes. By comparing the different actinide series, one can directly read off the tendency of the strength of the acetate complexes. Th(IV) forms by far the strongest complexes, while Np(V) tends to build the weakest complexes. The binding constants of U(VI) and Am(III) are rather similar and lie in between the two others. This sequence follows the usual order of increasing strength of actinide complexes $\text{AnO}_2^+ < \text{An}^{3+} \approx \text{AnO}_2^{2+} < \text{An}^{4+}$, which mirrors the effective charge of the actinide.⁷¹

4. SUMMARY AND CONCLUSIONS

The application of CE coupled to ICP-MS has proven to be a very suitable and appropriate analytical tool for the determination of the binding constants of complexes of different actinides with acetate. In particular, operation at very low concentrations is a benefit that allowed the investigation of systems in the environmentally relevant range. The results determined by this method for U(VI), Np(V), Th(IV), and Am(III) are given in Table 6. They are in good agreement with the available literature given for higher concentrations of the respective actinide. We were able to determine three successive complexes and the respective complex binding constants for U(VI) and Am(III), five for Th(IV), and only one for Np(V). Concerning the last, there is disagreement in the literature about the number of complexes. With this work we were able to show that no negative Np(V) acetate complex is formed, and thus just a 1:1 complex is to be expected. Our values may be used as a database for the long-term safety analysis of a future nuclear waste repository since they provide more accurate information about the actual conditions in such a system.

In order to improve further the databases for these concerns, the CE-ICP-MS system may be used in future works for the investigation of other actinides with acetate (e.g., plutonium), for the determination of binding constants with different ligands (such as citrate) and for different temperature ranges.

■ ASSOCIATED CONTENT

Supporting Information

The Supporting Information is available free of charge on the ACS Publications website at DOI: 10.1021/acs.inorgchem.8b03407.

Electropherograms of all measurement series, detailed composition of all samples, equations used to fit the experimental data, comparison of different extrapolations to zero ionic strength (PDF)

AUTHOR INFORMATION

Corresponding Authors

*(C.W.) E-mail: willberg@uni-mainz.de.

*(T.R.) E-mail: treich@uni-mainz.de.

ORCID

Tobias Reich: 0000-0002-5600-3951

Notes

The authors declare no competing financial interest.

ACKNOWLEDGMENTS

We thank Dr. J. Aupiais for fruitful discussions and helpful remarks on the topic of determining stability constants by CE-ICP-MS and two anonymous reviewers for their comments that improved the manuscript. This work was financially supported by the Federal Ministry for Economic Affairs and Energy (BMWi) under Contract No. 02E10981.

ABBREVIATIONS

AcOH, acetic acid; An, actinide; aq, dissolved in aqueous solution; CE-ICP-MS, capillary electrophoresis-inductively coupled plasma mass spectrometry; COX, Callovo-Oxfordian clay; DOM, dissolved organic matter; EOF, electroosmotic flow; (E)XAFS, (extended) X-ray absorption fine structure; OPA, Opalinus clay; UV-vis-near-IR, ultraviolet visible near-infrared; XAS, X-ray absorption spectroscopy.

REFERENCES

- (1) Hoth, P.; Wirth, H.; Reinhold, K.; Bräuer, V.; Krull, P.; Feldrappe, H. *Endlagerung radioaktiver Abfälle in Deutschland*; BGR Bundesanstalt für Geowissenschaften und Rohstoffe: Hannover/Berlin, Germany, 2007.
- (2) NAGRA; *Projekt Opalinuston Bericht NTB 02-03*, 2002.
- (3) Gompfer, K. *Radioaktivität und Kernenergie*; Forschungszentrum Karlsruhe: Karlsruhe, Germany, 2000; pp 153–168.
- (4) Grambow, B. Mobile fission and activation products in nuclear waste disposal. *J. Contam. Hydrol.* **2008**, *102*, 180–186.
- (5) Poinssot, C.; Geckeis, H. *Radionuclide Behaviour in the Natural Environment - Science, implications and lessons for the nuclear industry*; Woodhead Publishing: Oxford, UK, 2012.
- (6) Courdouan, A.; Christl, I.; Meylan, S.; Wersin, P.; Kretzschmar, R. Characterization of dissolved organic matter in anoxic rock extracts and in situ pore water of the Opalinus Clay. *Appl. Geochem.* **2007**, *22*, 2926–2939.
- (7) Courdouan, A.; Christl, I.; Meylan, S.; Wersin, P.; Kretzschmar, R. Isolation and characterization of dissolved organic matter from the Callovo-Oxfordian formation. *Appl. Geochem.* **2007**, *22*, 1537–1538.
- (8) Choppin, G. R. The role of natural organics in radionuclide migration in natural aquifer systems. *Radiochim. Acta* **1992**, *58-59*, 113–120.
- (9) Ahrland, S.; Bjellerup, L.; Rubin, I.; Saluste, E.; Stjernholm, R.; Ehrensvärd, G. On the complex chemistry of the uranyl ion. IV. The complexity of uranyl acetate. *Acta Chem. Scand.* **1951**, *5*, 199–219.
- (10) Ahrland, S.; Kullberg, L.; Roti, I.; Okinaka, H.; Kosuge, K.; Kachi, S. Thermodynamics of metal complex formation in aqueous solution. III. A calorimetric study of hydrogen sulphate and uranium(VI) sulphate, acetate, and thiocyanate. *Acta Chem. Scand.* **1971**, *25*, 3677–3691.
- (11) Bailey, E. H.; Mosselmans, J. F. W.; Schofield, P. F. Uranyl acetate speciation in aqueous solutions—An XAS study between 25°C and 250°C. *Geochim. Cosmochim. Acta* **2004**, *68*, 1711–1722.

(12) Lucks, C.; Rossberg, A.; Tsushima, S.; Foerstendorf, H.; Scheinost, A. C.; Bernhard, G. Aqueous uranium(VI) complexes with acetic and succinic acid: Speciation and structure revisited. *Inorg. Chem.* **2012**, *51*, 12288–12300.

(13) Sladkov, V. Uranyl complexation with acetate studied by means of affinity capillary electrophoresis. *J. Chromatogr. A* **2013**, *1289*, 133–138.

(14) Sladkov, V. Interactions of uranyl with acetate in aqueous solutions at variable temperatures. *J. Chem. Thermodyn.* **2014**, *71*, 148–154.

(15) Meinrath, G.; Kwiatek, D.; Hnatejko, Z.; Lis, S. Direct spectroscopic speciation of the complexation of U(VI) in acetate solution. *Monatsh. Chem.* **2014**, *145*, 1689–1696.

(16) Takao, K.; Takao, S.; Scheinost, A. C.; Bernhard, G.; Hennig, C. Complex formation and molecular structure of neptunyl(VI) and –(V) acetates. *Inorg. Chem.* **2009**, *48*, 8803–8810.

(17) Rao, L.; Tian, G.; Srinivasan, T. G.; Zanonato, P.; Di Bernardo, P. Spectrophotometric and calorimetric studies of Np(V) complexation with acetate at various temperatures from $T = 283$ to 343 K. *J. Solution Chem.* **2010**, *39*, 1888–1987.

(18) Usherenko, L. N.; Skorik, N. A. Stability of acetate complexes of scandium and thorium in water and aqueous ethanol mixtures. *Radiokhimiya* **1971**, *13*, 646–648.

(19) Tedesco, P. H.; Anon, M. C. Thorium–acetate and thorium–propionate complexes. *J. Inorg. Nucl. Chem.* **1972**, *34*, 2271–2276.

(20) Sergeev, G. M.; Astrashkova, L. G.; Yagodinskaya, N. N. Investigation of the formation of complexes of Th(IV) with acetic acid by the pH-potentiometric titration method. *Radiokhimiya* **1970**, *12*, 392–393.

(21) Moore, R. C.; Borkowski, M.; Bronikowski, M. G.; Chen, J.; Pokrovsky, O. S.; Xia, J.; Choppin, G. R. Thermodynamic modeling of actinide complexation with acetate and lactate at high ionic strength. *J. Solution Chem.* **1999**, *28*, 521–531.

(22) Portanova, R.; Tomat, G.; Cassol, A.; Magon, L. Equilibrium of thorium(IV) with monocarboxylic ligands. *J. Inorg. Nucl. Chem.* **1972**, *34*, 1685–1690.

(23) Portanova, R.; Di Bernardo, P.; Traverso, O.; Mazzocchin, G. A.; Magon, L. Thermodynamic properties of actinide complexes-II. Thorium(IV)–acetate system. *J. Inorg. Nucl. Chem.* **1975**, *37*, 2177–2179.

(24) Rao, L.; Zanonato, P.; Di Bernardo, P. Interaction of actinides with carboxylates in solution: Complexation of U(VI), Th(IV), and Nd(III) with acetate at variable temperatures. *J. Nucl. Radiochem. Sci.* **2005**, *6*, 31–37.

(25) Choppin, G. R.; Schneider, J. K. The acetate complexing by trivalent actinide ions. *J. Inorg. Nucl. Chem.* **1970**, *32*, 3283–3288.

(26) Grenthe, I.; Yhland, M.; Salmenperä, A.; Block-Bolten, A.; Toguri, J. M.; Flood, H. On the stability of the acetate, glycolate and thioglycolate complexes of trivalent europium and americium. *Acta Chem. Scand.* **1962**, *16*, 1695–1712.

(27) Moskvina, A. I. Complex formation of the actinides with anions of acids in aqueous solutions. *Radiokhimiya* **1969**, *11*, 458–460.

(28) Moskvina, A. I. Investigation of the complex formation of trivalent plutonium, americium, and curium in acetate solutions by the ion exchange method. *Radiokhimiya* **1971**, *13*, 221–223.

(29) Moskvina, A. I. Investigation of the complex formation of trivalent plutonium and americium in acetate solution by a potentiometric method. *Radiokhimiya* **1971**, *13*, 224–230.

(30) Münze, R. Thermodynamische Funktionen der Komplexbildung und Ionenradien-I. Bestimmung der freien Enthalpie, Entropie und Enthalpie von Azetokomplexen der Lanthaniden und Aktiniden aus zwischenatomaren Donor-Akzeptorabständen. *J. Inorg. Nucl. Chem.* **1972**, *34*, 661–668.

(31) Rao, V. K.; Mahajan, G. R.; Natarajan, P. R. Hydrolysis and carboxylate complexation of trivalent americium. *Inorg. Chim. Acta* **1987**, *128*, 131–134.

- (32) Mishustin, A. I. Estimate of the stability constants of trivalent actinide and lanthanide complexes with O-donor ligands in aqueous solutions. *Russ. J. Inorg. Chem.* **2010**, *55*, 746–752.
- (33) Fröhlich, D. R.; Skerencak-Frech, A.; Bauer, N.; Rossberg, A.; Panak, P. J. The pH dependence of Am(III) complexation with acetate: an EXAFS study. *J. Synchrotron Radiat.* **2015**, *22*, 99–104.
- (34) Richard, L.; Grieve, M.; Duro, L. *ANDRA-TDB7 Task 3 Organics*; Selection of formation constants for acetate complexes of Ca and radionuclides, Amphos 21, 2011.
- (35) Martel, A. E.; Smith, R. M. *NIST Standard Reference Database 46.6*, version 8.0, 2004.
- (36) Kuczewski, B.; Marquardt, C. M.; Seibert, A.; Geckeis, H.; Kratz, J. V.; Trautmann, N. Separation of plutonium and neptunium species by capillary electrophoresis-inductively coupled plasma-mass spectrometry and application to natural groundwater samples. *Anal. Chem.* **2003**, *75*, 6769–6774.
- (37) Ambard, C.; Delorme, A.; Baglan, N.; Aupiais, J.; Pointurier, F.; Madic, C. Interfacing capillary electrophoresis with inductively coupled plasma mass spectrometry for redox speciation of plutonium. *Radiochim. Acta* **2005**, *93*, 665–673.
- (38) Stöbener, N.; Amayri, S.; Gehl, A.; Kaplan, U.; Malecha, K.; Reich, T. Sensitive redox speciation of neptunium by CE-ICP-MS. *Anal. Bioanal. Chem.* **2012**, *404*, 2143–2150.
- (39) Graser, C.-H.; Banik, N.; Bender, K. A.; Lagos, M.; Marquardt, C. M.; Marsac, R.; Montoya, V.; Geckeis, H. Sensitive redox speciation of iron, neptunium, and plutonium by capillary electrophoresis hyphenated to inductively coupled plasma sector field mass spectrometry. *Anal. Chem.* **2015**, *87*, 9786–9794.
- (40) Rundlett, K. L.; Armstrong, D. W. Methods for the determination of binding constants by capillary electrophoresis. *Electrophoresis* **2001**, *22*, 1419–1427.
- (41) Chen, Z.; Weber, S. G. Determination of binding constants by affinity capillary electrophoresis, electrospray ionization mass spectrometry and phase-distribution methods. *TrAC, Trends Anal. Chem.* **2008**, *27*, 738–748.
- (42) Dvorak, M.; Svobodova, J.; Benes, M.; Gas, B. Applicability and limitations of affinity capillary electrophoresis and vacancy affinity capillary electrophoresis methods for determination of complexation constants. *Electrophoresis* **2013**, *34*, 761–767.
- (43) Uselova-Vcelakova, K.; Zuskova, I.; Gas, B. Stability constants of amino acids, peptides, proteins, and other biomolecules determined by CE and related methods: Recapitulation of published data. *Electrophoresis* **2007**, *28*, 2145–2152.
- (44) Jiang, C.; Armstrong, D. W. Use of CE for the determination of binding constants. *Electrophoresis* **2010**, *31*, 17–27.
- (45) Stepanova, S.; Kasicka, V. Capillary electrophoretic methods applied to the investigation of peptide complexes. *J. Sep. Sci.* **2015**, *38*, 2708–2721.
- (46) Galievsky, V. A.; Stasheuski, A. S.; Krylov, S. N. Capillary electrophoresis for quantitative studies of biomolecular interactions. *Anal. Chem.* **2015**, *87*, 157–171.
- (47) Kuban, P.; Timerbaev, A. R. CE of inorganic species – A review of methodological advancements over 2009–2010. *Electrophoresis* **2012**, *33*, 196–210.
- (48) Timerbaev, A. R. Element speciation analysis using capillary electrophoresis: Twenty years of development and application. *Chem. Rev.* **2013**, *113*, 778–812.
- (49) Timerbaev, A. R.; Timerbaev, R. M. Recent progress of capillary electrophoresis in studying the speciation of actinides. *TrAC, Trends Anal. Chem.* **2013**, *51*, 44–50.
- (50) Sladkov, V. Affinity capillary electrophoresis in studying the complex formation equilibria of radionuclides in aqueous solutions. *Electrophoresis* **2016**, *37*, 2558–2566.
- (51) Timerbaev, A. R. Capillary electrophoresis coupled to mass spectrometry for biospeciation analysis: critical evaluation. *TrAC, Trends Anal. Chem.* **2009**, *28*, 416–425.
- (52) Tycova, A.; Ledvina, V.; Kleparnik, K. Recent advances in CE-MS coupling: Instrumentation, methodology, and applications. *Electrophoresis* **2017**, *38*, 115–134.
- (53) Topin, S.; Aupiais, J. The pentavalent actinide solution chemistry in the environment. *J. Environ. Radioact.* **2016**, *153*, 237–244.
- (54) Topin, S.; Aupiais, J.; Baglan, N.; Vercouter, T.; Vitorge, P.; Moisy, P. Trace metal speciation by capillary electrophoresis hyphenated to inductively coupled plasma mass spectrometry: Sulfate and chloride complexes of Np(V) and Pu(V). *Anal. Chem.* **2009**, *81*, 5354–5363.
- (55) Topin, S.; Aupiais, J.; Moisy, P. Direct determination of plutonium(V) and neptunium(V) complexation by carbonate ligand with CE-ICP-sector field MS. *Electrophoresis* **2009**, *30*, 1747–1755.
- (56) Topin, S.; Aupiais, J.; Baglan, N. Determination of the stability constants of nitrate complexes of Np(V) and Pu(V) using CE-ICP-MS. *Radiochim. Acta* **2010**, *98*, 71–75.
- (57) Petit, J.; Geertsen, V.; Beaucaire, C.; Stambouli, M. Metal complexes stability constant determination by hyphenation of capillary electrophoresis with inductively coupled plasma mass spectrometry: The case of 1:1 metal-to-ligand stoichiometry. *J. Chromatogr. A* **2009**, *1216*, 4113–4120.
- (58) Petit, J.; Aupiais, J.; Topin, S.; Geertsen, V.; Beaucaire, C.; Stambouli, M. Stability constants determination of successive metal complexes by hyphenated CE-ICPMS. *Electrophoresis* **2010**, *31*, 355–363.
- (59) Mendes, M.; Hamadi, S.; Le Naour, C.; Roques, J.; Jeanson, A.; Den Auwer, C.; Moisy, P.; Topin, S.; Aupiais, J.; Henning, C.; Di Giandomenico, M. Thermodynamic and structural study of protactinium(V) oxalate complexes in solution. *Inorg. Chem.* **2010**, *49*, 9962–9971.
- (60) Brunel, B.; Philippini, V.; Mendes, M.; Aupiais, J. Actinides oxalate complex formation as a function of temperature by capillary electrophoresis coupled with inductively coupled plasma mass spectrometry. *Radiochim. Acta* **2015**, *103*, 27–37.
- (61) Aupiais, J.; Bonin, L.; Den Auwer, C.; Moisy, P.; Siberchicot, B.; Topin, S. On the use of speciation techniques and *ab initio* modelling to understand tetravalent actinide behavior in a biological medium: An^{IV}DTPA case. *Dalton Trans.* **2016**, *45*, 3759–3770.
- (62) Bonin, L.; Aupiais, J.; Kerbaa, M.; Moisy, P.; Topin, S.; Siberchicot, B. Revisiting actinide-DTPA complexes in aqueous solution by CE-ICPMS and *ab initio* molecular dynamics. *RSC Adv.* **2016**, *6*, 62729–62741.
- (63) Rösch, F.; Dittrich, S.; Buklanov, G. V.; Milanov, M.; Khalkin, V. A.; Dreyer, R. Electromigration of carrier-free radionuclides. 12. Reactions of ²³⁹Np(V) with acetate and citrate ligands in neutral solutions. *Radiochim. Acta* **1990**, *49*, 29–34.
- (64) Janos, P. Role of chemical equilibria in the capillary electrophoresis of inorganic substances. *J. Chromatogr. A* **1999**, *834*, 3–20.
- (65) Goldberg, R. N.; Kishore, N.; Lennen, R. M. Thermodynamic quantities for the ionization reactions of buffers. *J. Phys. Chem. Ref. Data* **2002**, *31*, 231–370.
- (66) Tedesco, P. H.; Gonzalez Quintana, J. A. Equilibrium of complexes formation in chromium(III)-acetate and chromium(III)-propionate systems. *J. Inorg. Nucl. Chem.* **1970**, *32*, 2689–2696.
- (67) Hynes, M. J.; O'Dowd, M. Interactions of the trimethyltin(IV) cation with carboxylic acids, amino acids, and related ligands. *J. Chem. Soc., Dalton Trans.* **1987**, 563–566.
- (68) Grossmann, P. D.; Colburn, J. C., Eds. *Capillary Electrophoresis Theory and Practice*; Academic Press: San Diego, 1992.
- (69) Sursyakova, V. V.; Burmakina, G. V.; Rubaylo, A. I. Influence of analyte concentration on the stability constant values determined by capillary electrophoresis. *J. Chromatogr. Sci.* **2016**, *54*, 1253–1262.
- (70) Pokrovsky, O. S.; Choppin, G. R. Neptunium(V) complexation by acetate, oxalate and citrate in NaClO₄ media at 25°C. *Radiochim. Acta* **1997**, *79*, 167–171.
- (71) Choppin, G. R.; Jensen, M. P. Actinides in Solution: Complexation and Kinetics. In *The Chemistry of the Actinide and Transactinide Elements*, 3rd ed.; Morris, L. R.; Edelstein, N. M.; Fuger, J., Eds.; Springer: Dordrecht, 2006.

4.4 PROPIONATE LIGAND

As a further ligand, propionate, the anion of the propionic acid, was investigated. Propionic acid is the next member of the homologues series of carboxylic acids after the acetic acid. It is thus interesting to see the effect of the additional methylene group in the propionate ligand on the stability of the complexes formed with different actinides in comparison to the acetate ligand. The results of this investigation can also be used in the utilization of short-chain carboxylates as model substances for naturally occurring more complex molecules such as humic or fulvic acid and their interactions with actinides (for more details see the Introduction of the acetate manuscript, Section 4.3).

In these experiments all four actinides, namely Am(III), Th(IV), Np(V) and U(VI) were investigated in one and the same sample solution via CE-ICP-MS. This allows to significantly reduce the total amount of samples compared to the acetate series, where all actinides were measured individually. Furthermore, it again emphasizes the benefit of using ICP-MS as a multi-element detector. The feasibility of this approach should result from the low actinide concentrations and thus the very high excess of ligand. As a consequence, an impact of a competition of the different actinides for the free ligand can be ruled out.

4.4.1 INTRODUCTION

The actinide-propionate systems are less extensively studied compared with the respective acetate systems but nevertheless some examinations can be found in the literature. Again, all values given there are determined for actinide concentrations much higher than employed in the experiments of this work by CE-ICP-MS.

Cassol et al. [69CAS] investigated the relative stability of AnO_2^{2+} with monocarboxylate anions for $An = U, Np$ and Pu by potentiometry ($T = 20\text{ }^\circ\text{C}$, $I = 1\text{ M NaClO}_4$). They report on the order of stability of the complexes as $UO_2^{2+} > NpO_2^{2+} > PuO_2^{2+}$ for the actinides and on an increasing stability of the complexes with an increase in the basicity of the ligand but no stability constants are given. Hala et al. [62HAL] determined the ratio of the stability constants of U(V) and U(VI) with propionate by a polarographic method ($I = 1\text{ M NaNO}_3$) but also give no absolute values. Miyake et al. [67MIY] evaluated the U(VI)-propionate system by spectroscopy for both uranyl and propionate concentrations in the millimolar range. They found four consecutive complexes with the respective stability constants $\log(\beta_1) = 2.53 \pm 0.01$, $\log(\beta_2) = 4.68 \pm 0.04$, $\log(\beta_3) = 6.49 \pm 0.05$ and $\log(\beta_4) = 8.25 \pm 0.06$ at $T = 20\text{ }^\circ\text{C}$ and $I = 1\text{ M NaClO}_4$. Further stability constants for the 1:1 and the 1:1 and 1:2 complexes can be found to be $\log(\beta_1) = 3.03$ [68RAM] (pH-titration method in the region $\text{pH} = 1.5 - 3.5$, $T = 31\text{ }^\circ\text{C}$ and $I = 0.1\text{ M NaClO}_4$) and $\log(\beta_1) = 2.50 \pm 0.01$ and $\log(\beta_2) = 4.79 \pm 0.04$ [07KIR] (microcalorimetry, $c(UO_2^{2+}) = 3.75\text{ mM}$, $T = 25\text{ }^\circ\text{C}$ and $I = 1.0\text{ M}$

4. Determination of Stability Constants with CE-ICP-MS

NaClO₄), respectively. A capillary electrophoresis experiment with UV-Vis detection for the separation and simultaneous determination of U(VI) and several carboxylic acids (amongst others acetic and propionic acid) in the context of sorption experiments on silica and rutile is described by Sladkov et al. [11SLA].

For the NpO₂⁺-propionate system just the 1:1 complex is described in the literature. Vasiliev et al. [15VAS] investigated the complexation reaction in 0.5 – 4 M NaCl solutions in a temperature range of $T = 20 - 85$ °C via spectroscopic techniques. For $T = 25$ °C they determined the stability constant at zero ionic strength extrapolated by SIT (specific ion interaction theory) from their experimental results to be $\log(\beta^0_1) = 1.26 \pm 0.03$. Furthermore, they found a mainly bidentate binding of both the acetate and the propionate ligand for the 1:1 complex.

Sergeev [71SER] determined stability constants for the 1:1 and 1:2 complexes of Th(IV) with propionate for different Th⁴⁺:propionate ratios of 1:8, 1:10 and 1:15. The values are $\log(\beta_1) = 3.61 \pm 0.04$, $\log(\beta_2) = 6.93 \pm 0.05$, $\log(\beta_1) = 3.7 \pm 0.1$, $\log(\beta_2) = 6.96 \pm 0.04$ and $\log(\beta_1) = 3.6 \pm 0.1$, $\log(\beta_2) = 6.8 \pm 0.1$, respectively. Four consecutive complexes are described by Portanova et al. [72POR]. They obtained $\log(\beta_1) = 3.94 \pm 0.03$, $\log(\beta_2) = 7.25 \pm 0.07$, $\log(\beta_3) = 9.44 \pm 0.10$ and $\log(\beta_4) = 11.20 \pm 0.14$ by potentiometric investigations at $T = 20$ °C and $I = 1$ M NaClO₄. Significant lower values for the 1:1 complex were published by Tedesco et al. [72TED] by spectrometry ($\log(\beta_1) = 1.31$) and potentiometry ($\log(\beta_1) = 1.42$) for $T = 25$ °C and $I = 1$ M.

For the Am³⁺-propionate system no experimental results can be found in the literature. A stability constant for the 1:1 complex was estimated by Mishustin [10MIS] by integration of the ligand density distribution function which resulted in $\log(\beta^0_1) = 2.91$ but the results are systematically overestimated as annotated by the author. In the knowledge that actinides tend to build stronger complexes with a given ligand compared to the homologue lanthanides (see e.g. [83NAI]) one can employ the stability constants of Eu³⁺ with propionate for a rough comparison. The values for the first two complexes can be found in the literature as $\log(\beta_1) = 2.23$, $\log(\beta_2) = 3.74$ (potentiometry, $T = 20$ °C and $I = 0.1$ M NaClO₄) [64POW] and $\log(\beta_1) = 1.98$, $\log(\beta_2) = 3.28$ (pH titration, $T = 25$ °C and $I = 2.0$ M NaClO₄) [65CHO].

4.4.2 EXPERIMENTAL PROCEDURE

Initially, a 0.3 M propionic acid solution was produced. For the preparation of the different samples, in each case 20 mL aliquots of this solution were adjusted to the desired pH value by the addition of appropriate amounts of 11.6 M perchloric acid solution or 10 M NaOH solution. This way, 24 samples in the pH region from 0.73 – 5.46 were prepared. It was

4.4 Propionate Ligand

ensured by speciation calculations with the program Visual MINTEQ [14GUS], that under the experimental conditions in this pH range the formation of hydroxides can be neglected for all four actinides. All samples were brought to an equal ionic strength of $I = 0.3$ M by adding respective amounts of $\text{NaClO}_4 \cdot \text{H}_2\text{O}$. The detailed composition of the samples can be found in Appendix A5.2 (Table A1). After filtration through $0.2 \mu\text{m}$ syringe filters $200 \mu\text{L}$ of these solutions were used as the BGE for the flushing of the capillary.

For the samples for CE-ICP-MS measurements, stock solutions of the actinides Am(III), Th(IV) and Np(V) in 1 M HClO_4 and U(VI) in 0.1 M HClO_4 were used. The preparation of these solutions and the control of the concentrations were conducted as described in Section 4.3. As the only difference, U(VI) was, like Th(IV), prepared from the dilution of a ICP-MS standard solution of known concentration.

To 5 mL of the respective propionic acid solution described above, $5 \mu\text{L}$ of the Am(III) and the Np(V) stock solution and $10 \mu\text{L}$ of the Th(IV) and the U(VI) stock solution were added to yield actinide sample concentrations of $c(\text{Am(III)}) = c(\text{Np(V)}) = 5 \cdot 10^{-8} \text{ M}$ and $c(\text{Th(IV)}) = c(\text{U(VI)}) = 2 \cdot 10^{-7} \text{ M}$. The change in the ionic strength of the solution due to the addition of the actinides could be neglected because the sample volume is very small compared to the overall volume of the solution. The pH values of the sample solutions were measured again after the actinide addition and these results were used for the data evaluation.

$200 \mu\text{L}$ of these sample solutions together with $1 \mu\text{L}$ 2-bromopropane as the EOF marker were then measured by CE-ICP-MS at $U = 10 \text{ kV}$ and a capillary length of $l = 76 \text{ cm}$.

4.4.3 RESULTS AND DISCUSSION

In Figure 11 the measured effective electrophoretic mobilities μ_{eff} of the actinide-propionate series as a function of the free propionate concentration $[\text{Pro}^-]$ at $I = 0.3 \text{ M}$ are shown together with the associated fit curves. The corresponding electropherograms and the migration times t_i and t_{EOF} as well as the electrophoretic mobilities can be found in the Appendix A5.2 (Figure A1 – Figure A3 and Table A2). The fitting procedure was conducted as described in Section 4.1 with application of the constraints given there. Again, as in the acetate case, the highest measured electrophoretic mobility was set as the lower limit and the highest electrophoretic mobility as evaluated in Section 4.2 for the system without any ligands was set as the upper limit for the μ_i parameter of the free actinide.

4. Determination of Stability Constants with CE-ICP-MS

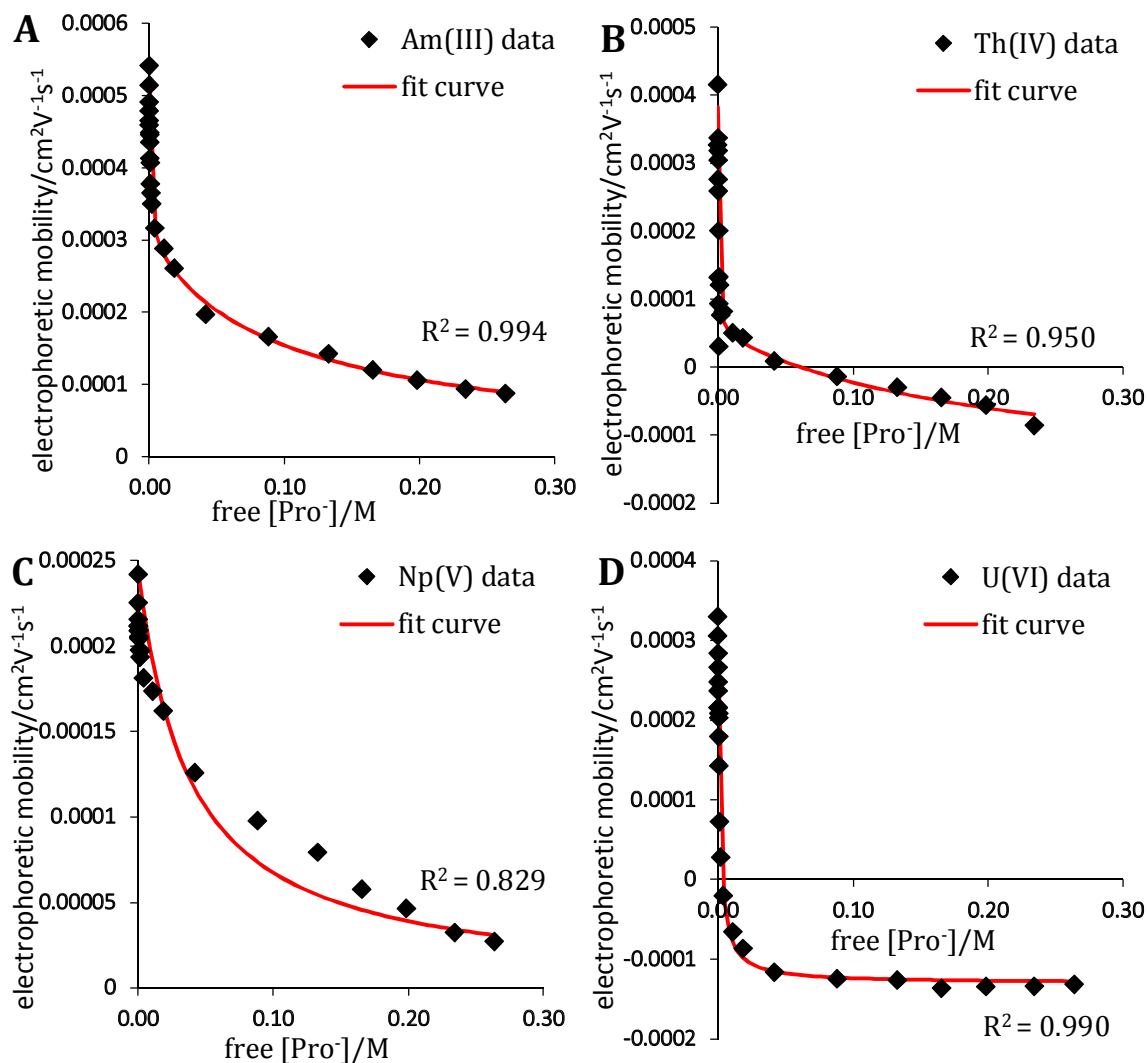


Figure 11: Measured effective electrophoretic mobilities μ_{eff} of the actinide-propionate series as a function of the free propionate concentration $[\text{Pro}^-]$ at $I = 0.3 \text{ M}$ with the related fit curve. **A:** Am(III), **B:** Th(IV), **C:** Np(V), **D:** U(VI).

The stability constants β_i (and $\log(\beta_i)$) for the actinides complexed by the propionate ligand determined at $I = 0.3 \text{ M}$ are presented in Table 7. The thermodynamic stability constants extrapolated to zero ionic strength by means of Equation (4.6) can also be found there. The respective electrophoretic mobilities of the individual species μ_i are summarized in Table 8. The uncertainties given for the β_i are resulting from the fitting procedure performed by the Origin 7 software. The ones for the electrophoretic mobilities were not derived from the fitting procedure since the μ_i were kept constant at the last iteration. They are estimated to be $\Delta\mu_i = 0.1 \cdot 10^{-4} \text{ cm}^2\text{V}^{-1}\text{s}^{-1}$ in all cases.

Table 7: Stability constants β_i for the different actinide–propionate complexes at $I = 0.3$ M and the corresponding values extrapolated to zero ionic strength. The limits of error $\Delta(\beta_i)$ are resulting from the fitting procedure.

actinide	i	β_i/M^{-i}	$\Delta\beta_i/M^{-i}$	$\log(\beta_i)$	$\Delta\log(\beta_i)$	$\log(\beta_i^0)$	$\Delta\log(\beta_i^0)$
Am(III)	1	1867	124	3.27	0.03	4.08	0.03
	2	40074	7947	4.60	0.09	5.95	0.09
	3	167682	23706	5.22	0.06	6.84	0.06
Th(IV)	1	$1.93 \cdot 10^5$	$3.32 \cdot 10^5$	5.29	0.75	6.36	0.75
	2	$8.92 \cdot 10^8$	$1.26 \cdot 10^9$	8.95	0.61	10.83	0.61
	3	$9.54 \cdot 10^{11}$	$1.70 \cdot 10^{12}$	11.98	0.78	14.40	0.78
	4	$2.07 \cdot 10^{13}$	$4.36 \cdot 10^{13}$	13.32	0.91	16.00	0.91
	5	$7.48 \cdot 10^{13}$	$1.41 \cdot 10^{14}$	13.87	0.82	16.56	0.82
Np(V)	1	26	12	1.42	0.20	1.69	0.20
U(VI)	1	1489	359	3.17	0.10	3.71	0.10
	2	931626	235900	5.97	0.11	6.78	0.11
	3	186917090	49129863	8.27	0.11	9.08	0.11

For Am(III) three successive stability constants for the 1:1, 1:2 and 1:3 complex could be identified. Since no negative values for the electrophoretic mobilities were obtained, the existence of the negatively charged 1:4 Am(III)-propionate was not considered for the data evaluation. The data set was also evaluated for the formation of just two successive complexes but the coefficient of determination R^2 in that case was slightly smaller than the one presented here. The value determined in this work for the 1:1 complex is in good agreement with the one estimated in [10MIS] to be $\log(\beta_i) = 2.91$ even though it is somewhat higher. The results for the 1:2 complex can just be compared to the homologue Eu(III) complex, which have considerably lower stability constants. This meets the expectations as already mentioned in the literature section above.

The investigation of the Th(IV)-propionate system results in both positive and negative values for the effective electrophoretic mobilities in dependence of the pH. This leads to the conclusion that five successive Th(IV)-propionate complexes have to be considered for the data evaluation because the 1:5 complex is the first negative one. As can be seen in Figure 11 B, the fitting procedure yields a satisfying curve with $R^2 = 0.950$. Nevertheless, the

4. Determination of Stability Constants with CE-ICP-MS

uncertainties of the resulting stability constants are very large (even larger than β_i itself). Again, like already noticed in the Th(IV)-acetate system, the high number of ligands leads to a high amount of fit parameters and thus to a system difficult to evaluate. Consequently, it seems reasonable to increase the number of samples for the determination of Th(IV) systems in order to gain more data and by that reduce the uncertainty values. In the available literature described above, the values for the 1:1 complex are quite scattered and the results from this work are, like in the Am(III) case, the highest ones. Only in [72POR] four consecutive Th(IV)-propionate complexes are investigated and the values given there are also significantly lower than the ones from this work. A negatively charged 1:5 complex is not described in the literature so no comparison of the $\log(\beta_5)$ value is possible. Nevertheless, due to the benefit from the possibility to discriminate between positive and negative complex species by the CE-ICP-MS method based on the sign of the effective electrophoretic mobilities, the assumption of the 1:5 species is reasonable.

Even though the neptunyl ion NpO_2^+ with the effective charge +1 is the actinide with the lowest charge, no negative electrophoretic mobilities could be measured in the pH region investigated. This suggests the formation of just the 1:1 compound. The respective fit curve of this evaluation can be seen in Figure 11 C. Due to the somewhat smaller coefficient of determination R^2 compared to the other systems it was also tried to fit the data for higher complexes of Np(V) with propionate but no result could be obtained. This finding is in accordance with the literature where also just the 1:1 species is described for Np(V). Again, the value for the stability constant determined in this work is higher than the one given in the reference [15VAS].

For U(VI) the formation of three and four consecutive propionate complexes was investigated because of the negative effective electrophoretic mobilities obtained during measurements. The better fitting curve could be obtained for the 1:3 system and the result is shown in Figure 11 D. In contrast to that, in [67MIY] four species are described. The stability constants given in the literature are lower than evaluated here.

In conclusion, the order of the stability constants β_i for the different actinide-propionate systems determined in this work follows the usual order of increasing strength of actinide complexes $\text{AnO}_2^+ < \text{An}^{3+} \approx \text{AnO}_2^{2+} < \text{An}^{4+}$, which mirrors the effective charge of the actinide [06CHO]. On the other hand, the values evaluated here are notably higher for all actinides compared to the available literature. Similar results were found for the actinide-acetate systems. Due to this conformities and similarities it stands to reason that the increase in the stability constants compared to the literature data described above is a consequence of the

much lower actinide concentrations employed in this work leading to a much higher excess of actinide over the ligand.

Table 8: Electrophoretic mobilities of the individual species μ_i for the different actinide–propionate complexes. The uncertainties are estimated to be $\Delta\mu_i = 0.1 \cdot 10^{-4} \text{ cm}^2 \text{ V}^{-1} \text{ s}^{-1}$ in all cases.

actinide	species	$\mu_i/10^{-4} \text{ cm}^2 \text{ V}^{-1} \text{ s}^{-1}$
Am(III)	Am^{3+}	5.4
	$[\text{Am}(\text{Pro})]^{2+}$	3.0
	$[\text{Am}(\text{Pro})_2]^+$	1.5
	$[\text{Am}(\text{Pro})_3]_{\text{aq}}$	0.0*
Th(IV)	Th^{4+}	6.0
	$[\text{Th}(\text{Pro})]^{3+}$	4.0
	$[\text{Th}(\text{Pro})_2]^{2+}$	1.5
	$[\text{Th}(\text{Pro})_3]^+$	0.5
	$[\text{Th}(\text{Pro})_4]_{\text{aq}}$	0.0*
	$[\text{Th}(\text{Pro})_5]^-$	-1.8
Np(V)	NpO_2^+	2.4
	$[\text{NpO}_2(\text{Pro})]_{\text{aq}}$	0.0*
U(VI)	UO_2^{2+}	3.3
	$[\text{UO}_2(\text{Pro})]^+$	1.9
	$[\text{UO}_2(\text{Pro})_2]_{\text{aq}}$	0.0*
	$[\text{UO}_2(\text{Pro})_3]^-$	-1.3

* held constant during the fitting procedure

Besides the stability constants a complete set of individual electrophoretic mobilities μ_i of the free species were obtained from the fitting procedure which is shown in Table 8. The order of the electrophoretic mobilities of the uncomplexed actinides mirrors the order of their charge $\mu_i(\text{NpO}_2^+) < \mu_i(\text{UO}_2^{2+}) < \mu_i(\text{Am}^{3+}) < \mu_i(\text{Th}^{4+})$. The same is true for species with an identical number of ligands, μ_i increases with increasing charge in the same sequence. Furthermore, for complexes with the same charge, the electrophoretic mobility decreases with an increasing number of ligands. This is reasonable because species with more ligands

4. Determination of Stability Constants with CE-ICP-MS

are larger and thus are more decelerated by the frictional force F_f that is the electrophoretic migration opposed (see Equation (2.3)).

4.5 COMPARISON OF ACETATE AND PROPIONATE

Acetic acid and propionic acid are, as already mentioned, both consecutive members of the homologues series of carboxylic acids. It therefore appears advisable to insert a more comprehensive consideration of the stability constants of the respective anions acetate and propionate determined by CE-ICP-MS experiments before presenting the results of the other ligands.

Generally speaking, due to the similarity between the two ligands, the complexation behavior of the actinides with these compounds is expected to be also very comparable. Thus, for all four actinides, the same number of maximum ligands was found, just one for Np(V), three for Am(III) and U(VI) and five for Th(IV). In order to compare the absolute values for the stability constants β_i one has to take a closer look at the respective acidity constants.

The acidity constant pK_a (see Equation (4.8)) increases in the row of the carboxylic acids. Thus, the pK_a of acetic acid is smaller than the one of propionic acid ($pK_{a,\text{acetic acid}}(0\text{ M}) = 4.76 < pK_{a,\text{propionic acid}}(0\text{ M}) = 4.87$, [04MAR]).

$$pK_a = -\log\left(\frac{[H^+][L^-]}{[HL]}\right). \quad (4.8)$$

In this case, L^- represents the acetate or the propionate anion, HL stands for the respective acid. By rearranging this formula for $[L^-]$ and inserting it into the definition for the stability constant β_i given in Equation (4.2) one obtains Equation (4.9).

$$\beta_i = \frac{[An-L_i^{(n-i)}]}{[An^{n+}]\left(\frac{10^{-pK_a} \cdot [HL]}{[H^+]}\right)^i}. \quad (4.9)$$

With Equation (4.9) a correlation between the acidity constant pK_a of a ligand with the respective stability constant β_i for the complexation of this ligand with a certain actinide is given. In general, one can derive from this formula that the complex is the weaker the lower the pK_a value is. The same findings were described by Bunting et al. [70BUN] who investigated the stability constants of several divalent metal ions complexed with different carboxylate anions.

Applied to the present case this leads to the conclusion that the $\log(\beta_i)$ values of the acetate complexes should be smaller than those of the propionate complexes. By comparing the respective values given in Table 6 (acetate paper) for acetate and Table 7 for propionate one can see that this is true for all the complexes investigated. Consequently, in the experiments

described in the previous two sections, a set of reasonable and conclusive stability constants were determined for actinides in low concentration ranges and the CE-ICP-MS method has proven to be a suitable analytical tool for such investigations.

On basis of Equation (4.9) one can additionally predict the trend of the $\log(\beta_i)$ for other members of the homologues row of the carboxylic acids. The complexes with formate as the first member in this series should have significantly lower $\log(\beta_i)$ values because of its smaller pK_s value, which is true for Th(IV) and U(VI) formates (on basis of the data given in the NIST database [04MAR]). The carboxylates following directly after propionate in contrast can be expected to have further increased values for the stability constants. At some point the differences in the acidity constants of the higher homologues of the carboxylic acids become very small so that the trend described above should also become less pronounced. Furthermore, it has to be noted that these considerations neither do take into account steric effects which become more important for larger carboxylates and may lead to weaker complexes nor consider the chelate effect in case of more binding possibilities in one ligand. This has to be kept in mind when using acetate or propionate as model ligands for the humic and fulvic acids as described above.

4.6 GLUCONATE LIGAND

4.6.1 INTRODUCTION

Gluconate, the anion of the gluconic acid, is known to build stable complexes with a large number of different metal cations in different oxidation states [64SAW]. In the context of the long-term safety assessment of a nuclear waste disposal, gluconate is currently investigated for different reasons. Firstly, it is employed in many studies as an analogue for isosaccharinic acid (ISA) [17DUD]. ISA was identified as one of the main degradation products of cellulose, which may be present in radioactive waste in form of contaminated papers, filters or cotton. By the complexation with ISA the radionuclides may be solubilized and thus mobilized [08KEI]. Consequently, a thorough understanding of the complexation mechanism based on these ligands and a trustworthy data set of the respective stability constants are of great interest. The available literature for the metal-ISA complexes is summarized in [08KEI]. In case of actinides, the works of Wieland, Tits et al. concerning Eu(III), Am(III) and Th(IV) with calcite [05TIT] and Th(IV) with hardened cement paste [02WIE] as well as of Rai et al. [03RAI] and Gaona et al. [08GAO] for tetravalent actinides are particularly emphasized. Furthermore, the use of cement and concrete in future nuclear waste disposals is discussed or it is already in use because of its good immobilization capability for radioactive metal ions (for more information see e.g. [96GOU], [09CHE]). In this context, gluconate is used as an additive in cement (for controlling the setting time and increasing the strength and water

4. Determination of Stability Constants with CE-ICP-MS

resistance) and concrete (to increase frost and crack resistance) [06RAM] and can moreover deal as a representative substance for different organic materials such as plasticizers that are added to cementitious mixtures [05TIT].

Regarding its chemical properties, some difficulties in the determination of the stability constants of actinides with gluconate have to be considered in the CE-ICP-MS measurements. The experiments are conducted in a low pH region for reasons already explained above. For acidic conditions, gluconate has just a weak or moderate ability to bind metal ions [07ZHA], which changes at higher pH values [06RAM]. This fact has to be kept in mind for the interpretation of stability constants determined in this work in comparison with the conditions in alkaline systems such as concrete and cement. Furthermore, in this pH range gluconate has a strong tendency to form lactone rings. For $\text{pH} > 2.5$ solely the δ -lactone (glucono-1,5-lactone) is formed, for $\text{pH} < 2$ both the δ -lactone and the γ -lactone (glucono-1,4-lactone) can occur [07ZHA]. The rate constants of the lactonization reaction at room temperature given in the literature in an acidic pH range ([88COM], [07ZHA]) can be converted to half-lives in the magnitude of several hours. By preparing all samples as directly as possible before the measurements, advantage was taken of this rather slow kinetic and the lactone formation could be neglected.

4.6.2 EXPERIMENTAL PROCEDURE

In the case of the gluconate investigations, a 0.3 M sodium gluconate stock solution was produced. From this solution, in the same way as for the acetate (see Section 4.3) and propionate (see Section 4.4) measurements 22 samples in the pH region from 0.87 – 4.78 were prepared. It was ensured by speciation calculations with the program Visual MINTEQ [14GUS], that under the experimental conditions in this pH range the formation of hydroxides can be neglected for all four actinides. All samples were brought to an equal ionic strength of $I = 0.3 \text{ M}$ by adding respective amounts of $\text{NaClO}_4 \cdot \text{H}_2\text{O}$. For the first samples it could not be prevented that the ionic strength is slightly higher than 0.3 M due to the required larger amounts of perchloric acid compared to the preparations starting from the respective acids instead of the sodium salt. As already depicted above, all samples were prepared directly prior to the measurements to minimize the lactate formation. The detailed composition of the samples can be found in Appendix A5.3 (Table A3).

Apart from the carboxylic acid group there are different hydroxyl groups in the gluconic acid molecule. These groups can also be partly deprotonated in dependence on the pH. This would thus lead to a different ligand $\text{Glu}_{-\text{H}^2-}$ (further details regarding different ligands in dependence on the degree of deprotonation can be found in the citrate series in the next section). In this case, the second deprotonation step only becomes significant in alkaline pH

regions ($pK_{a,2}(0.1 \text{ M}) = 13.0$ [07ZHA]) and could consequently be neglected in the presented experiments.

The preparation of the CE-ICP-MS samples and the actinide stock solutions as well as the experimental procedure for the measurements are identical to the procedure described for the acetate and propionate series. The actinide concentrations were $c(\text{Am(III)}) = 2.5 \cdot 10^{-7} \text{ M}$, $c(\text{Th(IV)}) = 1 \cdot 10^{-6} \text{ M}$, $c(\text{Np(V)}) = 5 \cdot 10^{-8} \text{ M}$ and $c(\text{U(VI)}) = 1.4 \cdot 10^{-7} \text{ M}$.

4.6.3 RESULTS AND DISCUSSION

In Figure 12 the measured effective electrophoretic mobilities μ_{eff} of the actinide-gluconate series as a function of the free gluconate concentration [Glu \cdot] at $I = 0.3 \text{ M}$ are shown together with the associated fit curves. The corresponding electropherograms and the migration times t_i and t_{EOF} as well as the electrophoretic mobilities can be found in the Appendix A5.3 (Table A4, Figure A4 – Figure A6). The fitting procedure was conducted as described in Section 4.1 with application of the constraints given there. Again, as in the acetate and in the propionate case, the highest measured electrophoretic mobility was set as the lower limit and the highest electrophoretic mobility as evaluated in Section 4.2 for the system without any ligands was set as the upper limit for the μ_i parameter of the free actinide.

The collected stability constants β_i (and $\log(\beta_i)$) for the actinides complexed by the gluconate ligand determined at $I = 0.3 \text{ M}$ are presented in Table 9. The thermodynamic stability constants extrapolated to zero ionic strength by means of Equation (4.6) are also given there. The uncertainties given for the β_i are again resulting from the fitting procedure given by the Origin 7 software.

As can be seen in Figure 12 A, the resulting effective electrophoretic mobilities for the Am(III) gluconate measurements become negative in the higher pH region starting from $\text{pH} = 3.87$. This is why the occurrence of the $\text{Am}(\text{Glu})_4^-$ species and thus of four consecutive Am(III) gluconate complexes was assumed for the fitting procedure. The corresponding fitting curve exhibits a satisfactory coefficient of determination of $R^2 = 0.986$ but the fitting procedure turned out to be strongly dependent on the starting parameters and small changes led to a breakdown of the fitting process. The presented results are the best values that could be obtained under the given circumstances. Since $\log(\beta_3)$ and $\log(\beta_4)$ are very similar, a fitting of the values under the assumption of just three complexes was also attempted, regardless the negative electrophoretic mobilities for the last samples. The respective R^2 value is then slightly smaller and the $\log(\beta_i)$ are in a comparable range. For a more conclusive final statement about the presence of the 1:4 Am(III) gluconate complex more samples in the pH region from $\text{pH} \approx 3.87$ upwards have to be measured. Tits et al. [05TIT] investigated the

4. Determination of Stability Constants with CE-ICP-MS

interaction of gluconic acid and Am(III) by batch type-sorption experiments at high pH. They determined the stability constant for the 1:1 complexation with the $\text{Glu}_{-3\text{H}^4}$ to be $\log(\beta^0) = 16.6 \pm 1$. In the literature, no further studies could be found concerning the stability constants of the Glu⁻ ligand as investigated in this work so the values presented here are the first for the given experimental conditions.

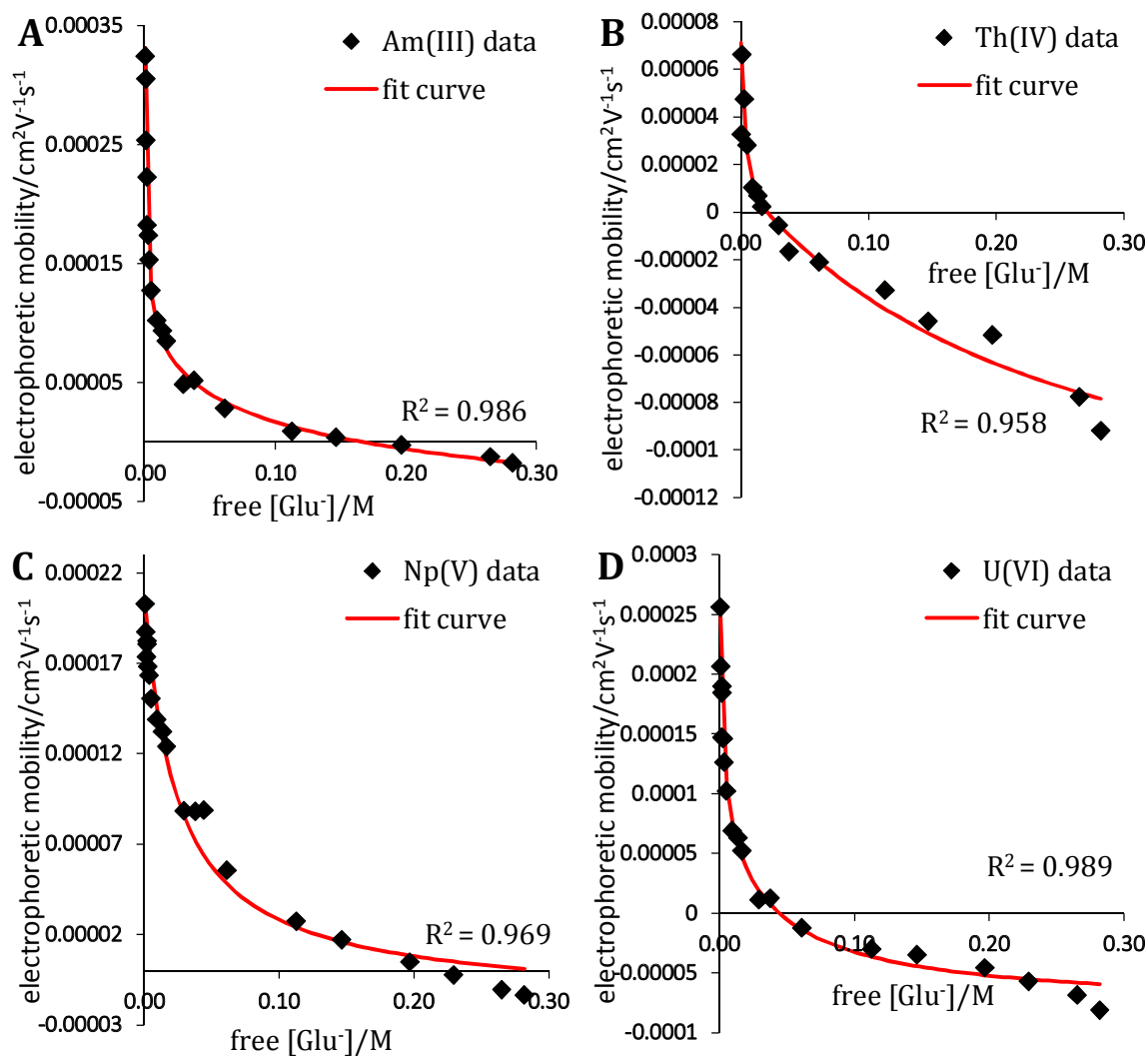


Figure 12: Measured effective electrophoretic mobilities μ_{eff} of the actinide-gluconate series as a function of the free gluconate concentration $[\text{Glu}^-]$ at $I = 0.3 \text{ M}$ with the related fit curve. **A:** Am(III), **B:** Th(IV), **C:** Np(V), **D:** U(VI).

4.6 Gluconate Ligand

Table 9: Stability constants β_i for the different actinide–gluconate complexes at $I = 0.3$ M and the corresponding values extrapolated to zero ionic strength. The limits of error $\Delta(\beta_i)$ are resulting from the fitting procedure.

actinide	i	β_i/M^{-i}	$\Delta\beta_i/M^{-i}$	$\log(\beta_i)$	$\Delta\log(\beta_i)$	$\log(\beta_i^0)$	$\Delta\log(\beta_i^0)$
Am(III)	1	512	183	2.71	0.16	3.51	0.16
	2	398108	54130	5.60	0.06	6.94	0.06
	3	10079094	2641523	7.00	0.11	8.62	0.11
	4	14618856	5333668	7.16	0.16	8.78	0.16
Th(IV)	1	$5.60 \cdot 10^4$	$2.73 \cdot 10^4$	4.75	0.21	5.82	0.21
	2	$2.89 \cdot 10^6$	$3.56 \cdot 10^6$	6.46	0.53	8.34	0.53
	3	$1.17 \cdot 10^9$	$8.93 \cdot 10^8$	9.07	0.33	11.49	0.33
	4	$3.29 \cdot 10^{10}$	$3.30 \cdot 10^{10}$	10.52	0.44	13.20	0.44
	5	$1.42 \cdot 10^{11}$	$1.20 \cdot 10^{11}$	11.15	0.37	13.84	0.37
Np(V)	1	45	5	1.65	0.05	1.92	0.05
	2	115	72	2.06	0.27	2.33	0.27
U(VI)	1	825	79	2.92	0.04	3.45	0.04
	2	43933	8616	4.64	0.09	5.45	0.09
	3	518654	104672	5.71	0.09	6.52	0.09

As in the case of Am(III), also in the Th(IV) measurements the appearance of negative effective electrophoretic mobilities implies the formation of a negatively charged Th(IV) gluconate species. Consequently, the fitting procedure was conducted with the assumption of five complexes. It has already been described in the acetate and propionate series that the great number of fitting parameters complicates the fitting operation. The same turned out to be true for the gluconate case. It was not possible to vary all parameters for the stability constants or the electrophoretic mobilities at the same time without aborting the fitting process. Therefore, in every iteration some parameters were held constant. Despite these difficulties, the results presented in Figure 12 C and Table 9 for the $\log(\beta_i)$ are quite satisfactory. As can be seen later in Table 10, the resulting electrophoretic mobilities are smaller than expected on basis of the previous series, but other starting parameters resulted in the same values. Again, literature provides only works in significantly higher pH ranges

4. Determination of Stability Constants with CE-ICP-MS

and the stability constants for multiple deprotonated ligands and mixed hydroxide complexes can be found ([05TIT], [08GAO], [11COL], [13COL1]), a comparison with the results from this work is therefore hardly possible.

For Np(V) two consecutive gluconate complexes were determined. In contrast to the acetate and the propionate series, also negative effective electrophoretic mobilities were measured suggesting the formation of the $\text{NpO}_2(\text{Glu})_2^-$ species. The resulting stability constants for $I = 0.3 \text{ M}$ are $\log(\beta_1) = 1.65 \pm 0.05$ and $\log(\beta_2) = 2.06 \pm 0.27$, which are in good agreement with the values determined by Zhang et al. [06ZHA] evaluated at $I = 1.0 \text{ M NaClO}_4$ at $\text{pH} = 6$ ($\log(\beta_1) = 1.48 \pm 0.03$ and $\log(\beta_2) = 2.14 \pm 0.09$).

The U(VI) gluconate system also exhibits negative values for the effective electrophoretic mobilities. Therefore, two different fitting procedures were conducted for the hypothesis of the formation of either three or four consecutive species. The resulting fitting curve obtained for the 1:3 scenario shown in Figure 12 D exhibits the better R^2 , therefore the $\text{UO}_2(\text{Glu})_3^-$ complex was set as the complex with the highest ligand number. In the available literature, just stability constants for the 1:1 species could be found. Zhang et al. [09ZHA] report on $\log(\beta_1) = 2.2 \pm 0.3$ on basis of calorimetric and potentiometric measurements at $I = 0.1 \text{ M NaClO}_4$ for $\text{pH} 2.5 - 4.2$. This is in good agreement with the results presented here. Much higher values of $\log(\beta_1) = 6.3 \pm 0.4$ at $\text{pH} = 7$ and $\log(\beta_1) = 19.9 \pm 2$ at $\text{pH} = 13.3$ (ion exchange method) are described by Warwick et al. [06WAR]. These differences prove noticeably the strong dependence of the complex forming capability of gluconate as a ligand on the pH value that has already been subjected. As for Th(IV), for U(VI) also further investigations in higher pH ranges and with mixed ligand systems are discussed in the literature [62SAW], [13COL2].

The associated electrophoretic mobilities of the individual species μ_i are summarized in Table 10. The uncertainties for the electrophoretic mobilities were not given from the fitting procedure since the μ_i were kept constant at the last iteration. They are estimated to be $\Delta\mu_i = 0.1 \cdot 10^{-4} \text{ cm}^2 \text{ V}^{-1} \text{ s}^{-1}$ in all cases. For Np(V), U(VI) and Am(III), the order of the electrophoretic mobilities of the uncomplexed actinides mirrors the order of their charge $\mu_i(\text{NpO}_2^+) < \mu_i(\text{UO}_2^{2+}) < \mu_i(\text{Am}^{3+})$. Contrary to this trend, for Th(IV) with the highest charge of +4 all electrophoretic mobilities are very small, but the presented results are the only values that could be obtained during the fitting procedure. For all approaches of fitting the data set with higher starting parameters for the μ_i either the same small values were obtained after few iterations or the fitting procedure was aborted. Besides the Th(IV) results, the same trends as in the propionate and acetate measurements were found, namely an increasing electrophoretic mobility with increasing charge for complexes with an identical number of

4.6 Gluconate Ligand

ligands and a decrease in μ_i with an increasing number of ligands for complexes with the same charge.

Table 10: Electrophoretic mobilities of the individual species μ_i for the different actinide-gluconate complexes. The uncertainties are estimated to be $\Delta\mu_i = 0.1 \cdot 10^{-4} \text{ cm}^2\text{V}^{-1}\text{s}^{-1}$ in all cases.

actinide	species	$\mu_i/10^{-4} \text{ cm}^2\text{V}^{-1}\text{s}^{-1}$
Am(III)	Am^{3+}	4.0
	$[\text{Am}(\text{Glu})]^{2+}$	2.0
	$[\text{Am}(\text{Glu})_2]^+$	1.0
	$[\text{Am}(\text{Glu})_3]_{\text{aq}}$	0.0*
	$[\text{Am}(\text{Glu})_4]^-$	-1.0
Th(IV)	Th^{4+}	1.1
	$[\text{Th}(\text{Glu})]^{3+}$	0.5
	$[\text{Th}(\text{Glu})_2]^{2+}$	0.1
	$[\text{Th}(\text{Glu})_3]^+$	0.02
	$[\text{Th}(\text{Glu})_4]_{\text{aq}}$	0.0*
	$[\text{Th}(\text{Glu})_5]^-$	-1.5
Np(V)	NpO_2^+	2.1
	$[\text{NpO}_2(\text{Glu})]_{\text{aq}}$	0.0*
	$[\text{NpO}_2(\text{Glu})_2]^-$	-0.2
U(VI)	UO_2^{2+}	3.3
	$[\text{UO}_2(\text{Glu})]^+$	0.9
	$[\text{UO}_2(\text{Glu})_2]_{\text{aq}}$	0.0*
	$[\text{UO}_2(\text{Glu})_3]^-$	-0.8

* held constant during the fitting procedure

4. Determination of Stability Constants with CE-ICP-MS

4.7 CITRATE LIGAND

4.7.1 INTRODUCTION

Citric acid (H_3Cit) is a naturally occurring organic acid with three carboxylate groups and one hydroxyl group. The three deprotonation steps of the carboxylate groups are all relevant in the pH region investigated in this work due to their respective acidity constants, $pK_{a,1}(0\text{ M}) = 3.13 \pm 0.01$, $pK_{a,2}(0\text{ M}) = 4.76 \pm 0.01$, $pK_{a,3}(0\text{ M}) = 6.40 \pm 0.02$ [05HUM]. The hydroxyl group, in contrast, just deprotonates at basic pH values. Consequently, for the investigation of the actinide-citric acid system, three different ligands, $H_{3-n}Cit^{n-}$ with $n = 1, 2, 3$ have to be considered, the fully deprotonated species Cit_{-H^4} can be neglected. Since it could be shown for different ligand systems with just one relevant deprotonation step, namely acetate, propionate and gluconate (as described in the previous sections), that CE-ICP-MS is a suitable and appropriate analytical technique for the determination of stability constants of actinides with such compounds in low concentration ranges, it should be tested in a further measurement series whether the method is also applicable to a more complicated ligand system.

Besides these more basic reasons for studying the actinide citrate interactions there are also practical interests in gaining a deeper knowledge of this compound. As in the case of acetate and propionate, the natural occurrence of citric acid and its deprotonated forms can influence the solubility of actinides and by that their migration behavior in the environment. Hence, many studies can be found in connection with the long-term safety assessment of a nuclear waste disposal, e.g. [05KAN], [12BER] for U(VI), [97POK] for Np(V), [87RAY], [96CHO], [06FEL] for Th(IV) and [02WAL], [12THA] for Am(III). Furthermore, it can be used as a small molecule model substance for natural organic matter (NOM) [00LEN]. In the processing of nuclear waste, for example in the liquid-liquid extraction of lanthanides and Am(III), citrate is found to have a beneficial impact when added as a buffer [14BRO]. It is further present in some radioactive waste storage tanks [07MAT]. Since citrate is the dominant binding agent of actinides in human urine [12HEL] and it is present in human blood serum, the interaction is also relevant for decorporation by chelating processes in biological systems in case of accidental intake [07BON], [08BON]. Moreover, studies on the effect of citrate on the interaction of microorganisms with actinides are described in the literature [97YON], [13OHN].

As indicated by the wide field of research topics summarized above, there can be found numerous studies concerning the determination of stability constants of actinides with citrate species in the literature. The results are rather scattered because of the experimental difficulties arising from the possibility of three different ligand species [71OHY]. A very

4.7 Citrate Ligand

thorough discussion of the available literature in combination with a selection of reliable stability constants for Am(III), Np(V) and U(VI) is given by Hummel et al. [05HUM] and for the comparison of the results obtained by the CE-ICP-MS measurements of this work it is referred to that overview. Also included in the discussion section following later are the results of more recent works: The U(VI)-citrate complexation was investigated by potentiometric and spectrometric measurements by Berto et al. [12BER] ($I = 0.1$ M, NaCl solution), Np(V) was examined also by spectrophotometry at $I = 1.0$ M by Bonin et al. [07BON]. More recent results for Am(III), given by three different groups, were obtained from solvent extraction at $I = 6.6$ m NaClO₄ [07MAT], from potentiometric titration experiments and extraction techniques ($I = 0.1 - 6.6$ m NaClO₄) [12THA] and from spectrophotometric titration at $I = 1.0$ M NaClO₄ [14BRO]. The first works concerning the Th(IV)-citrate interactions were conducted by Nebel et al. by potentiometric investigations [66NEB], [75NEB]. They determined the first two Th(IV)-Cit³⁻ complexes. Somewhat later, also by potentiometric measurements at $I = 0.1$ M in a chloride medium, Raymond et al. [87RAY] described three consecutive Cit³⁻ complexes and the 1:1 and 1:3 HCit²⁻ species. Solvent extraction with both NaClO₄ and NaCl as background electrolyte up to a high ionic strength of $I = 14$ m was used by Choppin et al. [96CHO] as the analytical method of choice. Bonin et al. [08BON] published stability constants for the 1:1 and 1:2 complexes of Th(IV) with all three possible citrate species investigated by spectrophotometry at $I = 0.3$ M in HNO₃ medium. Particular attention should be paid to the fact that actinide-citrate interaction investigations by electrophoresis methods are described in the literature. Rösch et al. [90ROS3] performed electromigration measurements of Np(V) in near neutral perchlorate solutions with an ionic strength of $I = 0.3$ M. With their experimental conditions, no continuous course of the measured effective electrophoretic mobility with increasing ligand concentration could be identified which was explained with a reduction of Np(V). CE was used for the speciation study of U(VI) in 0.02 M citrate buffer solution in the pH range from 2.5 to 5.5 by Boughammoura et al. [09BOU]. They described different monomeric and dimeric as well as mixed hydroxyl-citrate uranyl species. In good agreement with the results obtained in this work presented in the following, they measured no negative species up to pH = 3. In contrast, though, they determined up to four different peaks in one electropherogram, which is also contrary to the theory of a rapid equilibrium between the different species as depicted in Section 4.1. What both works have in common is that no stability constants are given. Zhang et al. [15ZHA] applied a multi-injection affinity capillary electrophoresis method and thus determined the stability constant for the 1:1 UO₂Cit⁻ species at pH = 1.98 ± 0.02, $I = 0.050$ M (HClO₄/NaClO₄) and varying citric acid concentrations. Besides these

4. Determination of Stability Constants with CE-ICP-MS

electrophoresis studies, no coupling of CE to ICP-MS for the investigation of actinide-citrate systems can be found in the literature.

It becomes obvious from all these data that not all stability constants for all theoretically possible ligand species are available and thus further investigations with new methods as conducted in this work are necessary to fill these gaps.

4.7.2 CITRATE SPECIATION

For the determination of stability constants of actinides with different citrate ligands by CE-ICP-MS it is important to know the exact species distribution of the respective citrate species. As already mentioned above, all three deprotonation steps of the carboxylate groups are relevant in the pH region investigated in this work. The acidity constants given in [05HUM] for zero ionic strength were extrapolated to $I = 0.3$ M by means of Equation (4.6) resulting in $pK_{a,1}(0.3 \text{ M}) = 2.86$, $pK_{a,2}(0.3 \text{ M}) = 4.22$, $pK_{a,3}(0.3 \text{ M}) = 5.59$. With these values, the percentage of the respective citrate species $H_{3-n}Cit^{n-}$ in dependence of the pH values adjusted in the samples were calculated by Equation (4.10)– (4.13).

$$c(H_3Cit) = c_{tot} \cdot \frac{(10^{-pH})^3}{(10^{-pH})^3 + (10^{-pH})^2 \cdot 10^{-pK_{a,1}} + 10^{-pH} \cdot 10^{-pK_{a,1}} \cdot 10^{-pK_{a,2}} + 10^{-pK_{a,1}} \cdot 10^{-pK_{a,2}} \cdot 10^{-pK_{a,3}}} \quad (4.10)$$

$$c(H_2Cit^-) = c_{tot} \cdot \frac{(10^{-pH})^2 \cdot 10^{-pK_{a,1}}}{(10^{-pH})^3 + (10^{-pH})^2 \cdot 10^{-pK_{a,1}} + 10^{-pH} \cdot 10^{-pK_{a,1}} \cdot 10^{-pK_{a,2}} + 10^{-pK_{a,1}} \cdot 10^{-pK_{a,2}} \cdot 10^{-pK_{a,3}}} \quad (4.11)$$

$$c(HCit^{2-}) = c_{tot} \cdot \frac{10^{-pH} \cdot 10^{-pK_{a,1}} \cdot 10^{-pK_{a,2}}}{(10^{-pH})^3 + (10^{-pH})^2 \cdot 10^{-pK_{a,1}} + 10^{-pH} \cdot 10^{-pK_{a,1}} \cdot 10^{-pK_{a,2}} + 10^{-pK_{a,1}} \cdot 10^{-pK_{a,2}} \cdot 10^{-pK_{a,3}}} \quad (4.12)$$

$$c(Cit^{3-}) = c_{tot} \cdot \frac{10^{-pK_{a,1}} \cdot 10^{-pK_{a,2}} \cdot 10^{-pK_{a,3}}}{(10^{-pH})^3 + (10^{-pH})^2 \cdot 10^{-pK_{a,1}} + 10^{-pH} \cdot 10^{-pK_{a,1}} \cdot 10^{-pK_{a,2}} + 10^{-pK_{a,1}} \cdot 10^{-pK_{a,2}} \cdot 10^{-pK_{a,3}}} \quad (4.13)$$

The resulting speciation diagram for a total citrate concentration of $c_{tot} = 0.3$ M is shown in Figure 13 based on the pH values of 16 samples that were prepared for the CE-ICP-MS investigation (the exact values are given in Appendix A5.4 (Table A5).

As can be seen from that diagram, all possible citrate species occur side by side in one and the same sample solution for nearly all pH values. This has to be taken into account for the data evaluation as described in more detail in the following.

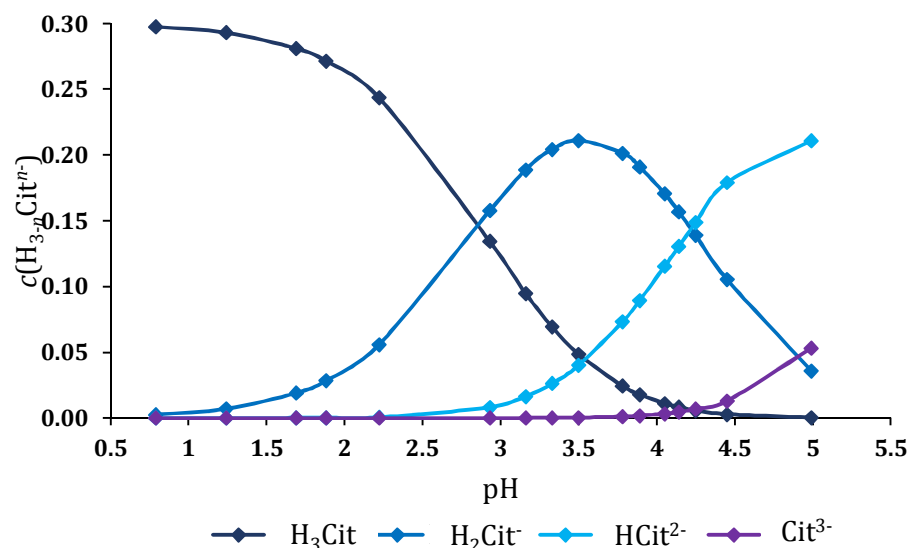


Figure 13: Citrate speciation diagram with the distribution of the different deprotonated species based on the pH values of 16 samples for the CE-ICP-MS measurement series.

4.7.3 EXPERIMENTAL PROCEDURE

A 0.3 M citric acid solution was produced from citric acid monohydrate. From this solution, in the same way as described before (see Sections 4.3 – 4.6), 16 samples in the pH region from 0.79 – 4.99 were prepared. Under the experimental conditions in this pH range the formation of hydroxides could be neglected for all four actinides because of the strong complex binding capability of the citrate species being present in great excess. In contrast to the measurement series described above, in the citrate series the ionic strengths I of the solutions were determined from measured values of the electrical conductivity κ by Equation (4.14) [96MAR] because of the more intricate sample composition with the different citrate species equilibria.

$$\log(I) = 1.159 + 1.009 \cdot \log(\kappa). \quad (4.14)$$

The ionic strength of $I = 0.3$ M was reached by adding respective amounts of $\text{NaClO}_4 \cdot \text{H}_2\text{O}$. Due to the required amounts of perchloric acid or sodium hydroxide for pH adjustment it could not be prevented that I is slightly higher than 0.3 M in the first sample and in the last two samples. In these cases no $\text{NaClO}_4 \cdot \text{H}_2\text{O}$ was added. The detailed sample compositions and the measured electrical conductivities κ are summarized in Appendix A5.4, Table A5.

The preparation of the CE-ICP-MS samples and the actinide stock solutions as well as the experimental procedure for the measurements are identical to the way described for the previous series. The actinide concentrations were $c(\text{Am(III)}) = 5.27 \cdot 10^{-8}$ M, $c(\text{Th(IV)}) = 1 \cdot 10^{-6}$ M, $c(\text{Np(V)}) = 5 \cdot 10^{-8}$ M and $c(\text{U(VI)}) = 1.4 \cdot 10^{-7}$ M.

4. Determination of Stability Constants with CE-ICP-MS

4.7.4 DATA EVALUATION

In order to determine the stability constants of the investigated actinides with the different citrate species the data evaluation cannot be carried out completely identical to the previous studies. Three different ligand species have to be considered, but just one value for the effective electrophoretic mobility can be measured. This value for μ_{eff} comprises all contributions of all actinide-citrate species. Therefore, Equation (4.4) can be written as depicted in Equation (4.15).

$$\mu_{\text{eff}} = \frac{\mu_0 + \sum_{i=1}^{N_1} \mu_i \beta_i [\text{Cit}^{3-}]^i + \sum_{j=1}^{N_2} \mu_j \beta_j [\text{HCit}^{2-}]^j + \sum_{k=1}^{N_3} \mu_k \beta_k [\text{H}_2\text{Cit}^-]^k}{1 + \sum_{i=1}^{N_1} \beta_i [\text{Cit}^{3-}]^i + \sum_{j=1}^{N_2} \beta_j [\text{HCit}^{2-}]^j + \sum_{k=1}^{N_3} \beta_k [\text{H}_2\text{Cit}^-]^k}. \quad (4.15)$$

The values N_1 , N_2 and N_3 are independent of each other and stand for the maximum number of ligands in the respective complex.

As a consequence, the free ligand concentration of just one citrate species cannot be employed as the x -value for the fitting procedure as conducted in the previous series with just one possible ligand species. In order to proceed still similar to those evaluation strategies, rather the pH value of the sample has to be set as the x -value instead of the free ligand concentration since the pH is the joint parameter for expressing all ligand concentrations. Hence, in Equation (4.15) the values for $[\text{Cit}^{3-}]$, $[\text{HCit}^{2-}]$ and $[\text{H}_2\text{Cit}^-]$ have to be replaced by the expressions given in Equations (4.11) – (4.13).

Based on these considerations it can quickly be recognized that the fitting equation becomes complicated to evaluate. Even for a small number of complexes formed, a great number of fitting parameters has to be applied. Under the little realistic assumption of just 1:1 complexes being formed, 7 fitting parameters are needed. A more realistic approach with 1:1 and 1:2 complexes already leads to 13 parameters and so on. Furthermore, there is also the possibility of mixed values for the maximum ligand numbers N_1 , N_2 and N_3 . With a data set of just 16 samples, it is unpromising to achieve conclusive results with this strategy.

In the framework of this study, therefore the application of an alternative approach was tested. As can be seen in Figure 13, the pH region investigated can be divided into parts with the predominance of one of the citrate species. These sections were evaluated individually by the application of Equation (4.4) as if just one ligand is present in the solution. Hereby, the classification was as follows: $0.79 < \text{pH} < 2.22$ for H_2Cit^- , $2.93 < \text{pH} < 3.89$ for HCit^{2-} and $4.05 < \text{pH} < 4.99$ for Cit^{3-} . In the last section, the Cit^{3-} is still not dominant, but it is described in the literature [05HUM] that the deprotonation can occur at much lower pH compared to the calculated values based on the $\text{p}K_a$ because of a strong interaction of the metal ion and

the ligand forming a more stable chelate complex. This effect can be expected in this case as well and the Cit^{3-} complexation can be determined.

For all fitting procedures, the same constraints as described in the previous sections were applied.

This approach of course is just an approximation since the contribution of the other species is neglected, but as shown later, the results are in parts quite satisfactory. For more significant values of the stability constants a greater number of samples has to be investigated to improve the available data set. Nevertheless, by the measurement series presented here it is possible to prove that CE-ICP-MS is in general also an appropriate analytical method for the investigation of such more complex ligand systems.

4.7.5 RESULTS AND DISCUSSION

All electropherograms and the migration times t_i of the respective actinides and t_{EOF} as well as the electrophoretic mobilities can be found in Appendix A5.4 (Table A6, Figure A7 – Figure A8).

AMERICIUM(III)

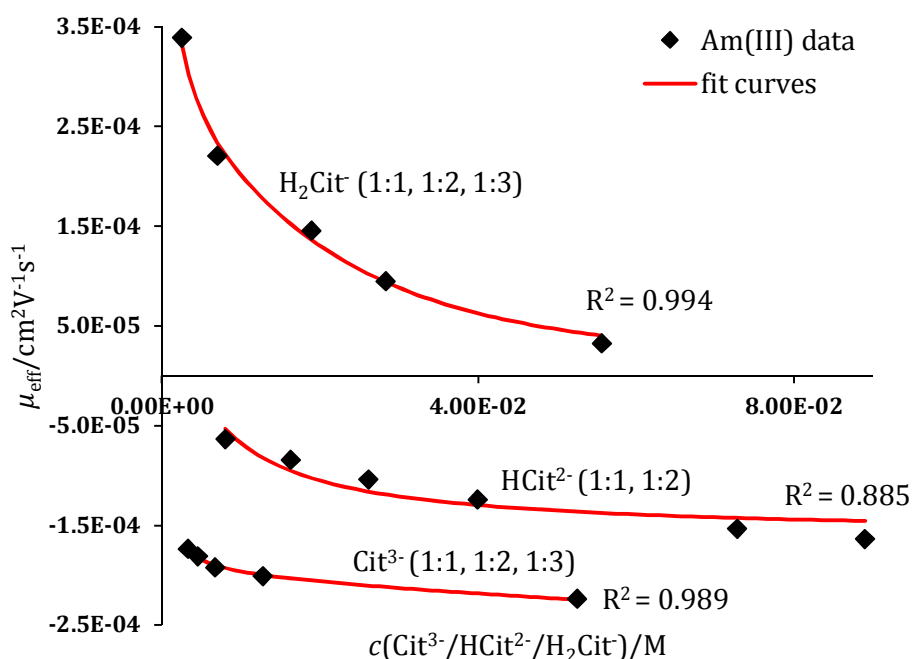


Figure 14: Measured effective electrophoretic mobilities μ_{eff} of the americium(III)-citrate series as a function of the respective free citrate species concentration [Cit^{3-} , HCit^{2-} , H_2Cit^-] at $I = 0.3 \text{ M}$ with the related fit curves. The classification is based on the predominance of the respective species at a given sample pH.

In Figure 14, the results of the measurements of the americium(III)-citrate series at $I = 0.3 \text{ M}$ are shown in terms of three different sections with the respective citrate species described

4. Determination of Stability Constants with CE-ICP-MS

above. Because of the presence of twice and thrice negatively charged ligand species in addition to the species with a charge of just -1 it is not surprising that the measured electrophoretic mobilities also become negative at quite low pH values compared to the previous measurement series. As can be seen, the fitting procedure led to a fit curve with satisfactory coefficients of determination R^2 for all of the sections. The best achievable results were obtained under the assumption of two consecutive complexes for the Am(III)-HCit²⁻ system and three for both the Am(III)-H₂Cit⁻ and the Am(III)-Cit³⁻ system. The obtained stability constants β_i (and $\log(\beta_i)$) at $I = 0.3$ M and the associated electrophoretic mobilities of the individual species μ_i are presented in Table 11.

Table 11: Stability constants β_i and electrophoretic mobilities of the individual species μ_i for the different Am(III)-citrate complexes at $I = 0.3$ M. The limits of error $\Delta(\beta_i)$ are resulting from the fitting procedure. The uncertainties $\Delta\mu_i$ are estimated to be $0.1 \cdot 10^{-4} \text{ cm}^2 \text{ V}^{-1} \text{ s}^{-1}$ in all cases.

species	β_i/M^{-i}	$\Delta\beta_i/M^{-i}$	$\log(\beta_i)$	$\Delta\log(\beta_i)$	$\mu_i/10^{-4} \text{ cm}^2 \text{ V}^{-1} \text{ s}^{-1}$
Am ³⁺					3.4
[Am(Cit)] _{aq}	9775	453	3.99	0.02	0.0*
[Am(Cit) ₂] ³⁻	20383173	833056	7.31	0.02	-2.0
[Am(Cit) ₃] ⁶⁻	58809707	3490254	7.77	0.03	-4.0
Am ³⁺					3.4
[Am(HCit)] ⁺	147618	19973	5.17	0.06	1.3
[Am(HCit) ₂] ²⁻	31637968	4285983	7.50	0.06	-1.6
Am ³⁺					6.3
[Am(H ₂ Cit)] ²⁺	766	125	2.88	0.07	1.9
[Am(H ₂ Cit) ₂] ⁺	9096	12771	3.96	0.61	1.0
[Am(H ₂ Cit) ₃] _{aq}	1248555	267871	6.10	0.09	0.0*

* held constant during the fitting procedure

Because of the performance of three fitting procedures also three values for the electrophoretic mobility μ_i of the free Am(III) ion are obtained. They are in good agreement for the Cit³⁻ and the HCit²⁻ system but differ from the H₂Cit⁻ system. Such differences can result from the fitting procedure. The average of all three values of $\mu(\text{Am(III)}) = 4.4 \cdot 10^{-4} \text{ cm}^2 \text{ V}^{-1} \text{ s}^{-1}$ is in good agreement with the results obtained from the other ligand systems. The other electrophoretic mobilities exhibit an overall trend of decreasing electrophoretic mobility

with decreasing charge. The two single positively charged species have similar μ_i whereby the $\mu([\text{Am}(\text{H}_2\text{Cit})_2]^+)$ is slightly lower than the corresponding $\mu([\text{Am}(\text{HCit})]^+)$ with just one ligand.

When comparing the stability constants of the different species for complexes with the same number of ligands it should be expected that the complex is the more stable the higher the charge of the ligand, because the higher charged ligands can bind two- or threedentate to the actinide ion leading to a stabilization of the complex due to chelation. [07HOL] This is true for the $\text{HCit}^{2-}/\text{H}_2\text{Cit}^-$ case, for the H_2Cit^- ligand the smallest stability constants were obtained. For the Cit^{3-} complexes on the other hand smaller $\log(\beta_i)$ were determined compared to the corresponding HCit^{2-} species. It seems thus necessary to assume that the Cit^{3-} results are too low. This is also substantiated by the available literature data. In the critical evaluation of [05HUM] considerably higher stability constants for two consecutive Cit^{3-} complexes are given for zero ionic strength ($\log(\beta^{0_1}) = 8.55 \pm 0.2$ and $\log(\beta^{0_2}) = 13.9 \pm 1.0$). Also two complexes were determined in more recent works: $\log(\beta_1) = 6.14 \pm 0.05$ and $\log(\beta_2) = 10.55 \pm 0.09$ in [07MAT] (6.6 m NaClO_4), $\log(\beta_1) = 7.05 \pm 0.08$ and $\log(\beta_2) = 11.67 \pm 0.08$ in [12THA] (0.3 M NaClO_4), $\log(\beta_1) = 6.93 \pm 0.01$ and $\log(\beta_2) = 10.3 \pm 0.5$ in [14BRO] (1.0 M NaClO_4). Because of these findings it was also tested whether the results can be fitted under the assumption of just two consecutive complexes but no fit could be obtained. Furthermore, the data evaluation was conducted with higher starting parameters for the $\log(\beta_i)$ values but either no fitting iteration was possible or the same smaller values presented here were obtained. Stability constants for the $\text{Am}(\text{III})\text{-HCit}^{2-}$ are just described in [05HUM] ($\log(\beta^{0_1}) = 6.5 \pm 1.0$ and $\log(\beta^{0_2}) = 10.8 \pm 1.0$) and in [14BRO] ($\log(\beta_1) = 9.56 \pm 0.04$). These values are inconsistent, the results from the review [05HUM] are in better agreement with the results obtained in the present work. For the $\text{Am}(\text{III})\text{-H}_2\text{Cit}$ species no $\log(\beta_i)$ could be found in the literature.

In order to test the data evaluation procedure and the results thus obtained for the $\text{Am}(\text{III})\text{-citrate}$ system, the effective electrophoretic mobility μ_{eff} was calculated for every sample by means of Equation (4.15) with the values given in Table 11. For μ_0 of the free $\text{Am}(\text{III})$ ion the average value of $\mu_0 = 4.4 \cdot 10^{-4} \text{ cm}^2 \text{ V}^{-1} \text{ s}^{-1}$ was inserted. The calculated electrophoretic mobilities were then compared to the measured μ_{eff} . The results are presented in Figure 15. As one can see, both values are in quite good agreement over a wide range of pH values. Only for the last samples in the higher pH region there is a clear difference between the measured and the calculated values of the electrophoretic mobilities. In this region the Cit^{3-} species has the greatest impact on μ_{eff} . Consequently, by this comparison it again becomes obvious that the $\log(\beta_i)$ for the Cit^{3-} complexes are too small. The stability constants of the other two ligand

4. Determination of Stability Constants with CE-ICP-MS

systems describe the experimental results satisfactorily, thus the data evaluation procedure itself is valid. More reliable results can be obtained by measuring more samples at more pH values to increase the number of data points for the fitting procedure in every pH region.

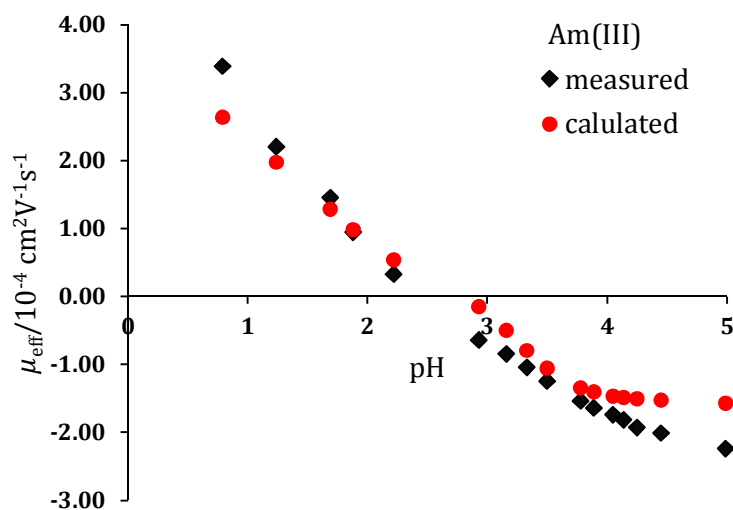


Figure 15: Comparison of the measured and the calculated effective electrophoretic mobility μ_{eff} of the Am(III)-citrate series at $I = 0.3 \text{ M}$.

THORIUM(IV)

The data evaluation as described above did not succeed for the Th(IV)-citrate series. As shown in Figure 16 already for the third sample, at a low $\text{pH} = 1.69$, the measured electrophoretic mobility becomes negative. This in combination with the high charge of +4 of the Th(IV) ion demands the assumption of at least five consecutive Th(IV)- H_2Cit^- complexes and three Th(IV)- HCit^{2-} to yield negative complex species. The fitting operation with the resulting high number of fitting parameters was not possible because of the low number of available data points.

Nevertheless, also because of the low pH value of the first negative electrophoretic mobility measured it was assumed that the Cit^{3-} species are dominant over the whole pH range. The other two ligand species were thus neglected completely. The effect of the deprotonation of protonated citrate ligands at lower pH, as described before because of a strong interaction of the metal ion and the ligand forming a more stable chelate complex, can be expected in this case to be very pronounced because of the high charge of Th(IV). This assumption of course increases the error in the resulting stability constants for the resulting Cit^{3-} species but at least allows for a rough evaluation of the measured data. Consequently, all electrophoretic mobilities were plotted against the $[\text{Cit}^{3-}]$ concentration and the fitting procedure as described before was conducted for just one ligand species. The results are depicted in Table 14.

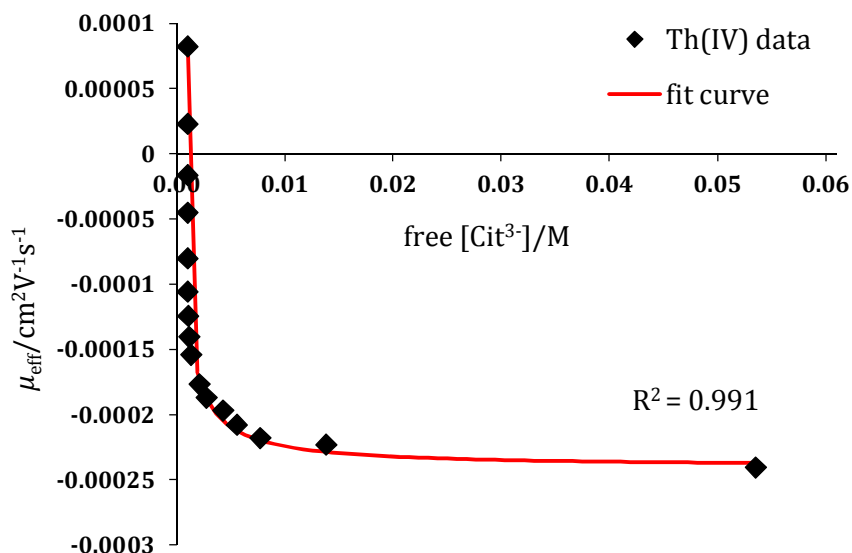


Figure 16: Measured effective electrophoretic mobilities μ_{eff} of the Th(IV)-citrate series as a function of the free citrate concentration $[\text{Cit}^{3-}]$ at $I = 0.3 \text{ M}$ with the related fit curve.

The obtained stability constants β_i (and $\log(\beta_i)$) at $I = 0.3 \text{ M}$ and the associated electrophoretic mobilities of the individual species μ_i are presented in Table 12.

Table 12: Stability constants β_i and electrophoretic mobilities of the individual species μ_i for the Th(IV)- Cit^{3-} complexes at $I = 0.3 \text{ M}$. The limits of error $\Delta(\beta_i)$ are resulting from the fitting procedure. The uncertainties $\Delta\mu_i$ are estimated to be $0.1 \cdot 10^{-4} \text{ cm}^2 \text{ V}^{-1} \text{ s}^{-1}$ in all cases.

species	β_i/M^{-i}	$\Delta\beta_i/\text{M}^{-i}$	$\log(\beta_i)$	$\Delta\log(\beta_i)$	$\mu_i/10^{-4} \text{ cm}^2 \text{ V}^{-1} \text{ s}^{-1}$
Th^{4+}					8.1
$[\text{Th}(\text{Cit})]^+$	$6.82 \cdot 10^{11}$	$9.84 \cdot 10^{10}$	11.83	0.06	0.1
$[\text{Th}(\text{Cit})_2]^{2-}$	$1.59 \cdot 10^{19}$	$4.61 \cdot 10^{18}$	19.20	0.13	-1.2
$[\text{Th}(\text{Cit})_3]^{5-}$	$1.16 \cdot 10^{22}$	$3.84 \cdot 10^{21}$	22.07	0.14	-2.4

The best fit results were attained for three consecutive Th(IV)- Cit^{3-} complexes with a good coefficients of determination of $R^2 = 0.991$. The evaluation for just the first two complexes was also possible but the corresponding R^2 was much worse ($R^2 = 0.811$). In comparison with the findings from Section 4.2 the resulting electrophoretic mobility of the free Th^{4+} ion is higher than the value determined there. Following, the constraint of an upper limit of the electrophoretic mobility could not be applied in this case.

First values for the stability constants of Th(IV) citrate complexes are given by Nebel et al. In two works they published $\log(\beta_i)$ values for the first two Cit^{3-} species: $\log(\beta_1) = 13$ and $\log(\beta_2) = 20.98$ in [66NEB] and $\log(\beta_1) = 11.82$ and $\log(\beta_2) = 20.38$ in [75NEB]. Also the first two values are given by Bonin et al. [08BON] ($\log(\beta_1) = 12.5 \pm 1$ and $\log(\beta_2) = 22.9 \pm 1$, 0.3 M

4. Determination of Stability Constants with CE-ICP-MS

HNO₃). Choppin et al. [96CHO] just report on the 1:1 Th(IV)-Cit³⁻ species with $\log(\beta_0) = 13.7 \pm 0.01$ for zero ionic strength. Three consecutive species, as in the present case, are described by Raymond et al. [87RAY]: $\log(\beta_1) = 11.611 \pm 0.039$, $\log(\beta_2) = 21.139 \pm 0.057$ and $\log(\beta_3) = 26.113 \pm 0.075$ (0.1 M chloride medium). Other citrate ligand species than Cit³⁻ are just mentioned in [87RAY] (1:1 and 1:3 HCit²⁻) and [08BON] (1:1 and 1:2 for both HCit²⁻ and H₂Cit⁻) but these species were not considered in the present work as explained above. As can be seen from the listing above, the literature data are quite scattered. Nevertheless, the values determined in this work fit quite well in this overall picture since they are all in the same order of magnitude. Consequently, the assumption of the predominance of the Cit³⁻ species with neglecting the other two seems (at least in parts) justified. Moreover, it can directly be concluded from the appearance of negative electrophoretic mobilities, that at least two consecutive Th(IV)-Cit³⁻ complexes are formed since the 1:1 species alone is not negative. For more reliable results and for a more satisfactory consideration of all three citrate species again more data points are needed.

NEPTUNIUM(V)

For the Np(V)-citrate system, the determination of stability constants of all three ligand species was possible. The experimental results together with the corresponding fit curves can be found in Figure 17.

The best fits with good R² values were obtained under the assumption of two consecutive complex species for both the Cit³⁻ and the HCit²⁻ ligand. In case of the H₂Cit⁻ ligand just the 1:1 complex was considered because of the all positive electrophoretic mobilities in the first pH region. The coefficient of determination R² is somewhat worse (but still the best result in comparison to the assumption of a 1:2 or even higher species) leading to a high error $\Delta\log(\beta_i)$ for the corresponding $\log(\beta_i)$. The resulting stability constants β_i (and $\log(\beta_i)$) at $I = 0.3$ M and the associated electrophoretic mobilities of the individual species μ_i are summarized in Table 13.

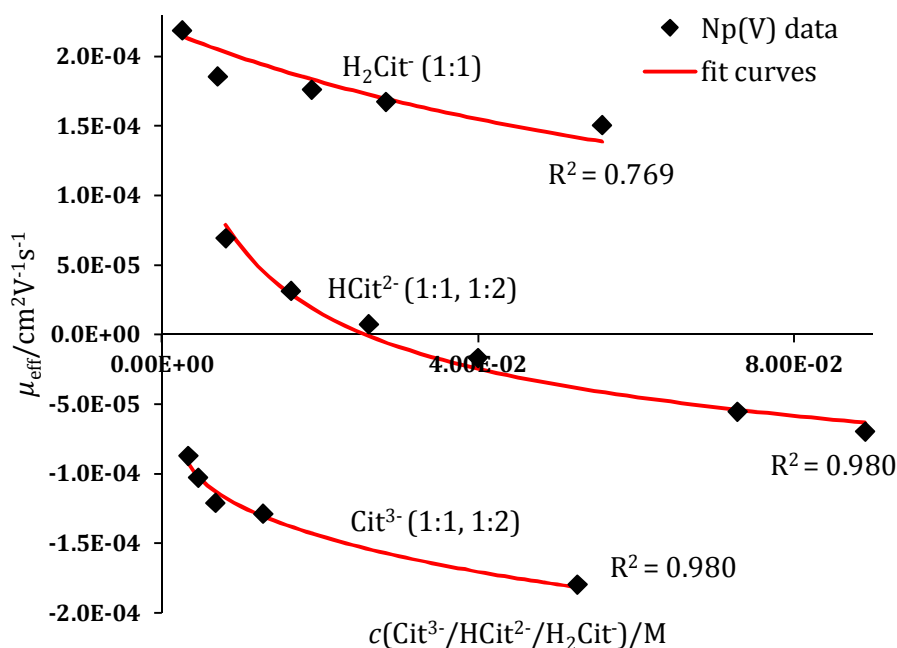


Figure 17: Measured effective electrophoretic mobilities μ_{eff} of the neptunium(V)-citrate series as a function of the respective free citrate species concentration $[\text{Cit}^{3-}, \text{HCit}^{2-}, \text{H}_2\text{Cit}^-]$ at $I = 0.3 \text{ M}$ with the related fit curves. The classification is based on the predominance of the respective species at a given sample pH.

Table 13: Stability constants β_i and electrophoretic mobilities of the individual species μ_i for the different Np(V)-citrate complexes at $I = 0.3 \text{ M}$. The limits of error $\Delta(\beta_i)$ are resulting from the fitting procedure. The uncertainties $\Delta\mu_i$ are estimated to be $0.1 \cdot 10^{-4} \text{ cm}^2 \text{ V}^{-1} \text{ s}^{-1}$ in all cases.

species	β_i/M^{-i}	$\Delta\beta_i/M^{-i}$	$\log(\beta_i)$	$\Delta\log(\beta_i)$	$\mu_i/10^{-4} \text{ cm}^2 \text{ V}^{-1} \text{ s}^{-1}$
NpO_2^+					2.4
$[\text{NpO}_2(\text{Cit})]^{2-}$	3680	719	3.57	0.08	-1.1
$[\text{NpO}_2(\text{Cit})_2]^{5-}$	58453	10385	7.31	0.02	-2.7
NpO_2^+					2.2
$[\text{NpO}_2(\text{HCit})]^-$	129	12	2.11	0.04	-0.5
$[\text{NpO}_2(\text{HCit})_2]^{3-}$	404	80	2.61	0.09	-2.0
NpO_2^+					2.2
$[\text{NpO}_2(\text{H}_2\text{Cit})]_{\text{aq}}$	11	29	1.02	1.20	0.0*

* held constant during the fitting procedure

The set of electrophoretic mobilities show a consistent trend for the correlation of the charge of the species and the respective value of μ_i . The three results for the free NpO_2^+ ion are in good agreement.

4. Determination of Stability Constants with CE-ICP-MS

It is further apparent from Table 13, that the stability constants increase with increasing charge of the ligand species (see discussion in the Am(III) section). The data evaluation of [05HUM] just reports on the stability constant of the 1:1 complex of Np(V) with the Cit³⁻ ligand. The value of $\log(\beta_1) = 3.68 \pm 0.05$ for zero ionic strength fits well with the result presented above for $I = 0.3$ M. Bonin et al. [07BON] examined two consecutive complexes for each of the ligand species at $I = 1.0$ M: $\log(\beta_1) = 1.6 \pm 0.2$ and $\log(\beta_2) = 2.4 \pm 0.5$ for Cit³⁻, $\log(\beta_1) = 2.0 \pm 0.2$ and $\log(\beta_2) = 3.2 \pm 0.3$ for HCit²⁻ and $\log(\beta_1) = 1.3 \pm 0.3$ and $\log(\beta_2) = 1.9 \pm 0.5$ for H₂Cit⁻. These results agree quite well with the values determined in the present work for the HCit²⁻ and the H₂Cit⁻ species, except for the fact that in [07BON] a second H₂Cit⁻ complex is described. However, as explained above, in the given case better results were obtained for just one complex. A greater disagreement appears for the Cit³⁻ ligand. The values by Bonin et al. are much smaller than those from this work. Since they are also smaller than the corresponding stability constants of the HCit²⁻ species, higher $\log(\beta_i)$ should be more probable, especially in combination with the good agreement with [05HUM].

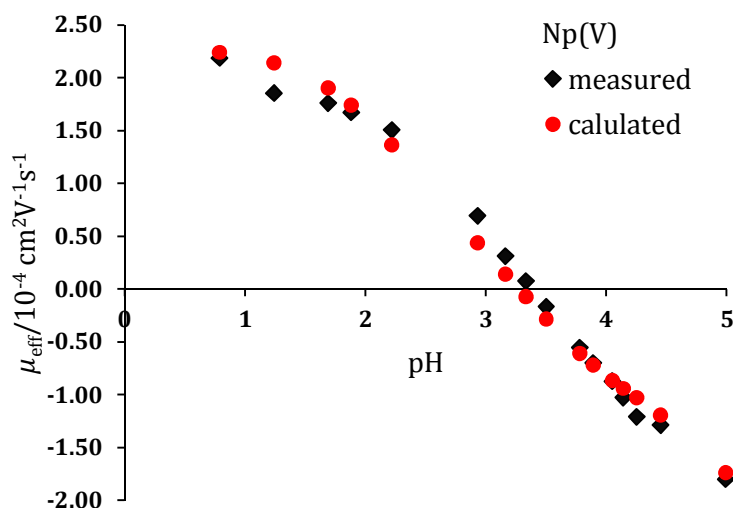


Figure 18: Comparison of the measured and the calculated effective electrophoretic mobility μ_{eff} of the Np(V)-citrate series at $I = 0.3$ M.

To verify these results, again the effective electrophoretic mobility μ_{eff} was calculated for every sample by means of Equation (4.15) with the values given in Table 13. As μ_0 for the free NpO_2^+ ion the average value of $\mu_0 = 2.3 \cdot 10^{-4} \text{ cm}^2 \text{ V}^{-1} \text{ s}^{-1}$ was used. The comparison of these values with the experimentally measured μ_{eff} is depicted in Figure 18. It can be seen from that figure that the results are in good agreement, which further approves the method of data evaluation applied here.

URANIUM(VI)

As for the Am(III)- and the Np(V)-citrate systems, the determination of stability constants of all three ligand species was possible for the U(VI) system. The experimental results together with the corresponding fit curves can be found in Figure 19.

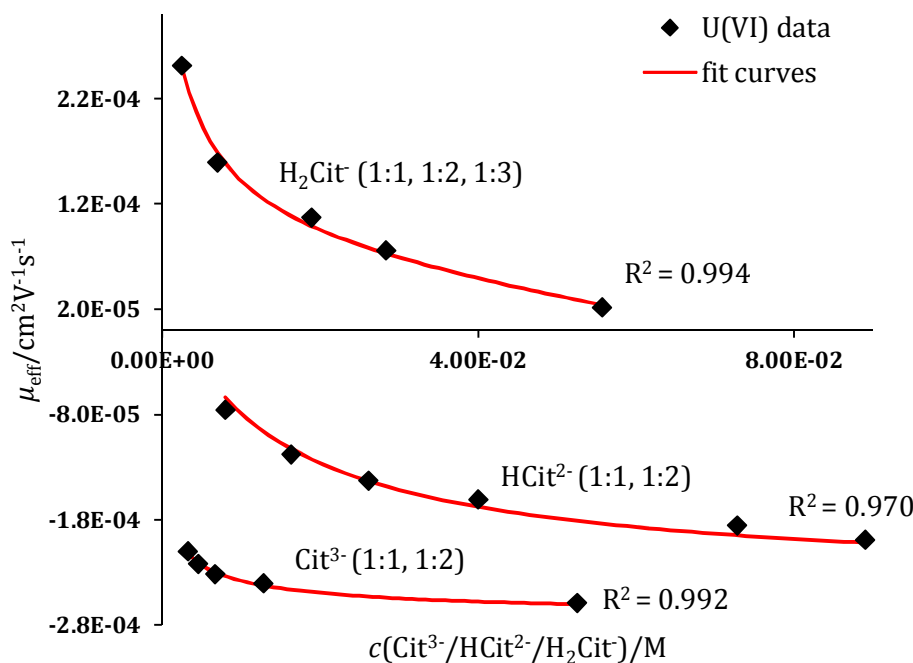


Figure 19: Measured effective electrophoretic mobilities μ_{eff} of the uranium(VI)-citrate series as a function of the respective free citrate species concentration $[\text{Cit}^{3-}]$, $[\text{HCit}^{2-}]$, $[\text{H}_2\text{Cit}^-]$ at $I = 0.3 \text{ M}$ with the related fit curves. The classification is based on the predominance of the respective species at a given sample pH.

As can be seen from the figure above, the best fitting results could be obtained by assuming three consecutive species for H_2Cit^- and two for both Cit^{3-} and HCit^{2-} with good coefficient of determination R^2 for all fits. In the case of HCit^{2-} executing the fitting procedure for three complexes instead of two was also possible leading to an even slightly better R^2 , but the individual errors of the resulting $\log(\beta_i)$ were very high. Moreover, the $\log(\beta_i)$ values for the second and third species became nearly identical. Because of these observations, the results presented here were considered more appropriate. The thus determined stability constants β_i (and $\log(\beta_i)$) at $I = 0.3 \text{ M}$ and the corresponding electrophoretic mobilities of the individual species μ_i are summarized in Table 14.

4. Determination of Stability Constants with CE-ICP-MS

Table 14: Stability constants β_i and electrophoretic mobilities of the individual species μ_i for the different U(VI)–citrate complexes at $I = 0.3$ M. The limits of error $\Delta(\beta_i)$ are resulting from the fitting procedure. The uncertainties $\Delta\mu_i$ are estimated to be $0.1 \cdot 10^{-4} \text{ cm}^2\text{V}^{-1}\text{s}^{-1}$ in all cases.

species	β_i/M^{-i}	$\Delta\beta_i/\text{M}^{-i}$	$\log(\beta_i)$	$\Delta\log(\beta_i)$	$\mu_i/10^{-4} \text{ cm}^2\text{V}^{-1}\text{s}^{-1}$
UO_2^{2+}					5.2
$[\text{UO}_2(\text{Cit})]^{2-}$	9242	1314	3.97	0.06	-2.2
$[\text{UO}_2(\text{Cit})_2]^{4-}$	751642	61954	5.88	0.04	-2.7
UO_2^{2+}					2.5
$[\text{UO}_2(\text{HCit})]_{\text{aq}}$	1866	132	3.27	0.03	0.0*
$[\text{UO}_2(\text{HCit})_2]^{2-}$	111815	7225	5.05	0.03	-2.4
UO_2^{2+}					3.7
$[\text{UO}_2(\text{H}_2\text{Cit})]^+$	257	21	2.41	0.03	0.7
$[\text{UO}_2(\text{H}_2\text{Cit})_2]_{\text{aq}}$	2531	780	3.40	0.13	0.0*
$[\text{UO}_2(\text{H}_2\text{Cit})_3]^-$	17951	3487	4.25	0.08	-2.4

* held constant during the fitting procedure

The three results for the free UO_2^{2+} ion are quite widely scattered but the average of these values of $\mu(\text{U(VI)}) = 3.8 \cdot 10^{-4} \text{ cm}^2\text{V}^{-1}\text{s}^{-1}$ is in a reasonable range compared to the results given in Section 4.2, Table 6. The other electrophoretic mobilities show a consistent trend for the correlation of the species charge and the respective value of μ_i .

Once more, as valid for Np(V), the stability constants increase with increasing charge of the ligand species (see discussion in the Am(III) section). Hereby, the differences between the $\log(\beta_i)$ of the Cit^{3-} species and the corresponding values for the HCit^{2-} species are very small, the complexes of the threefold deprotonated species are just slightly more stable than the ones complexed by HCit^{2-} . This may be an indication that too low Cit^{3-} stability constants are determined in this case. The values, which can be found in the literature substantiate this suspicion. In the data evaluation given in [05HUM], for $[\text{UO}_2(\text{Cit})]^{2-}$ a $\log(\beta^{0.1}) = 8.96 \pm 0.17$ for zero ionic strength is presented. This is much higher than the result determined here. The same is true for two more recent works by Berto et al. [12BER] ($\log(\beta_1) = 7.51 \pm 0.05$, $I = 0.1$ M NaCl) and by Zhang et al. [15ZHA] ($\log(\beta_1) = 9.73$, $I = 0.05$ M (Na, H)ClO₄, pH = 1.98). Due to this it was tried to start the fitting procedure with much higher starting values for the respective parameters but either no fit could be obtained or the same results as presented

here emerged. In the mentioned literature, also stability constants for the binuclear $[(\text{UO}_2)_2(\text{Cit})_2]^{2-}$ species are given: $\log(\beta_{0,2}^{\text{binuclear}}) = 21.3 \pm 0.5$ in [05HUM] and $\log(\beta_{2, \text{binuclear}}) = 19.5 \pm 0.01$ in [12BER]. Such species are neglected in the present evaluation which may be a reason for the discrepancies of the results. For the HCit^{2-} ligand only the stability constant of the 1:1 complex with U(VI) is mentioned in [05HUM] with a value of $\log(\beta_{0,1}) = 5.00 \pm 1.0$ for zero ionic strength. This result is in much better agreement with the data in Table 14. In [05HUM], no $\log(\beta)$ for U(VI)- H_2Cit^- are considered reliable enough to appear in the review, but two values can be found in the literature. In [75OHY], a value of $\log(\beta_1) = 2.79$ was determined by a cation exchange method ($I = 0.1 \text{ M}$, $\text{Na}(\text{H}_2\text{Cit})$ medium, $\text{pH} = 2.2 - 2.9$), $\log(\beta_1) = 1.53$ by spectroscopy ($I = 1.0 \text{ M}$, $((\text{H}, \text{Na})(\text{UO}_2)_{0.5})\text{Cit}$ medium) is published in [80VAN]. A comparison with the results presented here seems difficult because of the great difference of the literature values, but at least it can be shown that they are roughly in the same order of magnitude.

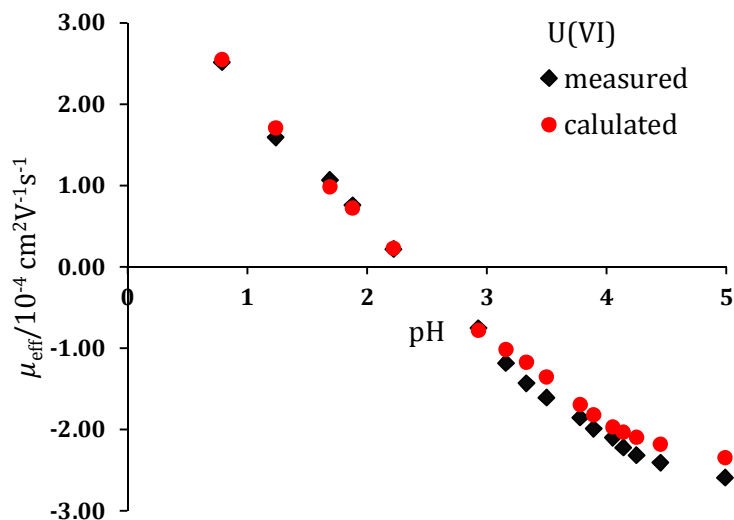


Figure 20: Comparison of the measured and the calculated effective electrophoretic mobility μ_{eff} of the U(VI)-citrate series at $I = 0.3 \text{ M}$.

Comparable to the Am(III) and Np(V) investigations, the effective electrophoretic mobility μ_{eff} was calculated for every sample by means of Equation (4.15) with the values given in Table 14. For the free UO_2^{2+} ion the average value of $\mu_0 = 3.8 \cdot 10^{-4} \text{ cm}^2 \text{ V}^{-1} \text{ s}^{-1}$ was used. The comparison of these values with the experimentally measured μ_{eff} is depicted in Figure 20. The good agreement of the experimental data points with those calculated is a satisfactory confirmation of the presented results, especially in view of the comparison with the literature data. As one can see, in the higher pH region, the calculated values are higher

4. Determination of Stability Constants with CE-ICP-MS

than the measured ones. This again is a clear sign that the determined stability constants for the Cit^{3-} species are too small since they are assumed to be the dominant species there.

4.7.6 CONCLUSION

The measurement series presented above shows that CE-ICP-MS in general is a suitable analytical tool for the stability constant investigation of the complex formation of actinides with compounds exhibiting more than one possible ligand species. Because of the more challenging data evaluation in comparison to simpler ligands, the measurement of more samples is required in order to obtain a wider amount of data points. Consequently, the experiments presented in this section are to be understood as a feasibility study demonstrating the general practicability of such investigations.

REMARK:

The citrate investigation described above was undertaken within the framework of the diploma thesis of Daniel Leichtfuß [17LEI2] under the guidance of Christian Willberger and Tobias Reich. Samples preparation and CE-ICP-MS measurements were conducted by Daniel Leichtfuß and Christian Willberger. The evaluation as presented here was conducted by Christian Willberger.

5. DETERMINATION OF REDOX KINETICS WITH CE-ICP-MS

5.1 INTRODUCTION

The measurement of kinetic parameters of reduction or oxidation processes of metal ions with a wide variety of reducing or oxidizing agents is another interesting application of the coupling of CE to ICP-MS. In this case, additionally to the already discussed capability of following actinide systems at low concentrations, the use of an ICP-MS as the detector allows for the investigation of a large number of different metals besides actinides, e.g. transition metals. Furthermore, if both redox partners are metals, it is possible to monitor the development of the concentrations of both the reductant and the oxidant at the same time thanks to ICP-MS being a multi element detection technique.

The theoretical background for the investigation of redox kinetics of actinides (or also other metals) is delineated in the 'Materials and Methods' section in '2.1 Capillary electrophoresis for determination of kinetics of redox reactions' of the kinetic publication [18WIL] presented in Section 5.2 of this work.

The method was employed for the determination of the kinetical parameters of the reduction of Np(V) to Np(IV) by different concentrations of HAHCl at different temperatures. The results are presented in the already mentioned kinetic publication [18WIL] depicted in Section 5.2. In addition to the findings presented in the publication the influence of iron on this reaction was investigated and the results are described subsequent to the manuscript.

A second redox system examined was the Pu(VI)/Fe(II) couple. The results of these experiments are summarized in Section 5.3. Since the measuring of iron ions by ICP-MS is impeded compared to other ions because of interferences occurring on the Fe masses, special attention was paid to the integration of the use of a octopole reaction system (ORS) to the kinetic determination experiments in order to overcome the interferences difficulties allowing the follow the development of both Pu(IV) and Fe(II) during the redox reaction within one and the same measurement.

5. Determination of Redox Kinetics with CE-ICP-MS

5.2 DETERMINATION OF KINETIC PARAMETERS OF THE REDOX REACTION OF NP(V) WITH HAHCL BY CE-ICP-MS

5.2.1 PUBLICATION: DETERMINATION OF KINETIC PARAMETERS OF REDOX REACTIONS USING CE-ICP-MS: A CASE STUDY FOR THE REDUCTION OF NP(V) BY HYDROXYLAMINE HYDROCHLORIDE

AUTHOR CONTRIBUTIONS:

The sample preparations and the CE-ICP-MS measurements were performed by Christian Willberger. Preceding experiments regarding this CE-ICP-MS application were conducted during the diploma thesis of Christian Willberger under the guidance of Nils Stöbener, Samer Amayri and Tobias Reich. Data evaluation was conducted by Christian Willberger. The conceptual planning of this investigation and the layout of the manuscript were done by Christian Willberger and Tobias Reich. The manuscript was written by Christian Willberger. The cover picture was designed by Christian Willberger.

Further Remarks:

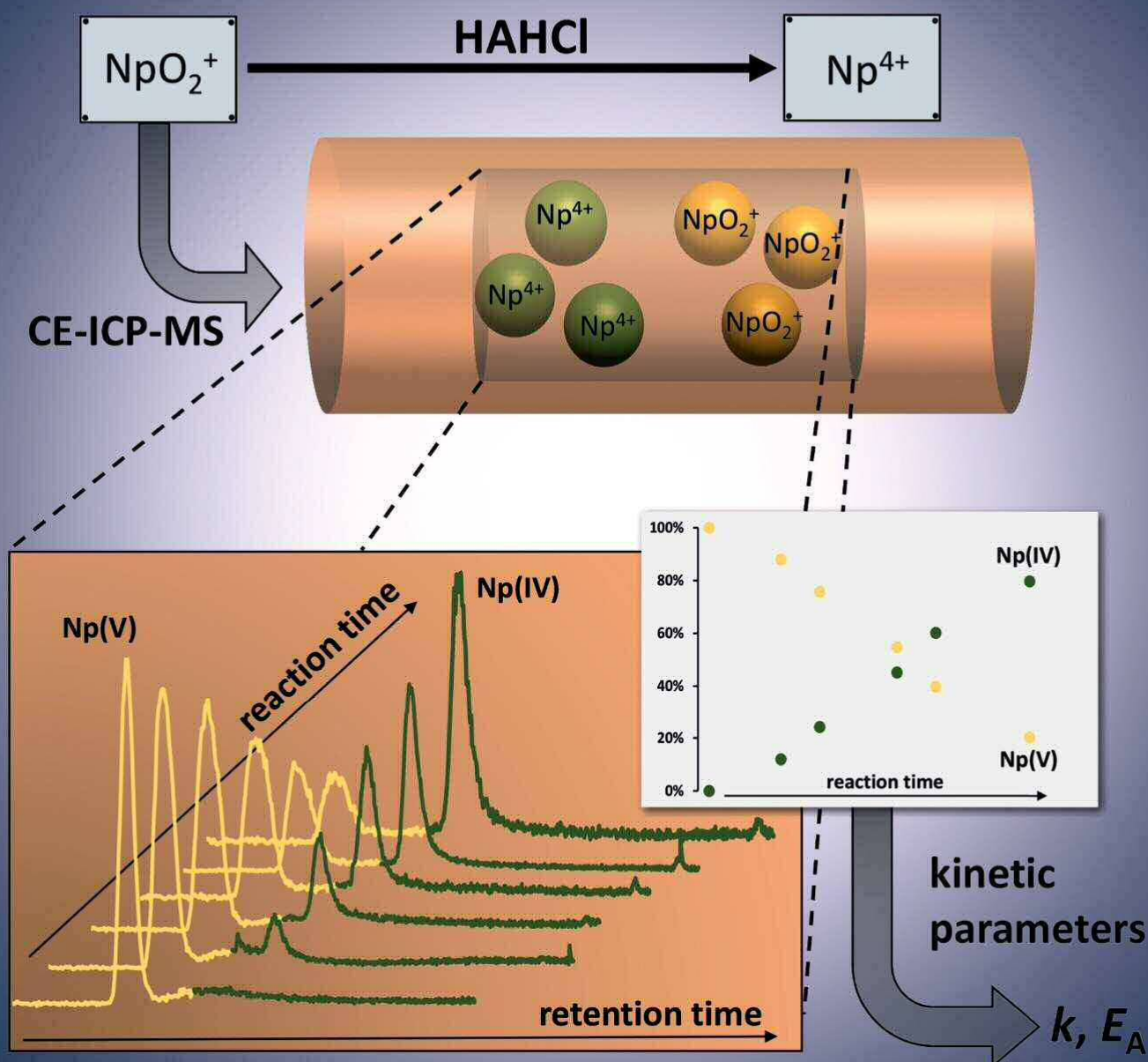
The additional figures S-1 to S-3 mentioned in the manuscript are presented in the Supporting Information that can be found in the APPENDIX A6.

The numbering of the pages, tables, figures and equations within the manuscript and in the Supporting Information has remained unchanged and thus is not in accordance with the numbering of the rest of this work. The same is true for the citations.

ELECTROPHORESIS

Liquid Phase Separation Techniques
Microfluidics • Nanoanalysis • Proteomics

23'18



Christian Willberger
Samer Amayri
Tobias Reich 

Institut für Kernchemie,
Fritz-Strassmann-Weg 2,
Johannes Gutenberg-Universität,
Mainz, Germany

Received July 25, 2018
Revised August 30, 2018
Accepted August 30, 2018

Research Article

Determination of kinetic parameters of redox reactions using CE-ICP-MS: A case study for the reduction of Np(V) by hydroxylamine hydrochloride

The rate constants k of the reduction of 5×10^{-5} M Np(V) to Np(IV) by hydroxylamine hydrochloride (HAHCl) in 1 M HCl have been determined by CE-ICP-MS in the temperature range of $\vartheta = 30\text{--}70^\circ\text{C}$ and with varying concentrations of HAHCl from 1 to 7.2 M. The reaction was found to have (pseudo)first order kinetics with respect to HAHCl. The experimental results for k ranged from $0.0029(1) \text{ min}^{-1}$ ($\vartheta = 40^\circ\text{C}$, $c(\text{HAHCl}) = 3 \text{ M}$) to $0.039(7) \text{ min}^{-1}$ ($\vartheta = 60^\circ\text{C}$, $c(\text{HAHCl}) = 7.2 \text{ M}$). The activation energy of the reaction was determined as $E_A = (72 \pm 10) \text{ kJ/mol}$. These results and a comparison with literature data show that the coupling of CE to ICP-MS provides a powerful analytical tool for the investigation of the kinetic aspects of redox reactions of actinides at low concentrations. On the basis of this proof-of-principle study, the method presented here can be extended to the investigation of the kinetic parameters of other redox systems containing different actinides (or transition metals) and oxidants/reductants.

Keywords:

CE-ICP-MS / hydroxylamine hydrochloride / neptunium / rate constant / redox reaction

DOI 10.1002/elps.201800318



Additional supporting information may be found online in the Supporting Information section at the end of the article.

1 Introduction

A detailed knowledge about the kinetics of redox reactions of actinides is of great importance for many aspects concerning separation processes in nuclear fuel reprocessing. Data on the rate of change of oxidation states by means of reducing or oxidizing agents are of great interest since they provide information about the effectiveness of a particular separation process and allow more accurate calculations in computer simulations of such processes [1]. In addition, redox reactions affect strongly the speciation of actinides in environmental systems. This, for example, is important for statements about the long-term safety of a potential future nuclear waste

repository. A deep understanding of such speciations leads to a better understanding of the geochemical behavior and sorption or transport processes of radionuclides in the biosphere, since they are strongly correlated to the oxidation state (besides other factors) [2]. Therefore, here, too, the knowledge of kinetic parameters is of great benefit.

The reaction of hydroxylamine with actinides such as plutonium and neptunium is of great interest since it is commonly used, among others, as a reducing agent in industrial separation processes such as the PUREX process [3, 4]. In the case of neptunium, the oxidation state is not fully controlled. Thus, to prevent a distribution to different fractions during the process, many efforts towards an advanced PUREX process have been made [5]. Concomitant with that is the need for detailed information on kinetic data for neptunium reactions with different reducing agents.

There have been a large number of works published by the group of Koltunov et al. on the kinetics of the reduction of neptunium and plutonium by hydroxylamine [6] and hydroxylamine derivatives [7] in different media. The reduction of Np(V) was investigated in nitric acid solution in the temperature range of $61\text{--}92^\circ\text{C}$ and an ionic strength of $I = 4 \text{ M}$ by a spectrophotometric method [8]. El-Naggar et al. [9] used a solvent extraction method and spectrophotometry to also study

Correspondence: Christian Willberger and Dr. Tobias Reich, Institut für Kernchemie, Fritz-Strassmann-Weg 2, Johannes Gutenberg-Universität Mainz, 55112 Mainz, Germany
E-mail: willberg@uni-mainz.de; treich@uni-mainz.de

Abbreviations: **aq**, dissolved in aqueous solution; **HAHCl**, hydroxylamine hydrochloride; **HDEHP**, bis(2-ethylhexyl) phosphate; **KCE**, kinetic capillary electrophoresis; **LLE/LSC**, liquid-liquid extraction with liquid scintillation counting; **PUREX**, plutonium-uranium recovery by extraction

the reaction of Np(V) with hydroxylamine (and hydrazine) in nitric acid solution with and without small amounts of Fe³⁺ ions as catalyst. The experiments were carried out in a temperature range of 50–70°C. An examination with hydroxylamine hydrochloride (HAHCl) in perchloric acid solution at 70°C via absorption spectroscopy was performed by Inoue et al. [10]. They found that the reaction is much faster in a chloride medium compared to a nitrate medium. All works report unanimously on the need for elevated temperatures since the reaction is extremely slow at room temperature and on an order of reaction of one with respect to Np(V).

Capillary electrophoresis (CE), particularly in combination with ICP-MS (inductively coupled plasma mass spectrometry) as a highly sensitive detection method, has proven to be a very powerful tool for the determination of element speciations [11, 12] and stability constants of complexes [13], especially in the field of actinides [14, 15]. A variety of different CE methods for the study of the rate of affinity interactions of biomolecules summarized under the superordinate term kinetic capillary electrophoresis (KCE) is described in the literature [16–19]. Besides these biochemical applications, kinetic investigations with CE are rather scarce. Some studies have been published into the determination of hydrolysis constants of different chemical compounds [20–23] and into the reactivity of metal complexes and metal-based drugs in biological inorganic chemistry [24]. To our knowledge, almost no studies concerning the redox kinetics of metal ions, especially of actinides, have been described in the literature. Graser et al. [25] investigated the reduction of Pu(VI) by Fe(II) via CE-ICP-sector field-MS, but no rate constants were given in their paper. Nevertheless, they mentioned the capability to apply CE-ICP-MS to the determination of actinide redox kinetics.

In the present work, the kinetics of the reduction of Np(V) by HAHCl in a hydrochloric acid medium is investigated by CE-ICP-MS. A great benefit of the CE-ICP-MS system is the possibility to follow the reaction in very low concentration ranges with limits of detections of about 1×10^{-9} M [26]. This is orders of magnitude lower compared to the analytical methods used in former works [6–10] and allows for more accurate results in the investigation of actinides in environmental systems.

The experimental conditions were chosen for several reasons. Due to the fact that this work should demonstrate the applicability of the CE-ICP-MS system in the determination of rate constants of redox reactions with actinides, a preferably distinct reaction was selected. Therefore, a nitrate medium was avoided, because the oxidation of both hydroxylamine and Np(V) by HNO₃, the latter even being catalyzed by generated HNO₂, would influence and therefore complicate the kinetics of the Np(V) reduction. For similar reasons, the reaction was investigated in an all-chloride medium, allowing the assumption of a constant chloride concentration throughout all experiments, since this concentration also influences the rate of reduction [10]. Neptunium was the actinide of choice because just two species, Np(V) and Np(IV), are involved in the reaction [5]. Unlike plutonium [6b,6e], Np(III) is very

unstable under the experimental conditions and is very rapidly reoxidized to Np(IV) by oxygen from the air [8]. Finally, a comparison with the existing literature data allows an evaluation of our results and can prove that CE-ICP-MS is an appropriate analytical tool for the determination of rate constants of redox reactions with actinides in low concentration ranges.

2 Materials and methods

2.1 Capillary electrophoresis for determination of kinetics of redox reactions

Basics and theoretical considerations about CE are described extensively in the literature (e.g. see [27]); thus, here just the aspects applying to this work are summarized.

An electropherogram obtained from a CE-ICP-MS measurement basically provides two important pieces of information for the determination of kinetic parameters of redox processes:

- (i) Conclusions about the speciation of an ion *i* can be drawn from the electrophoretic mobility μ_i , which is calculated from the retention times t_i and t_{EOF} of the ion and the electro-osmotic flow (EOF), respectively. For a given capillary length *l* and high voltage *U* the electrophoretic mobility can be calculated from Equation (1):

$$\mu_i = \frac{l^2}{U} \left(\frac{1}{t_i} - \frac{1}{t_{\text{EOF}}} \right) \quad (1)$$

The electrophoretic mobility depends on the charge and on the size of the examined ion. Consequently, by determining μ_i one can make statements about the oxidation state of the ion and about possible complexations, since both influence size and charge and hence differences in the electrophoretic mobility.

- (ii) From the peak areas, the concentrations of the respective species can be evaluated. By calculating the shares of the peak areas of different species in an electropherogram at a specific time of reaction, one can determine the reaction progress at that time. Therefore, recording multiple electropherograms during the course of a redox reaction allows tracking the kinetics of this very reaction. From these data rate constants can finally be determined.

The mathematical analysis of the peak areas determined in the CE experiments then depends on the order of reaction of the investigated reaction. Because of the literature data [8–10], in this case a first-order reaction (effectively pseudo-first-order because of the great excess of HAHCl) with respect to Np(V) was assumed. Therefore, the rate law for Np(V) is given according to Equation (2) [28]:

$$\frac{d[\text{Np(V)}]}{dt} = -k[\text{Np(V)}] \quad (2)$$

The square brackets indicate concentrations, *t* is the reaction time and *k* the rate constant. From the integrated form

[Equation (3)] the rate constant can then be derived graphically. The index 0 describes the initial concentration.

$$\ln \left(\frac{[\text{Np(V)}]}{[\text{Np(V)}]_0} \right) = -kt \quad (3)$$

For the determination of k , thus just the ratio $[\text{Np(V)}]/[\text{Np(V)}]_0$ at different reaction times has to be known. For a first-order kinetics, the half-life of a reaction $t_{1/2}$ can be calculated from the rate constant according to Equation (4):

$$t_{\frac{1}{2}} = \frac{\ln(2)}{k} \quad (4)$$

In this work, k has been examined at different temperatures T . From these values one can calculate the activation energy E_A by an Arrhenius approach; the equation used is given in (5). A is the pre-exponential factor and R the ideal gas constant.

$$\ln(k) = \ln(A) - \frac{E_A}{RT} \quad (5)$$

In addition to the general requirements for the samples and the CE-ICP-MS system [12, 29, 30], the investigated redox system itself has to meet several demands for the determination of kinetic parameters:

- At least one redox pair has to have (at least) two species with different electrophoretic mobilities. These species have to be stable on the time scale of a CE experiment, meaning that the kinetics of the redox reaction must be slow compared to the duration of measurement (see also [31]).
- The species separated by CE must be unambiguously detectable by ICP-MS. This applies equally to other detection methods.
- The CE separation process (by applying a high voltage) and sample preparation (by dilution in the background electrolyte and adding the EOF marker) must not influence the equilibrium of the redox species. Hence, the redox process must not continue or return during sample preparation or in the capillary after sampling.

As shown later, all these points are fulfilled for the Np(V)-HAHCl redox system.

A great advantage of the coupling of CE to ICP-MS for the examination of the kinetics of redox reactions comes into effect if both of the redox partners are metal ions. In this case, there is the opportunity to follow the proportions of both redox pairs simultaneously throughout the reaction, allowing the determination of the rate constants for all participating reagents in parallel.

2.2 CE-ICP-MS system

The electrophoresis experiments were conducted with an Agilent 7100 CE system hyphenated to an Agilent 7500 ce (both Agilent Technologies, Santa Clara, CA, USA). A MiraMist

CE nebulizer (Burgener Research, Mississauga, Canada) was connected to a Scott-type spray chamber (AHS Analysentechnik, Tübingen, Germany) to achieve a preferably efficient coupling. Through a syringe pump (PicoPlus, Harvard Apparatus, Holliston, MA, USA) a make-up electrolyte consisting of 1.25% HNO₃ solution with 10% ethanol and 5 ppb ⁸⁹Y, ¹⁰³Rh, ¹⁴⁰Ce, and ²⁰⁹Bi (internal standards) was inserted. The flow rate was adjusted experimentally to 5 μL min⁻¹ as the optimal value.

Fused silica capillaries (Polymicro Technologies, Phoenix, AZ, USA) with an inner diameter of 50 μm and a length of 76 cm were used, while a high voltage of 25 kV was applied, leading to a current between 9 and 14 μA during measurements. A background electrolyte of 1 M acetic acid was used. The samples were prepared in conical micro-inserts of borosilicate glass (Carl Roth AG, Arlesheim, Switzerland), which were placed in polyethylene vials sealed with polyethylene olefin snap caps (both Agilent Technologies, Santa Clara, CA, USA). Sample introduction was by hydrodynamic injection (100 mbar for 8 s). The average time to record one electropherogram was about 15 min. Before every use the capillaries were preconditioned by flushing with MilliQ water, 0.1 M NaOH solution, 0.1 M HCl and the background electrolyte. Between the different runs the capillary was flushed with 1 M acetic acid for 15 min for cleaning purposes. Temperature was controlled at 25°C by the air-cooling device of the Agilent apparatus. Temperature rise in this system due to Joule heating was calculated to be on average 0.5°C and to not exceed 1°C [27].

The ICP-MS was used as a detector in the time-resolved analysis detection mode with a dwell time of 100 ms and a plasma power of 1550 W. The lens system and the argon flow rates were regulated by a tuning process carried out before every measurement. Carrier gas and make-up gas flow rates were adjusted to 0.86–1.15 and 0.28–0.77 L min⁻¹, respectively. Data processing was conducted with MassHunter Workstation software (G7200B, Agilent Technologies, Santa Clara, CA, USA).

2.3 Reagents

All chemicals used were of pro-analysis quality or better. To prevent clogging of the capillary, all solutions were filtered through 0.2 μm syringe filters (Nalgene, Rochester, NY, USA). The dilutions were performed with MilliQ water (18.2 MΩ, Synergy™ Millipore water system, Millipore GmbH, Schwalbach, Germany). Sodium hydroxide, 2-bromopropane, hydroxylamine hydrochloride (HAHCl), bis(2-ethylhexyl) phosphate (HDEHP), toluene, nitric acid (superpure) and rhodium ICP-MS standard solution were from Merck (Darmstadt, Germany). Acetic acid was supplied by Riedel-de Haën (Seelze, Germany), ethanol by AppliChem GmbH (Darmstadt, Germany) and hydrochloric acid by Fisher Scientific (Loughborough, UK). The ICP-MS elemental standard solutions for bismuth, cerium and yttrium were ordered from High-Purity Standards (Charleston,

SC, USA). As plasma gas, 4.6 Ar was used (Westfalen AG, Münster, Germany).

An in-house stock solution of a known concentration of $^{237}\text{Np(V)}$ in 1 M perchloric acid was used. No change from perchloric to hydrochloric medium was undertaken, since with a dilution by nearly three orders of magnitude during sample preparation (see Section 2.4) the stock solution medium becomes negligible. The concentration of the Np(V) stock solution was checked gamma-spectrometrically before the experiments with the γ -lines at 29.4 keV and 86.5 keV with a high-purity Ge-detector (GMX-13280-S, EG & G ORTEC, USA) with a Canberra InSpector 2000 DSP Portable Spectroscopic Workstation (model IN2K, Canberra Industries Inc., USA) and Genie 2000 Gamma software (V. 3.0, Canberra Industries Inc., USA). The gamma spectrometer was calibrated with a multiple gamma-ray emitting solution (serial number: 1850–27, Eckert & Ziegler Isotope Products, Braunschweig, Germany). The oxidation state of Np in the stock solution was verified by UV-Vis spectroscopy (Tidas 100, J&M Analytic AG, Essingen, Germany) with the absorption band at 981 nm.

2.4 Sample preparation

2.4.1 CE

The HAHCl was dissolved in 1 mL 1 M HCl to obtain the required concentration. This solution was tempered to the respective temperature in a water bath with a thermostat (Haake C10, Thermo Electron Corporation, Waltham, MA, USA). When the temperature was stable, 4.5 μL Np(V) stock solution was added to yield a Np(V) concentration of 5×10^{-5} M and a stopwatch was started. After different reaction times 3 μL samples were taken. The first sample was collected directly after the addition of Np to ensure that every time at the beginning of the reaction 100% Np(V) was present.

For CE-ICP-MS measurements the samples were transferred to the CE glass vials containing 197 μL of 1 M acetic acid and 1 μL of 2-bromopropane as the EOF marker (the EOF was detected on bromine mass 79 by ICP-MS). The Np concentration during measurements was 7.5×10^{-7} M.

2.4.2 LLE/LSC

As a further method besides CE-ICP-MS for the investigation of the distribution of the Np species liquid-liquid extraction (LLE) with liquid scintillation counting (LSC) was used (see Section 3.1). For this, a method introduced by Nitsche et al. [32] developed for the separation of Pu oxidation states was adapted and modified. From a reaction solution prepared identically to that described above, aliquots of 0.5 mL were taken at given times. The sample was then transferred into a vial containing 1.5 mL 1 M hydrochloric acid and 3 mL of a solution of 3 M HDEHP in toluene. The resulting two-phase mixture was shaken vigorously for 1 min on a vortex

mixer (SA8, Stuart, Staffordshire, UK). Phase separation resulted from centrifugation (3K30, Sigma, Osterode am Harz, Germany) for 5 min at 5000 rpm. For the analyses of the concentration of Np(IV) in the organic phase and Np(V) in the inorganic phase, 500 μL was taken from each phase and added to 10 mL Ultima Gold XR LSC cocktail (PerkinElmer, Waltham, MA, USA) each. This solution was finally quantified via LSC (300SL, Hidex, Turku, Finland). The proportions of the two Np species were calculated from the sum of the measured activities in the two phases.

2.5 Data treatment

The peak areas in the electropherograms were evaluated with MassHunter Workstation software. In doing so, attention was always paid to define similar peak markers in order to minimize possible errors resulting from different peak treatment. The area of the Np(V) peak was set in relation to the sum of the Np(IV) peak areas (for explanations see Section 3.2). The $[\text{Np(V)}]/[\text{Np(V)}]_0$ ratio was derived from the percentages of the peak areas calculated in one electropherogram, not from the concentrations directly. This also minimized error-containing factors in the results, since in CE-ICP-MS many aspects, such as the coupling device or the sample introduction, have an influence on the efficiency of the system. Furthermore, no calibration of the instrument was necessary. By calculating the shares of Np(V) and Np(IV) individually in each electropherogram, their ratio becomes independent of the actual measured concentrations.

Plotting the logarithm of the ratio of the neptunium species $\ln([\text{Np(V)}]/[\text{Np(V)}]_0)$ against the reaction time t allows determination of the rate constant k of the reaction at a given temperature T from Equation (3) by fitting the experimental curve with a linear fit function. The same applies for the examination of the activation energy E_A from a linear fit of the plot of $\ln(k)$ against $1/(RT)$ according to Equation (5).

3 Results and discussion

3.1 Conservation of $\text{Np(V)}/\text{Np(IV)}$ ratio between sampling and measurement

When using the CE-ICP-MS method as a reliable tool for the determination of kinetic parameters of redox reactions, it is of great importance that the $\text{Np(V)}/\text{Np(IV)}$ ratio in a sample at a given reaction time is preserved. Because of this, two important aspects concerning the reproducibility and the accuracy of the results obtained have to be considered. First, the percentages of the respective Np species must not be altered due to dilution effects and changes in the dissolving medium. Second, since there is a short period of time between sampling and the start of the measurement, the reaction has to be stopped completely once the sample is taken. For both cases, preliminary investigations were performed to exclude a distortion of the results.

3.1.1 Stability of samples with regard to dilution and changes in the solvent

During sample preparation, the reaction solution is diluted by almost two orders of magnitude. This also leads to a change in solvent from 1 M hydrochloric acid to mainly 1 M acetic acid. To guarantee that both of these factors do not alter the speciation in the solution, we compared the CE-ICP-MS results for one series with the findings obtained by a different method, namely LLE/LSC. The experiments were carried out as described in Section 2.4. The experimental conditions were a temperature of 50°C and a HAHCl concentration of 7.2 M.

In Fig. 1A the development of the percentages of Np(V) and Np(IV) at different times of the reaction are compared. Furthermore, in Fig. 1B the graphical determination of the rate constant measured by LLE/LSC is shown. As one can see from Fig. 1A both methods provide consistent results.

An overview of the rate constants k and the respective half-lives $t_{1/2}$ of the reaction obtained in five different series measured with CE-ICP-MS compared to the results shown here for the LLE/LSC series is given in Table 1. All values exhibit very good conformity, the rate constants determined by both methods are identical within the experimental uncertainties. In conclusion: under the experimental conditions used in this work there is no alteration in the Np(V)/Np(IV) ratio due to dilution or medium effects.

3.1.2 Stability of samples over time

It is known from the literature that the reduction of Np(V) by HAHCl at room temperature does not take place [8], or at least is extremely slow [10]. It is thus possible to stop the reaction and preserve the respective Np(V)/Np(IV) ratio by cooling an aliquot of the sample down to room temperature. This can be achieved by the dilution step since a very small volume of the heated sample is given to great excess of acetic acid at room temperature. Under this assumption, the transportation time, which is about 1–2 min from sample preparation to measurement, should not influence the Np(V)/Np(IV) ratio. Anyway, because the Np concentration in our work was orders of magnitude lower than that mentioned in the literature, we carried out additional investigations to prove this correct for our case. For this purpose, some samples were allowed to stand for several hours at room temperature. After this time, a further 1 μ L 2-bromopropane (it had to be added again due to its volatility) as EOF marker was added and the samples were measured again without further treatment. In five randomly selected samples from different series, reaction times, temperatures and HAHCl concentrations that had stood for 177–281 min, we observed Np(V) and Np(IV) percentages that did not vary by more than $\pm 3.5\%$. This is comparable to the limits of error for the integration of the peak areas. Consequently, within the transportation time, which was considerably shorter than the times investigated, no alteration of the sample occurs.

3.2 Interpretation of electropherograms of Np(V) and Np(IV)

To follow the redox kinetics of the reduction of Np(V) by HAHCl via CE-ICP-MS, all the peaks found have to be assigned unambiguously to either a Np(V) or a Np(IV) species. Only by this can determination of the Np(V) and Np(IV) proportions be carried out. In Fig. 2, examples of the developments of the electropherograms of two different series of measurements are shown. All the other series exhibited similar trends.

As one can see, between one and three peaks appear in the electropherograms. In all measurement series there is just one peak in the first electropherogram at the reaction time $t = 0$ min. Since the experiments were started from a pure Np(V) stock solution, this peak is assigned to a Np(V) species. This is also because the electrophoretic mobilities are in accordance with those given in the available literature for Np(V) in 1 M acetic acid ($\mu_i(\text{Np(V)}) = (2.0\text{--}2.4) \times 10^{-4} \text{ cm}^2 \text{ V}^{-1} \text{ s}^{-1}$) [25, 33]. In electropherograms of later points in the reaction progress there are two or three recognizable peaks. Therefore, the first peak with the highest electrophoretic mobility is always the Np(V) species, for the reasons already mentioned. For the later peaks there is one with a positive electrophoretic mobility and one appearing after the EOF marker. Generally speaking, all the detected species have a constant electrophoretic mobility (see Table 2). According to the literature [25, 33] the electrophoretic mobility of Np(IV) in 1 M acetic acid is $\mu_i(\text{Np(IV)}) = (1.2\text{--}1.4) \times 10^{-4} \text{ cm}^2 \text{ V}^{-1} \text{ s}^{-1}$. This again fits perfectly well with our values for the Np(IV) peak 1. The peak with the negative electrophoretic mobility is assigned also to a Np(IV) species. To verify this assignment, once again the comparison with the LLE/LSC experiments (see Section 3.1) can be considered. The results of the CE measurements can be reconciled with those of the LLE/LSC measurements if the areas of both the later peaks are added together.

Nevertheless, conclusions about the exact speciation of these Np species are difficult to draw just from CE-ICP-MS measurements. Since the first two peaks show good agreement with the available literature data measured in 1 M acetic acid alone, they should represent the respective acetate complexes of Np(V) and Np(IV) under these experimental conditions. The Np(IV) peak with the negative electrophoretic mobility, on the other hand, is not described in the literature. Because of this, it is thought to result from the HAHCl; more precisely, from the chloride ions. Both a negative Np(IV) chloride complex and the formation of a Np(IV) colloid are conceivable. It is known that colloid formation of tetravalent actinides is very likely, even in low pH ranges [34]. The latter could explain the very slow migration speed, due to its huge size and furthermore by the saturation of the positive charge on the surface by negative chloride ions. In any case, there is no identifiable systematic behavior in the appearance of the peaks. As can be seen in Fig. 2, both a dominant peak 1 [series in (a)] and a dominant peak 2 [series in (b)] is possible and

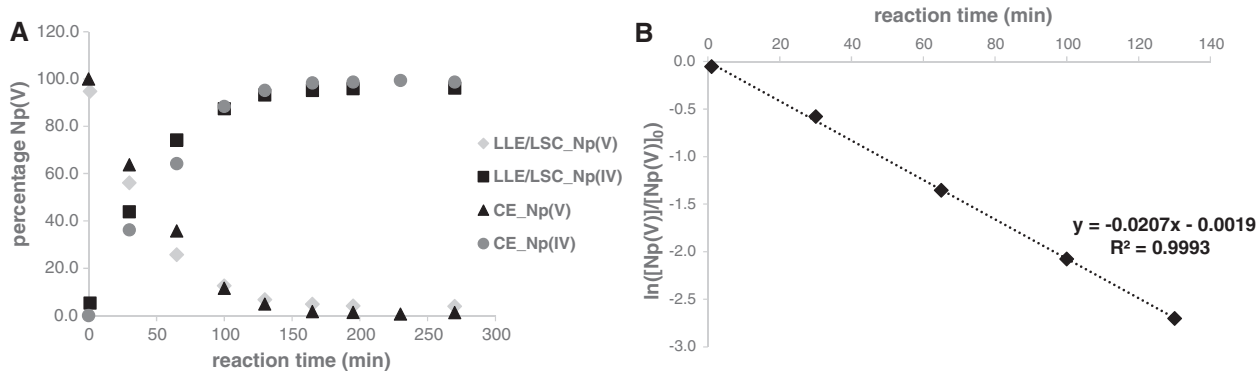


Figure 1. (A) Development of the percentages of Np(V) and Np(IV) at different reaction times determined by CE-ICP-MS compared to those from LLE/LSC. (B) Graphical determination of the rate constant measured by LLE/LSC at 50°C and [HAHCl] = 7.2 M.

Table 1. Comparison of rate constants determined by CE-ICP-MS and LLE/LSC at 50°C and [HAHCl] = 7.2 M

	CE-ICP-MS					LLE/LSC
	#1	#2	#3	#4	#5	
k (min ⁻¹)	0.020(1)	0.019(2)	0.023(2)	0.020(4)	0.024(1)	0.0207(3)
$t_{1/2}$ (min)	34(1)	36(3)	30(3)	36(5)	29(1)	33.5(0.5)
	Average		k (min ⁻¹) $t_{1/2}$ (min)		0.021(2) 33(3)	0.0207(3) 33.5(0.5)

Uncertainties are given in parenthesis applying to the last significant digit

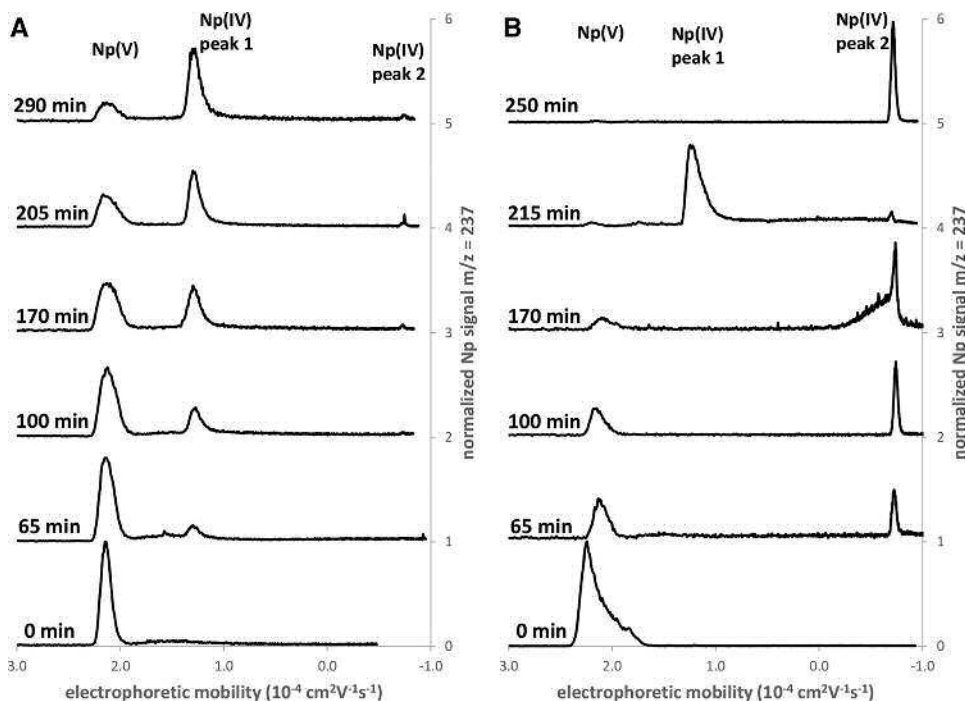


Figure 2. Development of the electropherograms during the redox reaction of Np(V) with HAHCl. (A) [HAHCl] = 1 M, ϑ = 60°C, (b) [HAHCl] = 3 M, ϑ = 60°C.

the ratio of peak 1 and peak 2 can change within one series [again in (b)].

Thus, for more detailed information about the exact speciations, further experiments with different analytical

techniques should be done. At this point we waived this because, for the evaluation of the kinetic parameters, just a distinct assignment of all peaks to one of the two Np oxidation states is necessary, and this was ensured, as described above.

Table 2. Electrophoretic mobilities of the measurement series shown in Fig. 2A and B as above

A)				B)			
Reaction time (min)	Electrophoretic mobilities ($10^{-4} \text{ cm}^2 \text{ V}^{-1} \text{ s}^{-1}$)			Reaction time (min)	Electrophoretic mobilities ($10^{-4} \text{ cm}^2 \text{ V}^{-1} \text{ s}^{-1}$)		
	Np(V)	Np(IV)			Np(V)	Np(IV)	
		peak 1	peak 2			peak 1	peak 2
0	2.14			0	2.24		
65	2.14	1.30	-0.72	65	2.15		-0.71
100	2.12	1.27	-0.73	100	2.16		-0.74
170	2.13	1.30	-0.73	170	2.10		-0.74
205	2.17	1.30	-0.75	215	2.20	1.25	-0.71
290	2.13	1.27	-0.74	250	2.14		-0.72

3.3 Dependence of the reduction kinetics on the HAHCl concentration and on the temperature

The reaction of HAHCl with Np(V) in 1 M hydrochloric acid was investigated at several temperatures ϑ between 30 and 70°C and at different initial concentrations c_0 of HAHCl in the range from 1 M to 7.2 M. The results obtained are shown in Supporting Information Fig. 1. All plots of $\ln([\text{Np(V)}]/[\text{Np(V)}]_0)$ against the reaction time t could be fitted very well with a linear function, confirming a first-order (or pseudo-first-order, respectively) kinetics with regard to Np(V). This is in accordance with the available literature [8–10]. As can be seen in Supporting Information Fig. 1, the rate of the reaction increases both with increasing temperature and with increasing concentration of HAHCl, which also accords with the results in the literature.

The rate constants k received from the fit functions of the plots in Supporting Information Fig. 1 are presented in Table 3. The respective half-lives were calculated from Equation (4). By inspection one can easily recognize that the rate of the reaction is in a reasonable range to be followed in the time scales of a CE experiment.

A direct comparison of the rate constants obtained in this work with the literature data is hardly possible because of the use of different reaction media. A variable

chloride ion concentration and the presence of nitric acid both influence the rate of the reaction. In any case, a qualitative discussion is possible. Inoue et al. [10] published a rate constant of $k = 0.067 \pm 0.003 \text{ mol}^{-3.7} \text{ L}^{3.7} \text{ min}^{-1}$ at 70°C and $[\text{HAHCl}] = 0.8\text{--}1.2 \text{ M}$, $[\text{H}^+] = 1.01\text{--}1.52 \text{ M}$ and $[\text{Np(V)}] = 2 \times 10^{-4} \text{--} 4 \times 10^{-3} \text{ M}$. This is in the same order of magnitude as the value determined in this work, $k = 0.011(1) \text{ min}^{-1}$, for comparable experimental conditions ($[\text{HAHCl}] = 1 \text{ M}$, $\vartheta = 70^\circ\text{C}$). The higher value in the literature can be explained by the higher H^+ ion concentration since a lower pH value accelerates the reaction. Koltunov et al. [8] determined a rate constant of $k = 0.03 \pm 0.001 \text{ mol}^{-1} \text{ min}^{-1}$ at 92°C in 1 M nitric acid. This also fits very well with our results extrapolated from those at 70°C, even though for comparison the influence of the nitric acid has to be taken into account. An additional difference in the resulting rate constants arises from the initial concentration of Np(V), which is several orders of magnitude lower than those in the literature.

3.4 Order of reaction with respect to HAHCl

To determine the order of reaction with regard to HAHCl, $\log(k)$ was plotted against the logarithm of the initial

Table 3. Rate constants k and half-lives $t_{1/2}$ of the reaction for different temperature and HAHCl concentrations

Temperature (°C)	[HAHCl]					
	7.2 M ^{a)}		3 M		1 M	
	k (min^{-1})	$t_{1/2}$ (min)	k (min^{-1})	$t_{1/2}$ (min)	k (min^{-1})	$t_{1/2}$ (min)
30	0.0064(3)	108(5)	-	-	-	-
40	0.012(1)	60(4)	0.0029(1)	235(8)	-	-
50	0.021(2)	33(3)	0.0084(5)	82(5)	0.0021(1)	330(16)
60	0.039(7)	18(4)	0.019(1)	37(2)	0.0054(5)	129(12)
70	-	-	-	-	0.011(1)	66(6)

a) average of repeated measurement series.

Uncertainties are given in parenthesis applying to the last significant digit.

Table 4. Orders of reaction with regard to HAHCl for different temperatures

Temperature (°C)	Order of reaction for HAHCl
60	1.07(4)
50	1.23(2)
40	1.62(5)

Uncertainties are given in parenthesis applying to the last significant digit.

Table 5. Activation energy and pre-exponential factor determined via Arrhenius approach

[HAHCl] (M)	E_A (kJ/mol)	ln(A)
7.2	60.6	18.7
3	80.1	25.0
1	74.2	21.5
Average	72(10)	22(3)

Uncertainties are given in parenthesis applying to the last significant digit.

concentrations of HAHCl for different temperatures. From that, a straight line with the slope accounting for the order of reaction for HAHCl was obtained (see Supporting Information Fig. 2). The results are summarized in Table 4.

In the literature, different results for the reaction order of hydroxylamine are given. Koltunov et al. [8] published a value of 1.0 for hydroxylamine nitrate. This differs from the data obtained by Inoue et al. [10], who determined an order of reaction of 1.6 for HAHCl. They also reported a combined influence of the hydroxylamine and of the chloride ions. The differences could hence be explained by the different counter ions, nitrate and chloride. For 40°C we also identified an order of reaction of 1.625 with regard to HAHCl, but by increasing the temperature to 50°C and 60°C these values reduced to 1.23(2) and 1.07(4), respectively. Accordingly, the mechanism of the reaction seems to be influenced by both the temperature and the initial concentration of HAHCl.

3.5 Determination of Arrhenius parameters

The activation energy E_A was determined via an Arrhenius approach with Equation (5) as described in Section 2.1. The respective plot is shown in Supporting Information Fig. 3. The results are shown in Table 5; in addition, the pre-exponential factor A from the Arrhenius equation is given.

As can be seen, an activation energy of $E_A = 72(10)$ kJ/mol resulted as an average value from the different measurement series at different concentrations of HAHCl. This value is significantly lower than that determined by Koltunov et al. [8] in nitric acid solution ($E_A = 105.4$ kJ/mol) again indicating a different influence of the nitric acid and the nitrate counter ions on the redox reaction.

4 Concluding remarks

Capillary electrophoresis has proved to be a powerful analytical technique for the investigation of the kinetic aspects of redox reactions of actinides. In particular, the coupling of CE to ICP-MS allows very sensitive measurements in low concentration ranges and is thus suitable for environmentally relevant systems. We performed measurements at $[Np(aq)] = 7.5 \times 10^{-7}$ M, but it could be shown that concentrations of Np in solution down to 10^{-9} M [26], with a sector field ICP-MS even down to 10^{-11} M [25], are feasible. Therefore, the concentration range of the redox reaction that is possible to examine can be extended from $[Np(aq)] = 5 \times 10^{-5}$ M in this case to Np concentrations of about 10^{-9} M.

We were able to determine a set of rate constants for the reaction of Np(V) with different initial concentrations of HAHCl in 1 M hydrochloric acid at various temperatures. The results obtained in this study are in good agreement with the available literature, as far as a comparison is possible due to differences in the medium and in the initial concentrations.

Furthermore, it could be shown that Np(V) and Np(IV) exhibit a difference in their electrophoretic mobilities large enough to clearly separate them by CE. Since these two Np species are the ones that are relevant under environmental conditions, CE-ICP-MS is also an appropriate tool for the investigation of geochemical redox processes of Np in aqueous solution.

In view of the satisfactory results shown in this work, the investigation of other redox systems is also very promising. Conceivable scenarios include both other actinides in different oxidation states and the reaction with diverse reductants or oxidants. Furthermore, the effective separation in CE combined with the capability of ICP-MS for multi-element detection enables the simultaneous detection of both redox partners; e.g., if both are metals.

This work was financially supported by the Federal Ministry for Economic Affairs and Energy under contract No. 02E10981. We thank Dr. Nils Stöbener for his support during preliminary CE-ICP-MS measurements.

The authors have declared no conflict of interest.

5 References

- [1] Taylor, R. J., May, I., *Sep. Sci. Technol.* 2001, 36, 1225–1240.
- [2] Choppin, G. R., *J. Radioanal. Nucl. Chem.* 2007, 273, 695–703.
- [3] Morss L. R., Edelstein, N. M., Fuger, J., Katz, J. J. (Eds.), Nash, K. L., Madic, C., Mathur, J. N., Laquement, J., *The Chemistry of the Actinide and Transactinide Elements – Chapter 24: Actinide Separation Science and Technology*, 3rd ed., Springer, Heidelberg, Germany, 2006.
- [4] Marchenko, V. I., Dvoeglazov, K. N., Volk, V. I., *Radiochemistry* 2009, 51, 329–344.

- [5] Morss, L. R., Edelstein, N. M., Fuger, J., Katz, J. J. (Eds.), Yoshida, Z., Johnson, S. G., Kimura, T., Krsul, J. R., *The Chemistry of the Actinide and Transactinide Elements – Chapter 7: Neptunium*, 3rd ed., Springer, Heidelberg, Germany, 2006.
- [6] a) Koltunov, V. S., Tikhonov, M. F., *Radiokhimiya* 1977, 19, 611–619; b) Koltunov, V. S.; Zhuravleva, G. I., *Radiokhimiya* 1978, 20, 94–101; c) Koltunov, V. S., Zhuravleva, G. I., *Radiokhimiya* 1978, 20, 661–669; d) Koltunov, V. S., Zhuravleva, G. I., Shapovalov, M. P., *Radiokhimiya* 1981, 23, 545–551; e) Koltunov, V. S., Zhuravleva, G. I., Shapovalov, M. P., *Radiokhimiya* 1981, 23, 552–558.
- [7] a) Koltunov, V. S., Baranov, S. M., Zharova, T. P., *Radiokhimiya* 1993, 35, 42–48; b) Koltunov, V. S., Baranov, S. M., Zharova, T. P., Abramina, E. V., *Radiokhimiya* 1993, 35, 49–53; c) Koltunov, V. S., Baranov, S. M., *Radiokhimiya* 1993, 35, 54–62; d) Koltunov, V. S., Baranov, S. M., Shapovalov, M. P., *Radiokhimiya* 1993, 35, 63–70; e) Koltunov, V. S., Baranov, S. M., Zharova, T. P., Shapovalov, M. P., *Radiokhimiya* 1993, 35, 71–78; f) Koltunov, V. S., Baranov, S. M., Zharova, T. P., Abramova, E. V., *Radiokhimiya* 1993, 35, 79–84; g) Koltunov, V. S., Baranov, S. M., Shapovalov, M. P., *Radiokhimiya* 1993, 35, 85–92; h) Koltunov, V. S., Baranov, S. M., *Radiokhimiya* 2000, 42, 218–222; i) Koltunov, V. S., Taylor, R. J., Baranov, S. M., Mezhev, E.A., May, I., *Radiochim. Acta* 1999, 86, 115–121; j) Koltunov, V. S., Baranov, S. M., *Radiokhimiya* 1993, 35, 11–21; k) Koltunov, V., *J. Nucl. Sci. Technol.* 2002, 39, 347–350.
- [8] Koltunov, V. S., Tikhonov, M. F., *Radiokhimiya* 1977, 19, 620–625.
- [9] El-Naggar, H. A., Gourisse, D., Masoud, M. S., *Radiochim. Acta* 1982, 31, 51–55.
- [10] Inoue, Y., Tochiyama, O., Kosaka, I., *J. Nucl. Sci. Technol.* 1987, 24, 724–729.
- [11] Hein, C., Sander, J. M., Kautenburger, R., *J. Anal. Bioanal. Tech.* 2014, 5, 225–233.
- [12] Timberbaev, A. R., *Chem. Rev.* 2013, 113, 778–812.
- [13] Jiang, C., Armstrong, D. W., *Electrophoresis* 2010, 31, 17–27.
- [14] Timberbaev, A. R., Timberbaev, R. M., *Trends Anal. Chem.* 2013, 51, 44–50.
- [15] Sladkov, V., *Electrophoresis* 2016, 37, 2558–2566.
- [16] Newman, C. I. D., Collins, G. E., *Electrophoresis* 2008, 29, 44–55.
- [17] Zheng, X., Bi, C., Li, Z., Podariu, M., Hage, D. S., *J. Pharm. Biomed. Anal.* 2015, 113, 163–180.
- [18] Galievsky, V. A., Stasheuski, A. S., Krylov, S. N., *Anal. Chem.* 2015, 87, 157–171.
- [19] Suzuki, N., Miyabe, K., *Anal. Chem.* 2017, 89, 10487–10495.
- [20] Chen, G., Ye, J., Bao, H., Yang, P., *J. Pharma. Biomed. Anal.* 2002, 29, 843–850.
- [21] Xing, X., Cao, Y., Wang, L., *J. Chromatogr. A* 2005, 1072, 267–272.
- [22] Zhang, L., Tong, P., Chen, G., *J. Chromatogr. A* 2005, 1098, 194–198.
- [23] Tong, P., Zhang, L., He, Y., Chi, Y., Chen, G., *Talanta* 2009, 77, 1790–1794.
- [24] Holtkamp, H., Grabmann, G., Hartinger, C. G., *Electrophoresis* 2016, 37, 959–972.
- [25] Graser, C.-H., Banik, N., Bender, K. A., Lagos, M., Marquardt, C. M., Marsac, R., Montoya, V., Geckeis, H., *Anal. Chem.* 2015, 87, 9786–9794.
- [26] Stöbener, N., Amayri, S., Gehl, A., Kaplan, U., Malecha, K., Reich, T., *Anal. Bioanal. Chem.* 2012, 404, 2143–2150.
- [27] Grossmann, P. D., Colburn, J. C. (Eds.), *Capillary Electrophoresis Theory and Practice*, Academic Press, San Diego, 1992.
- [28] Atkins, P. W., de Paula, J., *Physikalische Chemie*, 4th ed., Wiley-VCH, Weinheim, 2006.
- [29] Álvares-Llamas, G., del Rosario Fernández de la Campa, M., Sanz-Medel, A., *Trends Anal. Chem.* 2005, 24, 28–36.
- [30] Michalke, B., *Electrophoresis* 2005, 26, 1584–1597.
- [31] Sonke, J. E., Salters, V. J. M., *Analyst* 2004, 129, 731–738.
- [32] Nitsche, H., Lee, S., Gatti, R., *J. Radioanal. Nucl. Chem.* 1988, 124, 171–185.
- [33] Stöbener, N., Elementspeziation von Neptunium im Ultrasparenbereich, Ph.D. Thesis, Johannes Gutenberg University, Germany, 2013 (https://publications.ub.uni-mainz.de/theses/frontdoor.php?source_opus=3475)
- [34] Neck, V., Kim, J. I., *Radiochim. Acta* 2001, 89, 1–16.

5.2 Determination of Kinetic Parameters of the Redox Reaction of Np(V) with HAHCl by CE-ICP-MS

5.2.2 SUPPLEMENTARY INVESTIGATIONS: INFLUENCE OF IRON ON THE REDOX KINETICS OF THE REDUCTION OF Np(V) TO Np(IV) BY HYDROXYLAMINE HYDROCHLORIDE

In preceding experiments, conducted before the investigations presented in the publication above, it transpired that the rate constants of the reduction of Np(V) to Np(IV) by hydroxylamine hydrochloride (HAHCl) strongly varies with the choice of the batch of HAHCl. Older batches seemed to reduce the Np(V) ions much faster to Np(IV) than newer ones. Since these findings were not to be expected and no obvious explanation could be found at first glance, some analytical investigations such as XPS (X-ray photoelectron spectroscopy) measurements were undertaken to uncover differences in the respective HAHCl batches. The corresponding kinetic experiments and the analytical examinations are described in the diploma thesis of Christian Willberger [14WIL] and for more details it is referred to this work. In the experiments conducted in the time frame of the diploma thesis no differences in the individual HAHCl batches could be detected but at this point the assumption was established that the older batches contain iron to some extent either because of contaminations during the storage or because of impurities from the production process. The acceleration of the reduction reaction could then be explained by catalytic effects of the iron. For all experiments described in the manuscript above the same (newest) HAHCl batch was used to obtain reproducible and reliable results. Nevertheless, further examinations were undertaken to prove the assumption of iron impurities in older batches right and by that further support the results of the recent studies.

Firstly, two older HAHCl batches as well as the newest one used in the present work were tested for the presence of both Fe(II) and Fe(III) ions by the use of 5-sulfosalicylic acid (SSA) [02KAR]. If Fe(III) is present in solution, SSA forms a red complex together with this ions. After the addition of aqueous ammonia solution, the whole solution turns yellow in the alkaline region if Fe(II) is present indicating the complexation of both Fe(II) and Fe(III). For each batch, 1 g HAHCl was dissolved in 2 mL of 1 M HCl and 2 mL of 10 wt% SSA solution. A slight red coloring became visible for the two older batches and no coloring could be observed for the new batch. After the addition of 2 mL 28 wt% aqueous ammonia solution the first two batches turned yellow, the newest one again showed no change in color. Consequently, by that simple test it could be shown that, as expected, iron ions are present in the older HAHCl batches. The newest one contains no iron with a concentration higher than the limit of detection of this test. The red coloring after the SSA addition and the subsequent yellow coloring in the alkaline pH region suggest the presence of both Fe(II) and Fe(III) ions.

5. Determination of Redox Kinetics with CE-ICP-MS

Based on these findings it was then tested whether or not the iron ions in the older HAHCl batches are really the reason for the much higher reaction kinetics compared to the new batch. In order to do so three reduction reactions of Np(V) to Np(IV) were compared at 40 °C. The experimental approach of the reduction was exactly identical to the procedure described in the manuscript in Section 5.2.1. 2 g of the respective HAHCl was dissolved in 4 mL 1 M HCl ($c(\text{HAHCl}) = 7.2 \text{ M}$) and 66 μL Np(V) solution was added to yield a Np concentration of $c(\text{Np}) = 6 \cdot 10^{-4} \text{ M}$. In the first reaction, the oldest HAHCl batch was used. For the second data series, the newest batch without iron, the result for $c(\text{HAHCl}) = 7.2 \text{ M}$ at 40 °C presented in the manuscript above, was employed. For the third reaction, one spade point of $\text{FeCl}_3 \cdot 6 \text{ H}_2\text{O}$ was added to the newest HAHCl batch to achieve an artificial iron contamination. Samples were taken at given reaction times and the Np(V)/Np(IV) ratio in the samples was determined by liquid-liquid extraction (LLE) and LSC measurements (or CE-ICP-MS as in the second case). The experimental procedure and conditions for the LLE/LSC measurements were again kept completely identical to the ones conducted for the kinetic publication. The reaction times and the experimental results are summarized in Table 15 - Table 17.

Table 15: Results of the measurement series of the reduction of Np(V) to Np(IV) at 40 °C and $c(\text{HAHCl}) = 7.2 \text{ M}$: reaction 1, old batch.

reaction time/min	activity/Bq (determined by LLE/LSC, uncertainty $\pm 5\%$)			percentages	
	Np(V)	Np(IV)	Np(total)	Np(V)	Np(IV)
1	3.75	0.13	3.88	96.6	3.4
20	1.38	1.30	2.68	51.5	48.5
40	0.74	2.00	2.74	26.9	73.1
60	0.50	2.62	3.12	16.1	83.9
80	0.27	2.74	3.01	8.8	91.2
100	0.22	2.92	3.14	6.9	93.1
130	0.23	3.05	3.28	6.9	93.1
160	0.18	2.90	3.08	5.7	94.3
190	0.16	2.78	2.94	5.5	94.5

5.2 Determination of Kinetic Parameters of the Redox Reaction of Np(V) with HAHCL by CE-ICP-MS

Table 16: Results of the measurement series of the reduction of Np(V) to Np(IV) at 40 °C and $c(\text{HAHCl}) = 7.2 \text{ M}$: reaction 2, new batch. These results are taken from the kinetic manuscript obtained by CE-ICP-MS measurements.

reaction time/min	percentages	
	Np(V)	Np(IV)
0	95.5	4.5
30	78.2	21.8
65	62.4	37.6
100	34.0	66.0
130	23.6	76.4
165	13.3	86.7
195	9.3	90.7
230	6.8	93.2
270	4.5	95.5

Table 17: Results of the measurement series of the reduction of Np(V) to Np(IV) at 40 °C and $c(\text{HAHCl}) = 7.2 \text{ M}$: reaction 3, new batch + one spade point of $\text{FeCl}_3 \cdot 6 \text{ H}_2\text{O}$.

reaction time/min	activity/Bq (determined by LLE/LSC, uncertainty $\pm 5\%$)			percentages	
	Np(V)	Np(IV)	Np(total)	Np(V)	Np(IV)
1	3.77	0.43	4.20	89.8	10.2
10	0.81	2.13	2.94	27.6	72.4
20	0.26	2.50	2.76	9.4	90.6
30	0.21	2.77	2.98	7.0	93.0
40	0.22	2.68	2.90	7.5	92.5
50	0.17	2.61	2.78	6.2	93.8
60	0.21	2.57	2.78	7.7	92.3
70	0.18	2.69	2.87	6.3	93.7

5. Determination of Redox Kinetics with CE-ICP-MS

The graphical determination of the rate constants of the three reactions is shown in Figure 21. As can be seen, for reaction 1 (old HAHCl batch) and reaction 2 (new HAHCl batch + $\text{FeCl}_3 \cdot 6 \text{H}_2\text{O}$) the $[\text{Np}(\text{V})_t]/[\text{Np}(\text{V})_0]$ ratio becomes constant for higher reaction times. This is an indication for the reaction being near or even already in equilibrium. Since kinetical parameters has to be determined away from the equilibrium the respective fits were just performed in the non-constant region.

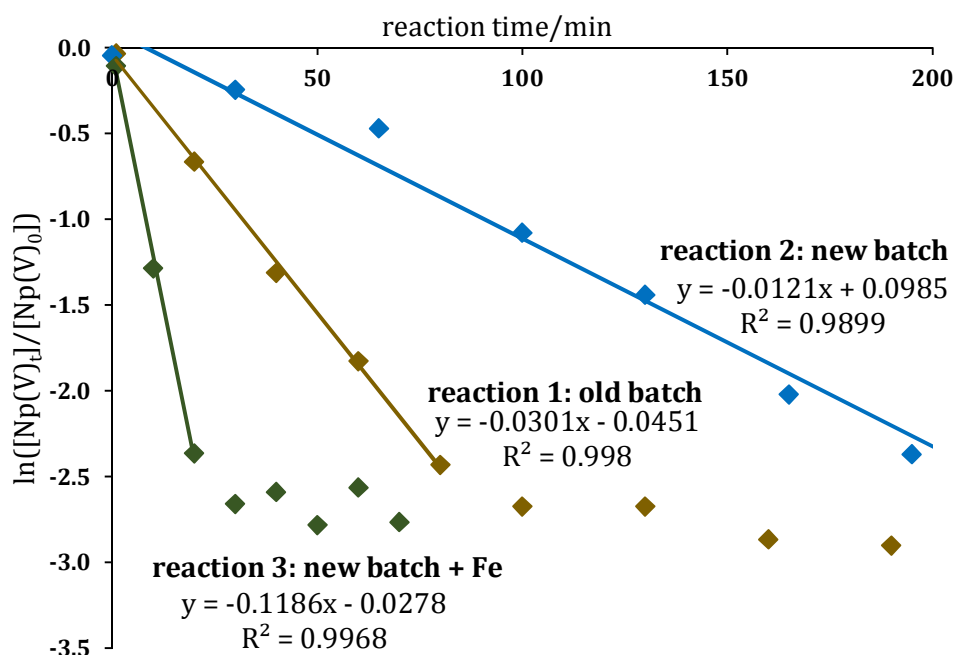


Figure 21: Graphical determination of the rate constants of the three reductions of Np(V) to Np(IV) at 40 °C and $c(\text{HAHCl}) = 7.2 \text{ M}$ with three different HAHCl batches.

The resulting rate constants k and the corresponding half times $t_{1/2}$ of the reactions can be found in Table 18.

Table 18: Rate constants k and half times $t_{1/2}$ of the measurement series of the reduction of Np(V) to Np(IV) at 40 °C with three different HAHCl batches: reaction 3, new batch + one spade point of $\text{FeCl}_3 \cdot 6 \text{H}_2\text{O}$.

reaction	rate constant $k/$ min^{-1}	half time of the reaction $t_{1/2}/$ min
1, old batch	0.0301 (± 0.002)	23.0 (± 1.5)
2, new batch	0.0121 (± 0.001)	57.3 (± 4.7)
3, new batch + $\text{FeCl}_3 \cdot 6 \text{H}_2\text{O}$	0.1186 (± 0.01)	5.8 (± 0.5)

As can be seen from these results, the rate constants k vary significantly with the choice of the HAHCl batch. The reduction of Np(V) to Np(IV) with the HAHCl from the old batch 1 is about twice as fast as the corresponding one with the HAHCl from the new batch 2. For

5.3 Determination of Kinetic Parameters of the Redox Reaction of Pu(VI) with Fe(II) by CE-ICP-MS

experiment 3, the artificial iron contamination, a half time of the reaction $t_{1/2}$ being 1 order of magnitude faster was obtained. Since in the latter case the iron concentration is expected to be much higher than in the first case, this order of the reduction kinetics is reasonable.

The results from these investigations show that the iron content in a HAHCl batch has a decisive influence on the rate constant of the reduction of Np(V) to Np(IV). From the fact that in experiment 3 a much higher reaction kinetic was obtained compared to experiment 1 it can be concluded that a very small iron content, significantly less than the one spade point added in experiment 3, is enough to have a notable effect on the rate constant. This leads to the conclusion that it has to be ensured in the experiments that the HAHCl is completely free from any iron impurities in order to yield repeatable and comparable rate constants k .

5.3 DETERMINATION OF KINETIC PARAMETERS OF THE REDOX REACTION OF PU(VI) WITH FE(II) BY CE-ICP-MS

5.3.1 INTRODUCTION

Besides radioactive elements as for example the actinides or fission products also non-radioactive elements have to be examined for the long-term safety assessment of a future nuclear waste disposal. Iron is one of those elements most frequently occurring in deep geological repositories. It is naturally present both dissolved in groundwater and as part of minerals such as the oxides magnetite ($\text{Fe(II/III)}_2\text{O}_4$) or hematite ($\text{Fe(III)}_2\text{O}_3$), the hydroxides goethite (FeOOH) or iron(II)-hydroxide (Fe(OH)_2), the carbonate siderite (FeCO_3), as iron(II)- and iron(III) sulfates and as the sulfide pyrite (FeS_2). [12SEH] Furthermore, an anthropogenic input of iron through steel containers and the like as packing material and the waste itself containing iron materials has to be considered. The corrosion of such materials and the dissolving of the minerals lead to the presence of both Fe(II) and Fe(III) ions in high concentrations in the direct surrounding of the radioactive waste. The oxidizing or reducing capability of Fe(III) and Fe(II), respectively, can have a great impact on the oxidation state of redox sensitive actinides and by that on their mobilization or immobilization in the environment of the repository. [19MA]

Based on these circumstances, in the present section the redox reaction of Pu(VI) with Fe(II) was examined by CE-ICP-MS. As already demonstrated in the previous section, the coupling of CE to ICP-MS allows for the retracing of the redox kinetics of actinides with reducing or oxidizing agents. Since, in contrast to the Np(V)/HAHCl couple, in the current case both reaction partners are metals the benefit of being able to separate and detect both the Pu species and the Fe species at the same time should be investigated.

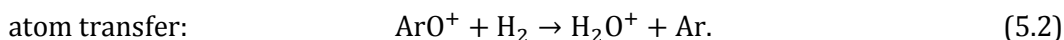
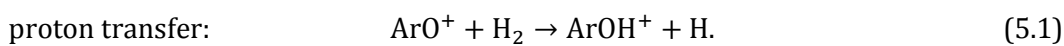
5. Determination of Redox Kinetics with CE-ICP-MS

The kinetics of the reduction of Pu(VI) by Fe(II) were already investigated with a spectrophotometric method in HClO₄ medium in the temperature range between 0 °C and 25 °C and a ionic strength of $I = 0.05 - 2.0$ M by Newton and Baker [63NEW]. They state that the reaction is fast at room temperature and of first order in view of both reactants. In principle, the redox potentials are sufficient to completely reduce Pu(VI) to Pu(III) but at concentrations in the range of $c = 10^{-4}$ M for both reactants, just the first reduction step of Pu(VI) to Pu(V) was found to be of interest. For the reaction mechanism a Pu(V)-Fe(III) intermediate dimer was postulated. It has to be noted that both the presence of complexing ions such as chloride and the hydrogen concentration have an influence on the rate of the reaction which is described to be quite complicated. In the case of a higher percentage of Fe(III) ions in the reaction solution the back reaction, Pu(V) is then reoxidized to Pu(VI), has to be considered. In a previous work Newton et al. [60NEW] additionally examined the Pu(IV) reduction by Fe(II). A more recent study of the reduction of Pu(VI) by Fe(II) was conducted by Graser et al. [15GRA]. Comparable to the present work, they also used CE-ICP-(SF)-MS as the analytical technique to follow both the changes in the percentages of the different Pu oxidation states and in the Fe(II)/Fe(III) couple. The reaction was investigated in a 0.1 M HClO₄ solution at pH = 1 and a great excess of Fe(II) was applied ($c(\text{Fe(II)}) = 2.0 \cdot 10^{-6}$ M, $c(\text{Pu(VI)}) = 5.0 \cdot 10^{-10}$ M). In their work, no rate constants are given, but they report a complete reduction of Pu(VI) to Pu(III) within 100 min.

For the separation and subsequent detection of Fe(II) and Fe(III) two challenges have to be taken into consideration. In the aqueous phase, the presence of Fe(II) and Fe(III) is possible. These two ions exhibit very similar charge-to-radius ratios and because of that they are hard to separate in the applied electric field of a CE experiment. An approach to increase the separability and by that overcome this difficulty is the selective complexation of Fe(III) with ethylenediaminetetraacetate (EDTA) and Fe(II) with 1,10-phenanthroline (phen). This method and its applicability in CE experiments was introduced by Schäffer et al. [96SCH] (further investigations can be found in [97POZ]) and is also applied in the work of Graser et al. [15GRA] mentioned above. The separation effect is based on a great difference in the respective stability constants. The Fe(III)(EDTA)⁻ complex has a high stability constant of $\log(k) = 25.2$ whereas the comparable Fe(II)(EDTA)²⁻ complex is much weaker with $\log(k) = 14.3$. The opposite trend accounts for the Fe(II)(phen)₃²⁺/Fe(III)(phen)₃³⁺ couple, here the Fe(II) complex is the more stable one ($\log(k(\text{Fe(II)}(\text{phen})_3^{2+})) = 21.2$, $\log(k(\text{Fe(III)}(\text{phen})_3^{3+})) = 14.4$). The data are taken from [96SCH] and the references cited therein. In the present work, this approach was also utilized and the experimental results are presented in the following.

5.3 Determination of Kinetic Parameters of the Redox Reaction of Pu(VI) with Fe(II) by CE-ICP-MS

The second challenge is the detection of the iron ions by ICP-MS. In this MS method, the analytes are ionized in an argon plasma. This leads to a high concentration of dimers and trimers such as $^{40}\text{Ar}^{14}\text{N}^+$ (mass 54), $^{40}\text{Ar}^{16}\text{O}^+$ (mass 56) and $^{40}\text{Ar}^{16}\text{O}^1\text{H}^+$ (mass 57) composed from the Ar atoms and atoms from the surrounding air creating a great background signal on the corresponding masses [04WIL]. Unfortunately, since the natural distribution of the four stable iron isotopes is 5.845% ^{54}Fe , 91.754% ^{56}Fe , 2.119% ^{57}Fe and 0.282% ^{58}Fe [04LID], these masses conform exactly to the masses of Fe ions that should be detected. As one can see, on all Fe masses with a significant natural isotopic abundance, a superimposition with Ar interferences is to be expected. In order to circumvent this difficulty, the application of the so called octopole reaction system (ORS) was introduced. The ORS is an additional component located between the ion lens chamber and the analyzer chamber inside the ICP-MS system (see Figure 4). Three different modes of operation are possible, H_2 -mode (reaction mode), He-mode (collision mode) and no-gas mode. Via a gas supply, H_2 or He can be introduced in the ORS in dependence of the mode to be used. In the reaction mode, hydrogen gas is utilized to remove the Ar interferences by reactions of the dimers or trimers with the H_2 molecules. In the case of Fe, the interferences can be reduced by either a proton transfer reaction (Equation (5.1)) or an atom transfer reaction (Equation (5.2)).



In both cases the dimer with the mass 56 is converted to a molecule or atom with a different mass and the background signal is thus decreased. The Fe atoms do not react with the H_2 gas, consequently there should be no significant loss of signal. [04WIL]

In the second mode, the He collision mode, no reaction takes place. The dimers are rather destroyed by impacts with the He gas if the collision energy is great enough to break the bond in the dimer or trimer. Even if the collision energy is lower than the required energy for the bond breaking the polyatomic ions are reduced compared to the monoatomic analyte because of a higher collision cross section. The larger polyatomic ions collide more often with the He atoms, thus loose energy on their path through the ORS and by that they are efficiently removed from the ion beam. Nevertheless, in this mode collisions of Fe ions with the He atoms cannot be completely avoided which leads to a lowering of the limit of detection. The same applies, to a smaller extent, for the H_2 mode because of collisions of the Fe ions with the H_2 molecules. Still, these reductions in the limits of detection are accepted because the great minimization of the background signal prevails. [04WIL]

5. Determination of Redox Kinetics with CE-ICP-MS

5.3.2 PRECEDING STUDY 1: MEASUREMENT OF IRON WITH THE ORS

In view of the investigation of the reaction of Pu(VI) with Fe(II) by CE-ICP-MS, the application of the ORS system described above was implemented and some preceding studies were realized to compare the different modes amongst each other. First of all ICP-MS measurements were conducted to find the optimal ORS gas and experimental conditions for the following CE-ICP-MS measurements. The results are presented in the following section.

For the experimental realization, a 10 ppb Fe ICP-MS standard containing the natural iron isotope distribution was prepared in 4% HNO₃ (supra pure) solution. The iron background signal was measured both in a 4% HNO₃ (supra pure) solution and in a MilliQ water sample. To all samples, Ir ICP-MS standard was added to yield 100 ppt as the internal standard. The optimal gas flow rates for the ORS were identified by the combination of an auto-tuning procedure and a subsequent systematic variation of the respective gas flow until the best signal was obtained. The rates were thus set to 3.5 ml min⁻¹ for the collision mode (He gas) and 4.0 mL min⁻¹ for the reaction mode (H₂ gas). The iron isotopes investigated were ⁵⁴Fe and ⁵⁶Fe, the other two isotopes ⁵⁷Fe and ⁵⁸Fe were not examined because those are irrelevant for further experiments due to their small natural abundance.

The results are summarized in Table 19. Each value is a mean of six consecutive measurements on the respective masses, the uncertainties given are the relative standard deviations (RSD). All results were corrected to the ¹⁹³Ir internal standard signal. The Fe signal in the Fe sample was background corrected by the subtraction of the Fe signal in the 4% HNO₃ sample.

In all modes and for both Fe isotopes, the Fe signal is significantly higher in the 4% HNO₃ sample compared to the MilliQ water sample. Since the HNO₃ solution was prepared from a supra pure acid a contamination with iron is unlikely. The raise in Fe signal can rather be explained by the additional introduction of both O and N atoms directly into the plasma from the HNO₃ solution. By that the dimer production for both ⁴⁰Ar¹⁴N⁺ (mass 54) and ⁴⁰Ar¹⁶O⁺ (mass 56) is increased and more isobaric interferences are detected on the iron masses.

In general, the Fe signals are reduced when the ORS is applied even though the iron content in the sample is identical. Consequently, it is possible to reduce the background signal due to isobaric interferences on the masses 54 and 56 using the reaction or collision mechanism described above. For comparing the H₂ and the He mode, the share of the Fe signal resulting from the sample Fe was related to the respective Fe signal created from the sum of the background signal and the sample signal (see last column in Table 19). Thus it is possible to see which percentage of the signal can be assigned to the sample and which is just resulting

5.3 Determination of Kinetic Parameters of the Redox Reaction of Pu(VI) with Fe(II) by CE-ICP-MS

from background signal. It can be concluded, that in He mode the Fe signal is reduced but no improvement of the signal-to-background ratio can be obtained. In the H₂ mode in contrast, this ratio could be improved significantly for both Fe isotopes. Consequently, the reaction mode of the ORS with the optimized parameters determined in this preceding examination (H₂ flow rate: 4.0 mL min⁻¹) was set as most suitable for the measurement of Fe isotopes.

Table 19: Results of the ICP-MS measurements of ⁵⁴Fe and ⁵⁶Fe with the ORS system in no gas mode, H₂ mode and He mode.

isotope	mode	ICP-MS signal (¹⁹³ Ir corrected)/cps (± RSD)			Fe signal/ cps (corrected) *	sample Fe share/ % **
		MilliQ	4% HNO ₃	Fe sample		
⁵⁴ Fe	no gas	13489 (±3.4%)	129451 (±3.3%)	163799 (±2.9%)	34349 (±2.9%)	21.0
	H ₂	11988 (±3.3%)	114730 (±2.2%)	26844 (±0.9%)	12114 (±0.9%)	45.1
	He	21531 (±1.3%)	78145 (±1.0%)	94037 (±0.6%)	15893 (±0.6%)	16.9
⁵⁶ Fe	no gas	997765 (±1.7%)	1441590 (±2.0%)	12022582 (±1.9%)	580992 (±1.9%)	28.7
	H ₂	18334 (±2.5%)	41334 (±2.5%)	265034 (±0.5%)	1223700 (±0.5%)	84.4
	He	350740 (±1.0%)	523515 (±1.0%)	754235 (±0.9%)	230720 (±0.9%)	30.6

* corrected to ¹⁹³Ir and to the Fe background signal in the 4% HNO₃ sample

** share of sample Fe in total Fe signal including background

Based on these findings it should be tested whether the ORS system is also beneficial for the measurement of iron in the combination of ICP-MS with CE as investigated in this work. For that purpose, two CE-ICP-MS runs were performed with samples consisting just of 1 M AcOH which is used as the BGE in most of the CE-ICP-MS experiments. In these first measurements no iron was added to the samples, so that just the reduction of the background signal in the resulting electropherogram could be investigated. The experiments were undertaken with the H₂ mode as described above and with a high voltage of 25 kV, the detected mass was 56 because of its highest natural abundance. The resulting electropherograms can be found in Figure 22.

5. Determination of Redox Kinetics with CE-ICP-MS

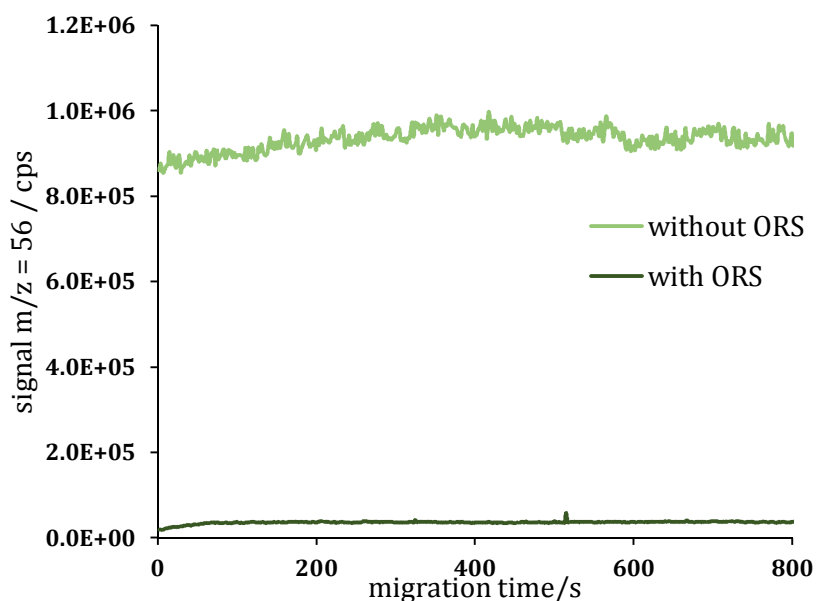


Figure 22: Effect of the ORS in H₂ mode on the electropherograms of the CE-ICP-MS background solution (1 M AcOH).

As can be seen clearly, in the electropherogram of 1 M AcOH with the ORS the background on the mass 56 is decreased dramatically in comparison to the corresponding electropherogram without the ORS. While in the latter, a background signal of about 10^6 cps is detected, with the use of the ORS this value diminishes to a value of about $4 \cdot 10^4$ cps. This order of magnitude can simultaneously be interpreted as a reference for the limit of detection of CE-ICP-MS iron measurements under the experimental conditions described above. Furthermore, the trend of the electropherogram is very constant without any spikes or interruptions. Thus, by the experiments presented above the capability of the application of an ORS in H₂ mode for the investigation of iron containing systems in CE-ICP-MS experiments could be proved.

5.3.3 PRECEDING STUDY 2: CE-ICP-MS MEASUREMENT OF Fe(II)-PHEN AND Fe(III)-EDTA COMPLEXES

As described in the introduction section, the separation of Fe²⁺ and Fe³⁺ ions by CE can be improved by the selective complexation of Fe(II) with phen and Fe(III) with EDTA. These complexes should exhibit considerably greater differences in their electrophoretic mobilities compared to the free iron ions. Before the investigation of the Fe(II)/Pu(VI) redox reaction, experiments should be executed to investigate the complexation behavior and the electrophoretic mobilities of the compounds of interest under the experimental conditions applied in the following kinetic experiments.

To do so, different solutions were prepared containing both Fe(II) and Fe(III). In each sample, Fe(ClO₄)₂ and Fe(ClO₄)₃ were dissolved in 0.1 M HClO₄, 1 M AcOH or in various mixtures of both to yield a Fe total concentration of $c(\text{Fe}_{\text{total}}) = 5 \cdot 10^{-4}$ M. All samples were prepared

5.3 Determination of Kinetic Parameters of the Redox Reaction of Pu(VI) with Fe(II) by CE-ICP-MS

under Ar atmosphere to prevent an oxidation of Fe(II) by oxygen from the air. The iron perchlorate salts and the perchloric acid background were chosen over other systems, e.g. chloride, because this anion has proven to be non-complexing and thus no competitive Fe complexes have to be considered. Details about these investigations via UV-Vis spectroscopy can be found in [17LEI1]. To each sample 1 mg phen and 5 mg EDTA were added. The detailed sample compositions are given in Table 20.

Table 20: Detailed sample compositions for the CE-ICP-MS investigations of the Fe(II)-phen and the Fe(III)-EDTA complexes. The total sample volume was $V = 200 \mu\text{L}$ in each sample.

sample	background in Fe sample	volume Fe(II/III) sample/ μL	CE dilution medium	1 M AcOH/ 0.1 M HClO ₄ ratio
1	1 M AcOH	5	195 μL 1 M AcOH	100/0
2	0.1 M HClO ₄	150	50 μL 1 M AcOH	75/25
3	0.1 M HClO ₄	100	100 μL 1 M AcOH	50/50
4	0.1 M HClO ₄	50	150 μL 1 M AcOH	25/75
5	0.1 M HClO ₄	5	195 μL 0.1 M HClO ₄	0/100

The resulting electropherograms of these five samples are shown in Figure 23. The applied voltage during CE separation was $U = 25 \text{ kV}$ and the masses 54 and 56 for the iron detection were investigated. During all measurements, the ORS in reaction mode was applied.

From the electropherograms presented in the following two points concerning the CE-ICP-MS detection of Fe(II/III) complexes with phen and EDTA can be recognized. Firstly, the quality of the electropherograms decreases with an increase of the percentage of the perchloric acid.

Only in a mostly AcOH medium satisfactory electropherograms without interruptions and with clearly distinguishable peaks can be obtained. Secondly, two individual peaks can be identified. This leads to the conclusion that the complexation of Fe(II) with phen and Fe(III) with EDTA really allows the separation of these two iron species. The resulting electrophoretic mobilities are summarized in Table 21.

5. Determination of Redox Kinetics with CE-ICP-MS

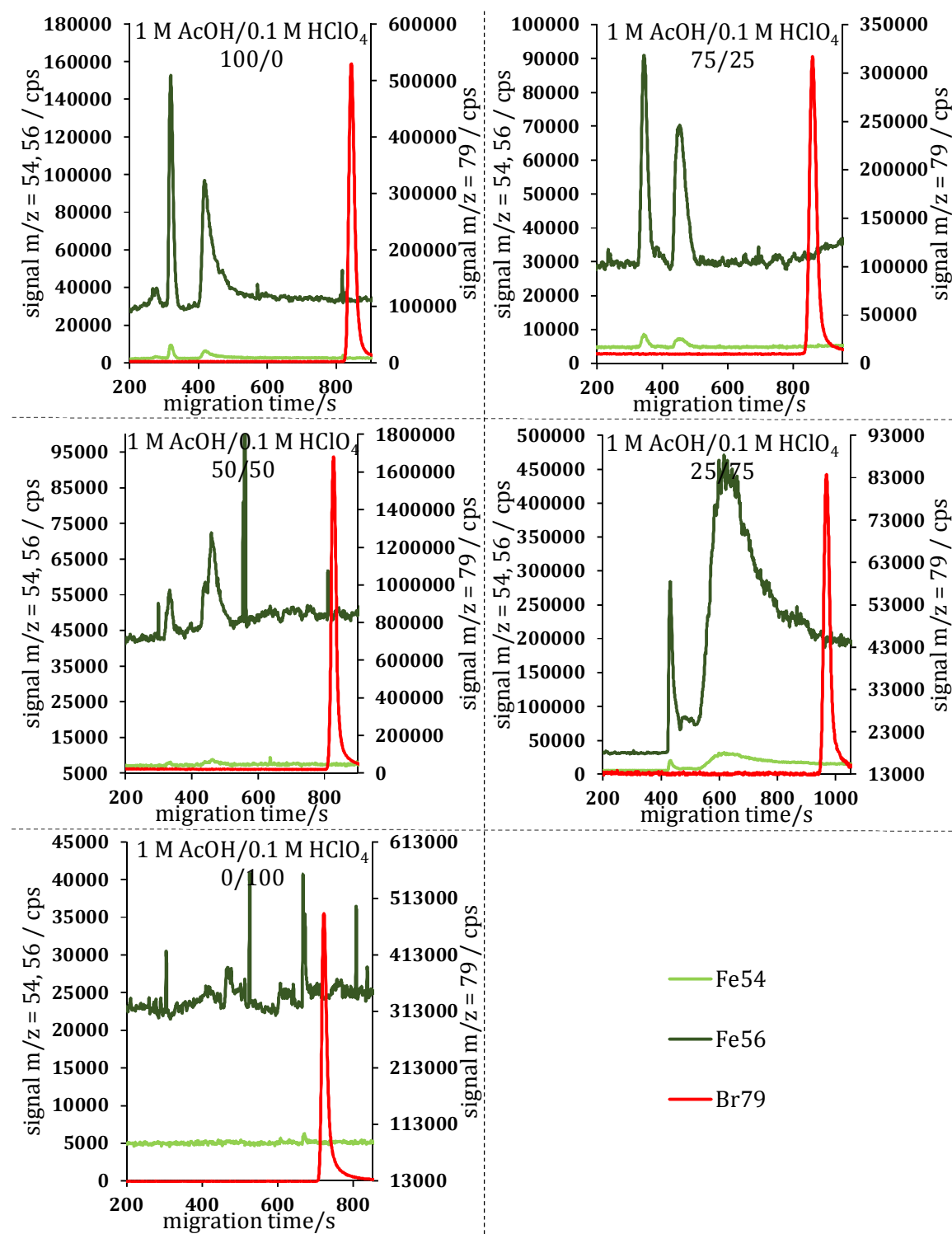


Figure 23: Electropherograms of the CE-ICP-MS measurements of Fe(II)-phen and Fe(III)-EDTA in 1 M AcOH and 0,1 M HClO₄ background medium.

Since the Fe(phen)_3^{2+} complex is positively charged and the Fe(EDTA)^- species exhibit a negative charge the first peak in the electropherograms was assigned to Fe(II) and the second one to Fe(III). The fact that the negatively charged Fe(III)-EDTA complex exhibits a positive electrophoretic mobility may be explained by the size of the ion. Due to the great EDTA ligand the whole molecule has a significant friction with the surrounding BGE and is thus dragged

5.3 Determination of Kinetic Parameters of the Redox Reaction of Pu(VI) with Fe(II) by CE-ICP-MS

along with the EOF. As a consequence, its forward movement is greater than the velocity in opposite direction and the overall electrophoretic mobility is positive.

Table 21: Electrophoretic mobilities of the Fe(phen)²⁺ and the Fe(EDTA)⁻ species investigated by CE-ICP-MS in different 1 M AcOH/0.1 M HClO₄ background media.

Sample	1 M AcOH/ 0.1 M HClO ₄ ratio	electrophoretic mobility $\mu_e/10^{-4} \text{ cm}^2\text{V}^{-1}\text{s}^{-1}$	
		Fe(phen) ²⁺	Fe(EDTA) ⁻
1	100/0	4.51 ± 0.12	2.81 ± 0.07
2	75/25	4.02 ± 0.10	2.41 ± 0.06
3	50/50	4.13 ± 0.11	2.24 ± 0.06
4	25/75	2.97 ± 0.07	1.36 ± 0.03
5	0/100	1.75 ± 0.06	0.27 ± 0.03

Taking a closure look on the development of the electrophoretic mobilities of the two Fe species with changing background medium one can notice, that the mobility decreases with increasing percentage of perchloric acid. As already described in Section 2.1.3 the ionic strength *I* of the BGE is one of the parameters having an influence on μ_e . Since the increase in the share of HClO₄ leads to an increase in *I* at this point it can be seen from experimental results what has already been depicted in general terms in Section 2.1.3: The electrophoretic mobility decreases with an increasing ionic strength. Besides the ionic strength of course all other parameters described in the theory section have an influence on the measured μ_e because of the changes in the BGE.

5.3.4 KINETICS OF THE REDOX REACTION OF PU(VI) WITH FE(II)

The kinetic parameters of the reduction of Pu(VI) by Fe(II) were investigated by LLE/LSC and by CE-ICP-MS measurements. LLE/LSC experiments were conducted because this method has proven in previous kinetic studies (see Section 5.2.1) to be an appropriate complementary technique to verify and compare the results obtained from CE-ICP-MS investigations. Details about the experimental procedure for the separation of Pu oxidation states by LLE/LSC using HDEHP and PMBP can be found in the APPENDIX A3.

5. Determination of Redox Kinetics with CE-ICP-MS

SAMPLE PREPARATION AND EXPERIMENTAL PROCEDURE

For the experiments, a $8 \cdot 10^{-7}$ M $^{239}\text{Pu(VI)}$ solution was prepared in 0.1 M HClO_4 . The $^{239}\text{Pu(VI)}$ stock solution was produced by evaporating an in-house ^{239}Pu solution until near dryness and subsequent dissolving in 1 M HClO_4 . During the evaporation process, a few grains of NaF were added to destroy Pu colloids and 3 drops of concentrated HNO_3 were added to prevent the solution from exploding because of organic molecules. The Pu solution was then purified by ion exchange chromatography. The eluate was again evaporated two times until near dryness and dissolved in 1 M HClO_4 . The Pu(VI) oxidation state was checked by UV-Vis spectroscopy, the concentration of the solution was determined via LSC.

The redox reaction was investigated for two different Pu/Fe ratios, namely 1:3 in the LLE/LSC measurements and 1:4000 in the CE-ICP-MS experiments. In the first case, a $2.4 \cdot 10^{-6}$ M Fe(II) solution was prepared from $\text{Fe}(\text{ClO}_4)_2$ in 0.1 M HClO_4 , in the second case a $3.2 \cdot 10^{-3}$ M Fe(II) solution was employed. The 1:3 ratio was chosen because of stoichiometric aspects since a threefold excess of Fe(II) is needed in theory to reduce Pu(VI) completely to Pu(III). The 1:4000 ratio on the other hand was chosen to allow a comparison with the results from [15GRA] where this relation was employed.

The Pu(VI) and the Fe(II) solutions were tempered to the aspired temperature in an ice bath for the 10 °C measurements and in a thermostat (Haake C10, Thermo Electron Corporation, Waltham, MA, USA) for the measurements at room temperature and at elevated temperature. The reaction was started by combining 3 mL of each solution. After certain time intervals the reaction progress was examined by LLE/LSC or CE-ICP-MS. The ^{239}Pu concentration during the redox reaction was thus $4 \cdot 10^{-7}$ M. The Pu(VI) content at the beginning of the reaction was set as 100% in all data evaluations.

LLE/LSC MEASUREMENTS

At first, the reduction of Pu(VI) by Fe(II) was investigated for the Pu/Fe ratio of 1:3 at 10 °C, 23 °C and 30 °C by LLE/LSC. The results of the measurements are summarized in Table 22 – Table 24 and the development of the shares of the different Pu oxidation states is depicted in Figure 24 – Figure 26. The LLE/LSC results are presented in terms of Pu(VI) and Pu(rest). In this case, Pu(rest) describes all other Pu oxidation states including colloidal Pu besides Pu(VI). This procedure was chosen since only the decrease of Pu(VI) is of interest for the determination of the kinetic parameters of the redox reaction.

5.3 Determination of Kinetic Parameters of the Redox Reaction of Pu(VI) with Fe(II) by CE-ICP-MS

Table 22: Results of the determination of the reduction kinetics of Pu(VI) with Fe(II), ratio 1:3, by LLE/LSC at 10 °C.

time/min	activity/Bq		percentages/%	
	Pu(VI)	Pu(rest)	Pu(VI)	Pu(rest)
0	4.912 ± 0.246	0.772 ± 0.039	100.0	0.0
15	3.342 ± 0.167	2.212 ± 0.111	60.2	39.8
30	2.563 ± 0.128	2.987 ± 0.149	46.2	53.8
45	1.932 ± 0.097	3.567 ± 0.178	35.1	64.9
60	1.606 ± 0.080	3.987 ± 0.199	28.7	71.3
75	1.258 ± 0.063	4.461 ± 0.223	22.0	78.0
90	0.924 ± 0.046	4.658 ± 0.233	16.6	83.4

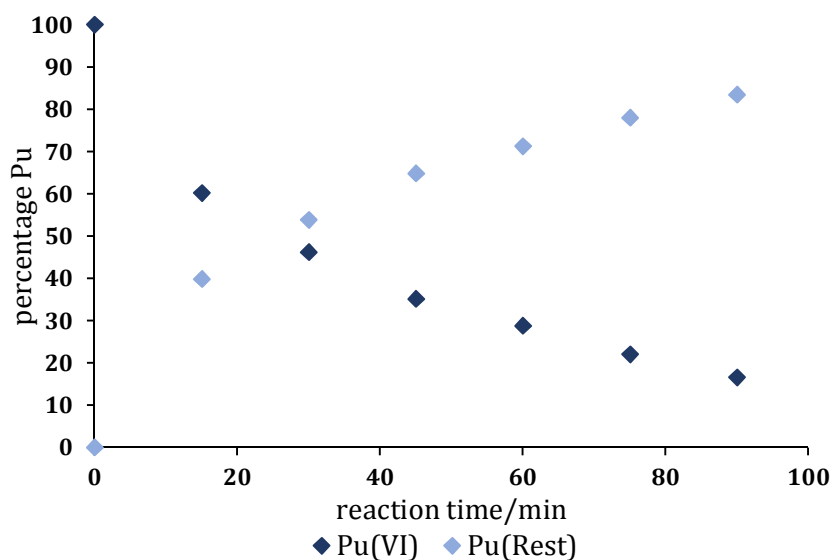


Figure 24: Development of the Pu(VI) and Pu(rest) percentages for the determination of the reduction kinetics of Pu(VI) with Fe(II), ratio 1:3, by LLE/LSC at 10 °C.

5. Determination of Redox Kinetics with CE-ICP-MS

Table 23: Results of the determination of the reduction kinetics of Pu(VI) with Fe(II), ratio 1:3, by LLE/LSC at 23 °C.

time/min	activity/Bq		percentages/%	
	Pu(VI)	Pu(rest)	Pu(VI)	Pu(rest)
0	5.762 ± 0.288	0.525 ± 0.026	100.0	0.0
12	3.490 ± 0.175	2.510 ± 0.126	58.2	41.8
24	2.428 ± 0.121	3.665 ± 0.183	39.8	60.2
36	1.690 ± 0.085	4.713 ± 0.236	26.4	73.6
48	1.135 ± 0.057	4.922 ± 0.246	18.7	81.3
60	0.831 ± 0.041	5.415 ± 0.271	13.3	86.7

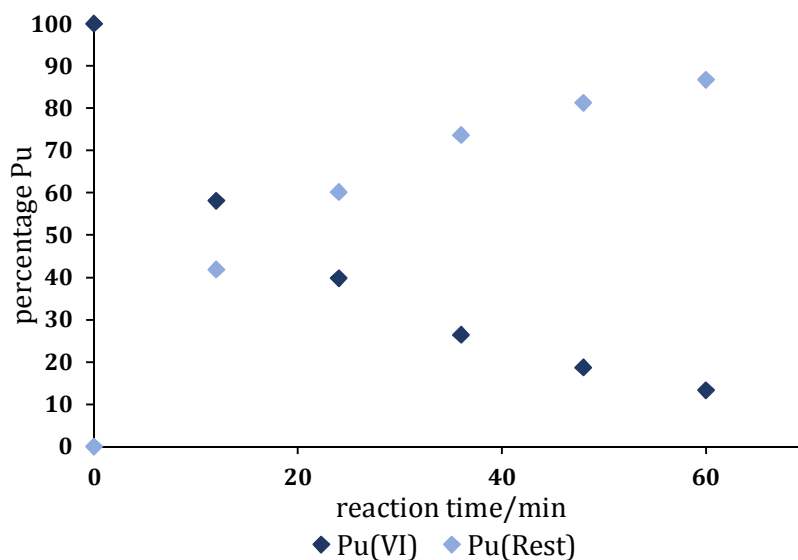


Figure 25: Development of the Pu(VI) and Pu(rest) percentages for the determination of the reduction kinetics of Pu(VI) with Fe(II), ratio 1:3, by LLE/LSC at 23 °C.

5.3 Determination of Kinetic Parameters of the Redox Reaction of Pu(VI) with Fe(II) by CE-ICP-MS

Table 24: Results of the determination of the reduction kinetics of Pu(VI) with Fe(II), ratio 1:3, by LLE/LSC at 30 °C.

time/min	activity/Bq		percentages/%	
	Pu(VI)	Pu(rest)	Pu(VI)	Pu(rest)
0	4.806 ± 0.240	0.798 ± 0.039	100.0	0.0
9	3.121 ± 0.156	2.272 ± 0.110	57.9	42.1
18	2.406 ± 0.120	3.414 ± 0.170	41.3	58.7
27	1.783 ± 0.089	3.973 ± 0.199	31.0	69.0
36	1.261 ± 0.063	4.430 ± 0.222	22.2	77.8
45*	1.056 ± 0.053	4.612 ± 0.230	18.6	81.4
54*	0.829 ± 0.041	4.947 ± 0.247	14.4	85.6

* not used for data evaluation because the reaction is already in equilibrium

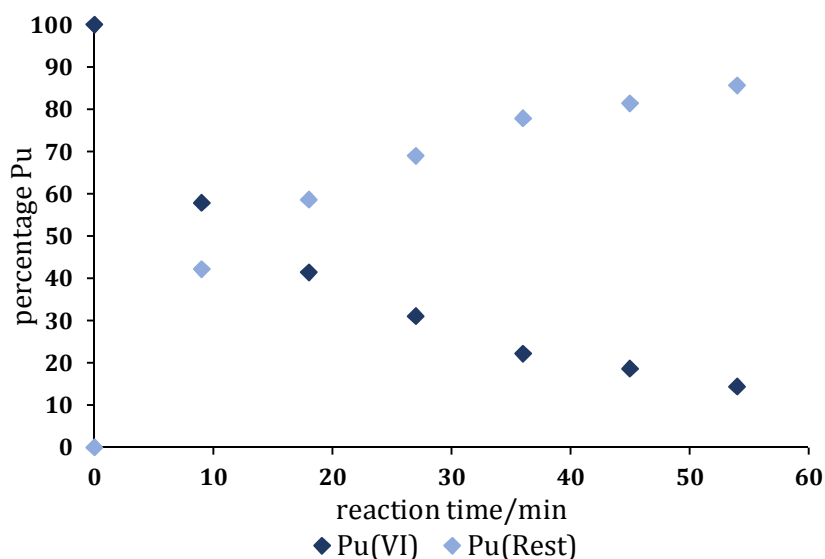


Figure 26: Development of the Pu(VI) and Pu(rest) percentages for the determination of the reduction kinetics of Pu(VI) with Fe(II), ratio 1:3, by LLE/LSC at 30 °C.

As one can see, for all three temperatures the reaction takes place and Pu(VI) is reduced by Fe(II). For the data evaluation the same approach as already described in Section 5.2.1 was employed. In this case also a first order reaction kinetic was assumed. The graphical determination of the rate constants k and the corresponding half lifes $t_{1/2}$ is shown in Figure 27, the resulting values are summarized in Table 25. The reduction at 30 °C was already near equilibrium after 36 min, thus the last two values are not used for the fitting

5. Determination of Redox Kinetics with CE-ICP-MS

procedure. These two data points are marked in grey in Figure 27. The fits were performed with Origin 7 software (OriginLab Corporation, Northampton, Massachusetts, USA).

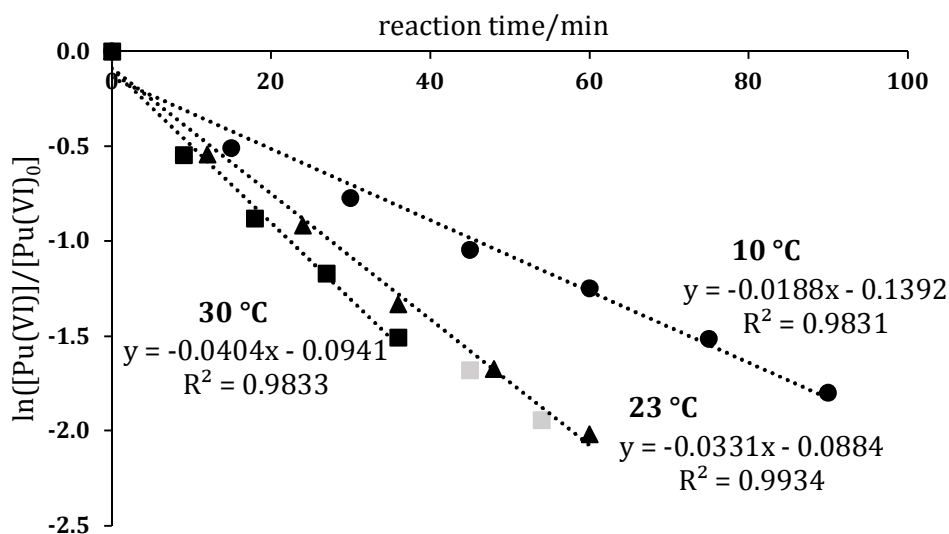


Figure 27: Graphical determination of the kinetical parameters of the reduction kinetics of Pu(VI) with Fe(II), ratio 1:3, by LLE/LSC. The data points in grey are not used for the fits since the reaction was already in equilibrium at this times.

Table 25: Resulting rate constants k and corresponding half lifes $t_{1/2}$ of the reduction of Pu(VI) by Fe(II), ratio 1:3, by LLE/LSC.

temperature/°C	k/min^{-1}	$t_{1/2}/\text{min}$
10	0.0188 ± 0.0011	36.9 ± 2.2
23	0.0331 ± 0.0014	20.9 ± 0.9
30	0.0404 ± 0.0031	17.2 ± 1.3

The results indicate that the assumption of a first order reaction kinetic with respect to Pu(VI) is reasonable. The rate constants increase with increasing temperature, the corresponding half lifes consequently decrease. 30 °C is set as an upper limit for the investigations of the given reaction because at higher temperatures the reaction should be too fast to investigate with the method employed in this work.

From the three rate constants determined at different temperatures an Arrhenius evaluation was performed as described in Section 5.2.1 in order to determine the activation energy of the Pu(VI) reduction by Fe(II). The resulting value for the activation energy is $E_A = (27.7 \pm 2.2)$ kJ/mol.

5.3 Determination of Kinetic Parameters of the Redox Reaction of Pu(VI) with Fe(II) by CE-ICP-MS

CE-ICP-MS MEASUREMENTS

The CE-ICP-MS measurements were conducted with a Pu(VI)/Fe(II) ratio of 1:4000. Besides the already mentioned fact that this is the same ratio as in [15GRA], a second aspect had been taken into consideration. Preceding experiments with a 1:3 ratio revealed, that the produced Pu(III) is not stable under the acidic conditions needed for the CE-ICP-MS measurements, it is rapidly reoxidized to Pu(IV). The rate constants of the reduction consequently are influenced by this redox process and the results are not trustworthy. The 1:4000 ratio in contrast turned out to be capable of stabilizing Pu(III), very likely because of the great excess of Fe(II). The reaction was investigated at 10 °C and 23 °C. The redox reaction was performed as described for the LLE/LSC measurements. For the CE-ICP-MS measurements, 200 μ L samples were taken without further dilution, just 1 μ L 2-bromopropane were added as the EOF-marker. The applied voltage during CE was $U = 25$ kV. The determination of the peak areas and the data evaluation was conducted as described in detail in Section 2.5 in the kinetic manuscript (see Section 5.2.1).

The resulting electropherograms for both temperature measurement series are summarized in Figure 28, the corresponding results for the peak areas and the electrophoretic mobilities are given in Table 26 for 10 °C and in Table 27 for 23 °C.

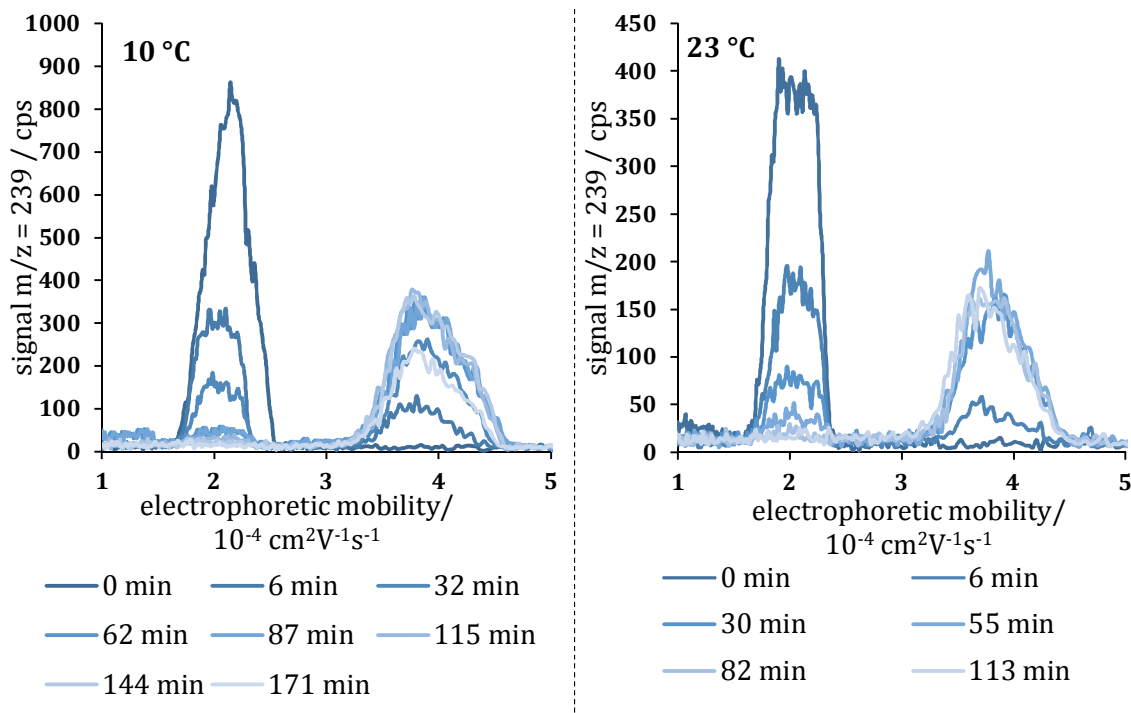


Figure 28: Electropherograms of the CE-ICP-MS measurement of the reduction of Pu(VI) by Fe(II) at 10 °C and 23 °C, $U = 25$ kV. The first peak in both electropherograms is assigned to Pu(VI), the second one to Pu(III).

5. Determination of Redox Kinetics with CE-ICP-MS

Table 26: Results of the determination of the reduction kinetics of Pu(VI) with Fe(II), ratio 1:4000, by CE-ICP-MS at 10 °C.

time/ min	peak area/cps		percentages/%		electrophoretic mobility/ $10^{-4} \text{ cm}^2\text{V}^{-1}\text{s}^{-1}$	
	Pu(VI)	Pu(III)	Pu(VI)	Pu(III)	Pu(VI)	Pu(III)
0	32034 ± 3203	0	100,0	0,0	2.14 ± 0.06	-
6	12345 ± 1235	2771 ± 277	81,7	18,3	2.10 ± 0.06	3.80 ± 0.11
32	5453 ± 545	7298 ± 730	42,8	57,2	2.02 ± 0.06	3.90 ± 0.11
62	2937 ± 294	10527 ± 1053	21,8	78,2	2.03 ± 0.06	3.82 ± 0.11
87	1529 ± 153	10359 ± 1036	12,9	87,1	2.08 ± 0.06	3.87 ± 0.11
115*	1048 ± 105	12130 ± 1213	8,0	92,0	2.00 ± 0.06	3.89 ± 0.12
144*	648 ± 65	12015 ± 1202	5,1	94,9	2.02 ± 0.07	3.97 ± 0.12
171*	0	7051 ± 705	0,0	100,0	-	3.85 ± 0.12

* not used for data evaluation because the reaction is already in equilibrium

Table 27: Results of the determination of the reduction kinetics of Pu(VI) with Fe(II), ratio 1:4000, by CE-ICP-MS at 23 °C.

time/ min	peak area/cps		percentages/%		electrophoretic mobility/ $10^{-4} \text{ cm}^2\text{V}^{-1}\text{s}^{-1}$	
	Pu(VI)	Pu(III)	Pu(VI)	Pu(III)	Pu(VI)	Pu(III)
0	16789 ± 1679	0	100,0	0,0	2.10 ± 0.06	-
6	6924 ± 692	1183 ± 118	85,4	14,6	2.10 ± 0.06	3.72 ± 0.11
30	2557 ± 256	4219 ± 422	37,7	62,3	2.03 ± 0.06	3.90 ± 0.12
55	1194 ± 119	5538 ± 554	17,7	82,3	2.04 ± 0.07	3.87 ± 0.12
82	384 ± 38	4698 ± 470	7,6	92,4	2.08 ± 0.07	3.85 ± 0.12
113	0	4626 ± 463	0,0	100,0	-	3.76 ± 0.11

The peak with the faster electrophoretic mobility was assigned to Pu(III), the other peak was assigned to Pu(VI). As can be seen in Table 26 and Table 27, the corresponding electrophoretic mobilities are in good agreement with the findings from previous experiments (see [19WIL1]). No other Pu species were detected in the electropherograms.

5.3 Determination of Kinetic Parameters of the Redox Reaction of Pu(VI) with Fe(II) by CE-ICP-MS

The rate constants k and the corresponding half lives $t_{1/2}$ were determined as described before. The resulting fits are shown in Figure 29, the values are depicted in Table 28.

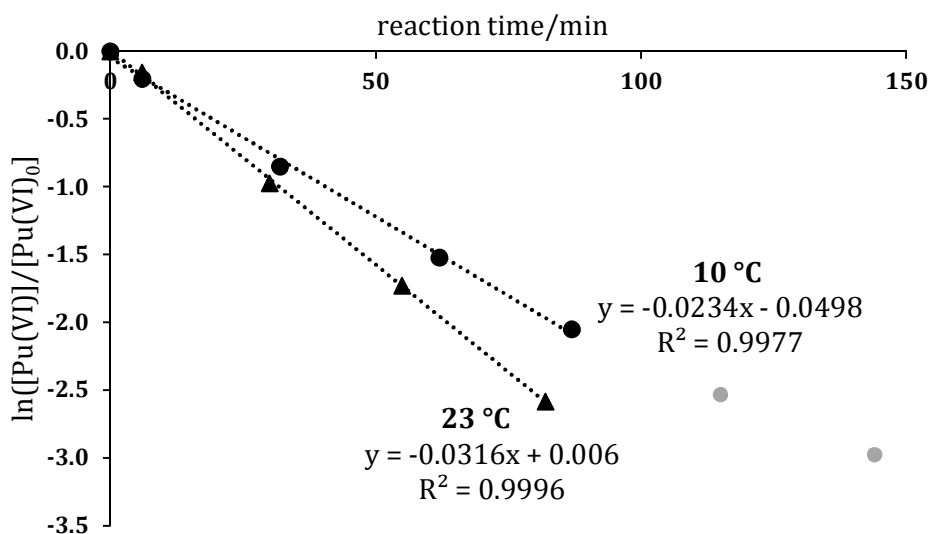


Figure 29: Graphical determination of the kinetical parameters of the reduction kinetics of Pu(VI) with Fe(II), ratio 1:4000, by CE-ICP-MS. The data points in grey are not used for the fits since the reaction was already in equilibrium at this times.

Table 28: Resulting rate constants k and corresponding half lives $t_{1/2}$ of the reduction of Pu(VI) by Fe(II), ratio 1:4000, by CE-ICP-MS.

temperature/°C	k/min^{-1}	$t_{1/2}/\text{min}$
10	0.0234 ± 0.0006	29.6 ± 0.8
23	0.0316 ± 0.0003	21.9 ± 0.2

Again, the experimentally determined results could be evaluated under the assumption of a reaction with a first order kinetic with respect to Pu(VI). The Arrhenius evaluation yielded an activation energy of $E_A = 16.1 \text{ kJ/mol}$.

5.3.5 DISCUSSION

The comparison of the results obtained from CE-ICP-MS measurements with the results from the LLE/LSC experiments shows a good agreement between the rate constants determined at the two temperatures 10 °C and 23 °C. The values are nearly identical within the limits of error for the 23 °C series. The deviation for the 10 °C series is somewhat higher which may be explained by the cooling procedure, which was just conducted by ice in a cooling bath, the temperature constancy was checked and adjusted by hand. Consequently, the activation energy resulting from the Arrhenius evaluation is also in quite good agreement, the differences may again be explained by the differences in the 10 °C rate constants. For more

5. Determination of Redox Kinetics with CE-ICP-MS

significant results, more measuring series must be conducted at different temperatures in order to get a higher statistical mass.

In the literature [15GRA], the presence of a Pu(IV) species in the course of the reduction reaction is described. As can be seen in the electropherograms presented in Figure 28, no such species could be detected in the present experiments. This difference may be explained by the use of a different ionic background. In the literature, a chloride medium was employed whereas in the present work chloride ions were avoided. Instead of these, perchlorate ions were used as the background because they are known to have non-complexing properties and the reaction as well as the CE-ICP-MS measurements should thus be less influenced. Both works agree in the fact, that the reduction is nearly complete after about 110 – 130 min. A direct comparison of the rate constants is not possible since no values for them are given in [15GRA].

The results from this section indicate that CE-ICP-MS is capable for the determination of kinetic parameters of redox reactions if both reaction partners are metals. In the case of redox reactions with iron it could be shown by preceding experiments that the use of an ORS system allows to overcome the difficulties arising from interferences with argon dimers.

REMARKS:

The kinetical investigations described above were undertaken within the framework of the diploma thesis of Saskia Leidich [17LE11] under the guidance of Christian Willberger and Tobias Reich. Samples preparation and CE-ICP-MS measurements were conducted by Saskia Leidich and Christian Willberger. The evaluation as presented here was conducted by Christian Willberger.

6. SUMMARY AND CONCLUSION

In the present work, CE-ICP-MS was employed for the investigation of different aspects of actinide chemistry in environmentally relevant concentrations in the context of the long-term safety assessment of a future disposal for high-level radioactive waste. The actinides examined in the experiments are thorium, uranium, neptunium, plutonium and americium.

First of all, the electrophoretic mobilities of the mentioned actinides with oxidation states reaching from +III to +VI were determined in a 1 M acetic acid BGE (Section 3.3). By comparing the results for redox stable actinide species (Am(III), Th(IV), Np(V) and U(VI)) with the electropherograms obtained for Pu it was possible to interpret all measured peaks and unequivocally ascertain the electrophoretic mobilities of the respective Pu species Pu(III)–Pu(VI). The trend in the electrophoretic mobilities was found to be $An(III) > An(VI) > An(V) > An(IV)$ for all actinides. This sequence can be explained by the effective charges of the respective actinides determined by speciation calculations. The electrophoretic mobilities of Am(III), U(VI) and U(IV) were measured for the first time under the given experimental conditions.

All samples were prepared in both 1 M HCl as a complexing medium and 1 M HClO₄ representing a non-complexing medium in order to investigate whether or not there is an influence of the medium of the stock solution on the results obtained in an 1 M acetic acid BGE. It could be shown that the electrophoretic mobility is independent of the chosen acid, the great excess of acetic acid during the electrophoretic migration makes the prior medium negligible.

Furthermore, as a result of these broad actinide mobility studies, a new systematic approach for the estimation of electrophoretic mobilities of actinides in oxidation states that are not stable during CE experiments could be introduced. Calculated values for Np(III), U(III) or U(V) could be thus presented. The validity of this new method could be proven by the comparison of calculated values with experimentally determined ones, e.g. for Np(VI) and U(IV).

On basis of the results obtained in this work it is now conceivable to use CE-ICP-MS also for the investigation of real samples, e.g. from long-term safety analysis experiments, with more complex background matrices. The knowledge of the electrophoretic mobilities of the given actinides and the trend throughout the oxidation states allows the interpretation of electropherograms with unknown sample compositions. A statement about the species distribution in environmental samples is thus possible. For a quantitative analysis of such samples some components, especially the coupling device, have to be developed further to

6. SUMMARY AND CONCLUSION

provide a more constant sample flow throughout all measurements and a calibration procedure has to be introduced.

In order to gain a deeper understanding of actinide behavior in the environment, more complex systems, as indicated above, representing naturally occurring BGEs were considered. Consequently, a further main aspect of this work was the investigation of interactions of actinides in the oxidation states III–VI with several organic ligands, namely acetate, propionate, gluconate and citrate (Section 4). The ligands were chosen with respect to their possible occurrence in a future geological nuclear waste repository and thus their importance in the corresponding long-term safety analysis.

In the present work, the stability constants of Am(III), Th(IV), Np(V) and U(VI) with acetate, propionate and gluconate were determined at an ionic strength of $I = 0.3$ M. By means of the Davies equation, these values were extrapolated to zero ionic strength. The results obtained here for low concentrations are in general in good agreement with literature data determined for higher concentration ranges with different analytical techniques.

The actinide-citrate system was challenging due to the three possible deprotonation steps of the citric acid (H_3Cit) in the pH range investigated in this work. Nevertheless, it could be demonstrated that CE-ICP-MS is also feasible for the examination of such a system of higher complexity. A simplified mathematical approach is presented to overcome the difficulties arising from the very complex fitting formulas resulting from this system. The stability constants thus obtained are comparable to values given in the literature, but for more significant results further measurement series are necessary to gain more data points.

Because of the positive results presented here, it is reasonable to expand the investigations to further ligand systems, not just in the context of nuclear waste disposal but also for a magnitude of other topics. In this case, it can be taken advantage of the possibility offered by CE-ICP-MS to measure several actinides within one and the same sample solution. In combination with the results from the mobility investigations, it is also very promising to examine the complexation of both the ligands presented here as well as further ligands for other actinides such as plutonium in different oxidation states. Here, because of the more complex redox chemistry of Pu, it has to be ensured that the oxidation state is fixed at any time without any doubt to avoid errors arising from mixed Pu species.

As a third application, in this work CE-ICP-MS was used for the investigation of kinetic parameters of actinide redox reactions (Section 5). The resulting rate constants were compared to rate constants obtained from another analytical technique, LLE/LSC, and by that it could be proved that the results from CE-ICP-MS are reliable.

First the reduction of Np(V) by hydroxylamine hydrochloride (HAHCl) was examined in 1 M HCl at different temperatures and concentrations of HAHCl (Section 5.2). A set of rate constants and the Arrhenius parameters could be obtained. The reaction turned out to be of (pseudo)first order with respect to both Np(V) and HAHCl.

The second reaction investigated was the reduction of Pu(VI) by Fe(II) (Section 5.3). The coupling of CE to ICP-MS offers the advantage of measuring multiple elements in varying oxidation states at the same time, which should be utilized in the experiments. Because of the difficulties resulting from isobaric interferences in the ICP-MS detection of Fe, the ORS was employed and the separation of Fe(II) and Fe(III) in this CE-ORS-ICP-MS was investigated. It was possible to clearly separate the two iron species by the selective complexation of Fe(II) by 1,10-phenanthroline (phen) and Fe(III) by EDTA and thus determine their electrophoretic mobilities.

The reaction turned out to be quite fast already at room temperature. Because of this the rate constants were investigated at 10 °C and at 23 °C in 1 M HClO₄. The reaction was found to be of first order kinetics with respect to Pu(VI) and again, the Arrhenius parameters were obtained.

Since it could be demonstrated that CE-ICP-MS is very useful in the determination of reaction kinetics, in future experiments it is very promising to investigate a variety of different actinide redox reactions with varying actinides in differing oxidation states and different redox partners. Especially metal redox partners are of potential interest since they can be examined in parallel.

In conclusion, in this work CE-ICP-MS has proven in three different application fields, namely mobility examination, stability constant determination and the investigation of redox reaction kinetics, to be a powerful and suitable analytical tool. In particular in the field of actinide chemistry with their wide redox species distribution and in the long-term safety assessment of nuclear waste disposals, where very low concentrations are of concern, the coupling of the separation capabilities of CE with the low detection limits of ICP-MS is very beneficial. The results obtained in this work for the stability constants and the kinetic parameters of the Pu(VI)/Fe(II) redox reaction can be used for the long-term safety assessment of radioactive waste. By a prove-of-principle study, the applicability of CE-ICP-MS for the determination of kinetic parameters of redox reactions could be demonstrated. These experiments can deal as a basis for future actinide CE-ICP-MS investigations.

REFERENCES

- [31ONS] Onsager, L.; Fuoss, R. M.: Irreversible Processes in Electrolytes. Diffusion, Conductance, and Viscous Flow in Arbitrary Mixtures of Strong Electrolytes. *J. Phys. Chem.* **1931**, *36*, 2689 – 2778.
- [60NEW] Newton, T. W.; Cowan, H. D.: The Kinetics of the Reaction Between Pu(IV) and Fe(II). *J. Phys. Chem.* **1960**, *64*, 244 – 247.
- [62HAL] Hala, J.; Okac, A.: Polarographische Verfolgung der Komplexe des Urans mit Propionat, Formiat and Monochloroacetat. *Collection Czechoslov. Chem. Commun.* **1962**, *27*, 1697 – 1701.
- [62SAW] Sawyer, D. T.; Kula, R. J.: Uranium(VI) Gluconate Complexes. *Inorg. Chem* **1962**, *1*, 303 – 309.
- [63NEW] Newton, T. W.; Baker, F. B.: The Kinetics of the Reaction Between Plutonium(VI) and Iron(II). *J. Phys. Chem.* **1963**, *67*, 1425 – 1432.
- [64SAW] Sawyer, D. T.: Metal-Gluconate Complexes. *Chem. Rev.* **1964**, *64*, 633 – 643.
- [64POW] Powell, J. E.; Kolat, R. S.; Paul, G. S.: Stability Constants of the Rare Earth Chelate Species Formed with Some Monocarboxylate Ligands. *Inorg. Chem.* **1964**, *3*, 518 – 520.
- [64SIL] Sillen, L. G.; Martell, A. E.; Bjerrum, J.: *Stability Constants of Metal-Ion Complexes*. Chemical Society, London, **1964**.
- [65CHO] Choppin, G. R.; Graffeo, A. J.: Complexes of Trivalent Lanthanide and Actinide Ions. II. Inner-Sphere Complexes. *Inorg. Chem.* **1965**, *4*, 1254 – 1257.
- [65RIC] Rice, C. L.; Whitehead, R.: Electrokinetical Flow in a Narrow Cylindrical Capillary. *J. Phys. Chem.* **1965**, *69*, 4017 – 4025.
- [66NEB] Nebel, D.; Urban, G.: Potentiometrische Untersuchungen zur Komplexbildung von Ce^{III}, Ce^{IV}, Th^{IV}, U^{IV} und Citrat in wässriger Lösung. *Z. Phys. Chem.* **1966**, *233*, 73 – 84.
- [67MIY] Miyake, C.; Nürnberg, H. W.: Co-Ordination Compounds of Actinides-I The Determination of the Stability Constants of Uranyl Complexes with Anions of Carboxylic Acids. *J. Inorg. Nucl. Chem.* **1967**, *29*, 2411 – 2429.
- [68RAM] Ramamoorthy, S.; Santappa, M.: Complexes of Uranyl Ion with Various Carboxylic Acids. *Curr. Sci.* **1968**, *14*, 403 – 404.
- [69CAS] Cassol, A.; Magon, L.; Tomat, G.; Portanova, R.: Relative Stabilities of Complexes of MO₂²⁺ (M = U, Np, and Pu) with Monocarboxylate Anions. *Inorg. Chim. Acta* **1969**, *3*, 639 – 643.
- [70BUN] Bunting, J. W.; Thong, K. M.: Stability Constants for Some 1:1 Metal-Carboxylate Complexes. *Can. J. Chem.* **1970**, *48*, 1654 – 1656.
- [71OHY] Ohyoshi, E.; Ohyoshi, A.: A Study of Complexes with a Polybasic Acid, Am(III) Citrate Complexes. *J. Inorg. Nucl. Chem.* **1971**, *33*, 4265 – 4273.
- [71SER] Sergeev, G. M.: The Stability of Propionate Complexes of Th(IV). *Radiokhimiya* **1971**, *13*, 900.

- [72POR] Portanova, R.; Tomat, G.; Cassol, A.; Magon, L.: Equilibria of Thorium(IV) with Monocarboxylate Ligands. *J. Inorg. Nucl. Chem.* **1972**, *34*, 1685 – 1690.
- [72TED] Tedesco, P. H.; Anon, M. C.: Thorium-Acetate and Thorium-Propionate Complexes. *J. Inorg. Nucl. Chem.* **1972**, *34*, 2271 – 2276.
- [74CHA] Chapman, A. J.: *Heat Transfer*. 3rd Ed., Macmillan, New York, **1974**.
- [75NEB] Nebel, D.; Anders, G.: Zur Komplexbildung und Solvatation einiger Actinide I. Untersuchungen zur Komplexbildung mit Acetat und Citrat. *Isotopenpraxis* **1975**, *11*, 152 – 155.
- [75OHY] Ohyoshi, E.; Oda, J.; Ohyoshi, A.: Complex Formation Between the Uranyl Ion and Citric Acid. *Bull. Chem. Soc. Jpn.* **1975**, *48*, 227 – 229.
- [80VAN] Vanura, P.; Kuca, L.: Citrate Complexes of Uranyl in Solutions with Higher Citrate Concentration. *Coll. Czechoslov. Chem. Comm.* **1980**, *45*, 41 – 53.
- [81CHU] Churaev, N. V.; Sergeeva, I. P.; Sobolev, V. D.; Derjaguin, B. V.: Examination of the Surface of Quartz Capillaries by Electrokinetic Methods. *J. Colloid Interface Sci.* **1981**, *84*, 451 – 460.
- [81SIN] Singh, R. K. P.; Sircar, J. K.; Yadava, J. R.; Yadava, P. C.; Yadava, K. L.: Stability Constants of Adipate Complexes of Copper(II), Nickel(II), Zinc(II), Cobalt(II), Uranyl(II) and Thorium(IV) Determined by Electrophoresis. *Electrochim. Acta* **1981**, *26*, 395 – 398.
- [83KEE] Keenan, J. H.; Chao, J.; Kaye, J.: *Gas Tables – International Version*. 2nd Ed., John Wiley & Sons, New York, **1983**.
- [83NAI] Nair, G. M.; Chander, K.: Stability Constants of Complexes of Plutonium(III) and Americium(III) with 5-Sulphosalicylic Acid. *J. Less Common Met.* **1983**, *92*, 29 – 34.
- [84FOU] Fourest, B.; Duplessis, J.; David, F.: Comparison of Diffusion Coefficients and Hydrated Radii for some Trivalent Lanthanide and Actinide Ions in Aqueous Solution. *Radiochim. Acta* **1984**, *36*, 191 – 195.
- [87FUJ] Fujiwara, S.; Honda, S.: Effect of Addition of Organic Solvent on the Separation of Positional Isomers in High-Voltage Capillary Zone Electrophoresis. *Anal. Chem.* **1987**, *59*, 487 – 490.
- [87HER] Herren, B. J.; Shafer, S. G.; van Alstine, J.; Harris, J. M.; Snyder, R. S.: Control of Electroosmosis in Coated Quartz Capillaries. *J. Colloid Interface Sci.* **1987**, *115*, 46 – 55.
- [87RAY] Raymon, D. P.; Duffield, J. R.; Williams, D. R.: Complexation of Plutonium and Thorium in Aqueous Environments. *Inorg. Chim. Acta* **1987**, *140*, 309 – 313.
- [87ROS] Rösch, F.; Herrmann, R.; Hung, T. K.; Milanov, M.; Khalkin, V. A.: Electromigration of Carrier-Free Radionuclides. IV. Oxalate and Tartrate Complexes of Ln(III) in Aqueous Solution. *J. Radioanal. Nucl. Chem.* **1987**, *111*, 319 – 327.
- [88COM] Combes, C. L.; Birch, G. G.: Interaction of D-Glucono-1,5-Lactone with Water. *Food Chem.* **1988**, *27*, 283 – 298.
- [88KNO] Knox, J. H.: Thermal Effects and Band Spreading in Capillary Electro-Separation. *Chromatographia* **1988**, *26*, 329 – 337.

REFERENCES

- [88NIT] Nitsche, H.; Lee, S.; Gatti, R.: Determination of Plutonium Oxidation States at Trace Levels Pertinent to Nuclear Waste Disposal. *J. Radioanal. Nucl. Chem.* **1988**, *124*, 171 – 185.
- [89ROS1] Rösch, F.; Reimann, T.; Buklanov, G. V.; Milanov, M.; Khalkin, V. A.; Dreyer, R.: Electromigration of Carrier Free Radionuclides. 13. Ion Mobilities and Hydrolysis of ²⁴¹Am-Am(III) in Aqueous Inert Electrolytes. *J. Radioanal. Nucl. Chem.* **1989**, *134*, 109 – 128.
- [89ROS2] Rösch, F.; Dietrich, S.; Buklanov, G. V.; Milanov, M.; Khalkin, V. A.; Dreyer, R.: Electromigration of Carrier Free Radionuclides. 11. Complex Formation of ²³⁹Np(V) with Oxalate, Tartrate and Sulphate in Neutral Inert Electrolytes. *Radiochim. Acta* **1989**, *48*, 205 – 211.
- [90HJE] Hjerten, S.: Zone Broadening in Electrophoresis with Special Reference to High-Performance Electrophoresis in Capillaries: An Interplay between Theory and Practice. *Electrophoresis* **1990**, *11*, 665 – 690.
- [90ROS1] Rösch, F.; Khalkin, V. A.: Ion Mobility of Trivalent f-Elements in Aqueous Electrolytes. *Radiochim. Acta* **1990**, *51*, 101 – 106.
- [90ROS2] Rösch, F.; Reimann, T.; Buklanov, V.; Milanov, M.; Khalkin, V. A.; Dreyer, R.: Electromigration of Carrier-Free Radionuclides. XIV. Complex Formation of ²⁴¹Am-Am(III) with Oxalate and Sulfate in Aqueous Solution. *J. Radioanal. Nucl. Chem.* **1990**, *140*, 159 – 169.
- [90ROS3] Rösch, F.; Dietrich, S.; Buklanov, G. V.; Milanov, M.; Khalkin, V. A.; Dreyer, R.: Electromigration of Carrier-Free Radionuclides. 12. Reactions of ²³⁹Np(V) with Acetate and Citrate Ligands in Neutral Solutions. *Radiochim. Acta* **1990**, *49*, 29 – 34.
- [90ROS4] Rösch, F.; Hung, T. K.; Dietrich, S.; Ludwig, R.; Buklanov, G. V.; Dreyer, R.; Khalkin, V. A.: Electromigration Studies of Carrier-Free ²³⁹Np(V) in Aqueous Solutions. *Isotopenpraxis* **1990**, *26*, 355 – 363.
- [92GRO] Grossman, P. D.; Colburn, J. C. (Eds.): *Capillary Electrophoresis - Theory and Practice*. Academic Press: San Diego, **1992**.
- [93ENG] Engelhardt, H.; Beck, W.; Kohr, J.; Schmitt, T.: Kapillarelektrophorese: Methoden und Möglichkeiten. *Angew. Chem.* **1993**, *105*, 659 – 680.
- [94REE] Reed, N. M.; Cairns, R. O.; Hutton, R. C.; Takaku, Y.: Characterization of Polyatomic Ion Interferences in Inductively Coupled Plasma Mass Spectrometry Using a High Resolution Mass Spectrometer. *J. Anal. At. Spectrom.* **1994**, *9*, 881 – 896.
- [95OLE] Olesik, J. W.; Kinzer, J. A.; Olesik, S. V.: Capillary Electrophoresis Inductively Coupled Plasma Mass Spectrometry for Rapid Elemental Speciation. *Anal. Chem.* **1995**, *67*, 1 – 12.
- [96CHO] Choppin, G. R.; Erten, H. N.; Xia, Y.-X.: Variation of Stability Constants of Thorium Citrate Complexes with Ionic Strength. *Radiochim. Acta* **1996**, *74*, 123 – 127.
- [96GOU] Gougar, M. L. D.; Scheetz, B. E.; Roy, D. M.: Ettringite and C-S-H Portland Cement Phases for Waste Ion Immobilization: A Review. *Waste Manage.* **1995**, *16*, 295 – 303.
- [96MAR] Marion, G. M.; Babcock, K. L.: Predicting Specific Conductance and Salt Concentration in Dilute Aqueous Solutions. *Soil Science* **1995**, *122*, 181 – 187.
- [96SCH] Schäffer, S.; Gareil, P.; Dezael, C.; Richard, D.: Direct Determination of Iron(II), Iron(III) and Total Iron as UV-Absorbing Complexes by Capillary Electrophoresis. *J. Chromatogr. A* **1996**, *740*, 151 – 157.

- [97HIE] Hiemenz, P. C.; Rajagopalan, R.: *Principles of Colloid and Surface Chemistry*. 3rd Edition, Marcel Dekker, Inc.: New York, **1997**.
- [97MAC] Macka, M.; Haddad, P. R.: Determination of Metal Ions by Capillary Electrophoresis. *Electrophoresis* **1997**, *18*, 2482 – 2501.
- [97POK] Pokrovsky, O. S.; Choppin, G. R.: Neptunium(V) Complexation by Acetate, Oxalate and Citrate in NaClO₄ Media at 25°C. *Radiochim. Acta* **1997**, *79*, 167 – 171.
- [97POZ] Pozniakova, S.; Padaruskas, A.; Schwendt, G.: Simultaneous Determination of Iron(II) and Iron(III) in Water by Capillary Electrophoresis. *Anal. Chim. Acta* **1997**, *351*, 41 – 48.
- [97SCA] Scapolan, S.; Ansoborlo, E.; Moulin, C.; Madic, C.: Etude de la Speciation de l'Uranium en Milieu Biologique Par Electrophorese Capillaire et Spectrofluorimetrie Laser a Resolution Temporelle. *Radioprotection* **1997**, *32*, 645 – 657.
- [97SUT] Sutton, K.; Sutton, R. M. C.; Caruso, J. A.: Inductively Coupled Plasma Mass Spectrometric Detection for Chromatography and Capillary Electrophoresis. *J. Chromatogr. A* **1997**, *789*, 85 – 126.
- [97YON] Yong, P.; Macaskie, L. E.: Removal of Lanthanum, Uranium and Thorium from the Citrate Complexes by Immobilized Cells of *Citrobacter* Sp. In a Flow-Through Reactor: Implications for the Decontamination of Solutions Containing Plutonium. *Biotechnol. Lett.* **1997**, *19*, 251 – 255.
- [98BAR] Barnes, R. M.: Capillary Electrophoresis and Inductively Coupled Plasma Mass Spectrometry: Status Report. *Fresenius J. Anal. Chem.* **1998**, *361*, 246 – 251.
- [98LIU1] Liu, B.-F.; Liu, L.-B.; Cheng, J.-K.: Separation of Thorium, Uranium and Rare-Earth Elements with 2-[(2-arsenophenyl)-azo]-1,8-dihydroxy-7-[(2,4,6-tribromophenyl)-azo]-naphthalene-3,6-disulfonic Acid by Capillary Electrophoresis. *Anal. Chim. Acta* **1998**, *358*, 157 – 162.
- [98LIU2] Liu, B.-F.; Liu, L.-B.; Cheng, J.-K.: Separation and Determination of Thorium, Uranium and Mixed Rare-Earth Elements as Their UV/Vis Absorbing Complexes by Capillary Zone Electrophoresis. *Talanta* **1998**, *47*, 291 – 299.
- [98MAC] Macka, M.; Nesterenko, P.; Andersson, P.; Haddad, P. R.: Separation of Uranium(VI) and Lanthanides by Capillary Electrophoresis Using On-Capillary Complexation with Arsenazo III. *J. Chromatograph. A* **1998**, *803*, 279 – 290.
- [98MCL] McLean, J. A.; Minnich, M. G.; Iacone, L. A.; Liu, H.; Montaser, A.: Nebulizer Diagnostics: Fundamental Parameters, Challenges, and Techniques on the Horizon. *J. Anal. At. Spectrom.* **1998**, *13*, 829 – 842.
- [98SCA] Scapolan, S.; Ansoborlo, E.; Moulin, C.; Madic, C.: Investigation by Time-Resolved Laser-Induced Fluorescence and Capillary Electrophoresis of the Uranyl-Phosphate Species: Application to Blood Serum. *J. Alloys Comp.* **1998**, *271-273*, 106 – 111.
- [98SUT] Sutton, K. L.; B'Hymer, C.; Caruso, A.: Ultraviolet Absorbance and Inductively Coupled Plasma Mass Spectrometric Detection for Capillary Electrophoresis-A Comparison of Detection Modes and Interface Designs. *J. Anal. At. Spectrom.* **1998**, *13*, 885 – 891.
- [98ZEM] Zemmann, A. J.; Schnell, E.; Volgger, D.; Bonn, G. K.: Contactless Conductivity Detection for Capillary Electrophoresis. *Anal. Chem.* **1998**, *70*, 563 – 567.

REFERENCES

- [99JAN] Janos, P.: Role of Chemical Equilibria in the Capillary Electrophoresis of Inorganic Substances. *J. Chromatogr. A* **1999**, 834, 3 – 20.
- [00DAY] Day, J. A.; Caruso, J. A.; Becker, J. S.; Dietze, H.-J.: Application of Capillary Electrophoresis Interfaced to Double Focusing Sector Field ICP-MS for Nuclide Abundance Determination of Lanthanides Produced Via Spallation Reactions in an Irradiated Tantalum Target. *J. Anal. At. Spectrom.* **2000**, 15, 1343 – 1348.
- [00GOM] Gompper, K.: Zur Abtrennung langlebiger Radionuklide. *Radioaktivität und Kernenergie*. Forschungszentrum Karlsruhe **2000**, 153 – 168.
- [00LEN] Lenhart, J. J.; Cabaniss, S. E.; MacCarthy, P.; Honeyman, B. D.: Uranium(VI) Complexation with Citric, Humic and Fulvic Acids. *Radiochim. Acta* **2000**, 88, 345 – 353.
- [00OZT] Öztekin, N.; Erim, F. B.: Separation and Direct UV Detection of Lanthanides Complexed with Cupferron by Capillary Electrophoresis. *J. Chromatogr. A* **2000**, 895, 263 – 268.
- [00TIM] Timerbaev, A. R.: Element Speciation Analysis by Capillary Electrophoresis. *Talanta* **2000**, 52, 573 – 606.
- [00TOD] Todoli, J.-L.; Maestre, S.; Mora, J.; Canals, A.; Hernandis, V.: Comparison of Several Spray Chambers Operating at Very Low Liquid Flow Rates in Inductively Coupled Plasma Atomic Emission Spectrometry. *Fresenius J. Anal. Chem.* **2000**, 368, 773 – 779.
- [01AGI] *Agilent 7500 Inductively Coupled Plasma Mass Spectrometry*. Rev. 1, H8974-90000, Agilent Technologies, USA, **2001**.
- [01COL] Collins, G. E.; Lu, Q.: Microfabricated Capillary Electrophoresis Sensor for Uranium(VI). *Anal. Chim. Acta* **2001**, 436, 181 – 189.
- [01DAV1] David, F. H.; Vokhmin, V. J.: Hydration and Entropy Model for Ionic and Covalent Monoatomic Ions. *Phys. Chem. A* **2001**, 105, 9704 – 9709.
- [01DAV2] David, F.; Vokhmin, V.; Ionova, G.: Water Characteristics Depend on the Ionic Environment. Thermodynamics and Modelisation of the Aquo Ions. *J. Mol. Liq.* **2001**, 90, 45 – 62.
- [01EVA] Evans III, L.; Collins, G. E.: Separation of Uranium(VI) and Transition Metal Ions with 4-(2-Thiazolylazo)resorcinol by Capillary Electrophoresis. *J. Chromatogr. A* **2001**, 911, 127 – 133.
- [01PAC] Pacheco, M. L.; Havel, J.: Capillary Zone Electrophoretic (CZE) Study of Uranium(VI) Complexation with Humic Acids. *J. Radioanal. Nucl. Chem.* **2001**, 248, 565 – 570.
- [01RUN] Rundlett, K. L.; Armstrong, D. W.: Methods for the Determination of Binding Constants by Capillary Electrophoresis. *Electrophoresis* **2001**, 22, 1419 – 1427.
- [01TIM] Timerbaev, A. R.: Element Speciation Analysis by Capillary Electrophoresis: What are the Hints on Becoming a Standard Analytical Methodology?. *Anal. Chim. Acta* **2001**, 433, 165 – 180.
- [02KAN] Kannamkumarath, S. S.; Wrobel, K.; Wrobel, K.; B'Hymer, C.; Caruso, J. A.: Capillary Electrophoresis-Inductively Coupled Plasma-Mass Spectrometry: An Attractive Complementary Technique for Elemental Speciation Analysis. *J. Chromatogr. A* **2002**, 975, 245 – 266.

- [02KAR] Karamanev, D. G.; Nikolov, L. N.; Mamatarkova, V.: Rapid Simultaneous Quantitative Determination of Ferric and Ferrous Ions in Drainage Waters and Similar Solutions. *Miner. Eng.* **2002**, *15*, 341 – 346.
- [02MUZ] Muzikar, J.; van de Goor, T.; Kenndler, E.: The Principle Cause for Lower Plate Numbers in Capillary Zone Electrophoresis with Most Organic Solvents. *Anal. Chem.* **2002**, *74*, 434 – 439.
- [02TAN] Tanner, S. D.; Baranov, V. I.; Bandura, D. R.: Reaction Cells and Collision Cells for ICP-MS: A Tutorial Review. *Spectrochim. Acta B* **2002**, *57*, 1361 – 1452.
- [02WAL] Wall, N. A.; Borkowski, M.; Chen, J.-F.; Choppin, G. R.: Complexation of Americium with Humic, Fulvic and Citric Acids at High Ionic Strength. *Radiochim. Acta* **2002**, *90*, 563 – 568.
- [02WIE] Wieland, E.; Tits, J.; Dobler, J. P.; Spieler, P.: The Effect of α -Isosaccharinic Acid on the Stability of and Th(IV) Uptake by Hardened Cement Paste. *Radiochim. Acta* **2002**, *90*, 683 – 688.
- [03AUP] Aupiais, J.; Delorme, A.; Baglan, N.: Determination of the Absolute Mobility and the Equivalent Ionic Conductivity of NpO_2^+ at 25 °C and at Infinite Dilution by Capillary Electrophoresis-Inductively Coupled Plasma-Mass Spectrometry. *J. Chromatogr. A* **2003**, *994*, 199 – 206.
- [03JAN] Janos, P.: Analytical Separation of Lanthanides and Actinides by Capillary Electrophoresis. *Electrophoresis* **2003**, *24*, 1982 – 1992.
- [03KUC] Kuczewski, B.; Marquardt, C. M.; Seibert, A.; Geckeis, H.; Kratz, J. V.; Trautmann, N.: Separation of Plutonium and Neptunium Species by Capillary Electrophoresis-Inductively Coupled Plasma-Mass Spectrometry and Application to Natural Groundwater Samples. *Anal. Chem.* **2003**, *75*, 6769 – 6774.
- [03LIU] Liu, Y.-M.; Cheng, J.-K.: Elemental Speciation Analysis in Capillary Electrophoresis. *Electrophoresis* **2003**, *24*, 1993 – 2012.
- [03MAU] Mauerhofer, E.; Rösch, F.: Dependence of the Mobility of Tracer Ions in Aqueous Perchlorate Solutions on the Hydrogen Ion Concentration. *Phys. Chem. Chem. Phys.* **2003**, *5*, 117 – 126.
- [03PAU] Paull, B.; King, M.: Quantitative Capillary Zone Electrophoresis of Inorganic Anions. *Electrophoresis* **2003**, *24*, 1892 – 1934.
- [03RAI] Rai, D.; Hess, N. J.; Xia, Y.; Rao, L.; Cho, H. M.; Moore, R. C.; Van Loon, L. R.: Comprehensive Thermodynamic Model Applicable to Highly Acidic to Basic Conditions for Isosaccharinate Reaction with Ca(II) and Np(IV). *J. Solution Chem* **2003**, *32*, 665 – 689.
- [03SON] Sonke, J. E.; Furbish, D. J.; Salters, V. J. M.: Dispersion Effects of Laminar Flow and Spray Chamber Volume in Capillary Electrophoresis-Inductively Coupled Plasma-Mass Spectrometry: A Numerical and Experimental Approach. *J. Chromatograph. A* **2003**, *1015*, 205 – 218.
- [04KAR] Karbowski, M.; Hubert, S.; Fourest, B.; Moulin, C.: Complex Formation of Uranium(VI) in Periodate Solutions. *Radiochim. Acta* **2004**, *92*, 489 – 494.

REFERENCES

- [04KOP] Koppenaar, D. W.; Eiden, G. C.; Barinaga, C. J.: Collision and Reaction Cells in Atomic Mass Spectrometry: Development, Status, and Application. *J. Anal. At. Spectrom.* **2004**, *19*, 561 – 570.
- [04LID] Lide, D. R., ed.: *CRC Handbook of Chemistry and Physics*. 84th Edition, CRC Press: Boca Raton, **2004**.
- [04MAR] Martel, A. E.; Smith, R. M. *NIST Standard Reference Database 46.6*, version 8.0, 2004.
- [04PET] Peterson, N. J.; Nikolajsen, R. P. H.; Mogensen, K. B.; Kutter, J. P.: Effect of Joule Heating on Efficiency and Performance for Microchip-Based and Capillary-Based Electrophoretic Separation Systems: A Closer Look. *Electrophoresis* **2004**, *25*, 253 – 269.
- [04SON] Sonke, J. E.; Salters, V. J. M.: Disequilibrium Effects in Metal Speciation by Capillary Electrophoresis Inductively Coupled Plasma Mass Spectrometry (CE-ICP-MS); Theory, Simulations and Experiments. *Analyst* **2004**, *129*, 731 – 738.
- [04WIL] Wilbur, S.; Soffey, E.; McCurdy, E.: Performance Characteristics of the Agilent 7500ce – The ORS Advantage for High Matrix Analysis. 5989-1041EN, Agilent Technologies, USA, **2004**.
- [04YAN] Yanes, G. E.; Miller-Ihli, N. I.: Use of a Parallel Path Nebulizer for Capillary-Based Microseparation Techniques Coupled With an Inductively Coupled Plasma Mass Spectrometer for Speciation Measurements. *Spectrochim. Acta B* **2004**, *59*, 883 – 890.
- [05ALI] Ali, I.; Gupta, V. K.; Aboul-Enein, H. Y.: Metal Ion Speciation and Capillary Electrophoresis: Application in the New Millennium. *Electrophoresis* **2005**, *26*, 3988 – 4002.
- [05ALV] Alvarez-Llamas, G.; del Rosario Fernandez de laCampa, M.; Sanz-Medel, A.: ICP-MS for Specific Detection in Capillary Electrophoresis. *Trends Anal. Chem.* **2005**, *24*, 28 – 36.
- [05AMB] Ambert, C.; Delorme, A.; Baglan, N.; Aupiais, J.; Pointurier, F.; Madic, C.: Interfacing Capillary Electrophoresis with Inductively Coupled Plasma Mass Spectrometry for Redox Speciation of Plutonium. *Radiochim. Acta* **2005**, *93*, 665 – 673.
- [05FOU] Fourest, B.; Sladkov, V.: Transport Methods as Complementary Tools for Speciation Purposes. *Radiochim. Acta* **2005**, *93*, 653 – 657.
- [05HUM] Hummel, W.; Anderegg, G.; Rao, L.; Puigdomenech, I.; Tochiyama, O.: *Chemical Thermodynamics of Compounds and Complexes of U, Np, Pu, Am, Tc, Se, Ni and Zr with Selected Organic Ligands*. 1st Edition, Elsevier: Amsterdam, **2005**.
- [05KAN] Kantar, C.; Gillow, J. B.; Harper-Arabie, R.; Honeyman, B. D.; Francis, A. J.: Determination of Stability Constants of U(VI)-Fe(III)-Citrate Complexes. *Environ. Sci. Technol.* **2005**, *39*, 2161 – 2168.
- [05MIC] Michalke, B.: Capillary Electrophoresis-Inductively Coupled Plasma-Mass Spectrometry: A Report on Technical Principles and Problem Solutions, Potential, and Limitations of This Technology As Well As on Examples of Application. *Electrophoresis* **2005**, *26*, 1584 – 1597.
- [05PRA] Prange, A.; Pröfrock, D.: Application of CE-ICP-MS and CE-ESI-MS in Metalloproteomics: Challenges, Developments, and Limitations. *J. Bioanal. Chem.* **2005**, *383*, 372 – 389.

- [05TIT] Tits, J.; Wieland, E.; Bradbury, M. H.: The Effect of Isosaccharinic Acid and Gluconic Acid on the Retention of Eu(III), Am(III) and Th(IV) by Calcite. *Appl. Geochem.* **2005**, *20*, 2082 – 2096.
- [05YAN] Yanes, G. E.; Miller-Ihli, N. I.: Parallel Path Nebulizer: Critical Parameters for Use With Microseparation Techniques Combined With Inductively Coupled Plasma Mass Spectrometry. *Spectrochim. Acta B* **2005**, *60*, 555 – 561.
- [06ATK] Atkins, P. W.; de Paula, J.: *Physikalische Chemie*. 4th Edition, Wiley VCH: Weinheim, **2006**.
- [06CHO] Morss, L. R.; Edelstein, N. M.; Fuger, J.; Katz, J. J. (Eds.); Choppin, G. R.; Jensen, M. P.: *The Chemistry of the Actinide and Transactinide Elements – Chapter 23: Actinides in Solution: Complexation and Kinetics*. 3rd Edition, Springer: Heidelberg, **2006**.
- [06EVE] Evenhuis, C. J.; Guijt, R. M.; Macka, M.; Marriott, P. J.; Haddad, P. R.: Temperature Profiles and Heat Dissipation in Capillary Electrophoresis. *Anal. Chem.* **2006**, *78*, 2684 – 2693.
- [06FEL] Felmy, A. R.; Cho, H.; Dixon, D. A.; Xia, Y.; Hess, N. J.; Wang, Z.: The Aqueous Complexation of Thorium with Citrate Under Neutral to Basic Conditions. *Radiochim. Acta* **2006**, *94*, 205 – 212.
- [06JOU] Jouyban, A.; Kenndler, E.: Theoretical and Empirical Approaches to Express the Mobility of Small Ions in Capillary Electrophoresis. *Electrophoresis* **2006**, *27*, 992 – 1005.
- [06KAU] Kautenburger, R.; Nowotka, K.; Beck, H. P.: Online Analysis of Europium and Gadolinium Species Complexed or Uncomplexed with Humic Acid by Capillary Electrophoresis-Inductively Coupled Plasma Mass Spectrometry. *Anal. Bioanal. Chem.* **2006**, *384*, 1416 – 1422.
- [06RAM] Ramachandran, S.; Fontanille, P.; Pandey, A.; Larroche, C.: Gluconic Acid: Properties, Applications and Microbial Production. *Food Technol. Biotechnol.* **2006**, *44*, 185 – 195.
- [06SAI] Saito, S.; Danzaka, N.; Hoshi, S.: Highly Sensitive Determination of Lanthanides by Capillary Electrophoresis with Direct Visible Detection After Precapillary Complexation with Aromatic Polyaminocarboxylate and Additionally Applying Dynamic Ternary Complexation with Nitrilotriacetic Acid. *Electrophoresis* **2006**, *27*, 3093 – 3100.
- [06SON] Sonke, J. E.; Salters, V. J. M.: Lanthanide-Humic Substances Complexation. I. Experimental Evidence for a Lanthanide Contraction Effect. *Geochim. Cosmochim. Acta* **2006**, *70*, 1495 – 1506.
- [06WAR] Warwick, P.; Evans, N.; Vines, S.: Studies on Metal Gluconic Acid Complexes. In: Van Isheghem, P. (ed.), *Scientific Basis for Nuclear Waste Management XXIX*, Materials Resource Society Symposium Proceedings, 932, Warrendale, PA, **2006**, 959 – 966.
- [06ZHA] Zhang, Z.; Clark, S. B.; Tian, G.; Zanonato, P. L.; Rao, L.: Protonation of D-Gluconate and its Complexation with Np(V) in Acidic to Nearly Neutral Solutions. *Radiochim. Acta* **2006**, *94*, 531 – 536.
- [07BON] Bonin, L.; Den Auwer, C.; Ansoborlo, E.; Cote, E.; Moisy, P.: Study of Np Speciation in Citrate Medium. *Radiochim. Acta* **2007**, *95*, 371 – 379.
- [07BUR] Bürger, S.; Banik, N. L.; Buda, R. A.; Kratz, J. V.; Kuczewski, B.; Trautmann, N.: Speciation of the Oxidation States of Plutonium in Aqueous Solutions by UV/Vis Spectroscopy, CE-ICP-MS and CE-RIMS. *Radiochim. Acta* **2007**, *95*, 433 – 438.

REFERENCES

- [07HOL] Holleman, A. F.; Wiberg, N.: *Lehrbuch der anorganischen Chemie*. 102nd Edition, Walter de Gruyter: Berlin, **2007**.
- [07KAU] Kautenburger, R.; Beck, H. P.: Complexation Studies with Lanthanides and Humic Acid Analyzed by Ultrafiltration and Capillary Electrophoresis-Inductively Coupled Plasma Mass Spectrometry. *J. Chromatograph. A* **2007**, *1159*, 75 – 80.
- [07KIR] Kirishima, A.; Onishi, Y.; Sato, N.; Tochiyama, O.: Determination of the Thermodynamic Quantities of Uranium(VI)-Carboxylate Complexes by Microcalorimetry. *J. Chem. Thermodynamics* **2007**, *39*, 1432 – 1438.
- [07MAT] Mathur, J. N.; Cernochova, K.; Choppin, G. R.: Thermodynamics and Laser Luminescence Spectroscopy of Binary and Ternary Complexation of Am³⁺, Cm³⁺ and Eu³⁺ with Citric Acid and Citric Acid + EDTA at High Ionic Strength. *Inorg. Chim. Acta* **2007**, *360*, 1785 – 1791.
- [07SON] Sonke, J. E.; Salters, V. J. M.: Capillary Electrophoresis-High Resolution Sector Field Inductively Coupled Plasma Mass Spectrometry. *J. Chromatograph. A* **2007**, *1159*, 63 – 74.
- [07STE] Stern, J. C.; Sonke, J. E.; Salters, V. J. M.: A Capillary Electrophoresis-ICP-MS Study of Rare Earth Element Complexation by Humic Acids. *Chem. Geol.* **2007**, *246*, 170 – 180.
- [07USE] Uselova-Vcelakova, K.; Zuskova, I.; Gas, B.: Stability Constants of Amino Acids, Peptides, Proteins, and Other Biomolecules Determined by CE and Related Methods: Recapitulation of Published Data. *Electrophoresis* **2007**, *28*, 2145 – 2152.
- [07ZHA] Zhang, Z.; Gibson, P.; Clark, S. B.; Tian, G.; Zanonato, P. L.; Rao, L.: Lactonization and Protonation of Gluconic Acid: A Thermodynamic and Kinetic Study by Potentiometry, NMR and ESI-MS. *J. Solution Chem.* **2007**, *36*, 1187 – 1200.
- [08AGI1] *Agilent 7500 ICP-MS Hardware Manual*. Rev. A, G3270-90106, Agilent Technologies, USA, **2008**.
- [08AGI2] *Agilent 7500 ICP-MS Tuning and Application Handbook*. Rev. A, G3270-90132, Agilent Technologies, USA, **2008**.
- [08BON] Bonin, L.; Cote, G.; Moisey, P.: Speciation of An(IV) (Pu, Np, U and Th) in Citrate Media. *Radiochim. Acta* **2008**, *96*, 145 – 152.
- [08CHE] Chen, Z.; Weber, S. G.: Determination of Binding Constants by Affinity Capillary Electrophoresis, Electrospray Ionization Mass Spectrometry and Phase-Distribution Methods. *Trends Anal. Chem.* **2008**, *27*, 738 – 748.
- [08GAO] Gaona, X.; Montoya, V.; Colas, E.; Grieve, M.; Duro, L.: Review of the Complexation of Tetravalent Actinides by ISA and Gluconate Under Alkaline to Hyperalkaline Conditions. *J. Contam. Hydrol.* **2008**, *102*, 217 – 227.
- [08KEI] Keith-Roach, M. J.: The Speciation, Stability, Solubility and Biodegradation of Organic Co-Contaminant Radionuclide Complexes: A Review. *Sci. Total Environ.* **2008**, *396*, 1 – 11.
- [08PHI] Philippini, V.; Vercouter, T.; Aupiais, J.; Topin, S.; Ambard, C.; Chausse, A.; Vitorge, P.: Evidence of Different Stoichiometries for the Limiting Carbonate Complexes Across the Lanthanide(III) Series: A Capillary Electrophoresis-Mass Spectrometry Study. *Electrophoresis* **2008**, *29*, 2041 – 2050.

- [08PIT] Pitois, A.; Aldave de Las Heras, L.; Betti, M.: Determination of Fission Products in Nuclear Samples by Capillary Electrophoresis-Inductively Coupled Plasma Mass Spectrometry (CE-ICP-MS). *Int. J. Mass Spectrom.* **2008**, *270*, 118 – 126.
- [08YIN] Yin, X.-B.; Li, Y.; Yan, X.-P.: CE-ICP-MS for Studying Interactions Between Metals and Biomolecules. *Trends Anal. Chem.* **2008**, *27*, 554 – 565.
- [09AGI] Agilent Technologies, Inc.: *Technical Note - Capillary Thermostatting in Capillary Electrophoresis*. Publication Number 5990-3407EN, **2009**.
- [09BEN] Benes, P.: Radiotracer Study of Thorium Complexation with Humic Acid at pH 2-11 Using Free-Liquid Electrophoresis. *Radiochim. Acta* **2009**, *97*, 273 – 281.
- [09BOU] Boughammoura, S.; M'halla, J.; Fourest, B.: Application of Capillary Electrophoresis to the Uranyl/Citrate System in Moderately Acidic Solutions. *J. Radioanal. Nucl. Chem.* **2009**, *280*, 547 – 559.
- [09CHE] Chen, Q. Y.; Tyrer, M.; Hills, C. D.; Yang, X. M.; Carey, P.: Immobilisation of Heavy Metal in Cement-Based solidification/Stabilisation: A Review. *Waste Manage.* **2009**, *29*, 390 – 403.
- [09JOH] Johns, C.; Breadmore, M. C.; Macka, M.; Ryvolova, M.; Haddad, P. R.: Recent Significant Developments in Detection and Method Development for the Determination of Inorganic Ions by CE. *Electrophoresis* **2009**, *30*, 53 – 67.
- [09KAU] Kautenburger, R.: Influence of Metal Concentration and the Presence of Competing Cations on Europium and Gadolinium Speciation with Humic Acid Analyzed by CE-ICP-MS. *J. Anal. At. Spectrom.* **2009**, *24*, 934 – 938.
- [09PET] Petit, J.; Geertsen, V.; Beaucaire, C.; Stambouli, M.: Metal Complexes Stability Constant Determination by Hyphenation of Capillary Electrophoresis with Inductively Coupled Plasma Mass Spectrometry: The Case of 1:1 Metal-to-Ligand Stoichiometry. *J. Chromatogr. A* **2009**, *1216*, 4113 – 4120.
- [09TIM] Timerbaev, A. R.: Capillary Electrophoresis Coupled to Mass Spectrometry for Biospeciation Analysis: Critical Evaluation. *Trends Anal. Chem.* **2009**, *28*, 416 – 425.
- [09TOP1] Topin, S.; Aupiais, J.; Moisy, P.: Direct Determination of Plutonium(V) and Neptunium(V) Complexation by Carbonate Ligand with CE-ICP-Sector Field MS. *Electrophoresis* **2009**, *30*, 1747 – 1755.
- [09TOP2] Topin, S.; Aupiais, J.; Baglan, N.; Vercouter, T.; Vitorge, P.; Moisy, P.: Trace Metal Speciation by Capillary Electrophoresis Hyphenated to Inductively Coupled Plasma Mass Spectrometry: Sulfate and Chloride Complexes of Np(V) and Pu(V). *Anal. Chem.* **2009**, *81*, 5354 – 5363.
- [09ZHA] Zhang, Z.; Helms, G.; Clark, S. B.; Tian, G.; Zanonato, P.; Rao, L.: Complexation of Uranium(VI) by Gluconate in Acidic Solutions: A Thermodynamic Study with Structural Analysis. *Inorg. Chem.* **2009**, *48*, 3814 – 3824.
- [10BAH] Bahga, S. S.; Bercovici, M.; Santiago, S. G.: Ionic Strength Effects on Electrophoretic Focusing and Separations. *Electrophoresis* **2010**, *31*, 910 – 919.
- [10HUH] Huhn, C.; Ramautar, R.; Wuhler, M.; Somsen, G. W.: Relevance and Use of Capillary Coatings in Capillary Electrophoresis–Mass Spectrometry. *Anal. Bioanal. Chem.* **2010**, *396*, 297 – 314.

REFERENCES

- [10JIA] Jiang, C.; Armstrong, D. W.: Use of CE for the Determination of Binding Constants. *Electrophoresis* **2010**, *31*, 17 – 27.
- [10LAU] Lauer, H. H.; Rozing, P.: *High performance capillary electrophoresis – a primer*. Agilent Technologies, **2010**.
- [10MEN] Mendes, M.; Hamadi, S.; Le Naour, C.; Roques, J.; Jeanson, A.; Den Auwer, C.; Moisy, P.; Topin, S.; Aupiais, J.; Henning, C.; Di Giandomenico, M.-V.: Thermodynamical and Structural Study of Protactinium(V) Oxalate Complexes in Solution. *Inorg. Chem.* **2010**, *49*, 9962 – 9971.
- [10MIS] Mishustin, A. I.: Estimate of the Stability Constants of Trivalent Actinide and Lanthanide Complexes with O-Donor Ligands in Aqueous Solutions. *Russ. J. Inorg. Chem.* **2010**, *55*, 746 – 752.
- [10MUS1] Musheev, M. U.; Filiptsev, Y.; Krylov, S. N.: Noncooled Capillary Inlet: A Source of Systematic Errors in Capillary-Electrophoresis-Based Affinity Analysis. *Anal. Chem.* **2010**, *82*, 8637 – 8641.
- [10MUS2] Musheev, M. U.; Filiptsev, Y.; Krylov, S. N.: Temperature Difference Between the Cooled and the Noncooled Parts of an Electrolyte in Capillary Electrophoresis. *Anal. Chem.* **2010**, *82*, 8692 – 8695.
- [10PET] Petit, J.; Aupiais, J.; Topin, S.; Geertsen, V.; Beaucaire, C.; Stambouli, M.: Stability Constant Determination of Successive Metal Complexes by Hyphenated CE-ICPMS. *Electrophoresis* **2010**, *31*, 355 – 363.
- [10TIM] Timerbaev, A. R.: Inorganic Species Analysis by CE- An Overview for 2007-2008. *Electrophoresis* **2010**, *31*, 192 – 204.
- [10TOP] Topin, S.; Aupiais, J.; Baglan, N.: Determination of the Stability Constants of Nitrate Complexes of Np(V) and Pu(V) Using CE-ICP-MS. *Radiochim. Acta* **2010**, *98*, 71 – 75.
- [11BIR] Birjkumar, K. H.; Bryan, N. D.; Kaltsoyannis, N.: Computational Investigation of the Speciation of Uranyl Gluconate Complexes in Aqueous Solution. *Dalton Trans.* **2011**, *40*, 11248 – 11257.
- [11CLA] Claveranne-Lamolere, C.; Aupiais, J.; Lespes, G.; Frayret, J.; Pili, E.; Pointurier, P.; Potin-Gautier, M.: Investigation of Uranium-Colloid Interactions in Soil by Dual Field-Flow Fractionation/Capillary Electrophoresis Hyphenated with Inductively Coupled Plasma-Mass Spectrometry. *Talanta* **2011**, *85*, 2504 – 2510.
- [11COL] Colas, E.; Grive, M.; Rojo, I.; Duro, L.: Solubility of $\text{ThO}_2 \cdot x\text{H}_2\text{O}(\text{am})$ in the Presence of Gluconate. *Radiochim. Acta* **2011**, *99*, 269 – 273.
- [11EVE] Evenhuis, C. J.; Musheev, M. U.; Krylov, S. N.: Universal Method for Determining Electrolyte Temperatures in Capillary Electrophoresis. *Anal. Chem.* **2011**, *83*, 1808 – 1814.
- [11SLA] Sladkov, V.; Zhao, Y.; Mercier-Bion, F.: Capillary Zone Electrophoresis for U(VI) and Short Chain Carboxylic Acid Sorption Studies on Silica and Rutile. *Talanta* **2011**, *83*, 1595 – 1600.
- [12BER] Berto, S.; Crea, F.; Daniele, P. G.; De Stefano, C.; Prenesti, E.; Sammartano, S.: Potentiometric and Spectrophotometric Characterization of the UO_2^{2+} -Citrate Complexes in Aqueous Solution, at Different Concentrations, Ionic Strength and Supporting Electrolytes. *Radiochim. Acta* **2012**, *100*, 13 – 28.

- [12HEL] Heller, A.; Barkleit, A.; Foerstendorf, H.; Tsushima, S.; Heim, K.; Bernhard, G.: Curium(III) Citrate Speciation in Biological Systems: A Europium(III) Assisted Spectroscopic and Quantum Chemical Study. *Dalton Trans.* **2012**, *41*, 13969 – 13983.
- [12LEG] Leguay, S.; Vercouter, T.; Topin, S.; Aupiais, J.; Guillaumont, D.; Miguirditchian, M.; Moisy, P.; Le Naour, C.: New Insights Into Formation of Trivalent Actinides Complexes with DTPA. *Inorg. Chem.* **2012**, *51*, 12638 – 12649.
- [12MOS] Möser, C.; Kautenburger, R.; Beck, H. P.: Complexation of Europium and Uranium by Humic Acids Analyzed by Capillary Electrophoresis-Inductively Coupled Plasma Mass Spectrometry. *Electrophoresis* **2012**, *33*, 1482 – 1487.
- [12POI] Poinssot, C.; Geckeis, H. (Eds.): *Radionuclide Behaviour in the Natural Environment – Science, Applications and Lessons for the Nuclear Industry*. Woodhead Publishing: Cambridge, **2012**.
- [12PRO] Präfrock, D.; Prange, A.: Inductively Coupled Plasma-Mass Spectrometry (ICP-MS) for Quantitative Analysis in Environmental and Life Science: A Review of Challenges, Solutions, and Trends. *Appl. Spectrosc.* **2012**, *66*, 843 – 868.
- [12SEH] Seher, H.; Bracke, G.: *Chemische Vorgänge in einem Endlager für hochradioaktive Abfälle in Ton- und Salzgestein*. Gesellschaft für Anlagen- und Reaktorsicherheit (GRS) mbH – Synthesebericht, GRS – 301, ISBN 978-3-939355-80-9, **2012**.
- [12SLA] Sladkov, V.: Effects of Non-Thermostated Capillary Inlet in Affinity Capillary Electrophoresis: Uranyl-Selenate System at Variable Temperatures. *J. Chromatograph. A* **2012**, *1263*, 189 – 193.
- [12STO] Stöbener, N.; Amayri, S.; Gehl, A.; Kaplan, U.; Malecha, K.; Reich, T.: Sensitive Redox Speciation of Neptunium by CE-ICP-MS. *Anal. Bioanal. Chem.* **2012**, *404*, 2143 – 2150.
- [12THA] Thakur, P.; Xiong, Y.; Borkowski, M.; Choppin, G. R.: Thermodynamic Modeling of Trivalent Am, Cm and Eu-Citrate Complexation in Concentrated NaClO₄ Media. *Radiochim. Acta* **2012**, *100*, 165 – 172.
- [13COL1] Colas, E.; Grive, M.; Rojo, I.; Duro, L.: The Effect of Gluconate and EDTA on Thorium Solubility Under Simulated Cement Porewater Conditions. *J. Solution Chem.* **2013**, *42*, 1680 – 1690.
- [13COL2] Colas, E.; Grive, M.; Rojo, I.: Complexation of Uranium(VI) by Gluconate in Alkaline Solutions. *J. Solution Chem.* **2013**, *42*, 1545 – 1557.
- [13DVO] Dvorak, M.; Svobodova, J.; Benes, M.; Gas, B.: Applicability and Limitations of Affinity Capillary Electrophoresis and Vacancy Affinity Capillary Electrophoresis Methods for Determination of Complexation Constants. *Electrophoresis* **2013**, *34*, 761 – 767.
- [13KLE] Kleparnik, K.: Recent Advances in the Combination of Capillary Electrophoresis with Mass Spectrometry: From Element to Single-Cell Analysis. *Electrophoresis* **2013**, *34*, 70 – 85.
- [13MEN] Mendes, M.; Leguay, S.; Le Naour, C.; Hamadi, S.; Roques, J.; Moisy, P.; Guillaumont, D.; Topin, S.; Aupiais, J.; Den Auwer, C.; Hennig, C.: Thermodynamic Study of the Complexation of Protactinium(V) with Diethylentriaminepentaacetic Acid. *Inorg. Chem.* **2013**, *52*, 7497 – 7507.

REFERENCES

- [13OHN] Ohnuki, T.; Kozai, N.; Sakamoto, F.; Suzuki, Y.; Yoshida, T.: Biological Change of Chemical States of Actinides and Lanthanides –Effect of Organic Acids-. *Energy Procedia* **2013**, *39*, 175 – 182.
- [13SLA] Sladkov, V.: Uranyl Complexation with Acetate Studied by Means of Affinity Capillary Electrophoresis. *J. Chromatogr. A* **2013**, *1289*, 133 – 138.
- [13STO] Stöbener, N.: Elementspeziation von Neptunium im Ultraspurenbereich. Ph.D. Thesis, Johannes-Gutenberg University Mainz, Germany, **2013**. (https://publications.ub.uni-mainz.de/theses/frontdoor.php?source_opus=3475)
- [13TIM1] Timerbaev, A. R.: Element Speciation Analysis Using Capillary Electrophoresis: Twenty Years of Development and Application. *Chem. Rev.* **2013**, *113*, 778 – 812.
- [13TIM2] Timerbaev, A. R.; Timerbaev, R. M.: Recent Progress of Capillary Electrophoresis in Studying the Speciation of Actinides. *Trends Anal. Chem.* **2013**, *51*, 44 – 50.
- [14BRO] Brown, M. A.; Kropf, A. J.; Paulenova, A.; Gelis, A. V.: Aqueous Complexation of Citrate with Neodymium(III) and Americium(III): A Study by Potentiometry, Absorption Spectrophotometry, Microcalorimetry and XAFS. *Dalton Trans.* **2014**, *43*, 6446 – 6454.
- [14GUS] Gustafsson, J. P.: *Geochemical Equilibrium Speciation Model*. Visual MINTEQ Ver. 3.1. KTH, Department of Land and Water, Resources Engineering, Stockholm, Sweden, 2014. <http://vminteq.lwr.kth.se/download/>
- [14HEI] Hein, C.; Sander, J. M.; Kautenburger, R.: Speciation via Hyphenation – Metal Speciation in Geological and Environmental Samples by CE-ICP-MS. *Anal. Bioanal. Tech.* **2014**, *5*, 225.
- [14KAU] Kautenburger, R.; Hein, C.; Sander, J. M.; Beck, H. P.: Influence of Metal Loading and Humic Acid Functional Groups on the Complexation Behavior of Trivalent Analyzed by CE-ICP-MS. *Anal. Chim. Acta* **2014**, *816*, 50 – 59.
- [14KUB] Kuban, P.; Timerbaev, A. R.: Inorganic Analysis Using CE: Advanced Methodologies to Face Old Challenges. *Electrophoresis* **2014**, *35*, 225 – 233.
- [14SHI] Shiri-Yekta, Z.; Nilchi, A.; Yaftian, M. R.; Yousefnia, H.: Separation and Direct UV Detection of Complexed Lanthanides, Thorium and Uranyl Ions with 2-Thenoyltrifluoroacetone by Using Capillary Zone Electrophoresis. *J. Radioanal. Nucl. Chem.* **2014**, *302*, 1143 – 1150.
- [14SLA] Sladkov, V.: Interaction of Uranyl with Acetate in Aqueous Solutions at Variable Temperatures. *J. Chem. Thermodyn.* **2014**, *71*, 148 – 154.
- [14STE] Stern, J. C.; Foustoukos, D. I.; Sonke, J. E.; Salters, V. J. M.: Humic Acid Complexation of Th, Hf and Zr in Ligand Competition Experiments: Metal Loading and pH Effects. *Chem. Geol.* **2014**, *363*, 241 – 249.
- [14WIL] Willberger, C.: Redoxspeziation von Neptunium mit CE-ICP-MS und UV-Vis-Spektroskopie. Diploma Thesis, Johannes-Gutenberg University Mainz, Germany, **2014**.
- [15BRU] Brunel, B.; Philippini, V.; Mendes, M.; Aupiais, J.: Actinide Oxalate Complexes Formation As a Function of Temperature by Capillary Electrophoresis Coupled with Inductively Coupled Plasma Mass Spectrometry. *Radiochim. Acta* **2015**, *103*, 27 – 37.

- [15GAL] Galievsky, V. A.; Stasheuski, A. S.; Krylov, S. N.: Capillary Electrophoresis for Quantitative Studies of Biomolecular Interactions. *Anal. Chem.* **2015**, *87*, 157 – 171.
- [15GRA] Graser, C.-H.; Banik, N. L.; Bender, K. A.; Lagos, M.; Marquardt, C. M.; Marsac, R.; Montoya, V.; Geckeis, H.: Sensitive Redox Speciation of Iron, Neptunium, and Plutonium by Capillary Electrophoresis Hyphenated to Inductively Coupled Plasma Sector Field Mass Spectrometry. *Anal. Chem.* **2015**, *87*, 9786 – 9794.
- [15HUY] Huynh, T.-N. S.; Bourgeois, D.; Basset, C.; Vidaud, C.; Hagege, A.: Assessment of CE-ICP/MS Hyphenation for the Study of Uranyl/Protein Interactions. *Electrophoresis* **2015**, *36*, 1374 – 1382.
- [15STE] Stepanova, S.; Kasicka, V.: Capillary Electrophoretic Methods Applied to the Investigation of Peptide Complexes. *J. Sep. Sci.* **2015**, *38*, 2708 – 2721.
- [15VAS] Vasiliev, A. N.; Banik, N. L.; Marsac, R.; Fröhlich, D. R.; Rothe, J.; Kalmykov, S. N.; Marquardt, C. M.: Np(V) Complexation with Propionate in 0.5-4 M NaCl Solutions at 20-85 °C. *Dalton Trans.* **2015**, *44*, 3837 – 3844.
- [15ZHA] Zhang, Y.; Li, L.; Huang, H.; Xu, L.; Li, Z.; Bai, Y.; Liu, H.: Binding Constant Determination of Uranyl-Citrate Complex by ACE Using a Multi-Injection Method. *Electrophoresis* **2015**, *36*, 1033 – 1039.
- [16AUP] Aupiais, J.; Bonin, L.; Den Auwer, C.; Moisy, P.; Siberchicot, B.; Topin, S.: On the Use of Speciation Techniques and Ab Initio Modelling to Understand Tetravalent Actinide Behavior in a Biological Medium: An^{IV}DTPA Case. *Dalton Trans.* **2016**, *45*, 3759 – 3770.
- [16BON] Bonin, L.; Aupiais, J.; Kerbaa, M.; Moisey, P.; Topin, S.; Siberchicot, B.: Revisiting Actinide-DTPA Complexes in Aqueous Solution by CE-ICP-MS and Ab Initio Molecular Dynamics. *RSC Adv.* **2016**, *6*, 62729 – 62741.
- [16CHE] Cheng, H.; Li, J.; Liu, J.; Ye, M.: Coupling Electrophoretic Separation with Inductively Coupled Plasma Spectroscopic Detection: Interfaces and Applications from Elemental Speciation, Metal-Ligand Interaction to Indirect Determination. *J. Anal. At. Spectrom.* **2016**, *31*, 1780 – 1810.
- [16HUY] Huynh, T.-N. S.; Vidaud, C.; Hagege, A.: Investigation of Uranium Interactions with Calcium Phosphate-Binding Proteins Using ICP/MS and CE-ICP/MS. *Metallomics* **2016**, *8*, 1185 – 1192.
- [16LI] Li, L.; Zhang, Y.; Li, X.; Shen, S.; Huang, H.; Bai, Y.; Liu, H.: study of the Interaction of Uranyl with Sulfated Beta-Cyclodextrin by Affinity Capillary Electrophoresis and Molecular Dynamics Simulation. *Electrophoresis* **2016**, *37*, 2567 – 2573.
- [16MEB] Mebert, A. M.; Tuttolomondo, A. V.; Alvarez Echazu, M. I.; Foglia, M. L.; Alvarez, G. S.; Vescina, M. C.; Santo-Orihuela, P. L.; Desimone, M. F.: Nanoparticles and Capillary Electrophoresis: A Marriage with Environmental Impact. *Electrophoresis* **2016**, *37*, 2196 – 2207.
- [16SLA] Sladkov, V.: Affinity Capillary Electrophoresis in Studying the Complex Formation Equilibria of Radionuclides in Aqueous Solutions. *Electrophoresis* **2016**, *37*, 2558 – 2566.
- [16TOP] Topin, S.; Aupiais, J.: The Pentavalent Actinide Solution Chemistry. *J. Environ. Radioact.* **2016**, *153*, 237 – 244.

REFERENCES

- [17ALE] Aleksenko, S. S.; Matczuk, M.; Timerbaev, A. R.: Characterization of Interactions of Metal-Containing Nanoparticles with Biomolecules by CE: An Update (2012-2016). *Electrophoresis* **2017**, *38*, 1661 – 1668.
- [17AND] Androniuk, I.; Landesman, C.; Henocq, P.; Kalinichev, A. G.: Adsorption of Gluconate and Uranyl on C-S-H Phases: Combination of Wet Chemistry Experiments and Molecular Dynamics Simulations for the Binary Systems. *Phys. Chem. Earth* **2017**, *99*, 194 – 203.
- [17AUP] Aupiais, J.; Younes, A.; Moisy, P.; Hennig, C.; Rossberg, A.; Brunel, B.; Kerbaa, M.; Vidaud, C.; Den Auwer, C.: Structural and Thermodynamical Investigation of An^{IV}LI(O)HOPO. *New J. Chem.* **2017**, *41*, 11291 – 11298.
- [17DUD] Dudas, C.; Kutus, B.; Böszörményi, E.; Peintler, G.; Kele, Z.; Palinko, I.; Sipos, P.: Comparison of the Ca²⁺ Complexing Properties of Isosaccharinate and Gluconate – Is Gluconate a Reliable Structural and Functional Model of Isosaccharinate. *Dalton Trans.* **2017**, *46*, 13888 – 13896.
- [17FRA] Franze, B.; Strenge, I.; Engelhard, C.: Separation and Detection of Gold Nanoparticles with Capillary Electrophoresis and ICP-MS in Single Particle Mode (CE-SP-ICP-MS). *J. Anal. At. Spectrom.* **2017**, *32*, 1481 – 1489.
- [17HAH] Hahn, R.; Hein, C.; Sander, J. M.; Kautenburger, R.: Complexation of Europium and Uranium with Natural Organic Matter (NOM) in Highly Saline Water Matrices Analysed by Ultrafiltration and Inductively Coupled Plasma Mass Spectrometry (ICP-MS). *Appl. Geochem.* **2017**, *78*, 241 – 249.
- [17HEI] Hein, C.; Sander, J. M.; Kautenburger, R.: New Approach of a Transient ICP-MS Measurement Method for Samples with High Salinity. *Talanta* **2017**, *164*, 477 – 482.
- [17KAU] Kautenburger, R.; Sander, J. M.; Hein, C.: Europium(III) and Uranium(VI) Complexation by Natural Organic Matter (NOM): Effect of Source. *Electrophoresis* **2017**, *38*, 930 – 937.
- [17LEI1] Leidich, S.: Untersuchung Redoxreaktion von Pu(VI) mit Fe(III) mittels CE-ICP-MS. Diploma Thesis, Johannes-Gutenberg University Mainz, Germany, **2017**.
- [17LEI2] Leichtfuß, D.: Untersuchungen zur aquatischen Chemie von Actiniden mittels CE-ICP-MS. Diploma Thesis, Johannes-Gutenberg University Mainz, Germany, **2017**.
- [17MOZ1] Mozhayeva, D.; Strenge, I.; Engelhard, C.: Implementation of Online Preconcentration and Microsecond Time Resolution to Capillary Electrophoresis Single Particle Inductively Coupled Plasma Mass Spectrometry (CE-SP-ICP-MS) and Its Application in Silver Nanoparticle Analysis. *Anal. Chem.* **2017**, *89*, 7152 – 7159.
- [17MOZ2] Mozhayeva, D.; Engelhard, C.: Separation of Silver Nanoparticles with Different Coatings by Capillary Electrophoresis Coupled to ICP-MS in Single Particle Mode. *Anal. Chem.* **2017**, *89*, 9767 – 9774.
- [17NOW] Nowak, P. M.; Wozniakiewicz, M.; Koscielniak, P.: Seven Approaches to Elimination of the Inherent Systematic Errors in Determination of Electrophoretic Mobility by Capillary Electrophoresis. *Anal. Chem.* **2017**, *89*, 3630 – 3638.
- [17SAG] „Standortauswahlgesetz vom 5. Mai 2017 (BGBl. I S. 1075), das zuletzt durch Artikel 2 Absatz 16 des Gesetzes vom 20. Juli 2017 (BGBl. I S. 2808) geändert worden ist.“

- [17SAU] Sauge-Merle, S.; Lemaire, D.; Evans, R. W.; Berthomieu, C.; Aupiais, J.: Revisiting Binding of Plutonium to Transferrin by CE-ICP-MS. *Dalton Trans.* **2017**, 46, 1389 – 1396.
- [17TYC] Tycova, A.; Ledvina, V.; Kleparnik, K.: Recent Advances in CE-MS Coupling: Instrumentation, Methodology, and Applications. *Electrophoresis* **2017**, 38, 115 – 134.
- [18AtG] „Atomgesetz in der Fassung der Bekanntmachung vom 15. Juli 1985 (BGBl. I S. 1565), das zuletzt durch Artikel 1 des Gesetzes vom 10. Juli 2018 (BGBl. I S. 1122, 1124) geändert worden ist.“
- [18BRU] Brulfert, F.; Aupiais, J.: Topological Speciation of Actinide-Transferrin Complexes by Capillary Isoelectric Focusing Coupled with Inductively Coupled Plasma Mass Spectrometry: Evidence of the Non-Closure of the Lobes. *Dalton Trans.* **2018**, 47, 9994 – 10001.
- [18FRA] Francisco, K. J. M.; do Lago, C. L.: Improving Thermal Control of Capillary Electrophoresis with Mass Spectrometry and Capacitively Coupled Contactless Conductivity Detection by Using 3D Printed Cartridge. *Talanta* **2018**, 185, 37 – 41.
- [18KUB] Kuban, P.; Hauser, P. C.: 20th Anniversary of Axial Capacitively Coupled Contactless Conductivity Detection in Capillary Electrophoresis. *Trends Anal. Chem.* **2018**, 102, 311 – 321.
- [18LUC] Luchini, C.; Leguay, S.; Aupiais, J.; Cannes, C.; Le Naour, C.: Complexation of Protactinium(V) with Nitrotriacetic Acid: A Study at the Tracer Scale. *New J. Chem.* **2018**, 42, 7789 – 7795.
- [18MAR] Martelat, B.; Isnard, H.; Vio, L.; Dupuis, E.; Cornet, T.; Nonell, A.; Chartier, F.: Precise U and Pu Isotope Ratio Measurements in Nuclear Samples by Hyphenating Capillary Electrophoresis and MC-ICPMS. *Anal. Chem.* **2018**, 90, 8622 – 8628.
- [18MEE] Meermann, B.; Nischwitz, V.: ICP-MS for the Analysis at the Nanoscale – A Tutorial Review. *J. Anal. At. Spectrom.* **2018**, 33, 1432 – 1468.
- [18MIC] Michalke, B.; Vinkovic-Vrcek, I.: Speciation of Nano and Ionic Form of Silver with Capillary Electrophoresis-Inductively Coupled Plasma Mass Spectrometry. *J. Chromatogr. A.* **2018**, 1572, 162 – 171.
- [18SLA] Sladkov, V.; Bessonov, A. A.; Roques, J.; Charushnikova, I. A.; Fedosseev, A.M.: Complexation of An(VI) with Succinic Acid in Aqueous Acid Solution: Uranyl vs. Plutonyl. *New J. Chem.* **2018**, 42, 7780 – 7788.
- [18WIL] Willberger, C. Amayri, S.; Reich, T.: Determination of Kinetic Parameters of Redox Reactions Using CE-ICP-MS: A Case Study for the Reduction of Np(V) by Hydroxylamine Hydrochloride. *Electrophoresis* **2018**, 39, 3013 – 3021.
- [19BUR] Burgener Research Operating Instructions Manual. Online Source: <http://burgenerresearch.com/MiraMistCEManual.html>, last accessed on 25.05.2019.
- [19MA] Ma, B.; Charlet, L.; Fernandez-Martinez, A.; Kang, M.; Made, B.: A Review of the Retention Mechanism of Redox-Sensitive Radionuclides in Multi-Barrier Systems. *Appl. Geochem.* **2019**, 100, 414 – 431.
- [19WIL1] Willberger, C.; Amayri, S.; Häußler, V.; Scholze, R.; Reich, T.: Investigation of the Electrophoretic Mobility of the Actinides Th and U–Am in Different Oxidation States. (*submitted for publication*).

REFERENCES

[19WIL2] Willberger, C.; Amayri, S.; Leichtfuß, D.; Reich, T.: Determination of the Stability Constants of the Actinides Am(III), Th(IV), Np(V), and U(VI) Using CE-ICP-MS. *Inorg. Chem.* **2019**, *58*, 4851 – 4858.

APPENDIX A1 – CALCULATION OF TEMPERATURE RISE DUE TO JOULE HEATING

In Section 2.1.3 the temperature rise due to Joule heating is discussed and a temperature profile inside the capillary is shown in Figure 3. The values and graphs given there were calculated as follows (the derivation follows [92GRO]).

The capillaries used in this work have an inner radius $r_c = 25 \mu\text{m}$. The radius of the fused silica layer is $r_2 = 171.5 \mu\text{m}$, that of the exterior polymer coating is $r_3 = 181.5 \mu\text{m}$. The capillary length is $l = 76 \text{ cm}$.

Firstly, the thermal conductivities k_{BGE} , k_f , k_p and k_{air} of the different materials (BGE, fused-silica, polyimide and air) have to be determined. Under the assumption, that k_{BGE} is independent of the ions present in the solution, it can be approximated by the thermal conductivity of water. This value is temperature dependent and was calculated for $\vartheta = 25 \text{ }^\circ\text{C}$ with a second order polynomial fit given in Equation (A1.1).

$$k_{\text{BGE}}(\vartheta) = 0.5605 + 1.998 \cdot 10^{-3}T - 7.765 \cdot 10^{-6}T^2. \quad (\text{A1.1})$$

By applying this equation, a thermal conductivity of $k_{\text{BGE}} = 0.606 \text{ W m}^{-1} \text{ K}^{-1}$ resulted which is in good agreement with a value of $k_{\text{BGE}} = 0.6 \text{ W m}^{-1} \text{ K}^{-1}$ that can be found in the literature [88KNO]. Consequently, the result given above was used throughout the complete calculation instead of using an iterative procedure to always include the temperature dependence of k_{BGE} . The other thermal conductivities are considered as temperature independent in the temperature region considered. The values are as follows: $k_f = 1.5 \text{ W m}^{-1} \text{ K}^{-1}$, $k_p = 1.55 \text{ W m}^{-1} \text{ K}^{-1}$ (both [92GRO]) and $k_{\text{air}} = 0.025 \text{ W m}^{-1} \text{ K}^{-1}$ [88KNO].

After that, the electrical conductivity of the buffer κ_e has to be determined. It is also a strong function of the temperature as well as of the composition of the buffer. It can be determined experimentally by measuring the electrical current I during an electrophoretic measurement that is generated at a given applied voltage U . With these values Equation (A1.2) can be used.

$$\kappa_e = \frac{I}{AU}. \quad (\text{A1.2})$$

The electrical current during typical experiments is $I = 10 - 13 \mu\text{A}$ for $U = 25 \text{ kV}$. The following calculations are undertaken with the upper limit of the electrical current in order to yield a maximum value for the temperature rise. With the capillary length $l = 76 \text{ cm}$ and a capillary cross section area $A = \pi r_c^2 = 1963.5 \mu\text{m}^2$ the electrical conductivity emerges as $\kappa_e = 0.201 \text{ S m}^{-1}$.

A very important parameter for the calculation of the temperature rise due to Joule heating is the so called heat transfer coefficient h which defines the possibility to dissipate the heat from the capillary to the surrounding medium. In the case of this work, a stream of forced air was used to cool the area around the capillary. In such a case, h can be calculated by Equation (A1.3), which is

APPENDIX A1 – CALCULATION OF TEMPERATURE RISE DUE TO JOULE HEATING

an empirical estimation for a capillary surrounded by forced air given in [74CHA] relating the Nusselt number Nu and the Reynolds number Re .

$$Nu = 0.615Re^{0.466}. \quad (A1.3)$$

The two variable Nu and Re are defined as depicted in Equations (A1.4) and (A1.5).

$$Nu = \frac{hd_3}{k_{\text{air}}}. \quad (A1.4)$$

$$Re = \frac{d_3 v_{\text{air}} \rho_{\text{air}}}{\eta_{\text{air}}}. \quad (A1.5)$$

By combining Equations (A1.3) – (A1.5) one obtains a term for the heat transfer coefficient h given in Equations (A1.6).

$$h = \frac{\left(0.615 \left(\frac{d_3 v_{\text{air}} \rho_{\text{air}}}{\eta_{\text{air}}}\right)^{0.466}\right) k_{\text{air}}}{d_3}. \quad (A1.6)$$

Hereby, v_{air} is the velocity of the forced air ($v_{\text{air}} = 10 \text{ m s}^{-1}$), ρ_{air} and η_{air} are the density and the viscosity of air, respectively ($\rho_{\text{air}} = 1.184 \text{ kg m}^{-3}$, $\eta_{\text{air}} = 1.85 \cdot 10^{-5} \text{ Pa s}$ [83KEE]). All values are given for 25 °C. The thus calculated result for the heat transfer coefficient is $h = 536.4 \text{ W m}^{-2} \text{ K}^{-1}$. This is a typical value for a forced air cooling devise, even though the values given in the literature are quite scattered. For a liquid cooling devise, h can be higher up to two orders of magnitude [04PET].

Last, the rate of power generation within the capillary volume per unit volume S has to be calculated as given in Equation (A1.7).

$$S = \frac{J^2}{\kappa_e}. \quad (A1.7)$$

The current density J is the electrical current I per capillary cross section area A (Equation (A1.8)).

$$J = \frac{I}{A}. \quad (A1.8)$$

With the values mentioned above, a current density of $J = 6.62 \cdot 10^3 \text{ A m}^{-2}$ arises which leads to a rate of power generation within the capillary volume per unit volume $S = 2.18 \cdot 10^8 \text{ W m}^{-3}$.

Now all the variables in Equation (2.13) are known and the temperature rise due to Joule heating can be calculated. The results for typical experimental current regions are given in Section 2.1.3. According to this, the temperature rise is smaller than 1 °C and thus does not significantly influence the measurements. Nevertheless, it has to be noted that the current in some experiments concerning the determination of stability constants (see Section 4) is considerably higher due to low pH values in the samples. In such cases the temperature rise is higher than in standard experiments and the results have to be checked thoroughly.

For the determination of the temperature profile shown in Figure 3, the temperature rise in all three different zones of the capillary was calculated separately. The formulas used are given in Equation (A1.9) (for the BGE region inside the capillary), Equation (A1.10) (for the fused silica layer) and Equation (A1.11) (for the BGE region inside the capillary). The variable r is always the radius measured from the center of the capillary.

$$T(r) - T_1 = \frac{sr_c^2}{4k_{\text{BGE}}} \left(1 - \left(\frac{r}{r_c} \right)^2 \right). \quad (\text{A1.9})$$

$$T(r) - T_2 = \frac{sr_c^2}{2k_f} \ln \left(\frac{r_2}{r} \right). \quad (\text{A1.10})$$

$$T(r) - T_a = \frac{sr_c^2}{2rh}. \quad (\text{A1.11})$$

APPENDIX A2 – CALCULATION OF UNCERTAINTIES

The estimation of the uncertainties was conducted, unless not stated otherwise, on basis of a Gaussian error propagation.

The uncertainty of the **electrophoretic mobility** $\Delta\mu$ is given by Equation (A2.1). The errors of the capillary length l , of the migration times t_i and t_{EOF} and of the high voltage U were set as $\Delta l = 0.3$ cm, $\Delta t_i = \Delta t_{\text{EOF}} = 5$ s and $\Delta U = 0.1$ kV.

$$\begin{aligned} \Delta\mu &= \pm \sqrt{\left(\frac{\partial\mu}{\partial l} \Delta l \right)^2 + \left(\frac{\partial\mu}{\partial U} \Delta U \right)^2 + \left(\frac{\partial\mu}{\partial t_i} \Delta t_i \right)^2 + \left(\frac{\partial\mu}{\partial t_{\text{EOF}}} \Delta t_{\text{EOF}} \right)^2} \\ &= \pm \sqrt{\left(\frac{2l}{U} \left(\frac{1}{t_i} - \frac{1}{t_{\text{EOF}}} \right) \cdot \Delta l \right)^2 + \left(-\frac{l^2}{U^2} \left(\frac{1}{t_i} - \frac{1}{t_{\text{EOF}}} \right) \cdot \Delta U \right)^2 + \left(-\frac{l^2}{U \cdot t_i^2} \cdot \Delta t_i \right)^2 + \left(\frac{l^2}{U \cdot t_{\text{EOF}}^2} \cdot \Delta t_{\text{EOF}} \right)^2}. \end{aligned} \quad (\text{A2.1})$$

For the **stability constants** β_i the errors resulting from the fitting operation given by the Origin 7 software were adopted. The errors of the $\log(\beta_i)$ were from that calculated using Equation (A2.2).

$$\Delta \log(\beta_i) = \pm \frac{\Delta\beta_i}{\beta_i \cdot \log(10)}. \quad (\text{A2.2})$$

The uncertainties of the **activity values** resulting from LSC measurements were $\pm 2\%$ deduced from the 10 000 counts or 15 min measuring time criterion. Since the previously conducted liquid-liquid extraction is also a source of error which was expected to have a greater impact on the overall error, $\pm 5\%$ was set as the total uncertainty range.

The error range of the **rate constants** k that were determined in the kinetic manuscript [18WIL] (see Section 5.2.1) is based on a standard deviation of different measurement series. In the investigations presented in Section 5.3 after the manuscript just one measurement series for each rate constant k was performed. Consequently, no standard deviation error could be calculated and

APPENDIX A2 – CALCULATION OF UNCERTAINTIES

the error was thus set as the average value obtained from the kinetic investigations to be $\Delta k = 8\%$. The errors of the corresponding half-lives $t_{1/2}$ were calculated based on these values by Equation (A2.3).

$$\Delta t_{1/2} = \pm \sqrt{\left(\frac{\partial t_{1/2}}{\partial k} \Delta k\right)^2} = \pm \sqrt{\left(-\frac{\ln(2)}{k^2} \cdot \Delta k\right)^2}. \quad (\text{A2.3})$$

In ICP-MS measurements, **counts per second cps** are obtained. The uncertainty is given by the evaluation software in terms of the relative standard deviation *RSD*, which is defined by the quotient of the standard deviation of a data set *SD* and the absolute value of the mean of the data set $|\bar{x}|$ as given in Equation (A2.4).

$$RSC = \frac{SD}{|\bar{x}|} \cdot 100. \quad (\text{A2.4})$$

The **peak areas** A_{Peak} in the electropherograms resulting from CE-ICP-MS measurements are evaluated with the MassHunter Workstation software. The peak boundaries are set manually and it was tried to define similar peak markers in order to minimize the errors. Nevertheless this leads to a quite high uncertainty which was set as $\Delta A_{\text{Peak}} = \pm 10\%$.

The uncertainties which are set as fixed values are listed in the following.

pH:	± 0.1
mass <i>m</i>:	± 1 mg
capillary length <i>l</i>:	± 0.3 cm
migration time <i>t_i</i>:	± 5 s
high voltage <i>U</i>:	± 0.1 kV

APPENDIX A3 – DETAILS ABOUT EXPERIMENTAL PROCEDURES

GAMMA SPECTROMETRY

The γ -spectra were measured with a high-purity Ge-detector (GMX-13280-S, EG & G ORTEC, USA) with a Canberra InSpector 2000 DSP Portable Spectroscopic Workstation (model IN2K, Canberra Industries Inc., USA) and Genie 2000 Gamma software (V. 3.0, Canberra Industries Inc., USA). The gamma-ray spectrometer was calibrated with a multiple gamma-ray emitting solution (serial number: 1850-27, Eckert & Ziegler Isotope Products, Braunschweig, Germany).

PH MEASUREMENTS

pH values were determined using a pH electrode (BlueLine 16 pH, Schott, Mainz, Germany) with a pH/ E_h meter (inoLab/Cond 720, WTW GmbH, Weilheim, Germany). Before every measurement, the electrode was calibrated by a three-point calibration with pH buffer solutions at pH 4.01, pH 6.86 and pH 9.81 (all HANNA Instruments, Woonsocket, Rhode Island, USA). The errors of the measured pH values were in general assumed to be ± 0.1 .

ELECTRICAL CONDUCTIVITY MEASUREMENTS

The electrical conductivity was measured using a standard conductivity cell (TetraCon 325, WTW, Weilheim, Germany) with a pH/ E_h meter (inoLab/Cond 720, WTW GmbH, Weilheim, Germany). The errors of the measured electrical conductivity were in general assumed to be $\pm 1.0 \text{ mS cm}^{-1}$.

LLE/LSC MEASUREMENTS

In some experiments liquid-liquid extraction (LLE) was used for the separation of different oxidation states of actinides. The basic principle of this technique are differences in the solubility and in the complexation behavior of the respective oxidation states of the actinides in two different, non-mixable phases. In the present work, for the separation of Np(V) and Np(IV) ions, 3 M HDEHP (2-bisethylhexylphosphate) in toluene was used as the organic phase and 1 M HCl solution as the aqueous phase. The plutonium oxidation states Pu(III), Pu(IV), Pu(V) and Pu(VI) as well as colloidal Pu were investigated by a combined LLE procedure using both a 0.5 M HDEHP in Toluol/1 M HCl system and a system containing 0.025 M PMBP (4-benzoyl-3-methyl-1-phenylpyrazole-5-one). The methodology is based on the description of Nitsche et al. [88NIT]. After the addition of the actinide solution to be separated the two-phase mixture was shaken vigorously on a vortex mixer (SA8, Stuart, Staffordshire, UK). Following, the two phases were re-separated by centrifugation (3K30, Sigma, Osterode am Harz, Germany) for 5 min at 5000 rpm. From each phase, 500 μL were taken and given to 10 mL Ultima Gold XR LSC cocktail (PerkinElmer, Waltham, Massachusetts, USA). For quantification, liquid scintillation counting

APPENDIX A3 – DETAILS ABOUT EXPERIMENTAL PROCEDURES

(LSC) was applied (300SL, Hidex, Turku, Finland). The measurements were programmed to stop either when 10 000 counts were detected or after 15 min, in dependence on which criterion was reached first. This correlates to an uncertainty of 2%. A background measurement was conducted before every series and the background counts were subtracted automatically by the data processing software.

APPENDIX A4 – SUPPORTING INFORMATION FOR THE MOBILITY PAPER (SECTION 3.3)

Supporting Information

Investigation of the Electrophoretic Mobility of the Actinides Th and U–Am in Different Oxidation States

Christian Willberger*, Samer Amayri, Verena Häußler, Raphael Scholze, Tobias Reich*

Institute of Nuclear Chemistry, Johannes Gutenberg University Mainz, 55099 Mainz, Germany

*Corresponding Authors

E-Mail: willberg@uni-mainz.de, treich@uni-mainz.de

Contents:

S-1: Detailed calculations for the acetate speciation of the metal ions and the resulting mean effective charge q_{eff} .

Table S-1: Species distribution of $5 \cdot 10^{-7}$ M metal ion in 1 M acetic acid at pH 2.38 calculated with Visual MINTEQ¹.

References

APPENDIX A4 – SUPPORTING INFORMATION FOR THE MOBILITY PAPER (SECTION 3.3)

S-1: Detailed calculations for the acetate speciation of the metal ions and the resulting mean effective charge q_{eff} .

The calculations were conducted with the program Visual MINTEQ (version 3.1)¹. The pH value and the concentrations of the different components were set as follows based on the experimental conditions used in this work.

$$c(\text{acetate}) = 1.0 \text{ M}$$

$$c(\text{Eu(III)}, \text{Am(III)}, \text{Th(IV)}, \text{Np(V)}, \text{U(VI)}) = 5 \cdot 10^{-7} \text{ M}$$

$$\text{pH} = 2.38$$

Based on the stability constants given in the literature, a species distribution of the different metal-acetate complexes was calculated. The detailed results are given in this supplementary section. The stability constants are taken from the ANDRA database² for the actinides U(VI), Np(V) and Th(IV) and from the NIST Database³ for trivalent metal ions Eu(III) and Am(III).

$$\text{Eu(III): } \log(\beta_1) = 2.77, \log(\beta_2) = 4.71, \log(\beta_3) = 5.52$$

$$\text{Am(III): } \log(\beta_1) = 2.8, \log(\beta_2) = 4.62, \log(\beta_3) = 5.51$$

$$\text{Th(IV): } \log(\beta_1) = 5.24, \log(\beta_2) = 9.44, \log(\beta_3) = 12.56, \log(\beta_4) = 14.38, \log(\beta_5) = 15.37$$

$$\text{Np(V): } \log(\beta_1) = 1.32, \log(\beta_2) = 3.42, \log(\beta_3) = 3.57$$

$$\text{U(VI): } \log(\beta_1) = 3.02, \log(\beta_2) = 5.20, \log(\beta_3) = 7.03$$

Knowing the distribution of the different species an effective charge q_{eff} of the respective ion was calculated as the weighted average charge taking into account all species according to the following formula.

$$q_{\text{eff}} = \frac{\sum_i q_i \cdot a_i}{100}, \quad (\text{Eq. S-1})$$

where q_i is the charge of the species and a_i is the corresponding fraction in percent.

The results of these calculations are summarized in Table S-1. The acetate ligand is abbreviated as Ac.

APPENDIX A4 – SUPPORTING INFORMATION FOR THE MOBILITY PAPER (SECTION 3.3)

Table S-1: Species distribution of $5 \cdot 10^{-7}$ M metal ion in 1 M acetic acid at pH 2.38 calculated with Visual MINTEQ¹.

Metal ion	Species	Charge q_i	Percentage/%	Effective charge q_{eff}
Eu(III)	Eu ³⁺	3	30.9	2.15
	EuAc ²⁺	2	53.1	
	EuAc ₂ ⁺	1	15.6	
	EuAc ₃ (aq)	0	0.4	
Am(III)	Am ³⁺	3	30.7	2.17
	AmAc ²⁺	2	56.4	
	AmAc ₂ ⁺	1	12.5	
	AmAc ₃ (aq)	0	0.4	
Th(IV)	Th ⁴⁺	4	0.0	0.97
	ThAc ³⁺	3	0.3	
	ThAc ₂ ²⁺	2	15.0	
	ThAc ₃ ⁺	1	66.7	
	ThAc ₄ (aq)	0	17.1	
	ThAc ₅ ⁻	-1	0.8	
Np(V)	NpO ₂ ⁺	1	88.7	0.85
	NpO ₂ Ac (aq)	0	7.2	
	NpO ₂ Ac ₂ ⁻	-1	4.1	
	NpO ₂ Ac ₂ ²⁻	-2	0.03	
U(VI)	UO ₂ ²⁺	2	13.8	0.68
	UO ₂ Ac ⁺	1	48.7	
	UO ₂ Ac ₂ (aq)	0	28.7	
	UO ₂ Ac ₂ ⁻	-1	8.7	

References:

- (1) Gustafsson, J. P.: *Geochemical equilibrium speciation model*. Visual MINTEQ Ver. 3.1. KTH, Department of Land and Water, Resources Engineering, Stockholm, Sweden, **2014**.
<http://vminteq.lwr.kth.se/download/>
- (2) Smith, R. M. NIST 46.6, 2003.
- (3) Richard, L.; Grivé, M.; Druo, L. Andra-TDB7 Task 3 – Organics Amphos 21, 2011.

APPENDIX A5 – DETAILED SAMPLE PREPARATIONS, RESULTS AND ELECTROPHEROGRAMS FROM STABILITY CONSTANT DETERMINATION

A5.1 ACETATE

Supporting Information

Determination of the Stability Constants of the Acetate Complexes of the Actinides Am(III), Th(IV), Np(V), and U(VI) Using Capillary Electrophoresis-Inductively Coupled Plasma Mass Spectrometry

Christian Willberger,* Daniel Leichtfuß, Samer Amayri, and Tobias Reich*

Institut für Kernchemie, Johannes Gutenberg-Universität Mainz, 55099 Mainz, Germany

*Corresponding authors

E-Mail: willberg@uni-mainz.de, treich@uni-mainz.de

Contents:

Figure S1: Electropherograms of the stability constant determination with the acetate ligand for Am(III) (series 1) at $U = 10$ kV and $I = 0.3$ M.

Figure S2: Electropherograms of the stability constant determination with the acetate ligand for Am(III) (series 2) at $U = 10$ kV and $I = 0.3$ M.

Figure S3: Electropherograms of the stability constant determination with the acetate ligand for Th(IV) (series 1) at $U = 10$ kV and $I = 0.3$ M.

Figure S4: Electropherograms of the stability constant determination with the acetate ligand for Th(IV) (series 2) at $U = 10$ kV and $I = 0.3$ M.

Figure S5: Electropherograms of the stability constant determination with the acetate ligand for Np(V) (series 1) at $U = 10$ kV and $I = 0.3$ M.

Figure S6: Electropherograms of the stability constant determination with the acetate ligand for Np(V) (series 2) at $U = 10$ kV and $I = 0.3$ M.

Figure S7: Electropherograms of the stability constant determination with the acetate ligand for Np(V) (series 3) at U = 10 kV and I = 0.3 M.

Figure S8: Electropherograms of the stability constant determination with the acetate ligand for U(VI) (series 1) at U = 10 kV and I = 0.3 M.

Figure S9: Electropherograms of the stability constant determination with the acetate ligand for U(VI) (series 2) at U = 10 kV and I = 0.3 M.

Table S1: Detailed sample composition and experimental results of the Am(III) acetate series 1.

Table S2: Detailed sample composition and experimental results of the Am(III) acetate series 2.

Table S3: Detailed sample composition and experimental results of the Th(IV) acetate series 1.

Table S4: Detailed sample composition and experimental results of the Th(IV) acetate series 2.

Table S5: Detailed sample composition and experimental results of the Np(V) acetate series 1.

Table S6: Detailed sample composition and experimental results of the Np(V) acetate series 2.

Table S7: Detailed sample composition and experimental results of the Np(V) acetate series 3.

Table S8: Detailed sample composition and experimental results of the U(VI) acetate series 1.

Table S9: Detailed sample composition and experimental results of the U(VI) acetate series 2.

Table S10: Comparison of the $\log \beta^0$ values for Th(IV) acetate complexes ($I = 0$).

Table S11: SIT parameters $\alpha(i,j)$ used for the extrapolation to $I = 0$ in Table S10.

Page S20: Detailed equations employed for the fitting procedure for each actinide-acetate system.

Page S21: References

Appendix A5 – Detailed Sample Preparations, Results and Electropherograms from Stability Constant Determination

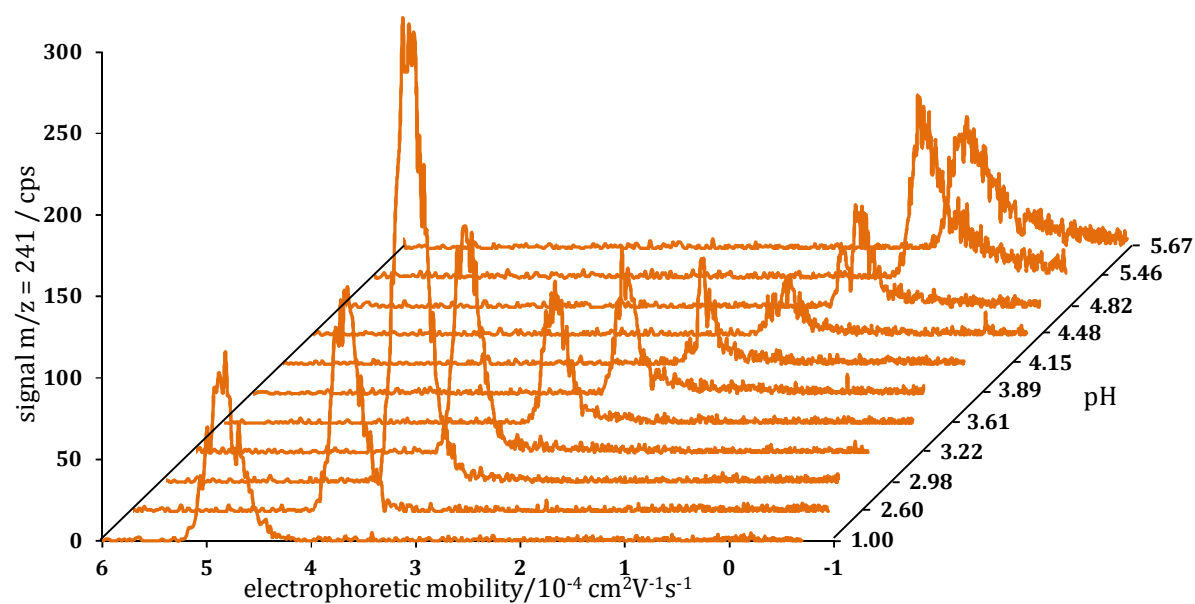


Figure S1: Electropherograms of the stability constant determination with the acetate ligand for Am(III) (series 1) at $U = 10 \text{ kV}$ and $I = 0.3 \text{ M}$.

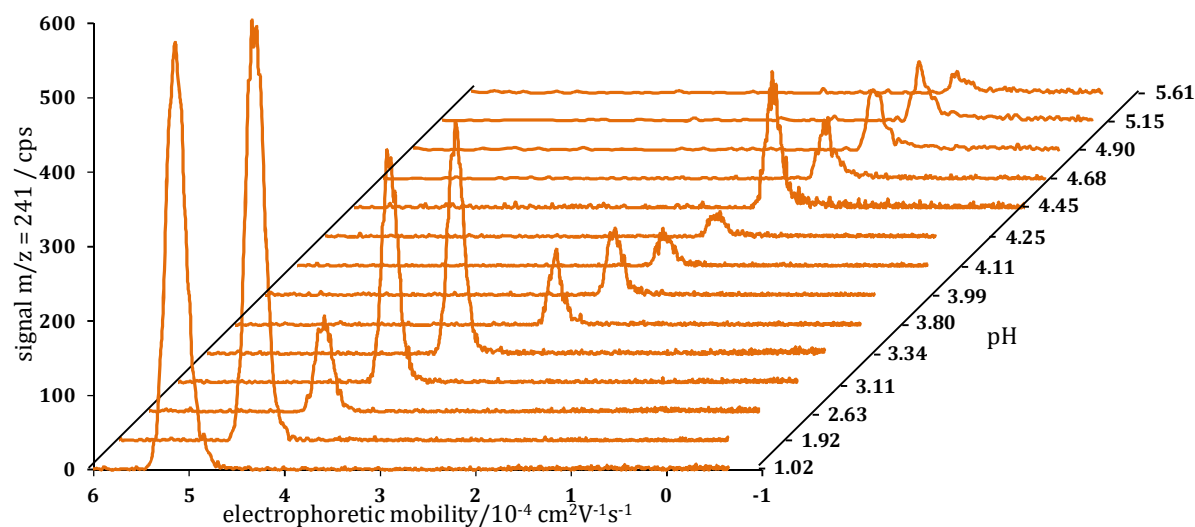


Figure S2: Electropherograms of the stability constant determination with the acetate ligand for Am(III) (series 2) at $U = 10 \text{ kV}$ and $I = 0.3 \text{ M}$.

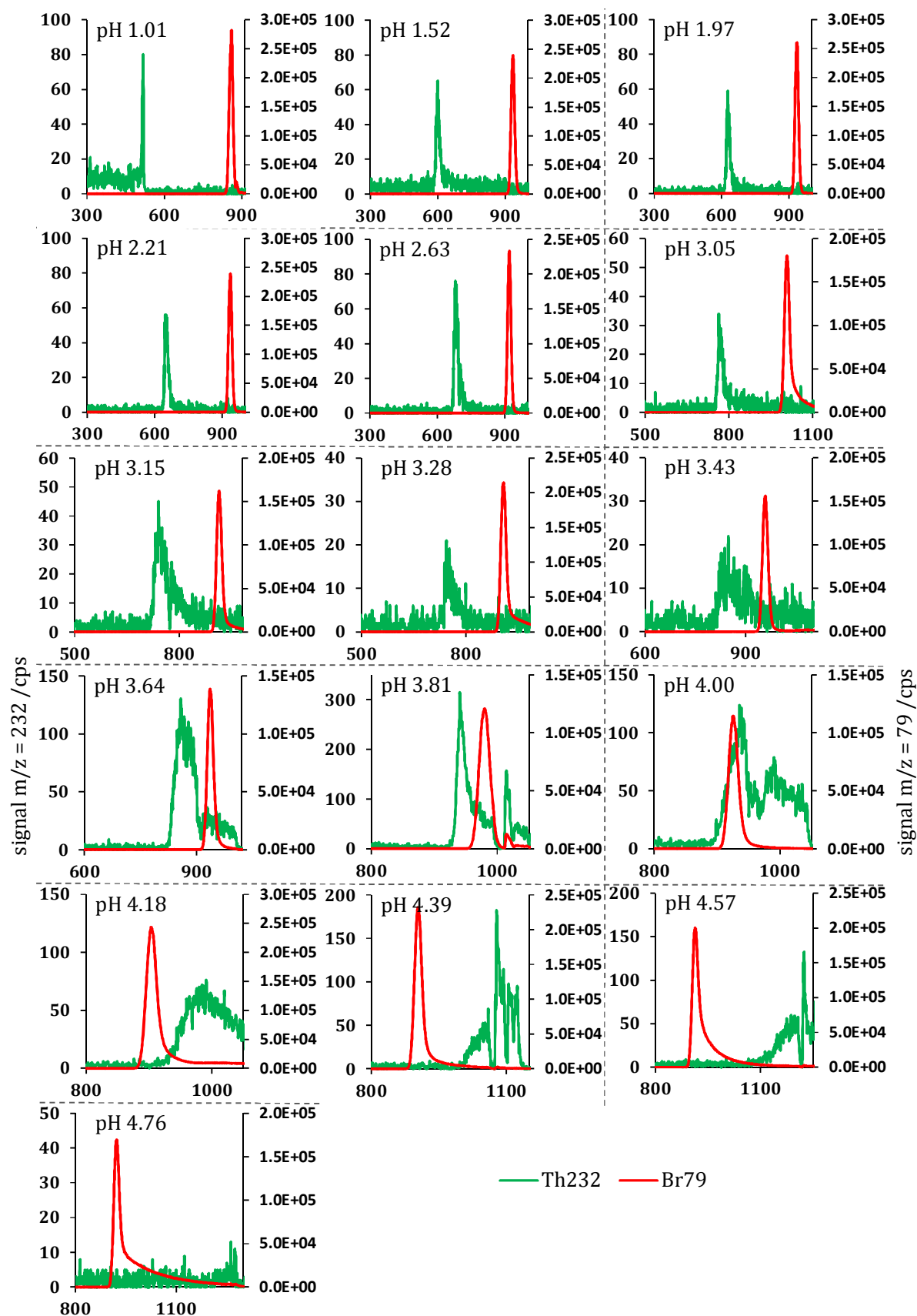


Figure S3: Electropherograms of the stability constant determination with the acetate ligand for Th(IV) (series 1) at $U = 10$ kV and $I = 0.3$ M.

Appendix A5 – Detailed Sample Preparations, Results and Electropherograms from Stability Constant Determination

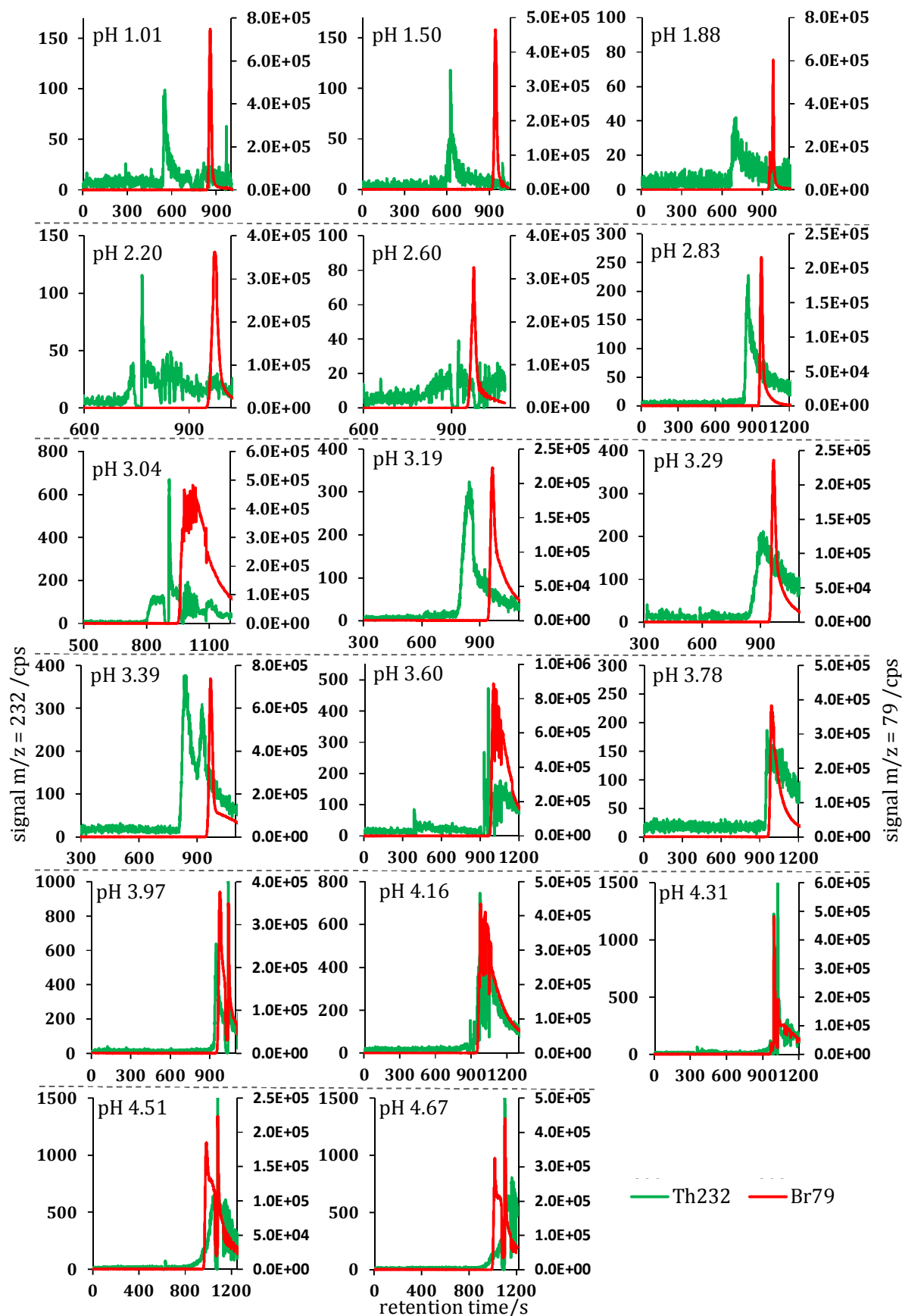


Figure S4: Electropherograms of the stability constant determination with the acetate ligand for Th(IV) (series 2) at $U = 10$ kV and $I = 0.3$ M.

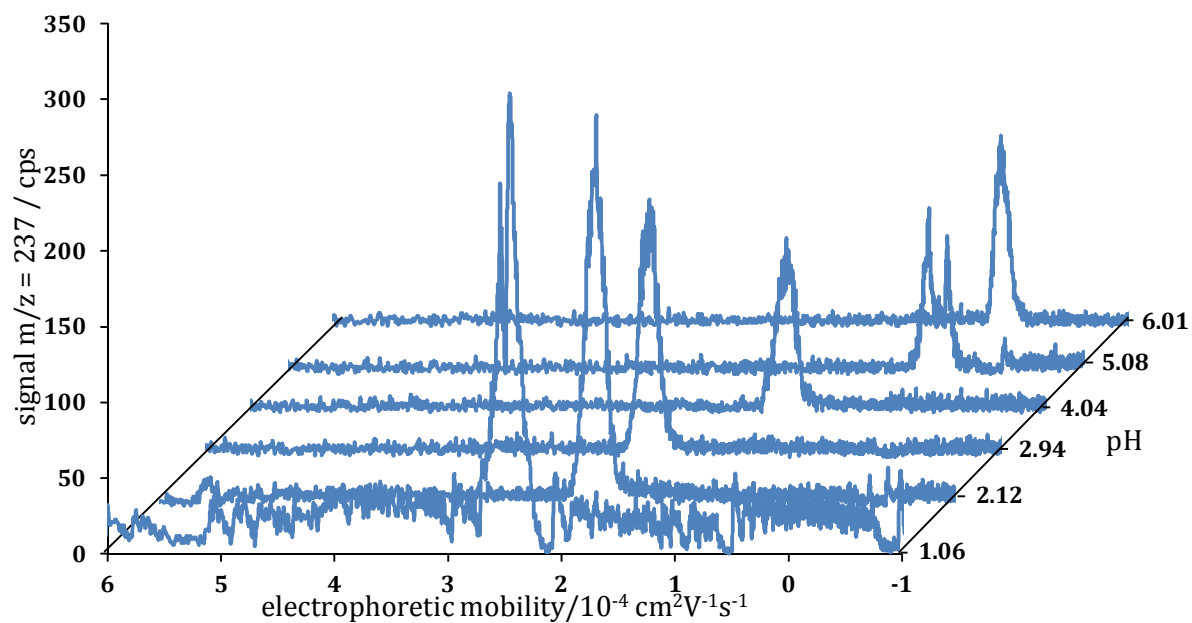


Figure S5: Electropherograms of the stability constant determination with the acetate ligand for Np(V) (series 1) at $U = 10$ kV and $I = 0.3$ M.

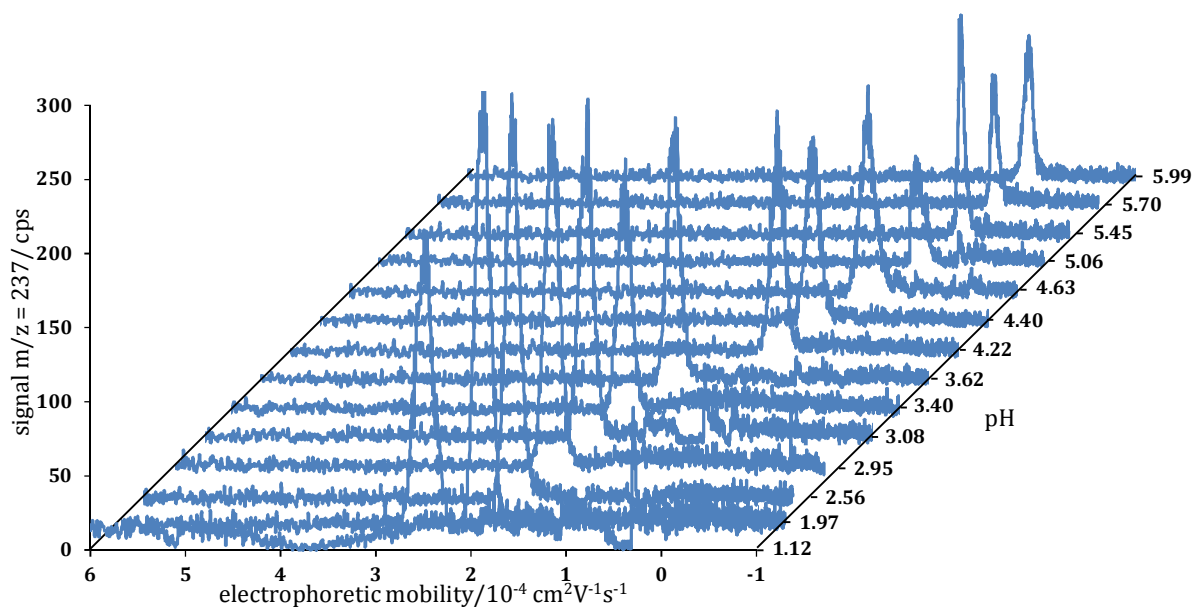


Figure S6: Electropherograms of the stability constant determination with the acetate ligand for Np(V) (series 2) at $U = 10$ kV and $I = 0.3$ M.

Appendix A5 – Detailed Sample Preparations, Results and Electropherograms from Stability Constant Determination

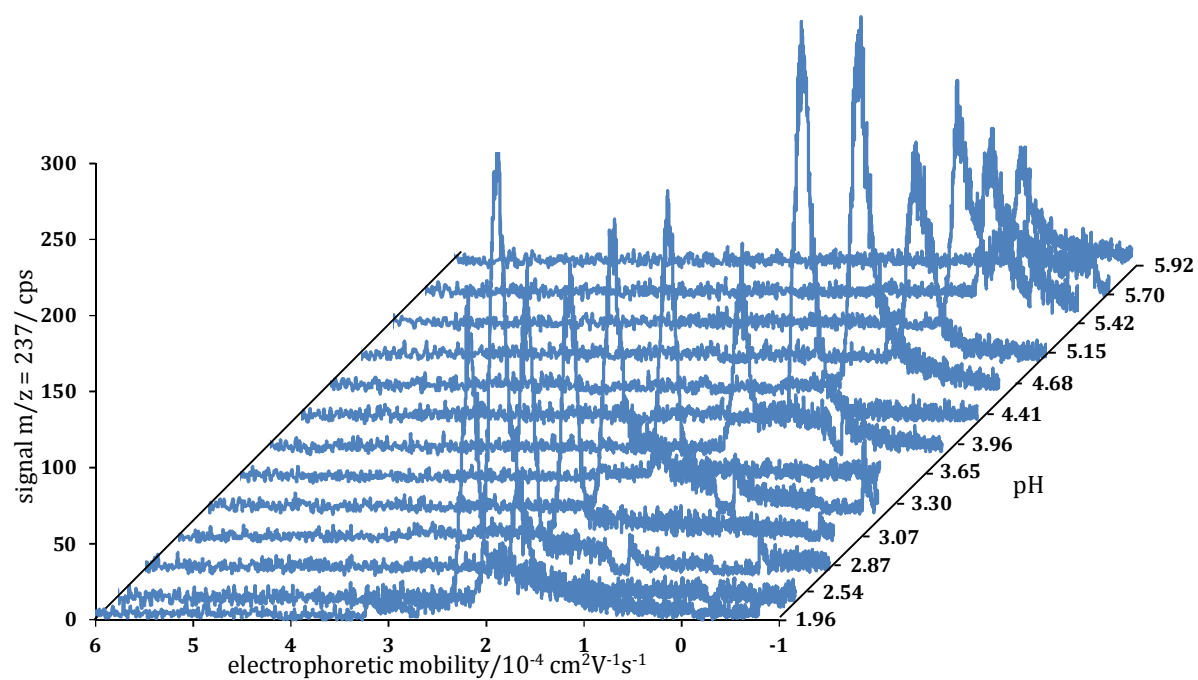


Figure S7: Electropherograms of the stability constant determination with the acetate ligand for Np(V) (series 3) at $U = 10 \text{ kV}$ and $I = 0.3 \text{ M}$.

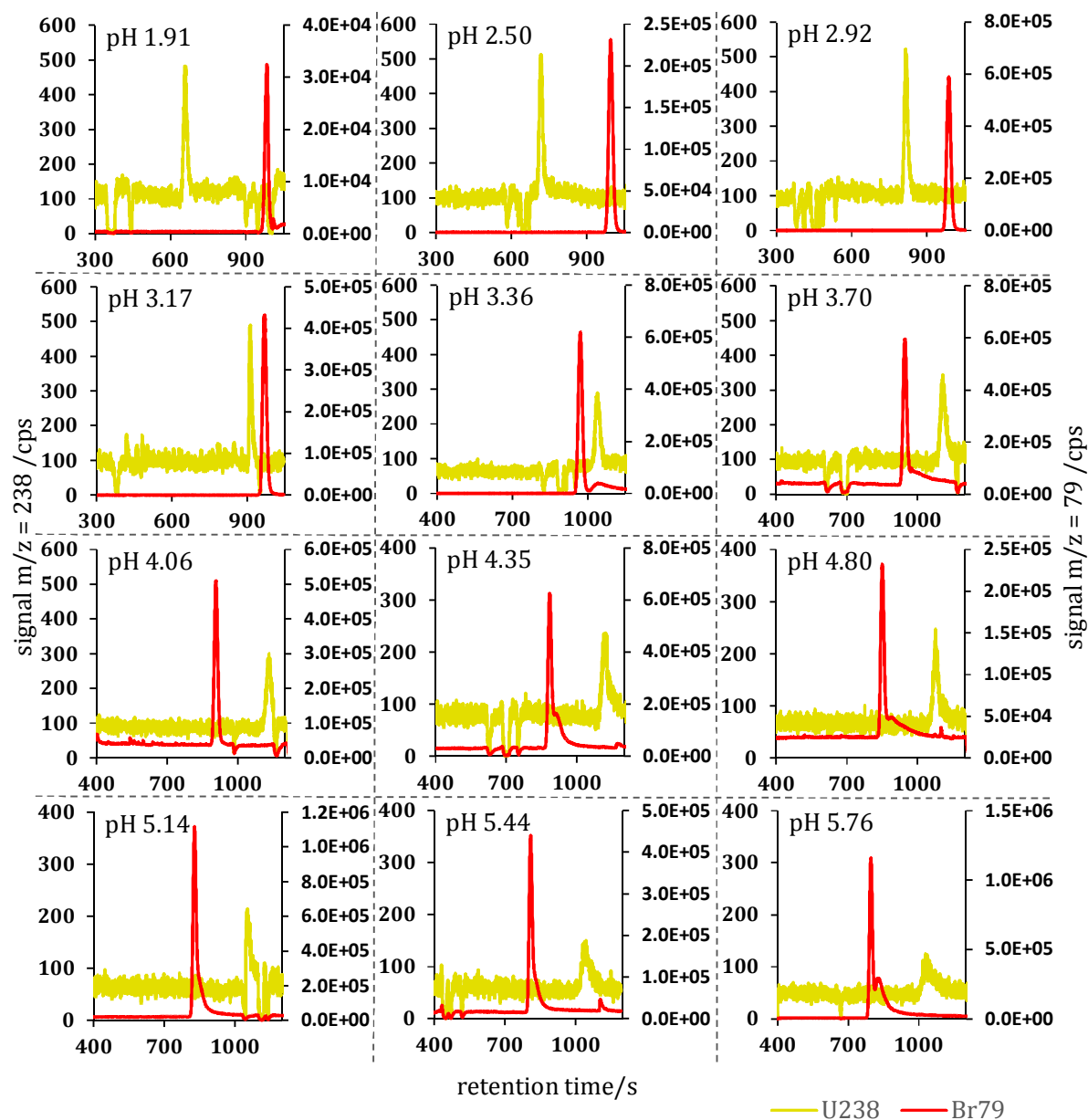


Figure S8: Electropherograms of the stability constant determination with the acetate ligand for U(VI) (series 1) at $U = 10$ kV and $I = 0.3$ M.

Appendix A5 – Detailed Sample Preparations, Results and Electropherograms from Stability Constant Determination

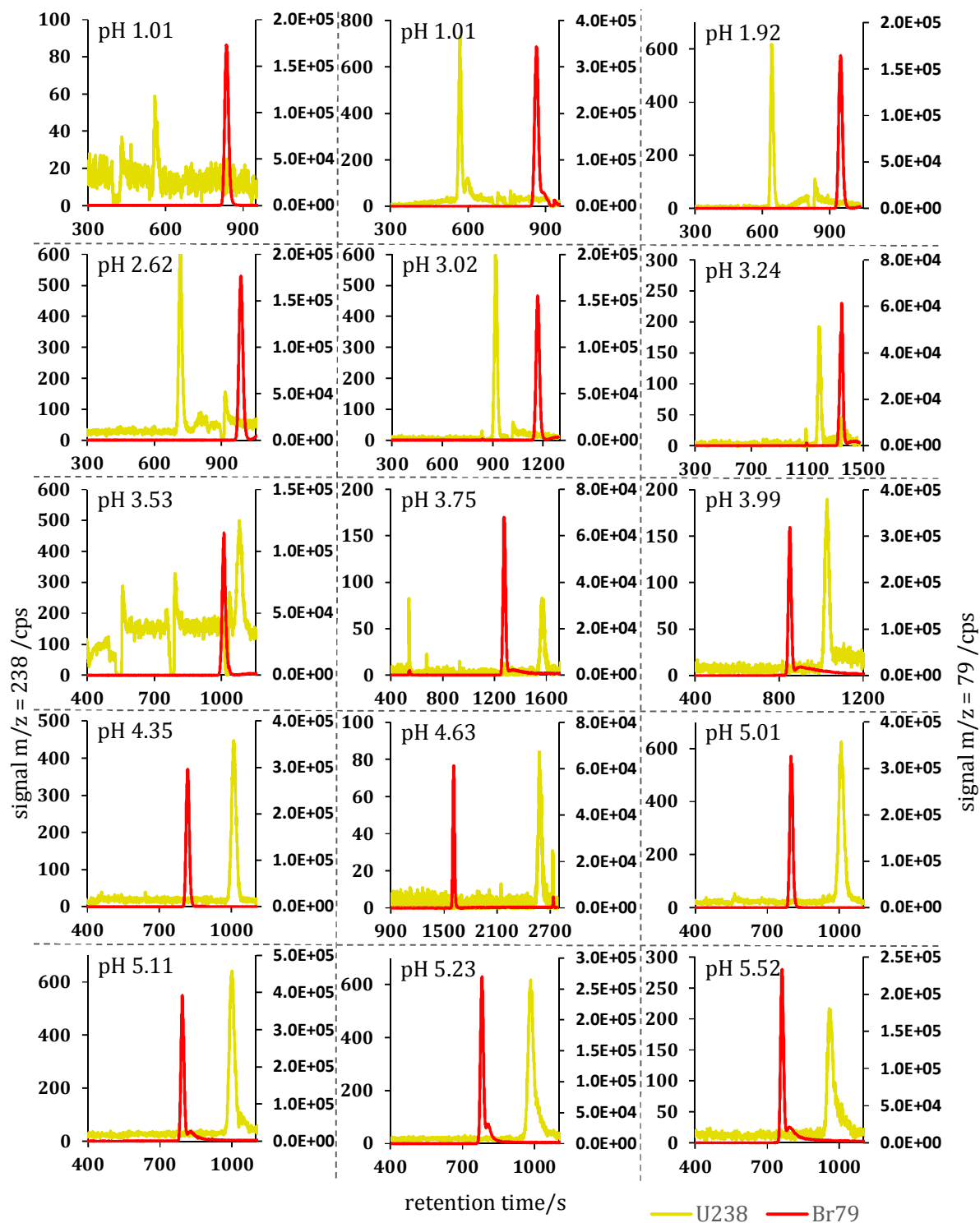


Figure S9: Electropherograms of the stability constant determination with the acetate ligand for U(VI) (series 2) at $U = 10$ kV and $I = 0.3$ M. The sample with $pH = 1.01$ was measured twice with consistent results.

Table S1: Detailed sample composition and experimental results of the Am(III) acetate series 1.

measured pH	free [AcO ⁻]/M	addition of (total sample volume V = 20 mL)			retention time/s		electrophoretic mobility/ 10 ⁻⁴ cm ² V ⁻¹ S ⁻¹
		HClO ₄ (11.6 M)/ μL	NaOH (10 M)/ μL	NaClO ₄ ·H ₂ O/ mg	t _{AN} /s	t _{EOF} /s	
1.00	9.48 · 10 ⁻⁵	172	0	565	498	851	4.82
2.60	0.00373	0	0	837	574	946	3.95
2.98	0.00879	0	10	815	598	976	3.74
3.22	0.0150	0	20	820	617	975	3.44
3.61	0.0342	0	50	785	646	946	2.83
3.89	0.0591	0	89	717	667	935	2.48
4.15	0.0926	0	155	627	699	922	2.00
4.48	0.147	0	245	499	725	885	1.44
4.82	0.203	0	380	308	727	847	1.13
5.46	0.270	0	590	14	760	849	0.80
5.67	0.281	0	605	0	779	851	0.63

Appendix A5 - Detailed Sample Preparations, Results and Electropherograms from Stability Constant Determination

Table S2: Detailed sample composition and experimental results of the Am(III) acetate series 2.

measured pH	free [AcO ⁻]/M	addition of (total sample volume V = 20 mL)			retention time/s		electrophoretic mobility/ 10 ⁻⁴ cm ² V ⁻¹ s ⁻¹
		HClO ₄ (11.6 M)/ μL	NaOH (10 M)/ μL	NaClO ₄ ·H ₂ O/ mg	t _n /s	t _{EOF} /s	
1.02	9.93 · 10 ⁻⁵	174	0	561	489	867	5.10
1.92	0.000787	20	0	806	546	969	4.58
2.63	0.00399	0	0	839	578	990	4.13
3.11	0.0117	0	13	825	598	989	3.79
3.34	0.0194	0	25	806	620	977	3.38
3.80	0.0499	0	73	738	656	936	2.61
3.99	0.0708	0	110	690	683	943	2.32
4.11	0.0868	0	140	648	682	917	2.16
4.25	0.108	0	180	587	704	910	1.85
4.45	0.141	0	260	477	699	870	1.61
4.68	0.181	0	340	366	725	872	1.33
4.90	0.215	0	420	254	732	863	1.18
5.15	0.245	0	490	153	765	885	1.01
5.61	0.278	0	600	0	917	1073	0.91

A5.1 ACETATE

Table S3: Detailed sample composition and experimental results of the Th(IV) acetate series 1. This series was not used for data evaluation due to inconsistent results.

measured pH	free [AcO ⁻]/M	addition of (total sample volume V = 20 mL)			retention time/s		electrophoretic mobility/ 10 ⁻⁴ cm ² V ⁻¹ s ⁻¹
		HClO ₄ (11.6 M)/ μL	NaOH (10 M)/ μL	NaClO ₄ ·H ₂ O/ mg	t _{AN} /s	t _{EO} /s	
1.01	9.70 · 10 ⁻⁵	172	0	564	518	859	4.44
1.52	0.000314	52	0	760	599	934	3.46
1.97	0.000883	17	0	817	627	936	3.00
2.21	0.00153	9	0	828	652	937	2.66
2.63	0.00399	0	0	844	680	919	2.19
3.05	0.0103	0	8	831	764	1008	1.81
3.15	0.0128	0	15	823	740	914	1.47
3.28	0.0170	0	20	814	744	908	1.39
3.43	0.0235	0	31	800	848	959	0.78
3.64	0.0364	0	48	773	857	936	0.56
3.81	0.0509	0	73	741	940	980	0.25
4.00	0.0721	0	108	689	936	926	-0.07
4.18	0.0971	0	155	624	990	903	-0.56
4.39	0.131	0	215	539	1048	903	-0.88
4.57	0.162	0	280	450	1175	913	-1.41
4.76	0.194	0	350	350	1251	923	-1.64

Appendix A5 – Detailed Sample Preparations, Results and Electropherograms from Stability Constant Determination

Table S4: Detailed sample composition and experimental results of the Th(IV) acetate series 2.

measured pH	free [AcO ⁻]/M	addition of (total sample volume V = 20 mL)			retention time/s		electrophoretic mobility/ 10 ⁻⁴ cm ² V ⁻¹ S ⁻¹
		HClO ₄ (11.6 M)/ μL	NaOH (10 M)/ μL	NaClO ₄ ·H ₂ O/ mg	t _{AN} /s	t _{OF} /s	
1.01	9.70 · 10 ⁻⁵	172	0	560	552	859	3.79
1.50	0.000300	52	0	757	625.08	943	3.16
1.88	0.000718	19	0	809	703	980	2.36
2.20	0.00150	9	0	823	765	974	1.64
2.60*	0.00373	0	0	839	923	975	0.34
2.83	0.00628	0	4	834	867	973	0.73
3.04	0.0101	0	10	830	909	974	0.43
3.19*	0.0140	0	15	820	845	966	0.87
3.29	0.0174	0	21	815	915	968	0.35
3.39**	0.0216	0	32	808	832	969	0.99
3.60	0.0335	0	50	787	964	1004	0.24
3.78	0.0480	0	75	763	956	990	0.21
3.97	0.0684	0	110	726	950	978	0.18
4.16	0.0941	0	155	673	974	978	0.02
4.31	0.118	0	215	623	993	995	0.01
4.51	0.152	0	285	541	1052	981	-0.40
4.67	0.179	0	350	464	1070	1017	-0.28

* outliers, not used for data evaluation

** two peaks were detected in this electropherogram, the second one was assigned to the acetate species

A5.1 ACETATE

Table S5: Detailed sample composition and experimental results of the Np(V) acetate series 1.

measured pH	free [AcO ⁻]/M	addition of (total sample volume V = 20 mL)			retention time/s		electrophoretic mobility/ 10 ⁻⁴ cm ² V ⁻¹ s ⁻¹
		HClO ₄ (11.6 M)/ μL	NaOH (10 M)/ μL	NaClO ₄ ·H ₂ O/ mg	t _{AN} /s	t _{EOF} /s	
1.06	0.000109	205	0	508	602	808	2.39
2.12	0.00125	15	0	819	705	956	2.09
2.94	0.00804	12	19	796	708	951	2.03
4.04	0.0772	60	190	478	757	909	1.24
5.08	0.238	60	440	127	786	826	0.35
6.01	0.291	13	480	147	772	783	0.10

Appendix A5 - Detailed Sample Preparations, Results and Electropherograms from Stability Constant Determination

Table S6: Detailed sample composition and experimental results of the Np(V) acetate series 2.

measured pH	free [AcO ⁻]/M	addition of (total sample volume V = 20 mL)			retention time/s		electrophoretic mobility/ 10 ⁻⁴ cm ² V ⁻¹ S ⁻¹
		HClO ₄ (11.6 M)/ μL	NaOH (10 M)/ μL	NaClO ₄ ·H ₂ O/ mg	t _{an} /s	t _{eof} /s	
1.12	0.000125	170	0	568	621	849	2.43
1.97	0.000883	17	0	813	705	965	2.15
2.56	0.00341	0	0	837	708	978	2.19
2.95	0.00822	0	10	829	720	966	1.99
3.08	0.0110	0	20	816	721	958	1.93
3.40	0.0221	0	39	789	724	945	1.81
3.62	0.0349	0	73	740	732	923	1.59
4.22	0.103	0	130	662	752	851	0.87
4.40	0.133	0	215	542	764	858	0.80
4.63	0.172	0	315	400	769	830	0.54
5.06	0.235	0	410	267	904	958	0.35
5.45	0.270	0	490	154	911	936	0.17
5.70	0.282	0	515	103	927	953	0.20
5.99	0.291	0	540	85	941	956	0.10

A5.1 ACETATE

Table S7: Detailed sample composition and experimental results of the Np(V) acetate series 3.

measured pH	free [AcO ⁻]/M	addition of (total sample volume V = 20 mL)			retention time/s		electrophoretic mobility/ 10 ⁻⁴ cm ² V ⁻¹ S ⁻¹
		HClO ₄ (11.6 M)/ μL	NaOH (10 M)/ μL	NaClO ₄ ·H ₂ O/ mg	t _{AN} /s	t _{EOF} /s	
1.96	0.000863	17	0	814	691	937	2.13
2.54	0.00325	0	0	843	711	959	2.05
2.87	0.00687	0	10	829	698	935	2.04
3.07	0.0108	0	20	812	705	932	1.94
3.30	0.0178	0	39	788	712	920	1.79
3.65	0.0371	0	73	742	724	911	1.59
3.96	0.0672	0	130	661	743	876	1.14
4.41	0.135	0	215	542	779	883	0.85
4.68	0.181	0	315	400	794	861	0.56
5.15	0.245	0	400	265	807	845	0.32
5.42	0.268	0	490	135	788	814	0.23
5.70	0.282	0	530	60	799	822	0.16
5.92	0.289	0	570	0	796	819	0.20

Appendix A5 – Detailed Sample Preparations, Results and Electropherograms from Stability Constant Determination

Table S8: Detailed sample composition and experimental results of the U(VI) acetate series 1.

measured pH	free [AcO ⁻]/M	addition of (total sample volume V = 20 mL)			retention time/s		electrophoretic mobility/ 10 ⁻⁴ cm ² V ⁻¹ s ⁻¹
		HClO ₄ (11.6 M)/ μL	NaOH (10 M)/ μL	NaClO ₄ ·H ₂ O/ mg	t _{an} /s	t _{eof} /s	
1.91	0.000769	17	0	813	657	984	2.92
2.50	0.00297	0	0	839	718	995	2.24
2.92	0.00769	0	10	828	814	988	1.25
3.12	0.0120	0	20	816	911	969	0.38
3.17	0.0134	0	39	789	904	960	0.37
3.36	0.0203	0	73	741	1068	1006	-0.33
3.70	0.0410	0	130	661	1108	946	-0.89
4.06	0.0799	0	215	541	1132	908	-1.26
4.35	0.124	0	315	401	1123	885	-1.38
4.80	0.200	0	415	260	1077	851	-1.43
5.14	0.244	0	490	154	1054	828	-1.49
5.44	0.269	0	538	87	1045	810	-1.60
5.76	0.284	0	560	56	1029	796	-1.65

A5.1 ACETATE

Table S9: Detailed sample composition and experimental results of the U(VI) acetate series 2.

measured pH	free [AcO ⁻]/M	addition of (total sample volume V = 20 mL)			retention time/s		electrophoretic mobility/ 10 ⁻⁴ cm ² V ⁻¹ S ⁻¹
		HClO ₄ (11.6 M)/ μL	NaOH (10 M)/ μL	NaClO ₄ ·H ₂ O/ mg	t _{AN} /s	t _{EOF} /s	
1.01	9.70 · 10 ⁻⁵	172	0	566	559	835	3.42
1.92	0.000787	17	0	813	641	950	2.93
2.62	0.00390	0	0	838	716	986	2.21
3.02	0.00962	0	10	831	916	1167	1.36
3.24	0.0156	0	20	816	1183	1346	0.59
3.53	0.0290	0	39	787	1079	1011	-0.36
3.75	0.0453	0	73	743	1566	1275	-0.84
3.99	0.0708	0	130	660	1028	851	-1.17
4.35	0.124	0	215	541	1008	818	-1.33
4.63	0.172	0	315	461	2580	1607	-1.35
5.01	0.229	0	415	261	1008	799	-1.50
5.11	0.241	0	490	156	1000	793	-1.51
5.23	0.253	0	538	87	984	781	-1.53
5.52	0.274	0	590	16	1008	781	-1.67

Appendix A5 – Detailed Sample Preparations, Results and Electropherograms from Stability Constant Determination

Table S10: Comparison of the $\log \beta^0$ values for Th(IV) acetate complexes ($l = 0$).

$\log \beta^0$				
i	Davies (see Tab. 6)	SIT	ANDRA ¹	NIST ²
1	4.73 ± 0.16	4.83 ± 0.37	5.24 ± 0.15	4.69
2	8.92 ± 0.09	9.04 ± 0.31	9.44 ± 0.15	8.18
3	12.16 ± 0.11	12.28 ± 0.34	12.56 ± 0.50	10.85
4	12.96 ± 0.87	13.03 ± 1.11	14.38 ± 0.50	12.44
5	14.39 ± 0.16	14.43 ± 0.46	15.37 ± 1.00	13.04

Table S11: SIT parameters $\varepsilon(i, j)$ used for the extrapolation to $l = 0$ in Table S10.

<i>i</i>	<i>j</i>	$\varepsilon(i, j)$ kg/mol	reference
Th ⁴⁺	ClO ₄ ⁻	0.70 ± 0.10	3
[Th(AcO)] ³⁺	ClO ₄ ⁻	0.6 ± 0.1	4*
[Th(AcO) ₂] ²⁺	ClO ₄ ⁻	0.4 ± 0.1	4*
[Th(AcO) ₃] ⁺	ClO ₄ ⁻	0.2 ± 0.01	4*
[Th(AcO) ₄](aq)	ClO ₄ ⁻	0 ± 0.1	4*
[Th(AcO) ₅] ⁻	Na ⁺	-0.05 ± 0.1	4*
AcO ⁻	Na ⁺	0.08 ± 0.01	3

* estimated value

A5.1 ACETATE

Detailed equations employed for the fitting procedure for each actinide-acetate system.

U(VI): $i = 0, 1, 2, 3$

$$\mu_{\text{eff}} = \frac{\mu_0(\text{UO}_2^{2+}) + \mu([\text{UO}_2(\text{AcO})]^+) \cdot \beta([\text{UO}_2(\text{AcO})_2]_{\text{aq}}) \cdot \beta([\text{UO}_2(\text{AcO})_2]_{\text{aq}}) \cdot [\text{AcO}^-]^{-2} + \mu([\text{UO}_2(\text{AcO})_3]^-) \cdot \beta([\text{UO}_2(\text{AcO})_3]^-) \cdot [\text{AcO}^-]^{-3}}{1 + \beta([\text{UO}_2(\text{AcO})]^+) \cdot [\text{AcO}^-] + \beta([\text{UO}_2(\text{AcO})_2]_{\text{aq}}) \cdot [\text{AcO}^-]^2 + \beta([\text{UO}_2(\text{AcO})_3]^-) \cdot [\text{AcO}^-]^3} \quad (\text{S1})$$

Np(V): $i = 0, 1$

$$\mu_{\text{eff}} = \frac{\mu_0(\text{NpO}_2^+) + \mu([\text{NpO}_2(\text{AcO})]_{\text{aq}}) \cdot \beta([\text{NpO}_2(\text{AcO})]_{\text{aq}}) \cdot [\text{AcO}^-]}{1 + \beta([\text{NpO}_2(\text{AcO})]_{\text{aq}}) \cdot [\text{AcO}^-]} \quad (\text{S2})$$

Th(IV): $i = 0, 1, 2, 3, 4, 5$

$$\frac{\mu_0(\text{Th}^{4+}) + \mu([\text{Th}(\text{AcO})]^{3+}) \cdot \beta([\text{Th}(\text{AcO})_2]^{2+}) \cdot \beta([\text{Th}(\text{AcO})_2]^{2+}) \cdot [\text{AcO}^-]^{-2} + \mu([\text{Th}(\text{AcO})_3]^+) \cdot \beta([\text{Th}(\text{AcO})_3]^+) \cdot [\text{AcO}^-]^{-3} + \mu([\text{Th}(\text{AcO})_4]_{\text{aq}}) \cdot \beta([\text{Th}(\text{AcO})_4]_{\text{aq}}) \cdot [\text{AcO}^-]^{-4} + \mu([\text{Th}(\text{AcO})_5]^-) \cdot \beta([\text{Th}(\text{AcO})_5]^-) \cdot [\text{AcO}^-]^{-5}}{1 + \beta([\text{Th}(\text{AcO})]^{3+}) \cdot [\text{AcO}^-] + \beta([\text{Th}(\text{AcO})_2]^{2+}) \cdot [\text{AcO}^-]^2 + \beta([\text{Th}(\text{AcO})_3]^+) \cdot [\text{AcO}^-]^3 + \beta([\text{Th}(\text{AcO})_4]_{\text{aq}}) \cdot [\text{AcO}^-]^4 + \beta([\text{Th}(\text{AcO})_5]^-) \cdot [\text{AcO}^-]^5} \quad \mu_{\text{eff}} = \quad (\text{S3})$$

Am(III): $i = 0, 1, 2, 3$

$$\mu_{\text{eff}} = \frac{\mu_0(\text{Am}^{3+}) + \mu([\text{Am}(\text{AcO})]^{2+}) \cdot \beta([\text{Am}(\text{AcO})_2]^{2+}) \cdot \beta([\text{Am}(\text{AcO})_2]^{2+}) \cdot [\text{AcO}^-]^{-2} + \mu([\text{Am}(\text{AcO})_3]_{\text{aq}}) \cdot \beta([\text{Am}(\text{AcO})_3]_{\text{aq}}) \cdot [\text{AcO}^-]^{-3}}{1 + \beta([\text{Am}(\text{AcO})]^{2+}) \cdot [\text{AcO}^-] + \beta([\text{Am}(\text{AcO})_2]^{2+}) \cdot [\text{AcO}^-]^2 + \beta([\text{Am}(\text{AcO})_3]_{\text{aq}}) \cdot [\text{AcO}^-]^3} \quad (\text{S4})$$

Appendix A5 – Detailed Sample Preparations, Results and Electropherograms from Stability Constant Determination

References

- (1) Richard, L.; Grieve, M.; Duro, L. *Andra-TDB7 Task 3 ? Organics*. Selection of formation constants for acetate complexes of Ca and radionuclides, Amphos 21, 2011.
- (2) Martel, A. E.; Smith, R. M. *NIST Standard Reference Database 46.6*, version 8.0, 2004.
- (3) Rand, M.; Fuger, J.; Grenthe, I.; Neck, V.; Rai, D. *Chemical Thermodynamics of Thorium* OECD-NEA: Paris, 2007.
- (4) Thoenen, T.; Hummel, W.; Berner, U.; Curti, E. *The PSI/NAGRA Chemical Thermodynamic Database 12/07*, Paul Scherrer Institut, PSI Bericht Nr. 14-04, 2014.

A5.2 PROPIONATE

Table A1: Detailed sample composition of the measurement series for the determination of the stability constants of actinides with propionate.

pH*	addition of (total sample volume $V = 20$ mL)			$c(\text{Pro}^-)/M$ with $pK_a(0.3\text{ M}) = 4.60^{**}$
	HClO_4 (11.6 M)/ μL	NaOH (10 M)/ μL	$\text{NaClO}_4 \cdot \text{H}_2\text{O}$ / mg	
0.73	260	0	412	$4.05 \cdot 10^{-5}$
0.81	180	0	532	$4.86 \cdot 10^{-5}$
1.06	110	0	652	$8.65 \cdot 10^{-5}$
1.13	80	0	704	$1.02 \cdot 10^{-4}$
1.31	48	0	759	$1.54 \cdot 10^{-4}$
1.49	30	0	790	$2.33 \cdot 10^{-4}$
1.60	20	0	807	$3.00 \cdot 10^{-4}$
1.73	10	0	823	$4.04 \cdot 10^{-4}$
1.87	5	0	831	$5.58 \cdot 10^{-4}$
1.19	2	0	834	$6.11 \cdot 10^{-4}$
2.00	0	0	831	$7.52 \cdot 10^{-4}$
2.10	0	3	830	$9.46 \cdot 10^{-4}$
2.24	0	8	789	$1.30 \cdot 10^{-3}$
2.45	0	16	810	$2.11 \cdot 10^{-3}$
2.74	0	24	799	$4.08 \cdot 10^{-3}$
3.18	0	55	800	$1.10 \cdot 10^{-2}$
3.42	0	86	781	$1.86 \cdot 10^{-2}$
3.81	0	114	715	$4.19 \cdot 10^{-2}$
4.22	0	177	602	$8.83 \cdot 10^{-2}$
4.50	0	250	468	$1.33 \cdot 10^{-1}$
4.69	0	310	359	$1.65 \cdot 10^{-1}$
4.89	0	370	295	$1.98 \cdot 10^{-1}$
5.15	0	450	181	$2.34 \cdot 10^{-1}$
5.46	0	520	109	$2.64 \cdot 10^{-1}$

* measured after actinide addition

** calculated by Equation (4.7) (based on $pK_a(0\text{ M}) = 4.87$ [04MAR])

Appendix A5 – Detailed Sample Preparations, Results and Electropherograms from Stability Constant Determination

Table A2: Experimental results of the actinide-propionate measurements. For the missing values no evaluable signal was obtained.

pH	migration time t_i/s				t_{EOF}/s	electrophoretic mobility/ $10^{-4} \text{ cm}^2\text{V}^{-1}\text{s}^{-1}$			
	Am(III)	Th(IV)	Np(V)	U(VI)		Am(III)	Th(IV)	Np(V)	U(VI)
0.73	467	520	616	563	831	5.41 ± 0.16	4.16 ± 0.13	2.42 ± 0.09	3.30 ± 0.11
0.81	487	578		591	860	5.14 ± 0.14	3.27 ± 0.10		3.06 ± 0.10
1.06	525	611	692	647	949	4.91 ± 0.13	3.37 ± 0.09	2.25 ± 0.07	2.84 ± 0.08
1.13	538	632	712	671	971	4.79 ± 0.12	3.18 ± 0.09	2.16 ± 0.07	2.66 ± 0.08
1.31	518	623	671	643	889	4.65 ± 0.13	2.77 ± 0.09	2.11 ± 0.08	2.48 ± 0.08
1.49	549	643	718	696	974	4.59 ± 0.12	3.05 ± 0.09	2.12 ± 0.07	2.37 ± 0.07
1.60	529	745	678	672	898	4.49 ± 0.12	1.32 ± 0.07	2.09 ± 0.08	2.16 ± 0.08
1.73	556	678	723	714	974	4.46 ± 0.11	2.59 ± 0.08	2.06 ± 0.07	2.16 ± 0.07
1.87	558	722	714	720	963	4.35 ± 0.11	2.01 ± 0.07	2.09 ± 0.07	2.03 ± 0.07
1.91	578	936	731	754	985	4.13 ± 0.11	0.31 ± 0.04	2.04 ± 0.07	1.79 ± 0.06
2.00	612	918	780	776	1078	4.07 ± 0.10	0.93 ± 0.04	2.05 ± 0.06	2.08 ± 0.06
2.10	627	854	780	842	1063	3.78 ± 0.09	1.33 ± 0.05	1.98 ± 0.06	1.43 ± 0.05
2.24	631	860	776	927	1049	3.65 ± 0.09	1.21 ± 0.05	1.94 ± 0.06	0.72 ± 0.04
2.45	594	827	705	889	929	3.50 ± 0.10	0.77 ± 0.05	1.97 ± 0.07	0.28 ± 0.05
2.74	654	891	772	1058	1020	3.16 ± 0.08	0.82 ± 0.05	1.81 ± 0.06	-0.20 ± 0.04
3.18	651	889	747	1081	963	2.88 ± 0.08	0.50 ± 0.05	1.74 ± 0.06	-0.66 ± 0.04
3.42	692	936	785	1185	1007	2.60 ± 0.07	0.43 ± 0.04	1.62 ± 0.06	-0.86 ± 0.04
3.81	769	1025	849	1318	1041	1.97 ± 0.06	0.09 ± 0.04	1.26 ± 0.05	-1.16 ± 0.03
4.22	794	1054	876	1321	1029	1.66 ± 0.06	-0.14 ± 0.04	0.98 ± 0.05	-1.24 ± 0.04
4.50	885	1201	980	1505	1132	1.42 ± 0.05	-0.29 ± 0.03	0.79 ± 0.04	-1.26 ± 0.03
4.69	938	1280	1043	1607	1165	1.20 ± 0.04	-0.44 ± 0.03	0.58 ± 0.03	-1.36 ± 0.03
4.89	889	1183	978	1409	1061	1.06 ± 0.05	-0.56 ± 0.03	0.47 ± 0.04	-1.34 ± 0.03
5.15	905	1260	1001	1407	1061	0.94 ± 0.05	-0.86 ± 0.03	0.33 ± 0.04	-1.34 ± 0.03
5.46	914		1011	1399	1061	0.88 ± 0.04		0.27 ± 0.04	-1.31 ± 0.03

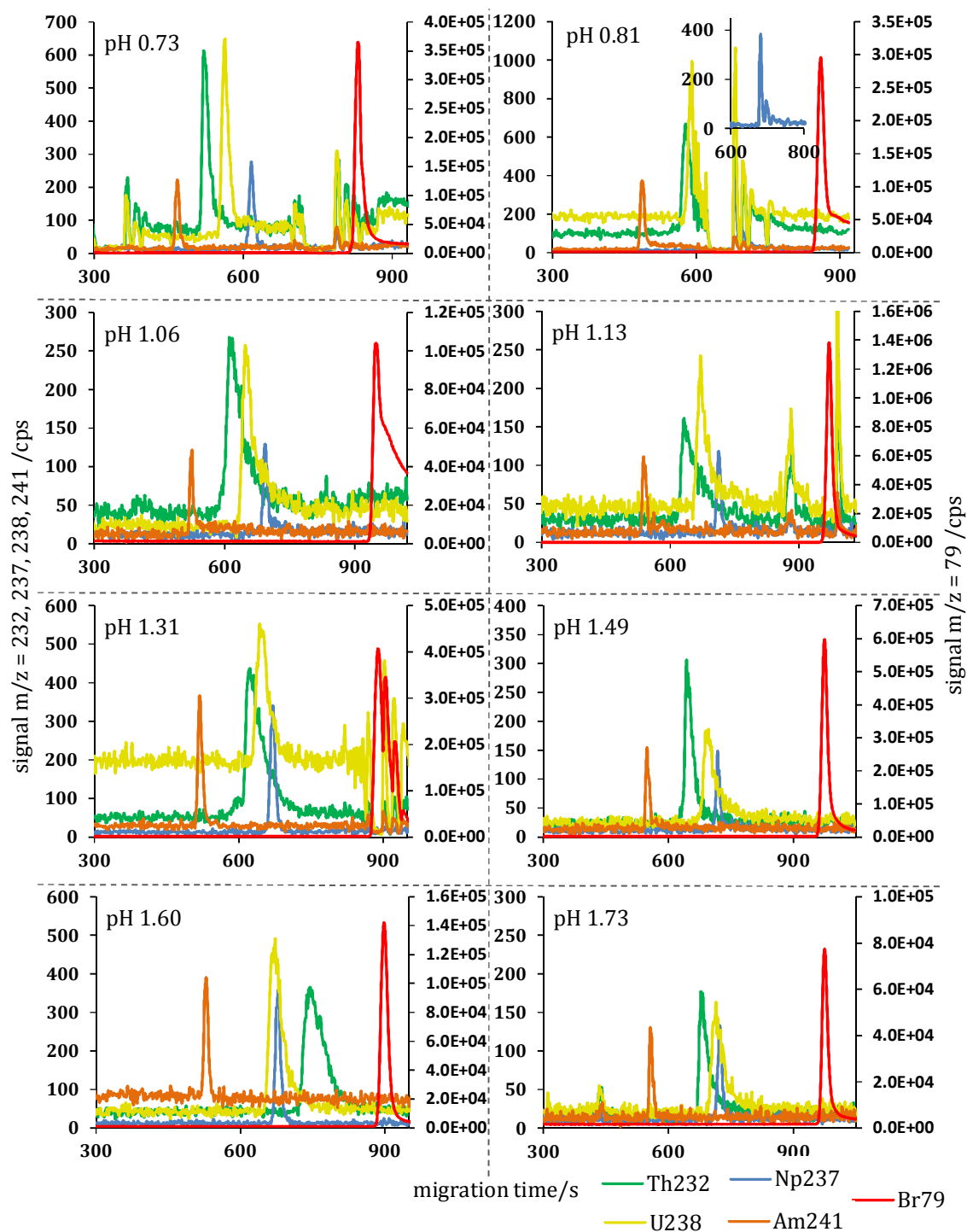


Figure A1: Electropherograms of the stability constant determination with the propionate ligand for the actinides U(VI), Np(V), Th(IV) and Np(V) at $U = 10$ kV and $I = 0.3$ M, $pH = 0.73 - 1.73$.

Appendix A5 – Detailed Sample Preparations, Results and Electropherograms from Stability Constant Determination

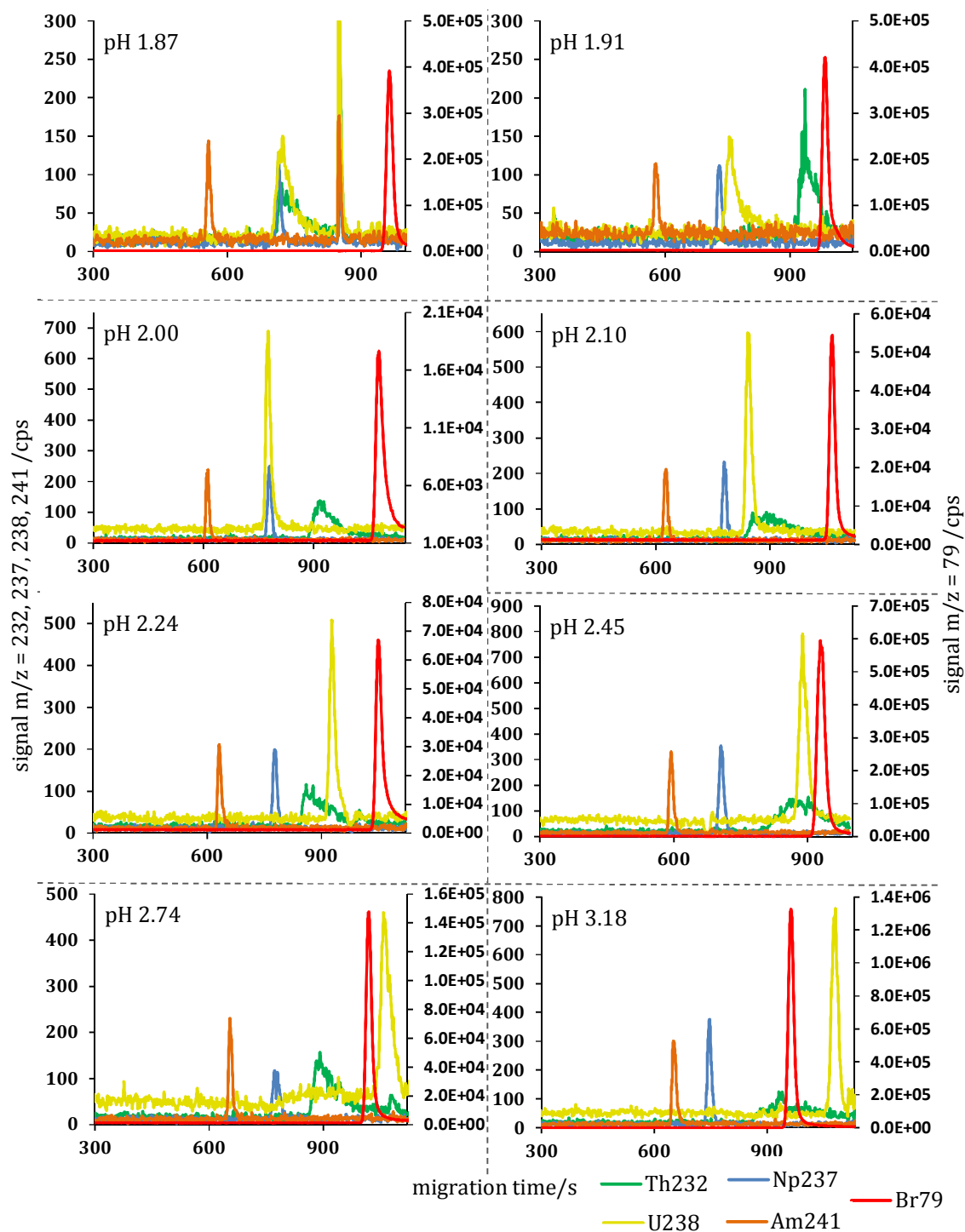


Figure A2: Electropherograms of the stability constant determination with the propionate ligand for the actinides U(VI), Np(V), Th(IV) and Np(V) at $U = 10$ kV and $I = 0.3$ M, $pH = 1.87 - 3.18$.

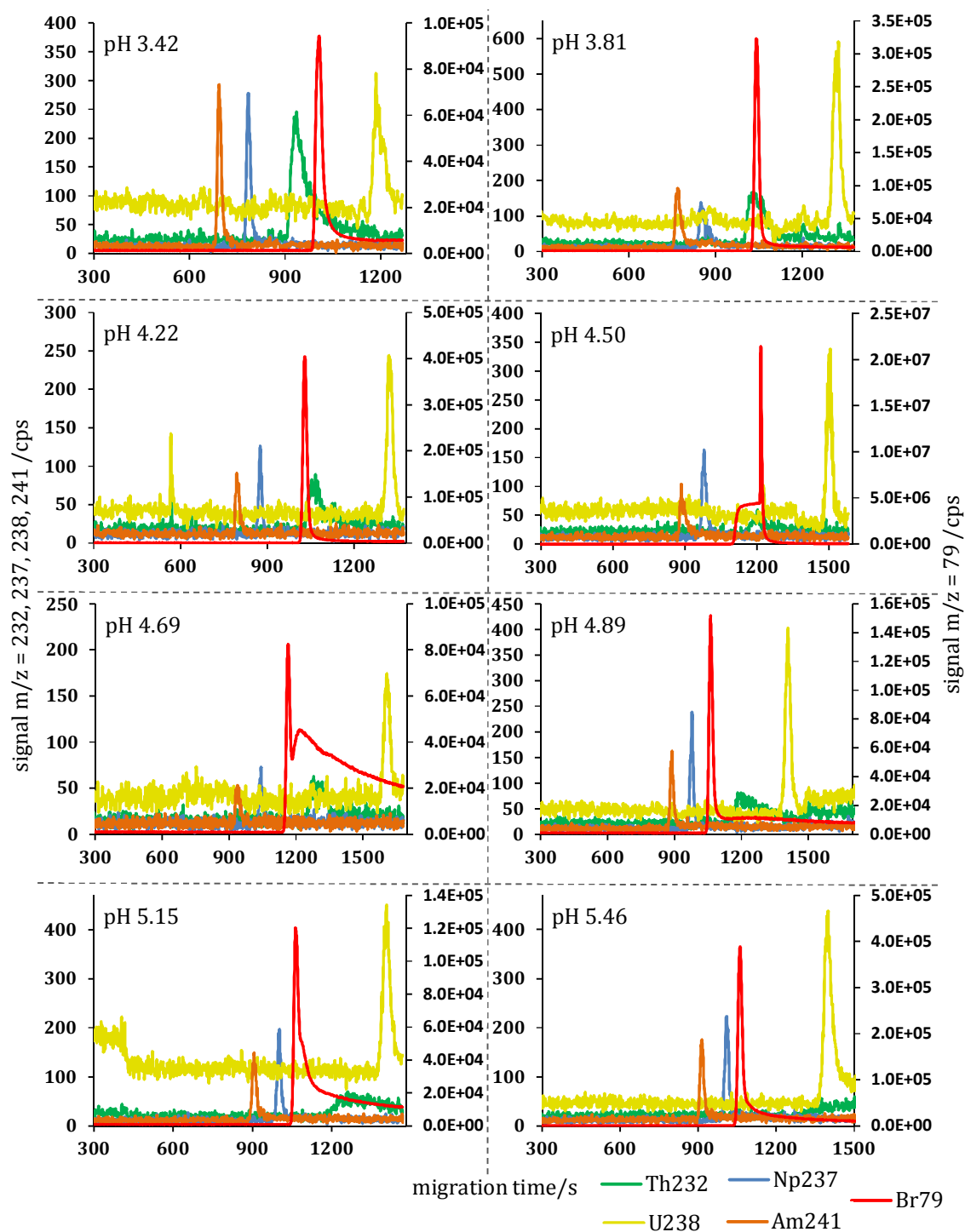


Figure A3: Electropherograms of the stability constant determination with the propionate ligand for the actinides U(VI), Np(V), Th(IV) and Np(V) at $U = 10$ kV and $I = 0.3$ M, $pH = 3.42 - 5.46$.

Appendix A5 – Detailed Sample Preparations, Results and Electropherograms from Stability Constant Determination

A5.3 GLUCONATE

Table A3: Detailed sample composition of the measurement series for the determination of the stability constants of actinides with propionate.

pH*	addition of (total sample volume $V = 20$ mL)			$c(\text{Glu}^-)/\text{M}$ with $\text{p}K_{\text{a},1}(0.3 \text{ M}) = 3.59^{**}$
	HClO_4 (11.6 M)/ μL	NaOH (10 M)/ μL	$\text{NaClO}_4 \cdot \text{H}_2\text{O}$ / mg	
0.87	625	0	0	$5.71 \cdot 10^{-4}$
1.17	600	0	0	$1.14 \cdot 10^{-3}$
1.17	565	0	0	$1.14 \cdot 10^{-3}$
1.39	552	40	0	$1.88 \cdot 10^{-3}$
1.40	550	20	0	$1.92 \cdot 10^{-3}$
1.40	550	20	0	$1.92 \cdot 10^{-3}$
1.57	500	0	0	$2.84 \cdot 10^{-3}$
1.67	490	0	0	$3.56 \cdot 10^{-3}$
1.83	485	0	0	$5.12 \cdot 10^{-3}$
2.10	460	0	0	$9.40 \cdot 10^{-3}$
2.27	460	0	35	$1.37 \cdot 10^{-2}$
2.36	450	0	0	$1.67 \cdot 10^{-2}$
2.63	400	0	68	$2.96 \cdot 10^{-2}$
2.75	400	0	0	$3.79 \cdot 10^{-2}$
2.83	300	0	286	$4.44 \cdot 10^{-2}$
3.00	350	20	0	$6.13 \cdot 10^{-2}$
3.37	220	0	145	$1.13 \cdot 10^{-1}$
3.57	250	100	0	$1.47 \cdot 10^{-1}$
3.87	170	70	0	$1.97 \cdot 10^{-1}$
4.10	150	120	0	$2.29 \cdot 10^{-1}$
4.47	50	20	0	$2.65 \cdot 10^{-1}$
4.78	20	10	0	$2.82 \cdot 10^{-1}$

* measured after actinide addition

** calculated by Equation (4.7) (based on $\text{p}K_{\text{a},1}(0 \text{ M}) = 3.86$ [64SIL])

Table A4: Experimental results of the actinide-gluconate measurements. Outliner values that were not considered in the fitting procedure are written in italics, for the missing values no evaluable signal was obtained.

pH	migration time t_i/s				t_{EOF}/s	electrophoretic mobility/ $10^{-4} \text{ cm}^2\text{V}^{-1}\text{s}^{-1}$			
	Am(III)	Th(IV)	Np(V)	U(VI)		Am(III)	Th(IV)	Np(V)	U(VI)
0.87	683	1043	798	743	1109	3.24 ± 0.08	0.33 ± 0.04	2.03 ± 0.06	2.56 ± 0.07
1.17	729	1043	752	771	1185	3.05 ± 0.07	0.66 ± 0.03	<i>2.80 ± 0.07</i>	<i>2.62 ± 0.06</i>
1.17	780	1145	856	832	1185	2.53 ± 0.06	0.17 ± 0.03	1.87 ± 0.05	2.06 ± 0.05
1.39	858	1180	869	905	1176	1.82 ± 0.05	<i>-0.02 ± 0.03</i>	1.74 ± 0.05	1.47 ± 0.05
1.40			992	980	1445			1.82 ± 0.04	1.90 ± 0.04
1.40	881		941	936	1334	2.22 ± 0.05		1.81 ± 0.04	1.84 ± 0.04
1.57	969	1229	978	1016	1367	1.74 ± 0.04	0.48 ± 0.03	1.68 ± 0.04	1.46 ± 0.04
1.67	1009		991	1058	1376	1.53 ± 0.04		1.63 ± 0.04	1.26 ± 0.03
1.83	965	1156	929	1007	1225	1.27 ± 0.04	0.28 ± 0.03	1.50 ± 0.04	1.02 ± 0.04
2.10	1103	1338	1031	1178	1370	1.02 ± 0.03	0.10 ± 0.02	1.39 ± 0.04	0.69 ± 0.03
2.27	1398	1768	1278	1508	1807	0.94 ± 0.02	0.07 ± 0.01	1.32 ± 0.03	0.63 ± 0.02
2.36	1487	1887	1350	1623	1901	0.85 ± 0.03	0.02 ± 0.01	1.24 ± 0.02	0.52 ± 0.02
2.63	1114	1243	1034	1200	1229	0.48 ± 0.03	<i>-0.05 ± 0.03</i>	0.88 ± 0.03	0.11 ± 0.03
2.75	1897	2444	1694	2175	2285	0.52 ± 0.01	<i>-0.17 ± 0.01</i>	0.88 ± 0.02	0.13 ± 0.01
2.83		1689	1347		1698		<i>0.02 ± 0.02</i>	0.89 ± 0.02	
3.00	1292	1452	1218	1421	1379	0.28 ± 0.02	<i>-0.21 ± 0.02</i>	0.56 ± 0.03	<i>-0.12 ± 0.02</i>
3.37	1183	1294	1140	1285	1205	0.09 ± 0.03	<i>-0.33 ± 0.03</i>	0.28 ± 0.03	<i>-0.30 ± 0.03</i>
3.57	1270	1427	1234	1389	1281	0.04 ± 0.03	<i>-0.46 ± 0.02</i>	0.17 ± 0.03	<i>-0.35 ± 0.02</i>
3.87	1239	1385	1220	1365	1232	<i>-0.03 ± 0.03</i>	<i>-0.52 ± 0.03</i>	0.05 ± 0.03	<i>-0.46 ± 0.03</i>
4.10	1554	1698	1310	1496	1303	<i>-0.71 ± 0.02</i>	<i>-1.03 ± 0.02</i>	<i>-0.02 ± 0.02</i>	<i>-0.57 ± 0.02</i>
4.47	1369	1618	1361	1578	1329	<i>-0.13 ± 0.02</i>	<i>-0.78 ± 0.02</i>	<i>-0.10 ± 0.02</i>	<i>-0.69 ± 0.02</i>
4.78	1401	1708	1387	1656	1343	<i>-0.18 ± 0.02</i>	<i>-0.92 ± 0.02</i>	<i>-0.14 ± 0.02</i>	<i>-0.81 ± 0.02</i>

Appendix A5 – Detailed Sample Preparations, Results and Electropherograms from Stability Constant Determination

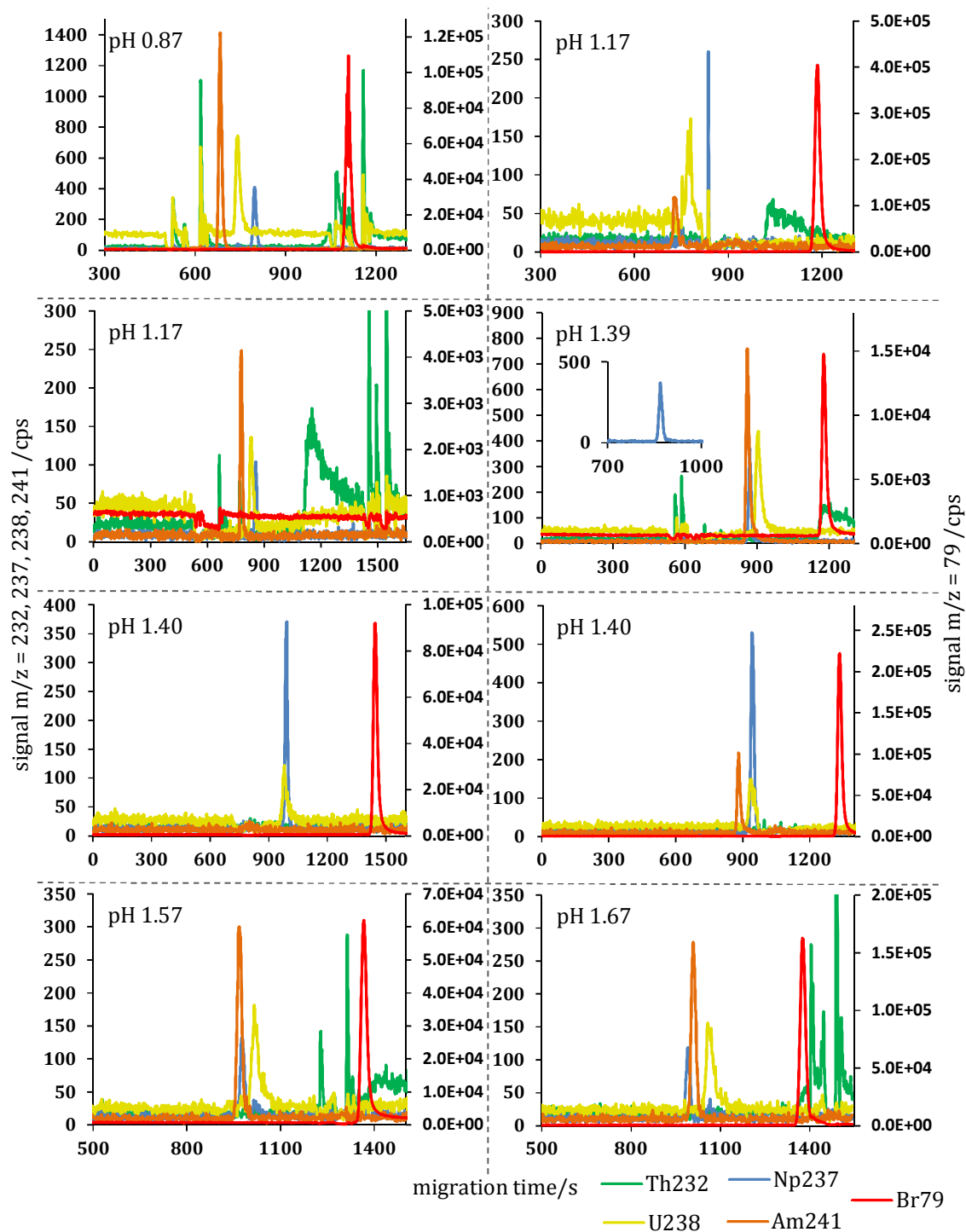


Figure A4: Electropherograms of the stability constant determination with the gluconate ligand for the actinides U(VI), Np(V), Th(IV) and Np(V) at $U = 10$ kV and $I = 0.3$ M, $pH = 0.87 - 1.67$.

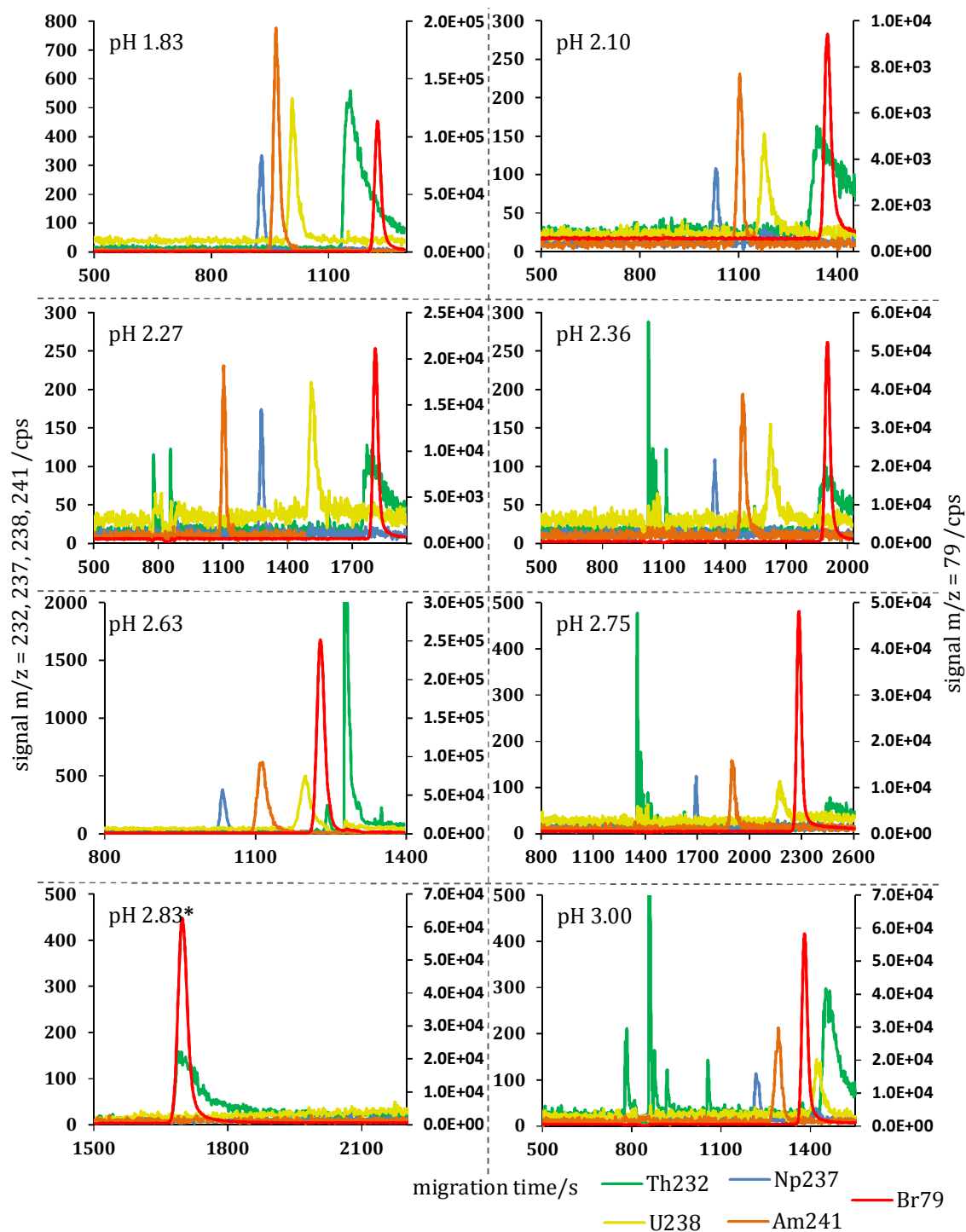


Figure A5: Electropherograms of the stability constant determination with the gluconate ligand for the actinides U(VI), Np(V), Th(IV) and Np(V) at $U = 10$ kV and $I = 0.3$ M, $pH = 1.83 - 3.00$.

* The measurement of the $pH = 2.83$ sample had to be restarted at 1500 s due to setting problems. This is why just the results starting from 1500 s are shown.

Appendix A5 – Detailed Sample Preparations, Results and Electropherograms from Stability Constant Determination

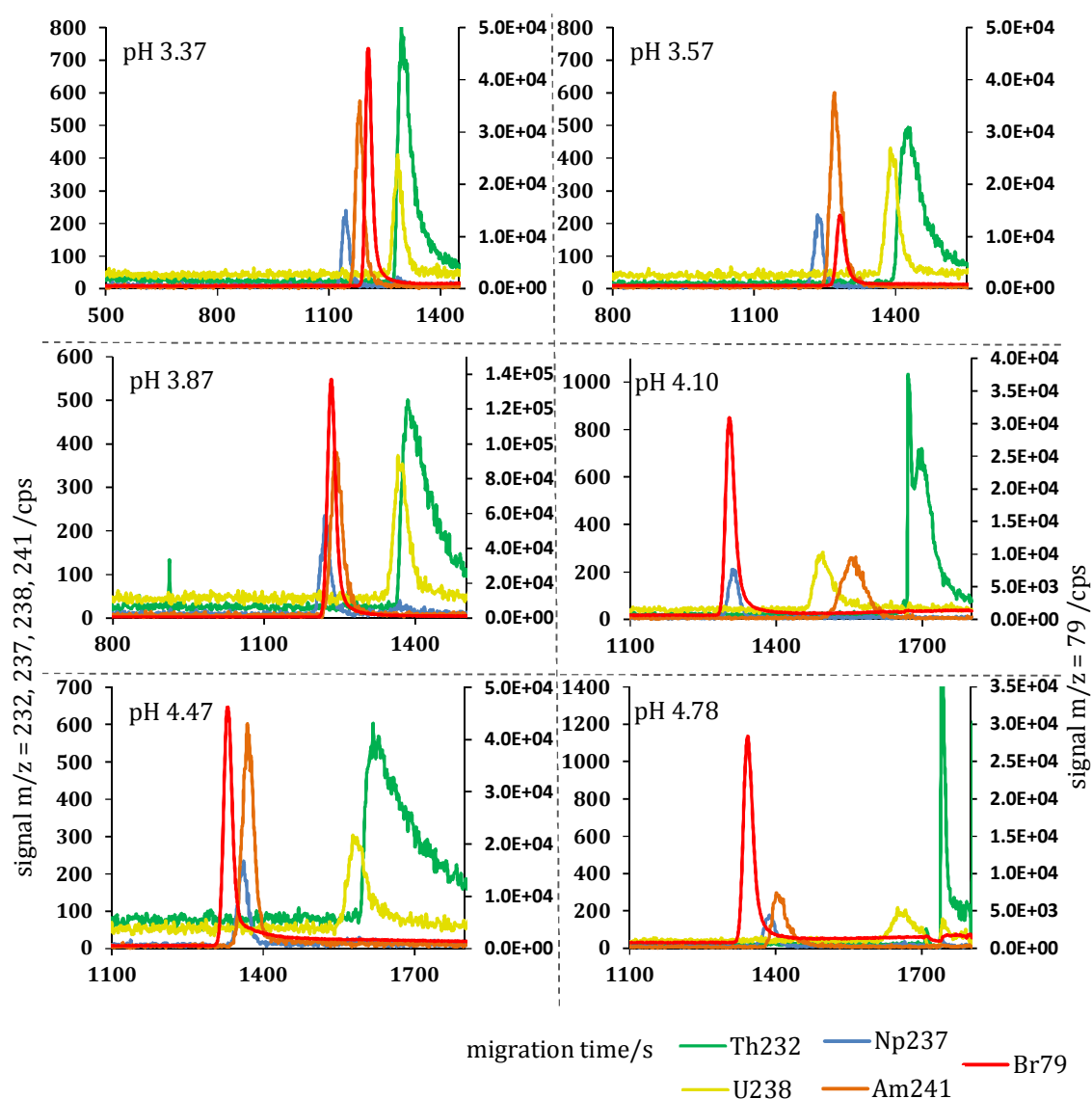


Figure A6: Electropherograms of the stability constant determination with the gluconate ligand for the actinides U(VI), Np(V), Th(IV) and Np(V) at $U = 10$ kV and $I = 0.3$ M, pH = 3.37 – 4.78.

A5.4 CITRATE

Table A5: Detailed sample composition of the measurement series for the determination of the stability constants of actinides with citrate.

pH*	addition of (total sample volume $V = 20$ mL)			$\kappa/\text{mS cm}^{-1}$	$c(\text{H}_{3-n}\text{Cit}^{n-})/\text{M}$ with $\text{p}K_{a,1}(0.3 \text{ M}) = 2.86$, $\text{p}K_{a,2}(0.3 \text{ M}) = 4.22$ and $\text{p}K_{a,3}(0.3 \text{ M}) = 5.59^{**}$		
	HClO_4 (11.6 M)/ μL	NaOH (10 M)/ μL	$\text{NaClO}_4 \cdot \text{H}_2\text{O}/$ mg		Cit^{3-}	HCit^{2-}	H_2Cit^{-}
0.79	172	0	0	38.30	$1.49 \cdot 10^{-11}$	$9.41 \cdot 10^{-7}$	$2.53 \cdot 10^{-3}$
1.24	52	0	374	14.19	$3.29 \cdot 10^{-10}$	$7.36 \cdot 10^{-6}$	$7.03 \cdot 10^{-3}$
1.69	0	0	737	5.52	$7.06 \cdot 10^{-9}$	$5.61 \cdot 10^{-5}$	$1.90 \cdot 10^{-2}$
1.88	0	41	788	4.27	$2.53 \cdot 10^{-8}$	$1.30 \cdot 10^{-4}$	$2.84 \cdot 10^{-2}$
2.22	0	115	774	4.63	$2.38 \cdot 10^{-7}$	$5.58 \cdot 10^{-4}$	$5.58 \cdot 10^{-2}$
2.93	0	360	577	9.28	$1.77 \cdot 10^{-5}$	$8.09 \cdot 10^{-3}$	$1.58 \cdot 10^{-1}$
3.16	0	450	495	11.24	$6.11 \cdot 10^{-5}$	$1.64 \cdot 10^{-2}$	$1.89 \cdot 10^{-1}$
3.33	0	515	431	12.76	$1.45 \cdot 10^{-4}$	$2.63 \cdot 10^{-2}$	$2.04 \cdot 10^{-1}$
3.50	0	600	368	14.26	$3.27 \cdot 10^{-4}$	$4.02 \cdot 10^{-2}$	$2.11 \cdot 10^{-1}$
3.78	0	710	257	16.92	$1.13 \cdot 10^{-3}$	$7.32 \cdot 10^{-2}$	$2.01 \cdot 10^{-1}$
3.89	0	780	205	18.14	$1.78 \cdot 10^{-3}$	$8.94 \cdot 10^{-2}$	$1.91 \cdot 10^{-1}$
4.05	0	850	139	19.71	$3.32 \cdot 10^{-3}$	$1.15 \cdot 10^{-1}$	$1.70 \cdot 10^{-1}$
4.14	0	960	0	21.00	$4.63 \cdot 10^{-3}$	$1.30 \cdot 10^{-1}$	$1.57 \cdot 10^{-1}$
4.25	0	1000	0	23.00	$6.80 \cdot 10^{-3}$	$1.49 \cdot 10^{-1}$	$1.39 \cdot 10^{-1}$
4.45	0	1070	0	24.00	$1.30 \cdot 10^{-2}$	$1.79 \cdot 10^{-1}$	$1.05 \cdot 10^{-1}$
4.99	0	3070	0	29.00	$5.30 \cdot 10^{-2}$	$2.11 \cdot 10^{-1}$	$3.58 \cdot 10^{-2}$

* measured after actinide addition

** calculated by Equation (4.12) – (4.15) (based on $\text{p}K_{a,1}(0 \text{ M}) = 3.13$, $\text{p}K_{a,2}(0 \text{ M}) = 4.76$, $\text{p}K_{a,3}(0 \text{ M}) = 6.40$ [05HUM])

Appendix A5 – Detailed Sample Preparations, Results and Electropherograms from Stability Constant Determination

Table A6: Experimental results of the actinide-citrate measurements.

pH	migration time t_i/s				t_{EOF}/s	electrophoretic mobility/ $10^{-4} \text{ cm}^2\text{V}^{-1}\text{s}^{-1}$			
	Am(III)	Th(IV)	Np(V)	U(VI)		Am(III)	Th(IV)	Np(V)	U(VI)
0.79	616	849	707	680	965	3.39 ± 0.09	0.82 ± 0.05	2.19 ± 0.07	2.51 ± 0.08
1.24	752	1014	789	818	1056	2.21 ± 0.06	0.23 ± 0.04	1.85 ± 0.06	1.59 ± 0.05
1.69	849	1114	812	900	1080	1.45 ± 0.05	-0.17 ± 0.03	1.76 ± 0.06	1.07 ± 0.05
1.88	925	1192	829	954	1091	0.95 ± 0.04	-0.45 ± 0.03	1.67 ± 0.05	0.76 ± 0.04
2.22	1016	1268	842	1036	1078	0.33 ± 0.04	-0.80 ± 0.03	1.50 ± 0.05	0.22 ± 0.04
2.93	1214	1332	949	1245	1070	-0.64 ± 0.03	-1.06 ± 0.03	0.69 ± 0.04	-0.76 ± 0.03
3.16	1285	1410	1021	1389	1081	-0.85 ± 0.03	-1.25 ± 0.03	0.31 ± 0.04	-1.18 ± 0.03
3.33	1332	1454	1060	1463	1074	-1.04 ± 0.03	-1.40 ± 0.03	0.07 ± 0.04	-1.43 ± 0.03
3.50	1398	1507	1109	1532	1074	-1.24 ± 0.03	-1.54 ± 0.03	-0.17 ± 0.03	-1.61 ± 0.03
3.78	1476	1568	1180	1605	1060	-1.54 ± 0.03	-1.77 ± 0.04	-0.55 ± 0.03	-1.85 ± 0.04
3.89	1508	1605	1210	1659	1056	-1.64 ± 0.04	-1.87 ± 0.04	-0.70 ± 0.03	-1.99 ± 0.04
4.05	1529	1628	1243	1690	1047	-1.74 ± 0.04	-1.97 ± 0.04	-0.87 ± 0.03	-2.10 ± 0.04
4.14	1527	1643	1265	1712	1032	-1.81 ± 0.04	-2.08 ± 0.04	-1.03 ± 0.04	-2.22 ± 0.04
4.25	1548	1663	1299	1730	1021	-1.92 ± 0.04	-2.18 ± 0.04	-1.21 ± 0.04	-2.32 ± 0.04
4.45	1581	1683	1319	1772	1020	-2.01 ± 0.04	-2.23 ± 0.04	-1.29 ± 0.04	-2.41 ± 0.04
4.99	1561	1634	1394	1725	972	-2.24 ± 0.04	-2.41 ± 0.04	-1.80 ± 0.04	-2.59 ± 0.05

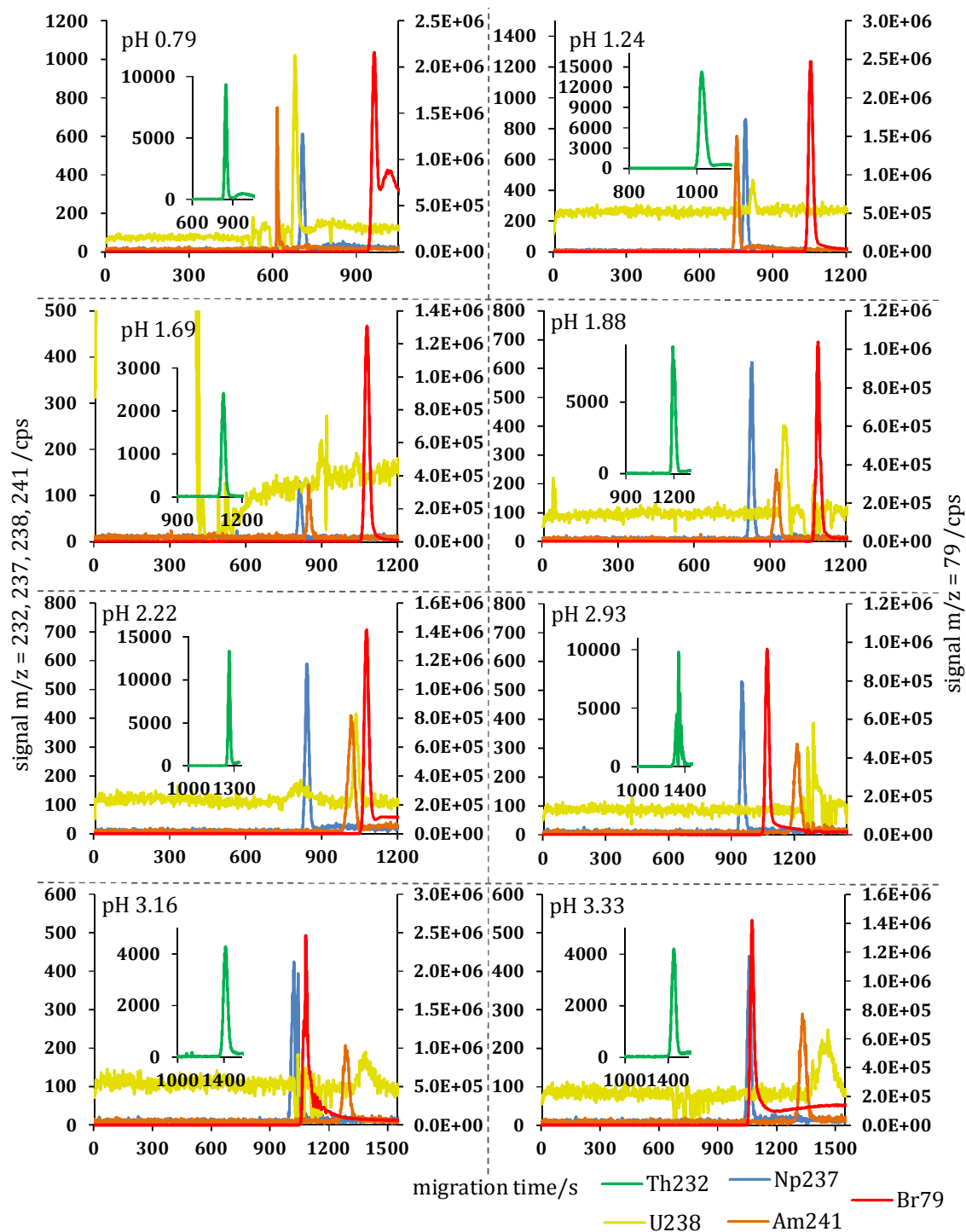


Figure A7: Electropherograms of the stability constant determination with the citrate ligand for the actinides U(VI), Np(V), Th(IV) and Np(V) at $U = 10$ kV and $I = 0.3$ M, pH = 0.79 – 3.33.

Appendix A5 – Detailed Sample Preparations, Results and Electropherograms from Stability Constant Determination

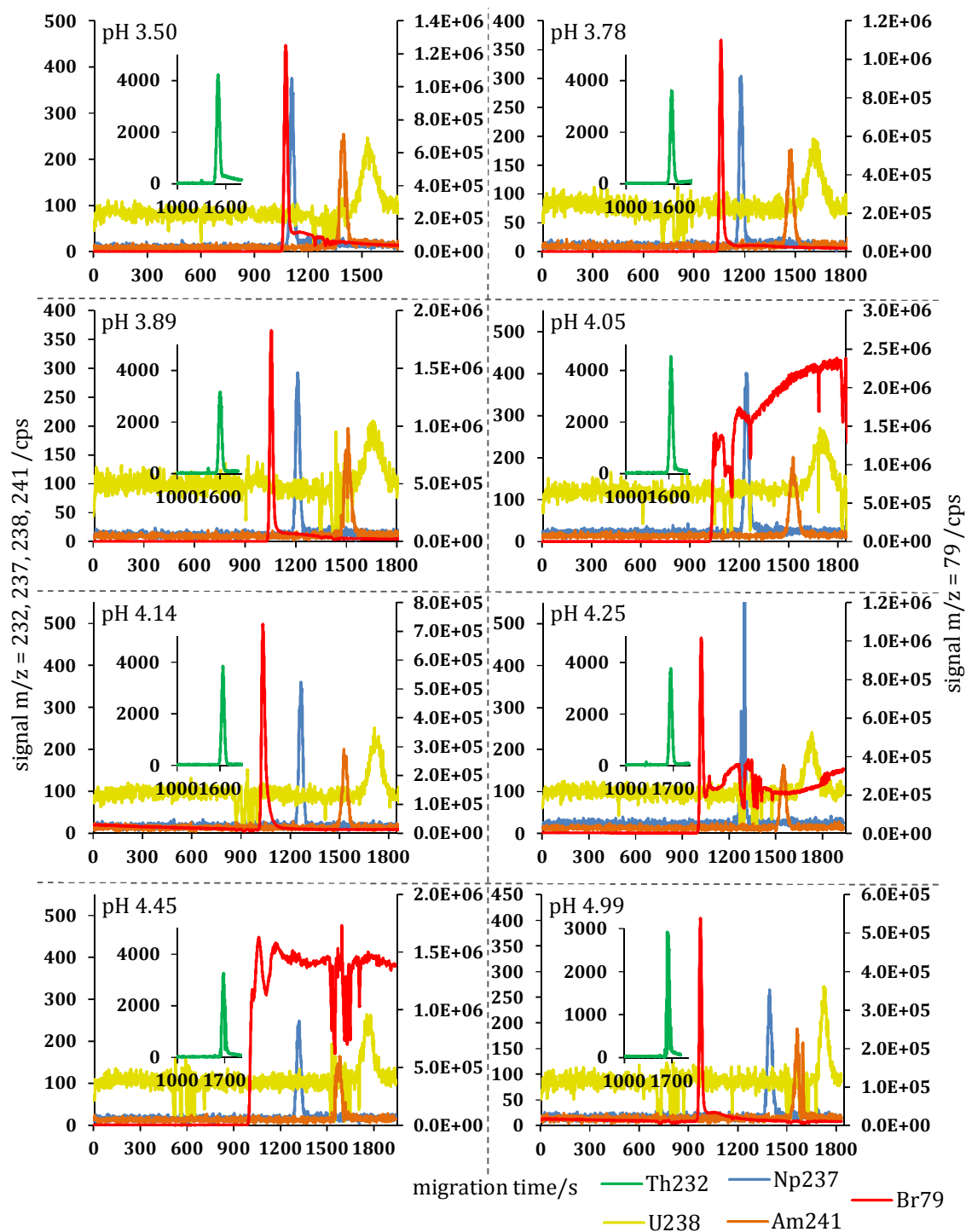


Figure A8: Electropherograms of the stability constant determination with the citrate ligand for the actinides U(VI), Np(V), Th(IV) and Np(V) at $U = 10$ kV and $I = 0.3$ M, pH = 3.50 – 4.99.

APPENDIX A6 – SUPPORTING INFORMATION FOR THE KINETIC PAPER (SECTION 5.2.1)

Supporting Information

Determination of Kinetic Parameters of Redox Reactions using CE-ICP-MS: A Case Study for the Reduction of Np(V) by Hydroxylamine Hydrochloride

Christian Willberger,* Samer Amayri, Tobias Reich*

Institute of Nuclear Chemistry, Johannes Gutenberg University Mainz, 55099 Mainz, Germany

*Corresponding authors

E-Mail: willberg@uni-mainz.de, treich@uni-mainz.de

Contents:

Figure S-1: **a)** Influence of the temperature on the rate constant of the reduction for different initial concentrations of HAHCl. **b)** Influence of the initial concentration of HAHCl on the rate constant of the reduction for different temperatures. The initial concentration of Np(V) was always 5×10^{-5} M.

Figure S-2: Dependence of the rate constant on the concentration of HAHCl.

Figure S-3: Arrhenius plot for determination of the activation energy of the reaction.

Appendix A6 – Supporting Information for the Kinetic Paper (Section 5.2.1)

Figure S-1: a) Influence of the temperature on the rate constant of the reduction for different initial concentrations of HAHCl. b) Influence of the initial concentration of HAHCl on the rate constant of the reduction for different temperatures. The initial concentration of Np(V) was always 5×10^{-5} M.

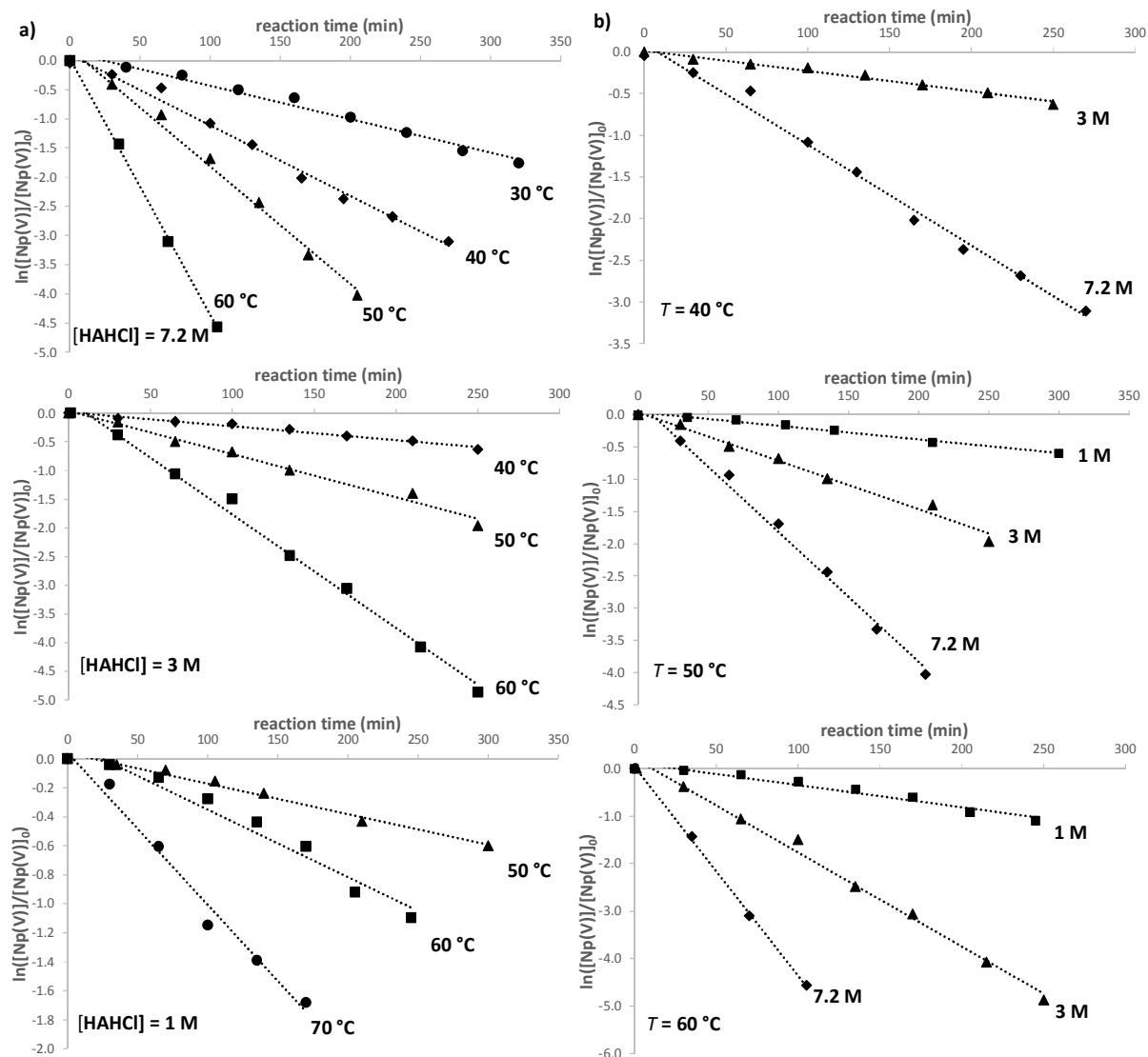


Figure S-2: Dependence of the rate constant on the concentration of HAHCl.

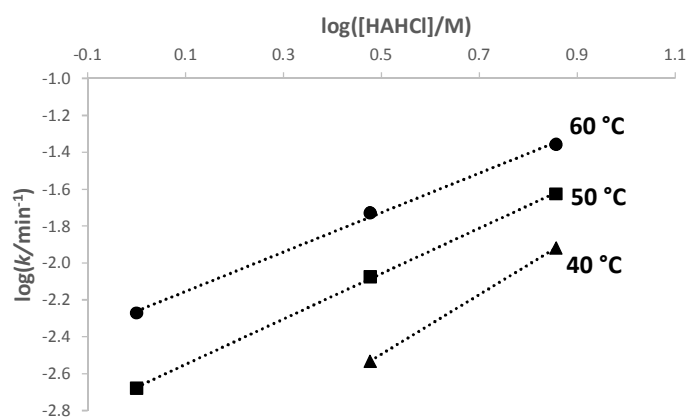
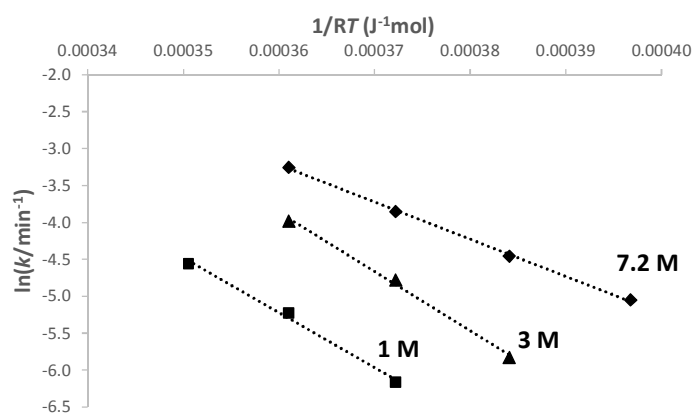


Figure S-3: Arrhenius plot for determination of the activation energy of the reaction.



DANKSAGUNG

Am Ende dieser Arbeit möchte ich die Gelegenheit nutzen und mich bei allen denjenigen bedanken, die mich während der langen Zeit dieser Arbeit unterstützt haben und damit zu ihrem Gelingen beigetragen haben.

An erster Stelle möchte ich mich bei Herrn Prof. Dr. Reich bedanken. Vielen Dank für die sehr gute Betreuung im gesamten Verlauf der Arbeit, nicht nur während der Promotion sondern auch schon vorher, während dem Forschungsmodul und der Diplomarbeit. Es war sehr hilfreich, jederzeit mit fachlichen Fragen und für das Finden von neuen Ideen zu dir kommen zu können. Das Thema hat mich sehr interessiert und großen Spaß gemacht.

Ein weiterer großer Dank geht an Dr. Samer Amayri. Er war bei vielen Messungen direkt oder indirekt beteiligt und hat immer bei fachlichen Fragen und technischen Problemen ausgeholfen. Außerdem habe ich immer sehr gerne mit dir in einem Büro gesessen und ich werde immer gerne daran zurückdenken.

Vielen Dank an Pascal Schönberg, Jogi Börner, Raphael Scholze, Verena Häußler, Saskia Leidich, Daniela Schönenbach, Tobias Stern, Steffen Koch und Felix Berg. Es war immer eine echt lustige Zeit, ihr habt sehr dazu beigetragen, dass ich die Promotionszeit gerne im Institut verbracht habe. Auch allen anderen aktuellen und ehemaligen Mitgliedern der Arbeitsgruppe Reich möchte ich für das sehr gute kollegiale Miteinander, die amüsanten Pausen und auch die schönen Zeiten abseits der Arbeit danken. Alle hier aufzuzählen würde den Rahmen sprengen und ich würde bestimmt auch unbeabsichtigt jemanden vergessen.

Das gleiche gilt für alle Mitarbeiter und Mitarbeiterinnen im Insitut für Kernchemie, sowohl aktuelle als auch ehemalige. Ich bin immer gerne ins Institut gekommen und wusste, dass ich egal an welcher Stelle, Hilfe bei meinen Anliegen bekommen kann. Vielen Dank dafür.

Danke auch an alle meine Freunde, die mich während der gesamten Zeit begleitet haben, während dem Studium und der Promotionszeit in Mainz, in meiner Zeit in der WG in Bretzenheim, die Jungs von Vitesse und meine Kumpels von ganz früher. Die Freizeit mit euch hat immer dazu geführt, dass ich wieder mit neuer Motivation an die Uni gehen konnte.

Ich danke auch meinen Kollegen an meiner neuen Arbeitsstelle dafür, dass ich so nett aufgenommen wurde und mir der Übergang von der Uni in die Berufswelt so leicht gemacht wurde. Die Arbeit mit euch macht mir wirklich Spaß und ich freue mich auf die Zeit die noch kommt.

Danke Alke, danke Phil, dafür, dass ihr die Arbeit Korrektur gelesen habt.

Besonders danken möchte ich natürlich auch meiner Familie. Ihr habt mir mein Studium ermöglicht, mich immer in jeder nur denkbaren Form unterstützt und immer an mich geglaubt, dafür kann man gar nicht genug danken! Vielen Dank Mama und Papa, vielen Dank Sandra!

Danke Maike, dass du während der stressigen Zeit der Arbeit an meiner Seite warst und mich unterstützt hast! Ich wüsste nicht worauf ich mich lieber einlassen würde, auch wenn ich nicht weiß, worauf ich mich eingelassen habe.

LIST OF ABBREVIATIONS

ACE	affinity capillary electrophoresis
An	actinides
Am	americium
Ac ⁻	acetate
AcOH	acetic acid
Ar	Argon
BGE	background electrolyte
Br	bromine
C ⁴ D	capacitively coupled contactless conductivity detector
CCD	contactless conductivity detection
CE	capillary electrophoresis
Cf	Californium
Cit ³⁻	Citrate
Cm	Curium
COX	Callovo-Oxfordian clay
cps	counts per second
DMF	<i>N,N</i> -dimethylformamide
DOM	dissolved organic matter
DTPA	diethylene triamine pentaacetic acid
EDTA	ethylene diamine tetraacetic acid
e.g.	exempli gratia \triangleq for example
EOF	electroosmotic flow
ESI-MS	electrospray ionization mass spectrometry
et al.	et alii/et aliae
EXAFS	extended X-ray absorption fine structure spectroscopy
Glu ⁻	gluconate
GluOH	gluconic acid
H ₃ Cit	citric acid
HA	humic acid
HAHCl	hydroxylamine hydrochloride
HDEHP	2-bisethylhexylphosphate
HIBA	hydroxyisobutyric acid
HOPO	hydroxypyridine oxide
HR-SF-ICP-MS	high resolution sector field inductively coupled plasma mass spectrometry
ICP-AES	inductively coupled plasma atomic emission spectroscopy
ICP-MS	inductively coupled plasma mass spectrometry
ICP-OES	inductively coupled plasma optical emission spectroscopy
ISA	isosaccharinic acid
L	ligand

LIST OF ABBREVIATIONS

Ln	lanthanides
M	metal
MC-ICP-MS	multi collector inductively coupled plasma mass spectrometry
Me	methyl
MS	mass spectrometry
NIR	near infrared
NOM	natural organic matter
Np	neptunium
OPA	Opalinus clay
ORS	octopole reaction system
Pa	protactinium
PMBP	4-benzoyl-3-methyl-1-phenylpyrazole-5-one
Pro-	propionate
ProOH	propionic acid
pH	potentia hydrogenii
phen	1,10-phenanthroline
ppb	parts per billion
Pu	plutonium
RF	radio frequency
RSC	relative standard deviation
rpm	rounds per minute
SD	standard deviation
SI	système international d'unités (international system of units)
SIT	specific ion interaction theory
SP-ICP-MS	single particle inductively coupled plasma mass spectrometry
SSA	5-sulfosalicylic acid
Th	thorium
U	uranium
UV-Vis	ultraviolet-visible (spectral region)
XAFS	X-ray absorption fine structure spectroscopy
XPS	X-ray photoelectron spectroscopy

LIST OF CHEMICALS

All reagents were of pro analysis quality or better. The actinide solutions of ^{237}Np , ^{239}Pu and ^{241}Am were prepared by dilution from in-house stock solutions. The preparation of the particular stock solution can be found in the respective experimental section.

chemical	supplier
acetic acid (99.8%)	Riedel-de Haën, Seelze, Germany
acetone	Fisher Scientific, Loughborough, United Kingdom
argon gas (4.6)	Westfalen AG, Münster, Germany
ammonia solution	Merck, Darmstadt, Germany
Bi ICP-MS standard (1000 $\mu\text{g ml}^{-1}$)	High-Purity Standards, Charleston, South Carolina, USA
2-bisethylhexylphosphate (HDEHP)	Merck, Darmstadt, Germany
2-bromoethanol	Alfa Aesar GmbH & Co KG, Karlsruhe, Germany
2-bromopropane	Merck, Darmstadt, Germany
Ce ICP-MS standard (1000 $\mu\text{g ml}^{-1}$)	High-Purity Standards, Charleston, South Carolina, USA
citric acid monohydrate	Merck, Darmstadt, Germany
Eu ICP-MS standard (1000 $\mu\text{g ml}^{-1}$)	Peak Performance, CPI International, Santa Rosa, California, USA
ethylenediaminetetraacetate (EDTA)	VWR International GmbH, Darmstadt, Germany
Fe ICP-MS standard (1000 $\mu\text{g ml}^{-1}$)	High-Purity Standards, Charleston, South Carolina, USA
hydrochloric acid (36%)	Fisher Scientific, Loughborough, United Kingdom
hydroxylamine hydrochloride	Merck, Darmstadt, Germany
iron(III) chloride hexahydrate	Merck, Darmstadt, Germany
iron(II) perchlorate	Sigma Aldrich, St. Louis, Missouri, USA
iron(III) perchlorate	Sigma Aldrich, St. Louis, Missouri, USA
MilliQ water (18.2 M Ω)	Synergy™ Millipore water system, Millipore GmbH, Schwalbach, Germany)
nitric acid	Merck, Darmstadt, Germany
perchloric acid (70%)	Riedel-de Haën, Seelze, Germany
1,10-phenanthroline (phen)	Alfa Aesar GmbH & Co KG, Karlsruhe, Germany
propionic acid	Acros Organics, Morris, New Jersey, USA
Rh ICP-MS standard (1000 $\mu\text{g ml}^{-1}$)	Merck, Darmstadt, Germany
5-sulfosalicylic acid	VWR International GmbH, Darmstadt, Germany
Th ICP-MS standard (1000 $\mu\text{g ml}^{-1}$)	Accu Trace™, Accu Standard, New Haven, Connecticut, USA
sodium fluoride	Merck, Darmstadt, Germany
sodium hydroxide (30%, Suprapure®)	Merck, Darmstadt, Germany
sodium gluconate	Sigma Aldrich, St. Louis, Missouri, USA
sodium perchlorate monohydrate	Merck, Darmstadt, Germany

LIST OF CHEMICALS

U ICP-MS standard (1000 $\mu\text{g ml}^{-1}$)	Peak Performance, CPI International, Santa Rosa, California, USA
^{238}U wires	Merck, Darmstadt, Germany
Y ICP-MS standard (1000 $\mu\text{g ml}^{-1}$)	High-Purity Standards, Charleston, South Carolina, USA

LIST OF UNITS

unit	full name (and the respective definition in SI-units)
A	ampere
Å	angstrom (1 Å = 10 ⁻¹⁰ m)
amu	atomic mass unit (1 amu = 1.660539 · 10 ⁻²⁷ kg)
C	coulomb (1 V = 1 A s)
cps	counts per second (1 cps = 1 s ⁻¹)
g	gram (1 g = 10 ⁻³ kg)
Hz	hertz (1 Hz = 1 s ⁻¹)
J	joule (1 J = 1 kg m ² s ⁻²)
K	kelvin
kg	kilogram
L	liter (1 L = 10 ⁻³ m ³)
m	meter
m	mol per kilogram (1 m = 1 mol kg ⁻¹)
min	minute (1 min = 60 s)
mol	mole
µm	micrometer (1 µm = 10 ⁻⁶ m)
M	mole per liter (1 M = 1 mol L ⁻¹ = 10 ³ mol m ⁻³)
N	newton (1 N = 1 kg m s ⁻²)
Pa	pascal (1 Pa = 1 kg m ⁻¹ s ⁻¹)
rpm	rounds per minute (min ⁻¹)
s	second
S	siemens (1 S = 1 A ² s ³ kg ⁻¹ m ⁻²)
V	volt (1 V = 1 kg m ² A ⁻¹ s ⁻³)
wt%	weight percent
W	watt (1 W = 1 kg m ² s ⁻³)
Ω	ohm (1 Ω = 1 kg m ² A ⁻² s ⁻³)

LIST OF VARIABLES AND CONSTANTS

variable/constant	Definition (Units are given in squared brackets.)
a	distance from the middle of a central ion to the beginning of the ionic vicinity in the Onsager-Fuoss model (see Eq. (2.5)) [Å]
A	capillary cross section area [μm^2]
A_{Peak}	peak area [cps = s^{-1}]
c	concentration [M]
C_n	coefficient in Eq. (2.5) given in [31ONS]
d_2	diameter of the fused silica layer of the capillary [μm]
d_3	diameter of the complete capillary including the polymer coating [μm]
d_c	inner capillary diameter [μm]
e	elementary charge ($e = 1.602176632 \cdot 10^{-19}$ C)
E	electric field strength [V cm^{-1}]
ε	permittivity [$\text{A s V}^{-1} \text{m}^{-1}$]
ε_0	permittivity in vacuum ($\varepsilon_0 = 8.854187 \cdot 10^{-12}$ A s $\text{V}^{-1} \text{m}^{-1}$)
ε_r	relative permittivity
γ_i	activity coefficient of a species i
Γ	twice ionic strength [M]
h	heat transfer coefficient between capillary and surrounding medium [$\text{W m}^{-2} \text{K}^{-1}$]
I	ionic strength [M]
I	electric current [A]
J	current density [A m^{-2}]
k	Boltzmann constant ($k = 1.38065 \cdot 10^{-23}$ J mol^{-1})
k_{air}	thermal conductivity of the air surrounding the capillary [$\text{W m}^{-1} \text{K}^{-1}$]
k_{BGE}	thermal conductivity of the BGE [$\text{W m}^{-1} \text{K}^{-1}$]
k_f	thermal conductivity of the fused silica layer [$\text{W m}^{-1} \text{K}^{-1}$]
k_p	thermal conductivity of the complete capillary including the polymer coating [$\text{W m}^{-1} \text{K}^{-1}$]
κ^{-1}	double layer thickness [10^{-9} m]
κ_e	electrical conductivity [S m^{-1}]
l	capillary length [cm]
m	mass [kg]
μ	electrophoretic mobility [$\text{cm}^2 \text{V}^{-1} \text{s}^{-1}$]
μ^0	electrophoretic mobility for zero ionic strength [$\text{cm}^2 \text{V}^{-1} \text{s}^{-1}$]
μ_{eff}	effective electrophoretic mobility [$\text{cm}^2 \text{V}^{-1} \text{s}^{-1}$]
N	Avogadro constant ($N = 6.022 \cdot 10^{23}$ mol^{-1})
N	maximum number of ligands in a given actinide-ligand complex system

List of Variables and Constants

Nu	Nusselt Number (dimensionless heat transfer coefficient)
η	viscosity [Pa s]
p	pressure [Pa]
π	mathematical constant ($\pi = 3.1415962$)
q	electric charge [C]
q_{eff}	effective electric charge [C]
φ	electric potential [V]
r	ionic radius [\AA]
r_2	radius of the fused silica layer of the capillary [μm]
r_3	radius of the complete capillary including the polymer coating [μm]
r_c	inner capillary radius [μm]
Re	Raynolds number
R^n	vectors in Eq. (2.5) given in [31ONS]
Rs	Resolution
ρ	density [kg m^{-3}]
RSD	relative standard deviation [%]
S	rate of power generation within the capillary volume per unit volume [W m^{-3}]
s	number of species
SD	standard deviation
t	time [s]
T	temperature [K]
T_o	temperature at the middle of the capillary [K]
T_a	ambient temperature of the medium surrounding the capillary [K]
ϑ	temperature [$^{\circ}\text{C}$]
U	voltage [V]
V	volume [m^3]
v	migration velocity [cm s^{-1}]
v_{air}	velocity of air over the capillary [m s^{-1}]
w	baseline width [s]
x	mole fraction
$ \bar{x} $	absolute value of the mean of a data set
z	charge number
ζ	zeta potential [V]

LIST OF FIGURES

Figure 1: Schematic layout of a capillary electrophoresis system.....	6
Figure 2: a) Cross section of a fused silica capillary with a schematic depiction of the electric double layer creating a flat EOF profile. b) Potential curve and EOF velocity profile. Figure based on a combination of [10LAU] and [92GRO].....	9
Figure 3: Cross section of the fused silica capillary with polymer coating (not true to scale). The temperature profile shown in red was evaluated with the conditions used in this work ($U = 25$ kV, 10 m s ⁻¹ forced air cooling at 25 °C). More details on the calculations are given in APPENDIX A1.....	12
Figure 4: Schematic overview of the general structure of the ICP-MS system with nebulizer and spray chamber used in this work. The figure is based on a combination of different illustrations in [08AGI1]. The red dotted line describes the path of the sample through the system.....	16
Figure 5: a) Schematic cross-section of the MiraMist CE nebulizer used in this work. b) Details of the tip of the nebulizer in cross section and top view with the respective gas and liquid flows. The figures are based on the Burgener Research Operating Instructions Manual [19BUR].	20
Figure 6: Resulting electropherograms for the comparison of two different EOF markers, 2-bromopropane and 2-bromoethanol, at $U = 25$ kV and $U = 10$ kV.	32
Figure 7: Table of Content Graphic for publication of the electrophoretic mobility manuscript.	34
Figure 8: Electropherograms of the CE-ICP-MS measurements of the actinides Am(III), Th(IV), Np(V) and U(VI) in a non-complexing medium in dependence of the pH value at $I = 0.3$ M and $U = 10$ kV ($U = 9$ kV for the sample at pH = 0.56).....	61
Figure 9: Trend of the electrophoretic mobilities of the actinides Am(III), Th(IV), Np(V) and U(VI) in a non-complexing medium in dependence of the pH value measured by CE-ICP-MS at $U = 10$ kV ($U = 9$ kV for the sample at pH = 0.56).	62
Figure 10: Table of Content Graphic for publication of the acetate manuscript.....	64
Figure 11: Measured effective electrophoretic mobilities μ_{eff} of the actinide-propionate series as a function of the free propionate concentration [Pro ⁻] at $I = 0.3$ M with the related fit curve. A: Am(III), B: Th(IV), C: Np(V), D: U(VI).....	76
Figure 12: Measured effective electrophoretic mobilities μ_{eff} of the actinide-gluconate series as a function of the free gluconate concentration [Glu ⁻] at $I = 0.3$ M with the related fit curve. A: Am(III), B: Th(IV), C: Np(V), D: U(VI).....	84

List of Figures

Figure 13: Citrate speciation diagram with the distribution of the different deprotonated species based on the pH values of 16 samples for the CE-ICP-MS measurement series.	91
Figure 14: Measured effective electrophoretic mobilities μ_{eff} of the americium(III)-citrate series as a function of the respective free citrate species concentration [Cit^{3-} , HCit^{2-} , H_2Cit^-] at $I = 0.3 \text{ M}$ with the related fit curves. The classification is based on the predominance of the respective species at a given sample pH.	93
Figure 15: Comparison of the measured and the calculated effective electrophoretic mobility μ_{eff} of the Am(III)-citrate series at $I = 0.3 \text{ M}$	96
Figure 16: Measured effective electrophoretic mobilities μ_{eff} of the Th(IV)-citrate series as a function of the free citrate concentration [Cit^{3-}] at $I = 0.3 \text{ M}$ with the related fit curve.	97
Figure 17: Measured effective electrophoretic mobilities μ_{eff} of the neptunium(V)-citrate series as a function of the respective free citrate species concentration [Cit^{3-} , HCit^{2-} , H_2Cit^-] at $I = 0.3 \text{ M}$ with the related fit curves. The classification is based on the predominance of the respective species at a given sample pH.	99
Figure 18: Comparison of the measured and the calculated effective electrophoretic mobility μ_{eff} of the Np(V)-citrate series at $I = 0.3 \text{ M}$	100
Figure 19: Measured effective electrophoretic mobilities μ_{eff} of the uranium(VI)-citrate series as a function of the respective free citrate species concentration [Cit^{3-}], [HCit^{2-}], [H_2Cit^-] at $I = 0.3 \text{ M}$ with the related fit curves. The classification is based on the predominance of the respective species at a given sample pH.	101
Figure 20: Comparison of the measured and the calculated effective electrophoretic mobility μ_{eff} of the U(VI)-citrate series at $I = 0.3 \text{ M}$	103
Figure 21: Graphical determination of the rate constants of the three reductions of Np(V) to Np(IV) at $40 \text{ }^\circ\text{C}$ and $c(\text{HAHCl}) = 7.2 \text{ M}$ with three different HAHCl batches.	120
Figure 22: Effect of the ORS in H_2 mode on the electropherograms of the CE-ICP-MS background solution (1 M AcOH).	126
Figure 23: Electropherograms of the CE-ICP-MS measurements of Fe(II)-phen and Fe(III)-EDTA in 1 M AcOH and $0,1 \text{ M HClO}_4$ background medium.	128
Figure 24: Development of the Pu(VI) and Pu(rest) percentages for the determination of the reduction kinetics of Pu(VI) with Fe(II), ratio 1:3, by LLE/LSC at $10 \text{ }^\circ\text{C}$	131
Figure 25: Development of the Pu(VI) and Pu(rest) percentages for the determination of the reduction kinetics of Pu(VI) with Fe(II), ratio 1:3, by LLE/LSC at $23 \text{ }^\circ\text{C}$	132
Figure 26: Development of the Pu(VI) and Pu(rest) percentages for the determination of the reduction kinetics of Pu(VI) with Fe(II), ratio 1:3, by LLE/LSC at $30 \text{ }^\circ\text{C}$	133

Figure 27: Graphical determination of the kinetical parameters of the reduction kinetics of Pu(VI) with Fe(II), ratio 1:3, by LLE/LSC. The data points in grey are not used for the fits since the reaction was already in equilibrium at this times.....134

Figure 28: Electropherograms of the CE-ICP-MS measurement of the reduction of Pu(VI) by Fe(II) at 10 °C and 23 °C, U = 25 kV. The first peak in both electropherograms is assigned to Pu(VI), the second one to Pu(III).....135

Figure 29: Graphical determination of the kinetical parameters of the reduction kinetics of Pu(VI) with Fe(II), ratio 1:4000, by CE-ICP-MS. The data points in grey are not used for the fits since the reaction was already in equilibrium at this times.....137

LIST OF TABLES

Table 1: Preconditioning program for new capillaries.	7
Table 2: Flushing program at the beginning of every measurement day.....	7
Table 3: Summary of the parameters and devices used in this work.....	21
Table 4: Summary of the publications on the determination of stability constants of actinides with different ligands. For more details concerning the experimental conditions such as BGE, ionic strength, temperature etc. and the results see the respective reference.	25
Table 5: Results of the comparison of two different EOF markers, 2-bromopropane and 0.2 M 2-bromoethanol, at $U = 25$ kV and $U = 10$ kV.....	33
Table 6: Values of the electrophoretic mobilities of the actinides Am(III), Th(IV), Np(V) and U(VI) in a non-complexing medium at different pH values.	62
Table 7: Stability constants β_i for the different actinide–propionate complexes at $I = 0.3$ M and the corresponding values extrapolated to zero ionic strength. The limits of error $\Delta(\beta_i)$ are resulting from the fitting procedure.	77
Table 8: Electrophoretic mobilities of the individual species μ_i for the different actinide–propionate complexes. The uncertainties are estimated to be $\Delta\mu_i = 0.1 \cdot 10^{-4} \text{ cm}^2 \text{ V}^{-1} \text{ s}^{-1}$ in all cases.	79
Table 9: Stability constants β_i for the different actinide–gluconate complexes at $I = 0.3$ M and the corresponding values extrapolated to zero ionic strength. The limits of error $\Delta(\beta_i)$ are resulting from the fitting procedure.	85
Table 10: Electrophoretic mobilities of the individual species μ_i for the different actinide–gluconate complexes. The uncertainties are estimated to be $\Delta\mu_i = 0.1 \cdot 10^{-4} \text{ cm}^2 \text{ V}^{-1} \text{ s}^{-1}$ in all cases.	87
Table 11: Stability constants β_i and electrophoretic mobilities of the individual species μ_i for the different Am(III)–citrate complexes at $I = 0.3$ M. The limits of error $\Delta(\beta_i)$ are resulting from the fitting procedure. The uncertainties $\Delta\mu_i$ are estimated to be $0.1 \cdot 10^{-4} \text{ cm}^2 \text{ V}^{-1} \text{ s}^{-1}$ in all cases.	94
Table 12: Stability constants β_i and electrophoretic mobilities of the individual species μ_i for the Th(IV)–Cit ³⁻ complexes at $I = 0.3$ M. The limits of error $\Delta(\beta_i)$ are resulting from the fitting procedure. The uncertainties $\Delta\mu_i$ are estimated to be $0.1 \cdot 10^{-4} \text{ cm}^2 \text{ V}^{-1} \text{ s}^{-1}$ in all cases.	97
Table 13: Stability constants β_i and electrophoretic mobilities of the individual species μ_i for the different Np(V)–citrate complexes at $I = 0.3$ M. The limits of error $\Delta(\beta_i)$ are resulting from the fitting procedure. The uncertainties $\Delta\mu_i$ are estimated to be $0.1 \cdot 10^{-4} \text{ cm}^2 \text{ V}^{-1} \text{ s}^{-1}$ in all cases.	99

Table 14: Stability constants β_i and electrophoretic mobilities of the individual species μ_i for the different Np(V)–citrate complexes at I = 0.3 M. The limits of error $\Delta(\beta_i)$ are resulting from the fitting procedure. The uncertainties $\Delta\mu_i$ are estimated to be $0.1 \cdot 10^{-4} \text{ cm}^2\text{V}^{-1}\text{s}^{-1}$ in all cases.....102

Table 15: Results of the measurement series of the reduction of Np(V) to Np(IV) at 40 °C and c(HAHCl) = 7.2 M: reaction 1, old batch.....118

Table 16: Results of the measurement series of the reduction of Np(V) to Np(IV) at 40 °C and c(HAHCl) = 7.2 M: reaction 2, new batch. These results are taken from the kinetic manuscript obtained by CE-ICP-MS measurements.....119

Table 17: Results of the measurement series of the reduction of Np(V) to Np(IV) at 40 °C and c(HAHCl) = 7.2 M: reaction 3, new batch + one spade point of $\text{FeCl}_3 \cdot 6 \text{H}_2\text{O}$119

Table 18: Rate constants k and half times $t_{1/2}$ of the measurement series of the reduction of Np(V) to Np(IV) at 40 °C with three different HAHCl batches: reaction 3, new batch + one spade point of $\text{FeCl}_3 \cdot 6 \text{H}_2\text{O}$120

Table 19: Results of the ICP-MS measurements of ^{54}Fe and ^{56}Fe with the ORS system in no gas mode, H_2 mode and He mode.....125

Table 20: Detailed sample compositions for the CE-ICP-MS investigations of the Fe(II)-phen and the Fe(III)-EDTA complexes. The total sample volume was $V = 200 \mu\text{L}$ in each sample.127

Table 21: Electrophoretic mobilities of the $\text{Fe}(\text{phen})^{2+}$ and the $\text{Fe}(\text{EDTA})^-$ species investigated by CE-ICP-MS in different 1 M AcOH/0.1 M HClO_4 background media.....129

Table 22: Results of the determination of the reduction kinetics of Pu(VI) with Fe(II), ratio 1:3, by LLE/LSC at 10 °C.....131

Table 23: Results of the determination of the reduction kinetics of Pu(VI) with Fe(II), ratio 1:3, by LLE/LSC at 23 °C.....132

Table 24: Results of the determination of the reduction kinetics of Pu(VI) with Fe(II), ratio 1:3, by LLE/LSC at 30 °C.....133

Table 25: Resulting rate constants k and corresponding half lifes $t_{1/2}$ of the reduction of Pu(VI) by Fe(II), ratio 1:3, by LLE/LSC.....134

Table 26: Results of the determination of the reduction kinetics of Pu(VI) with Fe(II), ratio 1:4000, by CE-ICP-MS at 10 °C.....136

Table 27: Results of the determination of the reduction kinetics of Pu(VI) with Fe(II), ratio 1:4000, by CE-ICP-MS at 23 °C.....136

Table 28: Resulting rate constants k and corresponding half lifes $t_{1/2}$ of the reduction of Pu(VI) by Fe(II), ratio 1:4000, by CE-ICP-MS.....137